

AD-A241 742



2

NAVAL POSTGRADUATE SCHOOL Monterey, California



THESIS

DTIC
ELECTE
OCT 28 1991
S B D

STUDY OF THE EFFECTS OF CENTRIFUGAL IN-
STABILITIES ON FLOW IN
A 40 TO 1 ASPECT RATIO RECTANGULAR
CURVED CHANNEL, FOR DEAN NUMBERS FROM
35 TO FULLY TURBULENT
CONDITIONS

by

William A. Fields, P.E.

December 1990

Thesis Advisor

P.M. Ligrani

Approved for public release; distribution is unlimited.

91-13998



Unclassified

Security classification of this page

REPORT DOCUMENTATION PAGE

a Report Security Classification Unclassified			1b Restrictive Markings		
2a Security Classification Authority			3 Distribution Availability of Report		
2b Declassification Downgrading Schedule			Approved for public release; distribution is unlimited.		
4 Performing Organization Report Number(s)			5 Monitoring Organization Report Number(s)		
6a Name of Performing Organization Naval Postgraduate School		6b Office Symbol (if applicable) 34	7a Name of Monitoring Organization Naval Postgraduate School		
6c Address (city, state, and ZIP code) Monterey, CA 93943-5000			7b Address (city, state, and ZIP code) Monterey, CA 93943-5000		
8a Name of Funding Sponsoring Organization Propulsion Directorate		8b Office Symbol (if applicable)	9 Procurement Instrument Identification Number MIPR C-30030-P		
8c Address (city, state, and ZIP code) US Army Aviation R/T Act AVSCON NASA-Lewis, Cleveland, Oh 45433			10 Source of Funding Numbers		
			Program Element No	Project No	Task No
			Work Unit Accession No		
11 Title (include security classification) STUDY OF THE EFFECTS OF CENTRIFUGAL INSTABILITIES ON FLOW IN A 40 TO 1 ASPECT RATIO RECTANGULAR CURVED CHANNEL, FOR DEAN NUMBERS FROM 35 TO FULLY TURBULENT CONDITIONS					
12 Personal Author(s) William A. Fields, P.E.					
13a Type of Report Master's Thesis		13b Time Covered From To		14 Date of Report (year, month, day) December 1990	
15 Page Count 192					
16 Supplementary Notation The views expressed in this thesis are those of the author and do not reflect the official policy or position of the Department of Defense or the U.S. Government.					
17 Cosati Codes			18 Subject Terms (continue on reverse if necessary and identify by block number)		
Field	Group	Subgroup	Dean vortices, Dean number, Rectangular curved channel.		
19 Abstract (continue on reverse if necessary and identify by block number)					
<p>The development and structure of Dean vortices in a high aspect ratio curved channel, were measured and studied for Dean numbers from 35 to fully turbulent conditions. Mean vorticity components were determined from measurements of the three components of mean velocity, which were measured using a miniature five-hole pressure probe. Streamwise, radial and spanwise vorticity components measured 120° from the start of curvature, show evidence of Dean vortices in the time-averaged flow field. Peak streamwise and peak spanwise vorticity, as well as streamwise circulation, generally increase as the Dean number increases from 60 to 240. Peak radial vorticity increases as Dean numbers vary from 60 to about 160. Spectra obtained from hot-wire probes show evidence of different frequency events, including twisting and undulation. Twisting is apparent for Dean numbers of 135 to 160 while undulation is observed at lower Dean numbers. Flow visualization results illustrate a variety of time dependent events in the channel.</p>					
20 Distribution Availability of Abstract			21 Abstract Security Classification		
<input checked="" type="checkbox"/> unclassified unlimited <input type="checkbox"/> same as report <input type="checkbox"/> DTIC users			Unclassified		
22a Name of Responsible Individual P.M. Ligrani			22b Telephone (include Area code) (408) 646-3382		22c Office Symbol ME/Li

DD FORM 1472, MAR

83 APR edition may be used until exhausted
All other editions are obsolete

security classification of this page

Unclassified

Approved for public release; distribution is unlimited.

Study of the Effects of Centrifugal Instabilities on Flow in
a 40 to 1 Aspect Ratio Rectangular
Curved Channel, for Dean Numbers from 35 to Fully Turbulent
Conditions

by

William A. Fields, P.E.
Lieutenant, United States Navy
Bachelor of Chemical Engineering, Manhattan College, 1982

Submitted in partial fulfillment of the
requirements for the degrees of

MASTER OF SCIENCE IN MECHANICAL ENGINEERING
and
MECHANICAL ENGINEER

from the


NAVAL POSTGRADUATE SCHOOL
December 1990

Author:

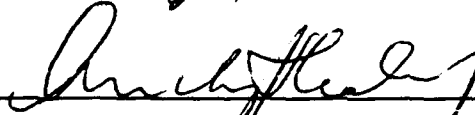


William A. Fields, P.E.

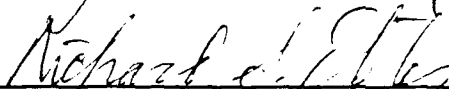
Approved by:



P.M. Ligrani, Thesis Advisor



Anthony J. Healey, Chairman,
Department of Mechanical Engineering



DEAN OF FACULTY AND GRADUATE STUDIES

ABSTRACT

The development and structure of Dean vortices in a high aspect ratio curved channel, were measured and studied for Dean numbers from 35 to fully turbulent conditions. Mean vorticity components were determined from measurements of the three components of mean velocity, which were measured using a miniature five-hole pressure probe. Streamwise, radial and spanwise vorticity components measured 120° from the start of curvature, show evidence of Dean vortices in the time-averaged flow field. Peak streamwise and peak spanwise vorticity, as well as streamwise circulation, generally increase as the Dean number increases from 60 to 240. Peak radial vorticity increases as Dean numbers vary from 60 to about 160. Spectra obtained from hot-wire probes show evidence of different frequency events, including twisting and undulation. Twisting is apparent for Dean numbers of 135 to 160 while undulation is observed at lower Dean numbers. Flow visualization results illustrate a variety of time dependent events in the channel.



Accession For	
NTIS GRA&I	<input checked="" type="checkbox"/>
DTIC TAB	<input type="checkbox"/>
Unannounced	<input type="checkbox"/>
Justification	
By	
Date (DD/MM/YY)	
Availability Codes	
Avail and/or	
Dist	Special
A-1	

TABLE OF CONTENTS

I. INTRODUCTION	1
A. BACKGROUND	1
B. OBJECTIVES	2
C. ORGANIZATION	3
II. CURVED CHANNEL	4
A. CHANNEL DESCRIPTION	4
B. DEAN NUMBER DETERMINATION	5
III. PROCEDURES FOR MEASUREMENT OF PRESSURE AND VELOCITY SURVEYS	7
A. PROBE DESCRIPTIONS	7
1. KIEL PROBE	7
2. FIVE-HOLE PRESSURE PROBE	7
B. EXPERIMENTAL DETAILS	8
C. PROBE CALIBRATION PROCEDURES AND RESULTS	9
D. CURVED CHANNEL MEASUREMENT PROCEDURES	10
1. TRAVERSING MECHANISM	10
2. MEASUREMENT PROCEDURE	11
3. DATA REDUCTION	12
IV. POWER SPECTRA PROCEDURES AND EQUIPMENT	14
A. HOT-WIRE PROBE	15

B. SIGNAL MEASUREMENT	15
C. SIGNAL PROCESSING AND ANALYSIS	16
V. FLOW VISUALIZATION APPARATUS AND PROCEDURE	18
A. SMOKE GENERATOR	18
B. CAMERA AND LIGHTING	19
C. VIDEO RECORDER, PRINTER AND MONITOR	20
VI. EXPERIMENTAL RESULTS	21
A. SURVEYS OF TIME-AVERAGED QUANTITIES	22
1. TOTAL PRESSURE AND STREAMWISE VELOCITY	22
2. VELOCITY PERTURBATION	23
3. VORTICITY COMPONENTS	24
a. STREAMWISE VORTICITY	24
b. STREAMWISE CIRCULATION	25
c. RADIAL VORTICITY	26
d. SPANWISE VORTICITY	26
B. SPECTRA OF HOT-WIRE SIGNAL MEASUREMENTS	26
C. FLOW VISUALIZATION	27
VII. SUMMARY AND CONCLUSIONS	32
APPENDIX A. FIGURES	34
APPENDIX B. UNCERTAINTY ANALYSIS	159
A. DEAN NUMBER UNCERTAINTY	159

1. CELESCO TRANSDUCER CALIBRATION UNCERTAINTY	159
2. PRESSURE DROP UNCERTAINTY	159
3. MASS FLOW RATE UNCERTAINTY	159
B. FIVE-HOLE PROBE VELOCITY MEASUREMENT UNCERTAINTY	160
1. VALIDYNE TRANSDUCER CALIBRATION UNCERTAINTY . .	160
2. PROBE CALIBRATION UNCERTAINTY	160
3. CURVED CHANNEL MEASUREMENT UNCERTAINTY	161
APPENDIX C. SOFTWARE DIRECTORY	162
A. KIEL PROBE PROGRAMS	162
B. FIVE-HOLE PRESSURE PROBE PROGRAMS	163
C. DATA PROCESSING	167
LIST OF REFERENCES	170
INITIAL DISTRIBUTION LIST	175

LIST OF FIGURES

Figure 1. Curved Channel Geometry	34
Figure 2. Schematic of One Dean Vortex Pair	34
Figure 3. Schematic of Test Facility	35
Figure 4. Test Facility (Side View)	36
Figure 5. Channel Inlet and Nozzle	37
Figure 6. Schematic of Support Block	38
Figure 7. Five-Hole Pressure Probe Geometry	39
Figure 8. Five-Hole Pressure Probe	40
Figure 9. Five-Hole Pressure Probe (100 μ between scale markings)	41
Figure 10. Pressure Probe Calibration Sled	42
Figure 11. Wind Tunnel Used For Probe Calibration	43
Figure 12. Curved Channel Traversing Mechanism, Transducers, Probe and Mount	44
Figure 13. C_{py} vs. Yaw Angle, 3.9 m/s	45
Figure 14. C_{pp} vs. Pitch Angle, 3.9 m/s	46
Figure 15. C_{pt} vs. Pitch Angle, 3.9 m/s	47
Figure 16. $C_{p_{12}}$ vs. Pitch Angle, 3.9 m/s	48
Figure 17. C_{p_s} vs. Pitch Angle, 3.9 m/s	49
Figure 18. Kiel Probe Total Pressure Contour, $De = 51.81$	50
Figure 19. Kiel Probe Total Pressure Contour, $De = 77.47$	51
Figure 20. Kiel Probe Total Pressure Contour, $De = 103.6$	52
Figure 21. Kiel Probe Total Pressure Contour, $De = 126.2$	53
Figure 22. Kiel Probe Total Pressure Contour, $De = 149.6$	54
Figure 23. Kiel Probe Total Pressure Contour, $De = 177.5$	55

Figure 24. Kiel Probe Total Pressure Contour, $De=202.7$	56
Figure 25. Kiel Probe Total Pressure Contour, $De=226.8$	57
Figure 26. Kiel Probe Total Pressure Contour, $De=252.4$	58
Figure 27. Kiel Probe Total Pressure Contour, $De=274.5$	59
Figure 28. Kiel Probe Total Pressure Contour, $De=302.0$	60
Figure 29. Kiel Probe Total Pressure Contour, $De=327.5$	61
Figure 30. Kiel Probe Total Pressure Contour, $De=350.7$	62
Figure 31. Kiel Probe Total Pressure Contour, $De=375.9$	63
Figure 32. Kiel Probe Total Pressure Contour, $De=402.8$	64
Figure 33. Kiel Probe Total Pressure Contour, $De=425.8$	65
Figure 34. Kiel Probe Total Pressure Contour, $De=450.2$	66
Figure 35. Kiel Probe Pressure Differentials	67
Figure 36. Five-Hole Probe Total Pressure Contours, $De=35.0$ to $De=111.8$	68
Figure 37. Five-Hole Probe Total Pressure Contours, $De=111.8$ to $De=187.7$	69
Figure 38. Five-Hole Probe Total Pressure Contours, $De=187.7$ to $De=275.4$	70
Figure 39. Five-Hole Probe Total Pressure Contours, $De=275.4$ to $De=428.6$	71
Figure 40. Five-Hole Probe Pressure Differentials	72
Figure 41. Streamwise Velocity Contours, $De=35.0$ to $De=111.8$	73
Figure 42. Streamwise Velocity Contours, $De=111.8$ to $De=187.7$	74
Figure 43. Streamwise Velocity Contours, $De=187.7$ to $De=275.4$	75
Figure 44. Streamwise Velocity Contours, $De=275.4$ to $De=428.6$	76
Figure 45. Plot of Velocity Vectors for $De=86.69$	77
Figure 46. Plot of Velocity Vectors for $De=99.9$	78
Figure 47. Plot of Velocity Vectors for $De=149.8$	79
Figure 48. Velocity Perturbation Contours, $De=35.0$ to $De=111.8$	80
Figure 49. Velocity Perturbation Contours, $De=111.8$ to $De=187.7$	81

Figure 50. Velocity Perturbation Contours, $De = 187.7$ to $De = 275.4$	82
Figure 51. Velocity Perturbation Contours, $De = 275.4$ to $De = 428.6$	83
Figure 52. Streamwise Perturbation Contours, $De = 35.0$ to $De = 111.8$	84
Figure 53. Streamwise Perturbation Contours, $De = 111.8$ to $De = 187.7$	85
Figure 54. Streamwise Perturbation Contours, $De = 187.7$ to $De = 275.4$	86
Figure 55. Streamwise Perturbation Contours, $De = 275.4$ to $De = 428.6$	87
Figure 56. Peak Streamwise Vorticity vs. Dean Number, Left Vortex Pair	88
Figure 57. Peak Streamwise Vorticity vs. Dean Number, Middle Vortex Pair	89
Figure 58. Peak Streamwise Vorticity vs. Dean Number, Right Vortex Pair	90
Figure 59. Vortex Circulation vs. Dean Number, Left Vortex Pair	91
Figure 60. Vortex Circulation vs. Dean Number, Middle Vortex Pair	92
Figure 61. Vortex Circulation vs. Dean Number, Right Vortex Pair	93
Figure 62. Radial Vorticity Contours, $De = 35.0$ to $De = 111.8$	94
Figure 63. Radial Vorticity Contours, $De = 111.8$ to $De = 187.7$	95
Figure 64. Radial Vorticity Contours, $De = 187.7$ to $De = 275.4$	96
Figure 65. Radial Vorticity Contours, $De = 275.4$ to $De = 428.6$	97
Figure 66. Peak Radial Vorticity vs. Dean Number, Left Vortex Pair	98
Figure 67. Peak Radial Vorticity vs. Dean Number, Middle Vortex Pair	99
Figure 68. Peak Radial Vorticity vs. Dean Number, Right Vortex Pair	100
Figure 69. Spanwise Vorticity Contours, $De = 35.0$ to $De = 111.8$	101
Figure 70. Spanwise Vorticity Contours, $De = 111.8$ to $De = 187.7$	102
Figure 71. Spanwise Vorticity Contours, $De = 187.7$ to $De = 275.4$	103
Figure 72. Spanwise Vorticity Contours, $De = 275.4$ to $De = 428.6$	104
Figure 73. Spanwise Vorticity vs. Radial Location	105
Figure 74. Peak Spanwise Vorticity vs. Dean Number, Left Vortex Pair	106
Figure 75. Peak Spanwise Vorticity vs. Dean Number, Middle Vortex Pair	107

Figure 76. Peak Spanwise Vorticity vs. Dean Number, Right Vortex Pair	108
Figure 77. Hot-wire Probe Mounting	109
Figure 78. Overview of the HP 3562A Signal Analyzer Measurement Process . . .	110
Figure 79. Typical Settings Used on the HP 3562A Signal Analyzer	111
Figure 80. Hot-wire Measurement Setup	112
Figure 81. Conventional Hot-wire Probe Spectra, $De = 40.3$ to $De = 145.3$	113
Figure 82. Conventional Hot-wire Probe Time Traces, $De = 40.3$ to $De = 145.3$. .	114
Figure 83. Conventional Hot-wire Probe Spectra, $De = 140.6$ to $De = 155.4$	115
Figure 84. Conventional Hot-wire Probe Time Traces, $De = 135.1$ to $De = 150.4$.	116
Figure 85. Conventional Hot-wire Probe Spectra, $De = 50.5$ to $De = 435.0$	117
Figure 86. Conventional Hot-wire Probe Spectrum, $De = 50.5$	118
Figure 87. Conventional Hot-wire Probe Spectrum, $De = 100.3$	119
Figure 88. Conventional Hot-wire Probe Spectrum, $De = 150.1$	120
Figure 89. Conventional Hot-wire Probe Spectrum, $De = 200.1$	121
Figure 90. Conventional Hot-wire Probe Spectrum, $De = 250.0$	122
Figure 91. Conventional Hot-wire Probe Spectrum, $De = 300.7$	123
Figure 92. Conventional Hot-wire Probe Spectrum, $De = 350.3$	124
Figure 93. Conventional Hot-wire Probe Spectrum, $De = 400.2$	125
Figure 94. Conventional Hot-wire Probe Spectrum, $De = 435.0$	126
Figure 95. Flow Visualization Radial Spanwise Plane	127
Figure 96. Schematic of Smoke Generator and Smoke Rake	128
Figure 97. Camera Control Unit (CCU) Front Panel	129
Figure 98. Flow Visualization, $De = 50.9$, $\theta = 40^\circ$ (inside), 1/15 Second Intervals . .	130
Figure 99. Flow Visualization, $De = 100.1$, $\theta = 40^\circ$ (inside), 1/15 Second Intervals .	131
Figure 100. Flow Visualization, $De = 150.7$, $\theta = 40^\circ$ (inside), 1/15 Second Intervals	132
Figure 101. Flow Visualization, $De = 200.5$, $\theta = 40^\circ$ (inside), 1/30 Second Intervals	133

Figure 102. Flow Visualization, $De = 250.8$, $\theta = 40^\circ$ (<i>inside</i>), 1/60 Second Intervals	134
Figure 103. Flow Visualization, $De = 300.3$, $\theta = 40^\circ$ (<i>inside</i>), 1/60 Second Intervals	135
Figure 104. Flow Visualization, $De = 350.3$, $\theta = 40^\circ$ (<i>inside</i>), 1/60 Second Intervals	136
Figure 105. Flow Visualization, $De = 400.4$, $\theta = 40^\circ$ (<i>inside</i>), 1/60 Second Intervals	137
Figure 106. Flow Visualization, $De = 425.0$, $\theta = 40^\circ$ (<i>inside</i>), 1/60 Second Intervals	138
Figure 107. Flow Visualization, $De = 50.9$, $\theta = 40^\circ$ (<i>outside</i>), 1/20 Second Intervals	139
Figure 108. Flow Visualization, $De = 100.0$, $\theta = 40^\circ$ (<i>outside</i>), 1/30 Second Intervals	140
Figure 109. Flow Visualization, $De = 150.5$, $\theta = 40^\circ$ (<i>outside</i>), 1/60 Second Intervals	141
Figure 110. Flow Visualization, $De = 200.3$, $\theta = 40^\circ$ (<i>outside</i>), 1/60 Second Intervals	142
Figure 111. Flow Visualization, $De = 250.6$, $\theta = 40^\circ$ (<i>outside</i>), 1/60 Second Intervals	143
Figure 112. Flow Visualization, $De = 300.7$, $\theta = 40^\circ$ (<i>outside</i>), 1/60 Second Intervals	144
Figure 113. Flow Visualization, $De = 350.7$, $\theta = 40^\circ$ (<i>outside</i>), 1/60 Second Intervals	145
Figure 114. Flow Visualization, $De = 400.9$, $\theta = 40^\circ$ (<i>outside</i>), 1/60 Second Intervals	146
Figure 115. Flow Visualization, $De = 425.3$, $\theta = 40^\circ$ (<i>outside</i>), 1/60 Second Intervals	147
Figure 116. Flow Visualization, $De = 200.4$, $\theta = 80^\circ$ (<i>inside</i>), 1/60 Second Intervals	148
Figure 117. Flow Visualization, $De = 250.3$, $\theta = 80^\circ$ (<i>inside</i>), 1/60 Second Intervals	149
Figure 118. Flow Visualization, $De = 300.3$, $\theta = 80^\circ$ (<i>inside</i>), 1/60 Second Intervals	150
Figure 119. Flow Visualization, $De = 50.9$, $\theta = 120^\circ$ (<i>inside</i>), 1/30 Second Intervals	151
Figure 120. Flow Visualization, $De = 75.5$, $\theta = 120^\circ$ (<i>inside</i>), 1/30 Second Intervals	152
Figure 121. Flow Visualization, $De = 75.5$, $\theta = 120^\circ$ (<i>inside</i>), 1/30 Second Intervals	153
Figure 122. Flow Visualization, $De = 75.5$, $\theta = 120^\circ$ (<i>inside</i>), 1/30 Second Intervals	154
Figure 123. Flow Visualization, $De = 100.6$, $\theta = 120^\circ$ (<i>inside</i>), 1/30 Second Intervals	155
Figure 124. Flow Visualization, $De = 125.5$, $\theta = 120^\circ$ (<i>inside</i>), 1/30 Second Intervals	156
Figure 125. Flow Visualization, $De = 150.5$, $\theta = 120^\circ$ (<i>inside</i>), 1/30 Second Intervals	157
Figure 126. Flow Visualization, $De = 200.8$, $\theta = 120^\circ$ (<i>inside</i>), 1/60 Second Intervals	158

NOMENCLATURE

A_{ch}	Cross Sectional Area of Curved Channel
A_{or}	Cross Sectional Area of Orifice
A_p	Cross Sectional Area of Outlet Pipe
\bar{C}	Average Transducer Calibration Coefficient
CCPF	Curved Channel Poiseuille Flow
C_{pp}	Probe Calibration Coefficient, Pitch
C_{ps}	Probe Calibration Coefficient, Static Pressure
C_{pt}	Probe Calibration Coefficient, Total Pressure
C_{pst}	Probe Calibration Coefficient, Total Static Pressure
C_{py}	Probe Calibration Coefficient, Yaw
d	Channel Height, $(r_o - r_i)$
d_{ely}	Radial Down-Wash Velocity Correction
d_{elz}	Spanwise Down-Wash Velocity Correction
d_p	Outlet Pipe Diameter
De	Dean Number, $(Re_{ch})\sqrt{d/r_i}$
\bar{E}	Average Transducer Voltage Reading
K	Flow Coefficient
K_p	Slope of Pitch Coefficient Calibration Curve
K_{st}	Slope of Total Static Coefficient Calibration Curve
K_y	Slope of Yaw Coefficient Calibration Curve
m	Mass Flow Rate
p'	Preliminary Pitch
P_{amb}	Ambient Pressure

P_{off}	Pitch Offset
\bar{P}	Average Pressure, $(P_2+P_3+P_4+P_5)/4$
P_1	Pressure Measured at Port One of Five Hole Probe
P_2	Pressure Measured at Port Two of Five Hole Probe
P_3	Pressure Measured at Port Three of Five Hole Probe
P_4	Pressure Measured at Port Four of Five Hole Probe
P_5	Pressure Measured at Port Five of Five Hole Probe
$P_{manometer}$	Manometer Pressure Reading
P_s	Static Pressure
P_t	Total Pressure
Re_{ch}	Channel Reynolds Number, $(\bar{U}d/\nu)$
Re_p	Pipe Reynolds Number, $(\bar{U}d_p/\nu)$
r_i	Curved Channel Inside Radius
r_o	Curved Channel Outside Radius
U	Total Velocity
\bar{U}	Mean Velocity
U_θ	Streamwise Velocity, also U_x
U_r	Radial Velocity, also U_y
U_x	Streamwise Velocity, also U_θ
U_y	Radial Velocity, also U_r
U_z	Spanwise Velocity
y/d	Normalized Radial Direction
Y	Expansion Coefficient
y_{len}	Radial Distance Between Port 1 and Center of Other Ports
z/d	Normalized Spanwise Direction
z_{len}	Spanwise Distance Between Port 1 and Center of Other Ports

Greek Symbols

δ	Uncertainty Estimate	.
Δ	Coefficient for determining Down-wash Velocity Correction	.
ΔP_{or}	Orifice Pressure Drop	v
Γ_x	Streamwise Circulation	
ρ	Density	
ν	Kinematic Viscosity	.
θ	Streamwise Location from Start of Curvature	.
ω_θ	Mean Streamwise Vorticity, also ω_x	.
ω_r	Mean Radial Vorticity, also ω_y	
ω_z	Mean Spanwise Vorticity	

ACKNOWLEDGMENT

I would like express my heartfelt thanks to several people who helped me make this work possible. Professor Ligrani, who guided my actions and provided encouragement through good times and bad. Professor Subramanian, whose software expertise and technical knowledge were invaluable, and who was there whenever I needed him. The Mechanical Engineering shop personnel, specifically Tom McCord, Charles Crow and Jim Selby, whose craftsmanship and concern for my work were outstanding. And finally to my family, Rooney, Billy and John, thank-you for providing me with the love and encouragement that sustained my effort until the end.

I. INTRODUCTION

Fully developed laminar channel flow does not maintain a parabolic velocity profile. Centrifugal instabilities in the flow result in counter-rotating vortex pairs, which initially form near the concave surface. The imposition of the centrifugal instabilities begin because centrifugal forces are greater on the fluid particles at the center of the channel than near the walls. Consequently, faster moving particles near the center are forced to move toward the concave surface, displacing the fluid particles located there. These displaced fluid particles move spanwise and then away from the concave surface. The path they follow is then like an arc, as shown in Figures 1 and 2. The resulting counter-rotating vortex pairs are known as Dean vortex pairs.

Even though flows near compressor blades and turbine blades are not channel flows, centrifugal instabilities result in the formation of counter-rotating vortex pairs near concave surfaces in all three situations. Similar effects are also present in combustion chambers, rocket nozzles as well as internal cooling passages of turbine blades. Predicting curved channel flow is an attractive first step in accounting for curvature in the practical environments because channel flow is a much simpler undertaking. Development of means to predict flows near concave surfaces in the practical environments will eventually lead to improved methods of protecting surfaces from exposure to hot gases. This will eventually allow higher inlet temperatures which result in greater efficiencies, improved power-to-weight ratios, and better engineering designs.

A. BACKGROUND

The first analytical study of curved channel ($d \ll r_c$) flow was performed by W.R. Dean [Ref. 1] in 1928. Dean found that the flow becomes unstable due to the effect of concave curvature when small disturbances are present. He also found that the critical

minimum flow velocity at which the small disturbances start to grow occurs when $\bar{U}d/\nu\sqrt{d/r_i}$ is above 36 for a channel with radius ratio near 1.0. This parameter is now known as the Dean number, De , where \bar{U} is the mean velocity in the channel, ν is the kinematic viscosity, d is the spacing between inner and outer walls of the channel, and r_i is the radius of curvature of the inner wall. Reid [Ref. 2] provides additional information on the neutral stability curve. Using a low aspect ratio curved channel, Hawthorne [Ref. 3] describes streamwise velocity distributions which result in curved channel flow. Cheng *et al.* [Ref. 4] show how flow visualization patterns in radial spanwise planes change with aspect ratios, where aspect ratio is varied from 1 to 12. Works by McKee [Ref. 5] and Flentie [Ref. 6] resulted in the first published work on high aspect ratio curved channel flow by Kelleher *et al.* [Ref. 7]. They show how streamwise velocity and Dean vortex pair spacing varies with Dean number. Finlay *et al.* [Refs. 8, 9] present a comprehensive analytical and numerical investigation of Dean vortices in high aspect ratio curved channel flow. Their work predicts two kinds of wavy Dean vortex flows, referred to as undulating Dean vortex flow and twisting Dean vortex flow [Ref. 10]. Experiments by Ligrani and Niver [Ref. 11], Finlay, Ligrani and Bland [Ref. 10], and Alfredsson and Persson [Ref. 12] confirm the presence of these secondary instabilities. Ligrani *et al.* [Refs. 11,13], Niver [Ref 14], Longest [Ref. 15], Ligrani *et al.* [Ref. 16], and Baun [Ref. 17] present additional results from the same curved channel used in the present study which has an aspect ratio of 40 to 1. A recent work by Finlay, Ligrani and Bland [Ref. 10] compares the numerical and experimental results when wavy vortex flow is present. Ligrani and Longest [Ref. 13] describe vortex pair appearance and disappearance events in curved channel flow.

B. OBJECTIVES

The primary objective of the present study is to measure flow characteristics in a curved channel with 40 to 1 aspect ratio at Dean numbers ranging from 35 to 425. A

miniature five-hole probe is used to obtain surveys of a number of time-averaged quantities, including total pressure, streamwise velocity, secondary flow vectors, streamwise vorticity, radial vorticity, and spanwise vorticity. Power spectra of the voltage fluctuations from a hot-wire probe sensing velocity fluctuations are used to show the frequencies of different events in the flow field. Unsteady Dean vortex behavior is illustrated by flow visualization results obtained over radial/spanwise planes at three streamwise locations.

C. ORGANIZATION

Chapter II describes curved channel. Chapter III describes the equipment and procedures used for measurement of pressure and velocity surveys. Chapter IV describes the procedures and equipment used to obtain power spectra. Chapter V gives equipment and procedures used to acquire flow visualization results. Experimental results are presented in Chapter VI. Summary and conclusions are presented in Chapter VII. Appendix A contains all of the figures. Appendix B presents the results of an uncertainty analysis from Baun [Ref. 17]. A software directory of the programs used in this study are presented in Appendix C.

II. CURVED CHANNEL

A. CHANNEL DESCRIPTION

The transparent curved channel is located in the laboratories of the Mechanical Engineering Department at the Naval Postgraduate School. Detailed explanations of the design and construction of the facility are found in Sieband [Ref. 18], Niver [Ref. 14], Ligrani and Niver [Ref. 11], and Baun [Ref. 17]. A schematic illustration [Ref. 14] and photograph [Ref. 18] of the rectangular curved channel are shown in Figures 3 and 4, respectively. The test facility equipment between plenum #1 and the blower exhaust is correctly represented in Figure 3. The photograph, Figure 4, shows a plenum/blower configuration that is no longer used. For the sake of continuity, a brief discussion of the channel is provided below.

The channel is an open circuit suction facility designed for low speed transition studies. Its primary function is in the study of the structural characteristics of the flow e.g., pressure, velocity, vorticity distributions, and flow visualization results. It is transparent because it is constructed of Lexan, a polycarbonate. The lip at the channel inlet is constructed of quarter circumference sections of 15.2 cm outside diameter pipe. To reduce spatial non-uniformities in the flow, an aluminum honeycomb and three fine mesh screens follow. This section is followed by a 20:1 contraction nozzle, whose contour is given by a fifth order polynomial. A photograph of the inlet section and nozzle is seen in Figure 5. The flow is accelerated through the nozzle into a 2.44 m long straight duct. This entry length provides fully developed flow at the inlet side of the curved section for Dean numbers less than 640 [Ref. 18]. The curved test section has an inner to outer radius ratio of 0.979 and turns the flow 180 degrees. The flow then enters another 2.44 m straight section before reaching another honeycomb, screens, and

a diffuser. The diffuser is followed by the outlet and blower plenums. A gate valve and orifice plate are used to control and regulate the flow in the channel, and are mounted between these two plenums on a 5.25 cm ID (2 inch schedule 40) pipe. A low pressure is maintained in the blower plenum by a 250W (one-third horsepower) motor. Rubber mounts and flexible couplings between the plenum and the blower as well as beneath the blower, isolate the channel from mechanical vibration. The side walls, longitudinal and cross beam supports maintain a cross section of 1.27 ± 0.015 cm by 50.8 ± 0.05 cm. [Ref. 16]

Flow properties in a radial/spanwise plane are measured after a miniature five-hole pressure probe is inserted through a slot cut in the curved section. The slot is 0.32 cm wide and 7.62 cm long and is located in the convex wall of the channel. The slot is aligned in the spanwise direction 5.08 cm from the centerline at a streamwise location of $\theta = 120^\circ$. A support block made of Lexan maintains the convex wall structural integrity and minimizes the deflection of the curved wall in the vicinity of the slot. The slot is lined with foam to eliminate air leakage when the pressure probe is inserted. A schematic illustration of the Lexan support block and foam sealing system [Ref. 17] is shown in Figure 6.

B. DEAN NUMBER DETERMINATION

The mass flow rate and Dean number are determined from measurements of the pressure drop across the ASME orifice plate. The pressure drop is measured with a Validyne Model PS309 digital pressure manometer. The signal is collected and processed using a Hewlett-Packard (HP) 3498A extender, HP 3497A data acquisition/control unit and a HP 300 Model 9000 computer. Additional details on the data acquisition system and computer are given in the following chapter.

The pressure drop is used to make a first guess at the Dean number by interpolating pressure drop versus Dean number data from Niver [Ref. 14]. Density is calculated using

the ideal gas law and ambient conditions. The expansion coefficient, Y , is calculated from Holman and Gajda [Ref. 19]. An initial mass flow rate is calculated from the initial estimate of the Dean number and pipe Reynolds number, Re_p . The latter is calculated using:

$$Re_p = \frac{\dot{m}d_p}{\rho v A_p} \quad \{1\}$$

The flow coefficient, K , is found by interpolation from the ASME tables [Ref. 20]. The mass flow rate is then updated using:

$$\dot{m} = KA_{or}Y\sqrt{2\rho\Delta P_{or}} \quad \{2\}$$

Iterations of this procedure are continued until the mass flow rate converges to within one percent of the previous value. A final estimate of the Dean number is then calculated using:

$$De = \left(\frac{\dot{m}}{\rho A_{ch}} \right) \left(\frac{d}{v} \right) \sqrt{\frac{d}{r_i}} \quad \{3\}$$

To set the curved channel up for a run at a particular Dean number, this procedure is implemented using the computer program DEAN15 described in the Appendix C. [Ref. 17]

III. PROCEDURES FOR MEASUREMENT OF PRESSURE AND VELOCITY SURVEYS

A detailed description of the fabrication, use, and calibration of the five-hole pressure probe is given by Ligrani *et al.* [Refs. 13,16, 21]. For completeness in thought and context, portions of these articles are presented below.

A. PROBE DESCRIPTIONS

1. KIEL PROBE

A miniature Kiel probe is used to measure time-averaged total pressure distributions, in a radial/spanwise plane, 120° from the start of curvature for Dean numbers from 50 to 450. This data is taken to qualify flow behavior of the channel after a thorough cleaning and reworking of the inlet apparatus. Secondly, these data are used to validate the performance of the five-hole pressure probe. The diameters of the Kiel probe shield and pressure port are 1.68 mm and 0.4 mm, respectively.

2. FIVE-HOLE PRESSURE PROBE

Two schematic illustrations and a photograph of the miniature five-hole pressure probe [Ref. 17] are shown in Figures 7, 8 and 9, respectively. In each, five tubes are evident such that the central tube is surrounded by four other tubes. The probe tip diameter is 1.38 mm, a value different from Baun [Ref. 17] (1.22 mm) because the probe was reconstructed by fitting a new tip to the original mounting cylinder. The end of each of the surrounding tubes is beveled at a 45° angle with respect to the centerline of the center tube. Each tube is constructed from stainless steel hypodermic tubing with inner and outer diameters of 0.203 mm and 0.406 mm. The five tubes were first joined by spot welds, bent in a 90° turn with a radius of about 1.5 mm and then silver soldered along

their length. Finally, a surface grinder was used to bevel the four outer tubes. This approach is slightly different from the one described by Treaster and Houtz [Ref. 22].

The probe tip extends 5.08 mm (four tip diameters) beyond the bend, as shown in Figure 7. This minimizes the effects of stem flow blockage at the measuring location. Similarly, the tip is 22.9 mm (19 tip diameters) from a 9.53 mm diameter mounting cylinder. This mounting cylinder was sized for easy mounting and handling.

The miniature five-hole pressure probe is designed to minimize the adverse effects of flow blockage and spatial resolution. When the probe is in place for measurements, the mounting cylinder is not exposed to the flow. A five hole rather than a four hole design was chosen because it is easier to calibrate, and because spatial resolution corrections are more readily applied [Ref. 21]. The tip is conical rather than prismatic to minimize flow blockage effects when the probe is near the wall.

B. EXPERIMENTAL DETAILS

Imperial Eastman 22-P-1/8 polyflo tubing is used to connect the pressure probes to the pressure transducers. To avoid pressure oscillations due to gas compressibility and flow passage constriction [Refs. 16,17], the maximum length of tubing used is 18 cm.

For pressure measurements using the Kiel probe, a Celesco Model LCVR variable reluctance differential pressure transducer is used with a full-scale range of 2 cm of water. Each port of the five-hole probe is connected to a Validyne Model DP103-06 variable reluctance differential pressure transducer with a full-scale range of 0.25 cm of water. At Dean numbers greater than 370, pressure ranges exceed those of the Validyne transducers and so, Celesco transducers are used instead. Each transducer signal is sent to a Celesco Model CD01D carrier demodulator, which converts outputs from the transducers to DC voltage signals which are proportional to pressure.

Using the computer program PROCAL, a calibration procedure similar to that described by Baun [Ref. 17] is used, except that a Validyne Model PS309 digital pressure

manometer is used instead of a standard fluid manometer. As expected, the calibration coefficients ($cm H_2O/volt$) of the Celesco transducers are ten times greater than those of the Validyne transducers.

The voltage signals are sent through an HP 3498A extender to an HP 3497A data acquisition control unit. These units then send data signals to the HP 300 Model 9000 computer to be processed and stored. In a procedure similar to that used by Baun [Ref. 17], 50 voltage signals are collected sequentially from each carrier demodulator. The mean and standard deviation of voltages from each channel are calculated. Sampling continues until 50 continuous samples from a particular channel are within 2.5 standard deviations of the previously calculated mean value.

C. PROBE CALIBRATION PROCEDURES AND RESULTS

The miniature five-hole probe is calibrated using procedures closely resembling those used by Baun [Ref. 17]. This is accomplished in an open circuit, subsonic wind tunnel illustrated in Figure 11. Manufactured by AEROLAB, the tunnel is located in the same Mechanical Engineering Laboratory as the curved channel. The calibration sled, shown in Figure 10, is mounted on the top of the walls of the test section. Before calibration begins, the probe is positioned in the flow using the sled so that yaw angle is zero. The computer program ORIENT is used to aid this procedure. The probe is considered to be at zero pitch angle when positioned vertically in the calibration sled. Calibration is undertaken using twenty-five angle combinations, i.e., five yaw angles at each of five pitch angles. For each angle combination, yaw, pitch, total, and total minus static pressure coefficients are calculated using equations given by [Refs. 16,17]:

$$C_{py} = (P_2 - P_3)/(P_1 - \bar{P}) \quad \{4\}$$

$$C_{pp} = (P_4 - P_5)/(P_1 - \bar{P}) \quad \{5\}$$

$$C_{pt} = (P_t - \bar{P}) / (P_1 - \bar{P}) \quad \{6\}$$

$$C_{pts} = (P_t - P_s) / (P_1 - \bar{P}) \quad \{7\}$$

and

$$C_{ps} = (P_1 - P_s) / (P_1 - \bar{P}) \quad \{8\}$$

Probe calibration results which correspond to a mean velocity of 3.9 m/s are presented in Figures 13 through 17. Figure 13 shows increasing values of C_{py} with increasing yaw angle, with $C_{py} = 0$ for zero yaw and pitch angles. Figure 14 shows C_{pp} increasing with increasing pitch angle, but shows $C_{py} = -0.25$ at zero pitch angle for all values of yaw angle. In Figure 15, C_{pt} , and in Figure 16, C_{pts} , both show a dependence on yaw angle at a given pitch angle. Figure 17 shows C_{pt} increasing slightly with pitch angle.

D. CURVED CHANNEL MEASUREMENT PROCEDURES

1. TRAVERSING MECHANISM

The probe is held in place within the channel using a mount which allows initial yaw angles and pitch angles to be adjusted within $\pm 0.1^\circ$ and $\pm 0.5^\circ$, respectively. This mount is attached to a travelling block whose position is controlled by an automated two-dimensional traversing mechanism [Ref 17]. A photograph [Ref. 17] of this equipment is seen in Figure 12. The block is moved using two leadscrews with a pitch of 1.27 mm (0.05 inch). A Superior Electric Type M092-FD-310 stepping/synchronous motor rotates each leadscrew. These motors are controlled by a Superior Electric MITAS Type PMS085-C2AR controller and a Superior Electric MITAS Type PMS085-D050 drive. These equipment direct the probe movement as directed by the HP 300 Model 9000 computer.

2. MEASUREMENT PROCEDURE

The probe is initially placed in the mount with the travelling block as close to the channel curved surface as possible. The probe is manually oriented so that it barely touches the concave wall. The probe mount is tightened and the probe is moved precisely to a radial location of $y/d = 0.5$ by the MITAS controller. The computer program ALIGN is then used to align the probe to zero yaw and pitch angles. When the probe is properly aligned with zero yaw angle and zero pitch angle, the pressure readings on opposing ports (i.e., 2 and 3, 4 and 5) are equal. Fine adjustments to probe orientation are accomplished by a specialized mount (seen in Figure 12), designed by Baun [Ref. 17].

Data collection begins with the probe 0.127 cm from the concave wall at the first spanwise position. The probe moves toward the convex wall as measurements are made. To move to the next spanwise position, the probe is moved 0.254 cm in the spanwise direction, then 0.127 cm in the reverse spanwise direction and finally toward the concave wall until it is 0.127 cm away. This positioning procedure is used to reduce the effects of leadscrew backlash and ensure repeatable data regardless of the direction of spanwise probe movement.[Ref. 17]

At each probe position in the channel, 100 pressures are sampled per pressure port, at a frequency of about five Hz. After the probe has moved to the next location, measurements are delayed ten seconds to avoid sampling when unsteadiness caused by probe movement is present in the flow. A full survey of pressure measurements using the five-hole probe requires about eight hours. Because the Kiel probe involves measurements of only one port, the elapsed time is much less. The entire traversing operation is computer controlled and performed late at night to minimize channel inlet disturbances caused by any sort of motion in the building.

3. DATA REDUCTION

Procedures similar to described used by Ligrani *et al.* [Refs. 16,21] are used for processing of data. The first step involves correcting pressures to account for spatial resolution effects using procedures described in [Ref. 21]. $C_{p'}$ and $C_{p''}$ are then determined using the same procedures described in [Ref. 16], except for the preliminary pitch calculation. For this, the following equation is employed:

$$p' = 8.458(C_{pp} + 0.2568) - p_{off} \quad \{9\}$$

p_{off} is zero for the five-hole probe arrangement used in this present study. After the yaw and pitch angles are known, a double interpolation procedure is employed to compute $C_{p''}$ and $C_{p'}$. Total velocity and three velocity components are then calculated. The final phase involves adjustments made to account for pressure and velocity gradients measured in the three-dimensional flow field [Ref. 21].

Using finite difference equations, distributions of the three components of mean velocity determine the three components of mean vorticity. Secondary flow vector magnitudes are used to calculate streamwise, radial and spanwise vorticity, using the following equations [Ref. 10]:

$$\omega_{\theta} = \frac{\partial U_r}{\partial z} - \frac{\partial U_z}{\partial r} \quad \{10\}$$

$$\omega_r = -\frac{\partial U_{\theta}}{\partial z} \quad \{11\}$$

$$\omega_z = \frac{U_{\theta}}{r} + \frac{\partial U_{\theta}}{\partial r} \quad \{12\}$$

U_θ , U_r and U_z represent the streamwise, radial and spanwise components of velocity. The streamwise derivatives are neglected for the determination of ω_r and ω_z . The first term in equation {12}, U_θ/r , is included in the determination of spanwise vorticity but was neglected in the study by Baun [Ref. 17].

IV. POWER SPECTRA PROCEDURES AND EQUIPMENT

Hot-wire anemometers are widely used for measurement of instantaneous velocity components in turbulent gas flows. Their operation relies on the fact that the electrical resistance of a metal conductor is a function of its temperature [Ref. 23]. The sensing element of a hot-wire probe is a very small diameter wire, usually made of platinum and/or tungsten. As such, the wire has high spatial resolution and provides little interference to flow. Hot-wire sensors are heated by electric current, where the amount of heat loss to the gas flow is directly related to the flow velocity. This relationship is determined by calibration [Ref. 24].

In this study, the hot-wire is used in the constant-temperature (or constant-resistance) mode of operation. As such, the hot-wire sensor forms one leg of a Wheatstone bridge. During operation, this bridge circuit is balanced with the hot-wire exposed to a zero-velocity flow field, and the resistance required to balance the bridge is the *cold* resistance. When the hot-wire is operated at elevated temperatures, its resistance is the *hot* resistance, determined by multiplying the cold resistance and the *overheat ratio*. Standard values of the overheat ratio range from 1.2 to 1.8. When hot-wire sensors are exposed to fluctuating velocities, a variable current feedback amplifier maintains the balance of the bridge, as well as the sensor resistance, by passing different levels of current to heat or cool the wire so that the average temperature along its length is maintained constant. The voltage required to keep the sensor resistance constant is then used as a measure of flow velocity fluctuations in the vicinity of the sensor.

The widespread use of hot-wire anemometry systems is due to several advantages. First, the small dimensions of the sensor provide very little flow blockage and alteration. Secondly, electronic system response is almost instantaneous and rapid fluctuations in

velocity components can be recorded with minimal electronic distortion. Third, system sensitivity is such that detection of fluctuations of only a few percent of the mean velocity can be recorded. Finally, electrical output of a hot-wire anemometer can be readily processed by both digital and analog systems.[Ref. 23]

A. HOT-WIRE PROBE

A DANTEC Type 55PO1, conventional hot-wire probe is used for the present study. The sensing wire is fabricated of platinum plated tungsten wire, five microns in diameter with a sensitive wire length of 1.25 mm. The wire is oriented so as to be sensitive to both the streamwise and spanwise velocity components. The probe is held in place by a DANTEC probe mount which is attached to a plug in the channel side wall. The location of the probe in the channel is $\theta=112^\circ$, $y/d=0.5$ with a spanwise location of 9.84 cm (3.875 in) or 10.16 cm (4.0 in) from the channel side wall. A photograph of the mounted hot-wire sensor is given in Figure 77.

B. SIGNAL MEASUREMENT

During measurements, the hot-wire probe is connected to a DANTEC 55M01 Standard Bridge using a five meter coaxial cable. The system is operated in the constant-temperature mode with an overheat ratio of 1.8, bridge gain of 3.0, and an HF FILTER setting of 2.0. The output signal from the DANTEC Bridge is passed through a DANTEC Model 56N20 Signal Conditioner, which filters and amplifies the voltage signal before it is sent to the signal analyzer and a B/K Precision Model 1476A 10 MHz oscilloscope. The high-pass filter of the signal conditioner is set at 0.1 Hz to remove the DC signal. To prevent aliasing, the low-pass filter is set at 0.1 or 0.3 kHz, depending on the frequency range being investigated. The gain setting is 100.

C. SIGNAL PROCESSING AND ANALYSIS

An HP 3562A Signal Analyzer is used to obtain spectra of signals from the hot-wire anemometer. The HP 3562A is a dynamic, dual-channel fast Fourier transformed (FFT) based analyzer with a 26.5 μ Hz-to-100 kHz frequency range and a 150 dB measurement range. The nominal maximum sampling rate for all channels is 256 kHz. A schematic diagram of the measurement process [Ref. 25] is given in Figure 78, and is also described below.

The analog to digital conversion (ADC) portion of the analyzer works in two steps. First, it *takes a picture* of the signal at one point in time. Second, this analog sample is converted to 14-bit digital words in a time record which is 2048 samples long. The measurement stage then begins after the analog signal is converted to digital data and properly scaled. In this part of the measurement process, data are filtered to an appropriate frequency span. Windowing is then performed using software and two specialized processors. The fast Fourier transform is subsequently implemented to convert the time varying signal to a frequency varying one. Next, the floating point processor (FPP) then provides the computational power necessary for averaging and calculating measurement displays. Signal averaging concludes the measurement portion, and the display portion begins.

The vector display used in the HP 3562A employs 1601 display points, so data must be compressed or expanded to fit on the display, as appropriate. With the display, the input data (view input), filtered input data (filtered input), or output data (measurement) may be presented. Input data are ones extracted at the output of the HP 3562A analog-to-digital converter, which have not been through the digital filter or measurement process. Filtered input data displays show input signals after they have been digitally filtered. Displays of output data show results after signals are filtered and processed according to settings selected by the user. [Ref. 26]

One channel is employed in the present study. The analyzer is used in the power spectrum mode of display with the trigger set to *free run*. A Hanning data window (Hann window) is utilized to attenuate the input signal at both ends of the record, forcing the signal to appear periodic. Time Averaging Off is selected so that the analyzer makes continual measurements with one average, erasing the result of each previous measurement. Time traces of the input signal are taken from the filtered input displays and are plotted in terms of volts versus seconds. Power spectra, taken from the measurement displays, are plotted with axes of (Volts^2/Hz) versus Hz. Typical settings of the HP 3562A Signal Analyzer used in this study are presented in Figure 79. A photograph showing the electronic components used to obtain the power spectra is given in Figure 80.

V. FLOW VISUALIZATION APPARATUS AND PROCEDURE

The apparatus used for flow visualization are now described, including the smoke generator, camera, lighting system, video recorder, video printer, and video monitor.

A. SMOKE GENERATOR

The smoke generator, which was first used by Morrison [Ref. 27], is shown schematically in Figure 96 [Ref. 28]. It consists of five main components: combustion chamber, reaction vessel, condensers, moisture separators, and smoke rake. Combustion takes place inside a 40.64 cm long, 6.27 cm inside diameter (2.5 inch schedule 40) steel pipe. Inside this chamber, smoke is produced from a mixture of hickory and mesquite wood chips, mixed in approximately equal amounts. The wood is initially ignited by passing current through a coil of several strands of 0.03175 cm (0.0125 in) diameter nickel-chromium wire, which is located beneath the wood chips, as compressed air at a pressure of 2-8 psig is passed through the pipe and between the wood chips. Different flow rates of smoke are produced by regulating the pressure level, and hence, the air supply to the combustion pipe. At the exit of the pipe, the smoke flows into a 1500 ml Pyrex reaction vessel where some unwanted combustion particles are removed. Next, it flows through two 44.5 cm Pyrex coiled Graham condensers where the smoke is cooled to temperatures near ambient. Two moisture separators, arranged in series, follow the condenser and allow additional moisture to be removed from the smoke. Each moisture separator consists of a cylindrical cavity 13.34 cm long and 11.43 cm in diameter, with loosely packed aluminum wool to increase the mass transfer surface area. These separators are connected to 1.22 cm inside diameter rubber tubing which carries the smoke to a manifold and rake located at the inlet of the curved channel. The rake contains nine

0.34 cm inside diameter tubes connected to the manifold which has an inside diameter of 2.24 cm.

B. CAMERA AND LIGHTING

A Smith-Victor 710-SG photographic floodlight is used to illuminate the smoke as flow visualization experiments are conducted. It is positioned so that light is directed radially outward toward the convex side of the curved channel. To prevent the Lexan of the curved section from deforming due to heat from the floodlight (it is rated at 600W), 2.54 cm thick, foam insulating material is placed along the outside of the convex wall.

A Dage-MTI CCD-72 Series Video Camera with an AMPEX Vidicon, 1:1.4 $f=25$ mm lens is used to photograph the flow patterns formed by the smoke. The camera head is connected to a control unit by means of a cable assembly. The camera is solid state and utilizes a high resolution CCD (Close Coupled Device) imager and high performance analog processor to provide an excellent combination of precision and flexibility. The camera head is quite small measuring 3.05 cm by 4.32 cm by 12.2 cm long and weighs 180 grams. The Camera Control Unit (CCU) has an IR cut filter and optical low-pass filter to minimize aliasing, and provides controls for gain and black level adjustment. An illustration of these controls on the front panel of the CCU are evident in Figure 97. Also apparent are the means to adjust bandwidth control, enhancement control, polarity reversal, gray scale stretch, and gamma settings. A test signal is also available to allow adjustment of the contrast of the image on a monitor [Ref. 29]. During this study, the gain is set at 4.62, the black level is set at 8.88, and the polarity switch is set to the positive position. Because the gain control is used in manual, the gray scale stretch feature is not used. For optimum sharpness with minimum noise, the bandwidth and edge enhancement settings are 2/3 of the maximum setting, and the gamma correction is set at 0.70.

A schematic showing the camera and lighting setup is presented in Figure 95 [Ref. 17]. With this arrangement, photographs of smoke patterns in radial/spanwise planes are taken at three locations on the curved section: $\theta = 40^\circ$, 80° , and 120° .

C. VIDEO RECORDER, PRINTER AND MONITOR

In order to obtain time histories of flow patterns, the CCU is connected to a Panasonic AG-1960 S-VHS video cassette recorder, which operates in the Super-VHS format, using a TDK XP-ST120 videotape. 7 cm by 10 cm hard copies of the individual images from the video are produced using a Mitsubishi P65U Video Copy Processor (VCP). The VCP allows the user to control contrast, print orientation, and scan type, as well as black and white levels, picture sharpness, gain and filter levels. In this study, the contrast and print orientation switches are set to normal. Scan selection is set to the field mode to best capture the rapidly varying flow phenomena. The black and white levels are varied to compensate for lighting differences due to smoke density. The sharpness, gain and filter selection are set to off. Print size and position may also be controlled using an additional menu. Here, the standard (default) settings for print size and position are utilized.

The video image is monitored during taping and playback on an Dage-MTI HR 1000 monitor. It provides 1000 TV lines of resolution on a 30.5 cm (12 inch) flat face, cathode ray tube (CRT) display. The monitor offers selectable underscan, variable video enhance, switchable 110/120 VAC operation, and brightness and contrast controls. The monitor is operated at 110 VAC with normal underscan and the enhancement, brightness and contrast controls turned fully clockwise. The Panasonic VCR allows the videotape to be viewed one field (1/60 second) at a time.

VI. EXPERIMENTAL RESULTS

This section presents surveys of measured total pressure, mean velocity, vortex circulation, mean vorticity and power spectra, as measured in a radial/spanwise plane located 120° from the start of curvature for Dean numbers from 35 to 450. Flow visualization results are also given for Dean numbers ranging from 50 to 425, and streamwise locations of 40° , 80° , and 120° . Data are collected at a total of 320 locations in the $\theta = 120^\circ$ radial/spanwise plane using a grid with eight radial (y/d) locations and 40 spanwise (z/d) locations. The spanwise locations are referenced to the channel centerline, increasing from $z/d = 4$ to $z/d = 8$ and spanning 5.08 cm. The Kiel probe and five-hole pressure probe are used to make pressure measurements. Pressure measurements obtained with the five-hole probe are used to determine the components of velocity. The components of vorticity are determined from these velocity components.

Power spectra results are collected at $\theta = 112^\circ$, $y/d = 0.5$ and spanwise locations of 9.84 cm or 10.16 cm from the channel side wall, which correspond to $z/d = 12.25$ and $z/d = 12.0$.

Flow visualization results are collected at two spanwise locations (labeled *inside* and *outside*) at $\theta = 40^\circ$. *Inside* refers to a portion of the radial/spanwise plane which extends from $z/d = 3.94$ to $z/d = 7.87$. *Outside* refers to a portion of the radial/spanwise plane which extends from $z/d = 12.99$ to $z/d = 16.93$. Each photograph in a particular sequence shows the concave surface at the bottom and the convex surface at the top. The time interval between individual photographs in different sequences vary from 1/15 second to 1/60 second.

A. SURVEYS OF TIME-AVERAGED QUANTITIES

Time-averaged results are presented in Figures 18 through 76. Of these, total pressure results from the Kiel probe are presented in Figures 18 through 35. Total pressure results from the five-hole probe are presented in Figures 36 through 40. Streamwise velocity contours are presented in Figures 41 through 44. Plots of velocity vectors in the curved channel flow are presented in Figures 45 through 47. Velocity perturbation contours are presented in Figures 48 through 51. Streamwise vorticity results are presented in Figures 52 through 58. Streamwise circulation results are presented in Figures 59 through 61. Radial vorticity results are presented in Figures 62 through 68. Spanwise vorticity results are lastly presented in Figures 69 through 76.

1. TOTAL PRESSURE AND STREAMWISE VELOCITY

Total pressure measurement results obtained using the Kiel probe are presented in Figures 18 through 35. These contour plots closely resemble results obtained with the five-hole pressure probe. Figure 35 shows linear increases of maximum and minimum values of total pressure with Dean number.

Total pressure and streamwise velocity measurement results obtained using the miniature five-hole pressure probe are given in Figures 36 through 44. Figure 40 shows a nearly linear increase of five-hole total pressure measurements with increasing Dean number. *Maximum* and *minimum* refer to the maximum and minimum pressure differences recorded for each Dean number. A comparison of the total pressure and streamwise velocity results indicates them to be qualitatively very similar for all Dean numbers investigated. Areas of low total pressure and low streamwise velocity develop near the concave wall as the Dean number increases from 35.03 to 61.92. Secondary flows generally move from the concave wall to the convex wall within these regions, which are present between pairs of counter-rotating vortices. They are referred to as upwash regions [Refs. 11,16], where upwash refers to the direction of flow with respect

to the concave surface. Plots of secondary flow velocity vectors which illustrate these upwash regions are presented for Dean numbers of 86.69, 99.90, 149.8 in Figures 45 through 47. At least three upwash regions are apparent in all three figures. As the Dean number increases above 149.8, Figures 36 through 43 show that the distance between the middle and right upwash regions decreases. At $De = 187.7$, only two upwash regions are evident. Further increases in Dean number (Figures 39 and 44) result in a spanwise uniform flow. Flow visualization from the present study as well as from Ligrani and Niver [Ref. 11], show that vortex pairs exist at these higher Dean numbers, but are not apparent in time-averaged measurements because of considerable vortex motion in the radial and spanwise directions [Ref. 17].

2. VELOCITY PERTURBATION

At small values of Dean number, the fluid motion in the curved channel is streamwise with no secondary flows. The velocity profile is nearly parabolic with a maximum which is shifted slightly closer to one wall (the concave surface) compared to flow in a straight channel. This is called *curved channel Poiseuille flow* (CCPF) [Refs. 8,9]. To show mean velocity deviations from CCPF, values of CCPF are subtracted from the measured streamwise velocity. This difference is then normalized using the bulk mean velocity, \bar{U} , for each Dean number studied to give the normalized velocity perturbation. Normalized velocity perturbation contours are presented in Figures 48 through 51. Figure 48 shows that the flow changes from a nearly spanwise uniform one to one with spanwise periodic perturbations as the Dean number increases from 35 to about 100. The most significant negative velocity perturbations occur at the same z/d locations as the upwash regions. Figures 50 and 51 show that the flow becomes spanwise uniform as the Dean number becomes greater than 250.

3. VORTICITY COMPONENTS

The three components of vorticity are determined from the three components of velocity using the computer program VORT!CITY, which implements equations {10},{11}, and {12} from Chapter III. Figures 52 through 76 present the results of these calculations along with circulation magnitudes determined from the streamwise component of vorticity. The contour plots of this section show positive vorticity as continuous lines, and negative vorticity as dashed lines. In the radial/spanwise plane with the flow directed away from the observer, positive streamwise vorticity is counterclockwise and negative streamwise vorticity is clockwise. Graphs showing the variation of vorticity with Dean number for each of three vortex pairs apparent in the contour plots (left, middle, and right), appear at the end of the group of plots for that particular vorticity component. The minimum value of negative vorticity is presented as an absolute value on these plots.

a. STREAMWISE VORTICITY

Streamwise vorticity results are shown in Figures 52 through 58. Figure 52 shows that the flow does not display spanwise periodic areas of positive and negative vorticity across the span of the measurement plane for Dean numbers less than 86.69. At $De = 99.9$, the three regions containing both positive and negative vorticity are apparent. Each area of positive and negative vorticity evidences a pair of counter-rotating vortices, or a *vortex pair*. As the Dean number increases, vorticity magnitudes in the pairs increase. The areas between the positive and negative vorticity regions in each pair are centered at the same z/d locations as the upwash regions. Figures 53 and 54 show that three pairs are replaced by two pairs as the Dean number increases from 149.8 to 175.5. $De = 175.5$ results show a small region of negative vorticity located at $y/d = 0.2, z/d = 6.3$ which is very close to a region of negative vorticity of a vortex pair located on the right-hand side of the measurement plane. These two areas of negative

vorticity are replaced by one large region at $De = 187.7$ (Figure 54), which is centered at $y/d = 0.4, z/d = 6.8$. As these events occur, the spanwise locations of pairs also change somewhat with time.

As the Dean number becomes greater than 250, areas of positive and negative vorticity are less apparent on the plots. The contour plots then show spanwise uniform time-averaged distributions of streamwise vorticity. Figures 56 through 58 show how the peak streamwise vorticity varies with Dean number. Plots are given for all three vortex pairs apparent in the contour plots. These are denoted as left, middle and right pairs according to their positions. Peak vorticity levels then generally increase with Dean number for all three cases.

b. STREAMWISE CIRCULATION

Circulation values of streamwise vorticity, Γ_x , are determined using the computer program CIRC1. This is done by summing the values of vorticity over a specified region, and then multiplying this result by the area corresponding to individual values of vorticity. Summing values of positive vorticity gives positive streamwise circulation and summing values of negative vorticity gives negative circulation. Figures 59 through 61 present values of positive and negative streamwise circulation versus Dean number. Figure 59 values are given for the left vortex pair and show a general increase with Dean number up to 138.7. Above $De = 138.7$, the positive circulation decreases and then increases, while the negative circulation continues to increase as the Dean number increases further. Figure 60 shows an increase of both positive and negative circulation for the middle vortex pair with Dean number for values up to 127.4. At greater Dean numbers, values of positive and negative circulation tend to decrease. Values of positive and negative circulation for the right vortex pair in Figure 61 both generally increase with Dean number for the entire range of values shown.

c. RADIAL VORTICITY

Radial vorticity distributions are presented in Figures 62 through 68. Spanwise periodicity is evident in results presented in Figures 62 and 63 for Dean numbers ranging from 73.63 to 226.8. At Dean numbers greater than 250.3, the time-averaged flow is spanwise uniform. Figures 66 through 68 show the variation of peak radial vorticity with Dean number for the left, middle and right vortex pairs. For all three situations, the values of positive and negative vorticity generally increase until $De = 149.8$, and then tend to decrease as the Dean number increases further.

d. SPANWISE VORTICITY

Spanwise vorticity distributions are given in figures 69 through 76. Results in Figure 69 for Dean numbers of 35.03 and 51.36 show a flow field which is nearly spanwise uniform. As the Dean number increases, some portions of the contours of positive spanwise vorticity move toward the concave wall, while contours of negative spanwise vorticity move toward the convex wall. In Figure 73, the data of Figures 71 and 72 are given in profile form. The time-averaged flow field becomes spanwise uniform for values of Dean number greater than 250.3. Figures 74 through 76 show the variation of peak spanwise vorticity with Dean number. In all three figures, positive and negative vorticity values increase approximately linearly with Dean number for the left, middle, and right pairs for the ranges of values shown.

B. SPECTRA OF HOT-WIRE SIGNAL MEASUREMENTS

Spectral results are presented in Figures 81 through 94. The streamwise and radial locations of the probe for all measurements are $\theta = 112^\circ$ and $y/d = 0.5$, respectively. The spanwise location for Figures 81 through 84 is 9.84 cm (3.875 in) from the channel wall or $z/d = 12.25$. The spanwise location for Figures 85 through 94 is 10.16 cm (4.0 in) from the channel wall or $z/d = 12.0$.

Figure 81 shows that the highest energy level for $De = 40.3$ is measured at 0.5-2.0 Hz. At this Dean number, four other broad spectral peaks also exist at 5-6 Hz, 7-9 Hz, 12-15 Hz and 17-19 Hz. As the Dean number increases up to 60.0, these peaks continue to be present as overall energy levels of the spectra increase. At $De = 135.2$, the highest energy level is measured at about 6 Hz. Only two other broad spectral peaks exist at 1-2 Hz and 12-14 Hz. At $De = 145.3$, individual broad peaks are not so apparent. The time traces in Figure 82 show that the dominant frequency increases from about 1.5 Hz (3 cycles/2 sec) for $De = 40.3$ to 5.5 Hz (11 cycles/2 sec) for $De = 135.2$.

Figure 83 shows that the highest energy level is measured at 5-6 Hz for $De = 140.6$. Two peaks at 1.5-2.0 Hz and 11-12 Hz are similar to the ones seen in Figure 81. Figure 83 also show large broad spectral peaks at 60-100 Hz for Dean number from 140.6 to 155.4. This results because of twisting Dean vortex flow, described by Finlay *et al.* [Refs. 9,10]. Figure 84 presents the time traces associated with the previous figure. Here, peak-to-peak amplitudes increase with Dean number.

Figure 85 shows a spectral survey for Dean numbers from 50.5 to 435.0. Individual spectra that make up this figure are also given in Figures 86 through 94. At $De = 50.5$, $De = 100.3$, and $De = 150.1$, a spectral peak at 60 Hz is present which is due to electronic noise. Figure 88 for $De = 150.1$ again shows a spectral peak at 80 Hz due to the presence of twisting Dean vortex flow.

C. FLOW VISUALIZATION

Flow visualization results are presented in Figures 98 through 126. Table I gives Dean numbers and streamwise locations for the different figures. Flow visualization results are given for $\theta = 40^\circ$, 80° , and 120° . Two portions of the radial/spanwise (*inside* and *outside*) are used. *Inside* refers to a radial/spanwise plane which extends from $z/d = 3.94$ to $z/d = 7.87$. *Outside* refers to a radial/spanwise plane which extends from $z/d = 12.99$ to $z/d = 16.93$. Time increases in each figure according to the frame numbers

to the left of each photograph. Each photograph shows a view with the concave surface on the bottom and the convex surface on the top.

Table 1. DEAN NUMBER AND LOCATION OF FLOW VISUALIZATION SEQUENCES

DEAN NUMBER	40° (inside)	40° (outside)	80° (inside)	120° (inside)
50	Figure 98	Figure 107		Figure 119
75				Figure 120
100	Figure 99	Figure 108		Figure 123
125				Figure 124
150	Figure 100	Figure 109		Figure 125
200	Figure 101	Figure 110	Figure 116	Figure 126
250	Figure 102	Figure 111	Figure 117	
300	Figure 103	Figure 112	Figure 118	
350	Figure 104	Figure 113		
400	Figure 105	Figure 114		
450	Figure 106	Figure 115		

Photographic sequences of results obtained at $\theta = 40^\circ(\text{inside})$ are now presented in Figures 98 through 106. Figure 98 ($De = 50.9$) shows evidence of flow in the spanwise direction. Dean vortex formation is not present as expected from the time-averaged contour plots. Figure 99 ($De = 100.1$) shows vortex pairs emerging from flow near the concave wall and disappearing into flow near the concave wall. Frames 7-17, 20-23, and 31-33 show spanwise flow above the vortex pairs. Figure 100 ($De = 150.7$) shows additional vortex pairs emerging from flow near the concave wall. Spanwise flow is clearly visible in frames 10-17. Figure 101 ($De = 200.5$) also shows a vortex pair emerging from flow near the concave wall in frames 3-5, and spanwise directed flow in frames 1-6. Frames 8-15 briefly show a spanwise periodic flow. Figure 102 ($De = 250.8$) shows the disappearance of a vortex pair due to its engulfment into the upwash of an adjacent

vortex pair in frames 22-32. Figure 103 ($De = 300.3$) shows a rocking motion of the vortex pairs. The poorly defined vortex pair in the middle of frame 1 moves slightly left, then right and then back to the left. It is more clearly evident in frame 30. Figure 104 ($De = 350.3$) also shows this rocking motion. A vortex disappearance event is evident in frames 3-9. Here, two vortex pairs are present near the middle of frame 3, one slightly right and one slightly left. The positive vortex of the pair to the right then merges with the negative vortex of the pair to the left. Frame 9 then shows the outline of a single vortex pair which replaces the two pairs present previously. Figure 105 ($De = 400.4$) shows vortex movement which is too rapid for the video camera to capture without blurriness. Here the image is focused but appears slightly blurry. This blurriness also results because smoke particles do not follow all of the higher frequency vortex motions (i.e., twisting or turbulence). Figure 106 ($De = 425.0$) shows a higher degree of the chaotic vortex motion than seen at $De = 400.4$. A variety of appearance and disappearance events are evident along with other complex vortex motions.

Photographic sequences of results obtained at $\theta = 40^\circ$ (*outside*) are now presented in Figures 107 through 115. Figure 107 ($De = 50.9$) shows approximately two cycles of spanwise flow where one cycle consists of flow from left to right and then back again. Figure 108 ($De = 100.0$) shows spanwise flow along with vortex pair formation. Frames 22-34 show a vortex pair forming to the left of the spanwise midpoint of the photographs. Figure 109 ($De = 150.5$) shows a more or less fully developed pairs as well as a vortex pair emerging from flow near the concave wall. The lifetime (over 2 seconds) of the more developed pair is unusually long for this Dean number. Typically, such pairs are present for less than one second. Figure 110 ($De = 200.3$) shows a rocking motion of the vortex pairs. Frames 7-15 show the emergence of a vortex pair from flow near the concave wall. Figure 111 ($De = 250.6$) also shows a rocking motion of the vortex pairs, as well as the disappearance (frames 3-14) of the vortex pair initially located in the

middle of frame 1. Figure 112 ($De = 300.7$) shows vortex formation as well as spanwise flow. Frames 14-19 show spanwise flow around the exterior of a vortex pair. Figure 113 ($De = 350.7$) shows a vortex pair forming between two existing vortex pairs. The outline of this newly formed vortex pair is particularly evident in frames 31-34. Figure 114 ($De = 400.9$) shows vortex pair formation along with a violent rocking motion in images which are somewhat blurred. Figure 115 ($De = 425.3$) shows vortex pair formation which is again present with fairly violent rocking motion.

Photographic sequences of results obtained at $\theta = 80^\circ$ (*inside*) are now presented in Figures 116 through 118. Figure 116 ($De = 200.4$) shows two interesting flow events. Frames 1-12 show one vortex pair splitting to form two vortex pairs. The outline of the initial single vortex pair is visible in frame 1. In frame 8, a downwash region is seen as a bright line at the spanwise centerline of the photograph, extending the full channel height. The downwash region is clearly visible in frame 12. The second flow event of interest is evident in frames 41-51, which show two adjacent vortex pairs joining to form one vortex pair. One vortex pair is located at the middle of frame 41, the other one is slightly to the left, and the upwash regions for each of the two vortex pairs are tilted toward each other. In frame 46 the two upwash regions are close enough to combine, resulting in one single vortex pair in frame 51. Figure 117 ($De = 250.3$) shows violent rocking of vortex pairs. In frames 6-11, the spanwise movement of the vortex pairs is so rapid that the images become blurry. Figure 118 ($De = 300.3$) shows similar behavior except that images are even more blurry.

Photographic sequences of results obtained at $\theta = 120^\circ$ (*inside*) are now presented by referring to photographic sequences presented in Figures 119 through 126. Figure 119 ($De = 50.9$) shows the formation of a vortex pair as it slowly drifts to the right. Frame 13 shows initial formation, just to the right of the spanwise centerline of the photograph. Figures 120 through 122 are photographic sequences of flows at

$De = 75.5$. Figure 120 shows two vortex pairs merging into one pair as the result of cancellation of individual vortices having opposite signs [Ref. 13]. Figure 121 shows two vortex pairs combining in frames 6-13 as a result of vortex pair engulfment [Ref. 13]. Frames 17-20 then show a new vortex pair emerging from flow near the concave wall. Frames 22-28 show that this newly formed pair then combines with the vortex pair directly to the left, also because of pair engulfment. Figure 122 shows a vortex pair disappearing into flow near the concave wall [Ref. 13]. Figures 123 ($De = 100.6$) and 124 ($De = 125.5$) show a gentle rocking of vortex pairs, while Figure 125 ($De = 150.5$) shows rocking vortex pairs which is higher in amplitude. Figure 126 ($De = 200.8$) show the emergence and disappearance of a vortex pair, which is located at the spanwise middle of the photograph in frame 8.

VII. SUMMARY AND CONCLUSIONS

A transparent curved channel with a 40 to 1 aspect ratio was utilized to study the structural characteristics of Dean vortices at Dean numbers from 35 to 400.

Mean velocity components and vorticity components are determined from time-averaged total pressure measurements measured using a miniature five-hole probe at a streamwise location of $\theta = 120^\circ$. At low Dean numbers, ($De = 35.03$ to $De = 61.92$), these results show flow which is spanwise uniform. As the Dean number increases, evidence of vortex pairs is apparent in flow which appears spanwise periodic. The time-averaged flow becomes less spanwise periodic and more spanwise uniform as Dean numbers become greater than 250.

Power spectra of voltage fluctuations from a hot-wire probe sensing velocity fluctuations were obtained at a streamwise location of $\theta = 112^\circ$. Twisting Dean vortex flow is evidenced by spectral peaks measured for $De = 140.6$ to $De = 155.4$. The frequency of the principal spectral peak increases from about 70 Hz to 85 Hz as the Dean number increases over this range.

Flow visualization results for streamwise locations of $\theta = 40^\circ$, 80° , and 120° , show a variety of unsteady Dean vortex pair behavior, including, spanwise directed flow, vortex pair appearance, vortex pair disappearance, vortex pair merging, and vortex pair rocking. Spanwise flow is evident for $De = 50$ and $De = 100$ for a streamwise location of $\theta = 40^\circ$. Vortex appearance and disappearance events are also apparent, becoming more so at this location as the Dean number increases. Results at $\theta = 80^\circ$ for $De = 200$ to $De = 300$ show vortex pairs with rocking motion. At $\theta = 120^\circ$, appearance and disappearance events are evident for Dean numbers of 50.9 to 200.8, and vortex pairs show rocking motion for Dean numbers of 100.6 to 150.5. As the streamwise location changes

from $\theta = 40^\circ$ to $\theta = 120^\circ$, appearance events, disappearance events, and vortex pair rocking occur at decreased Dean numbers.

APPENDIX A. FIGURES

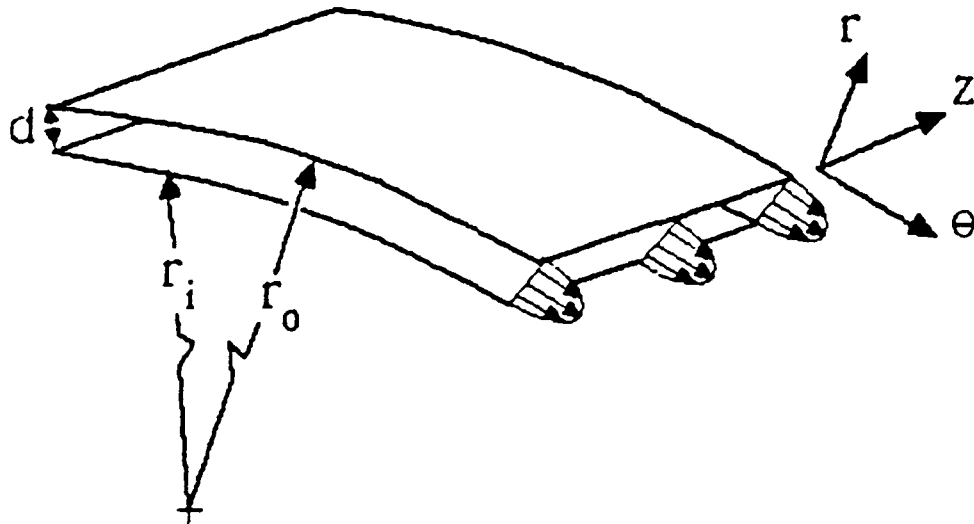


Figure 1. Curved Channel Geometry

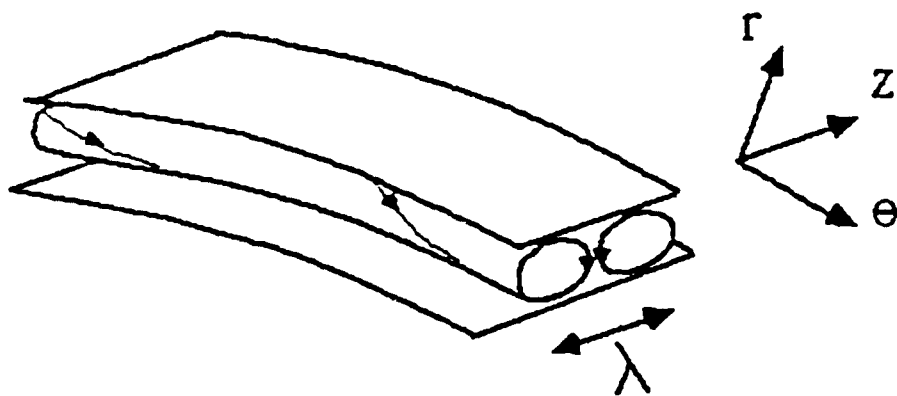


Figure 2. Schematic of One Dean Vortex Pair

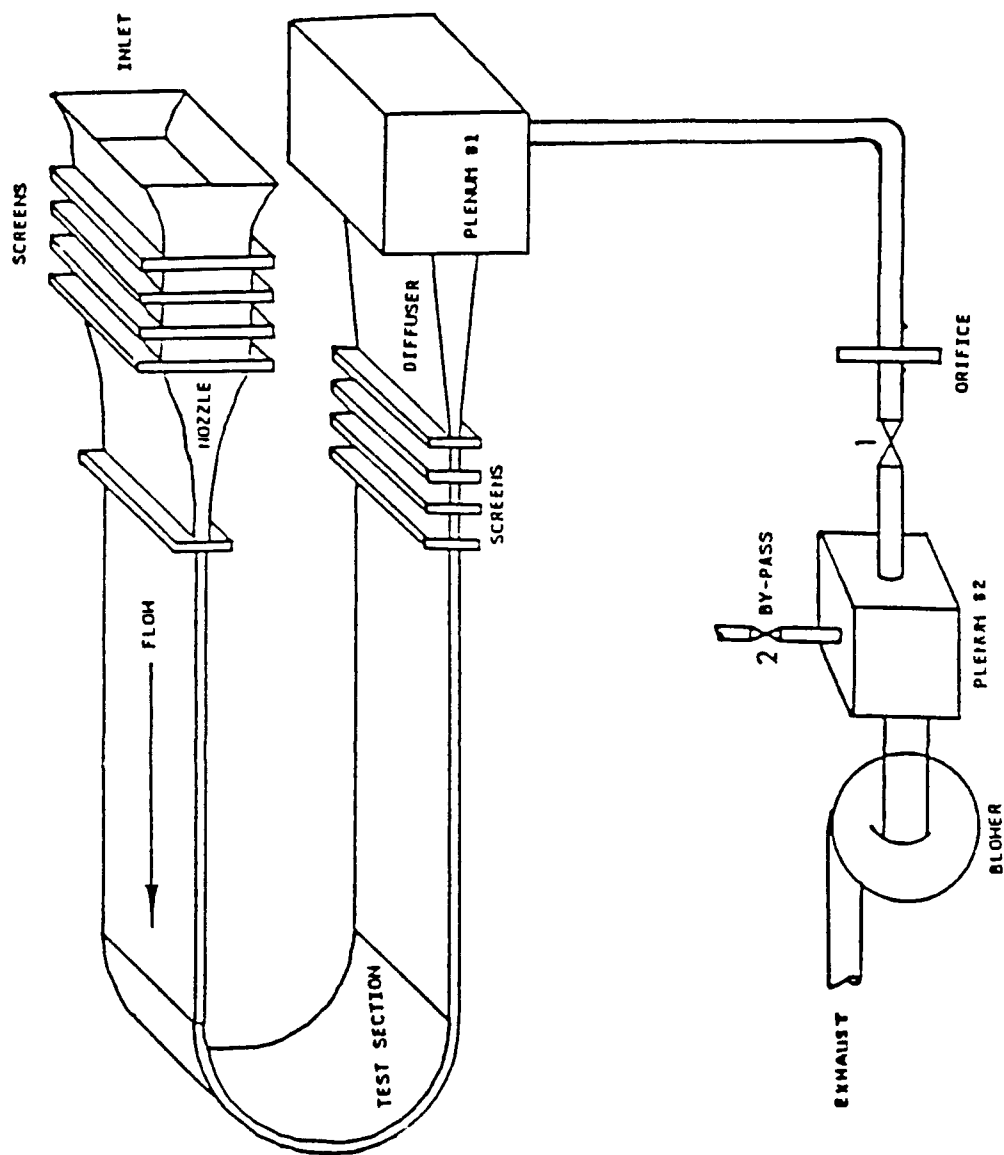


Figure 3. Schematic of Test Facility

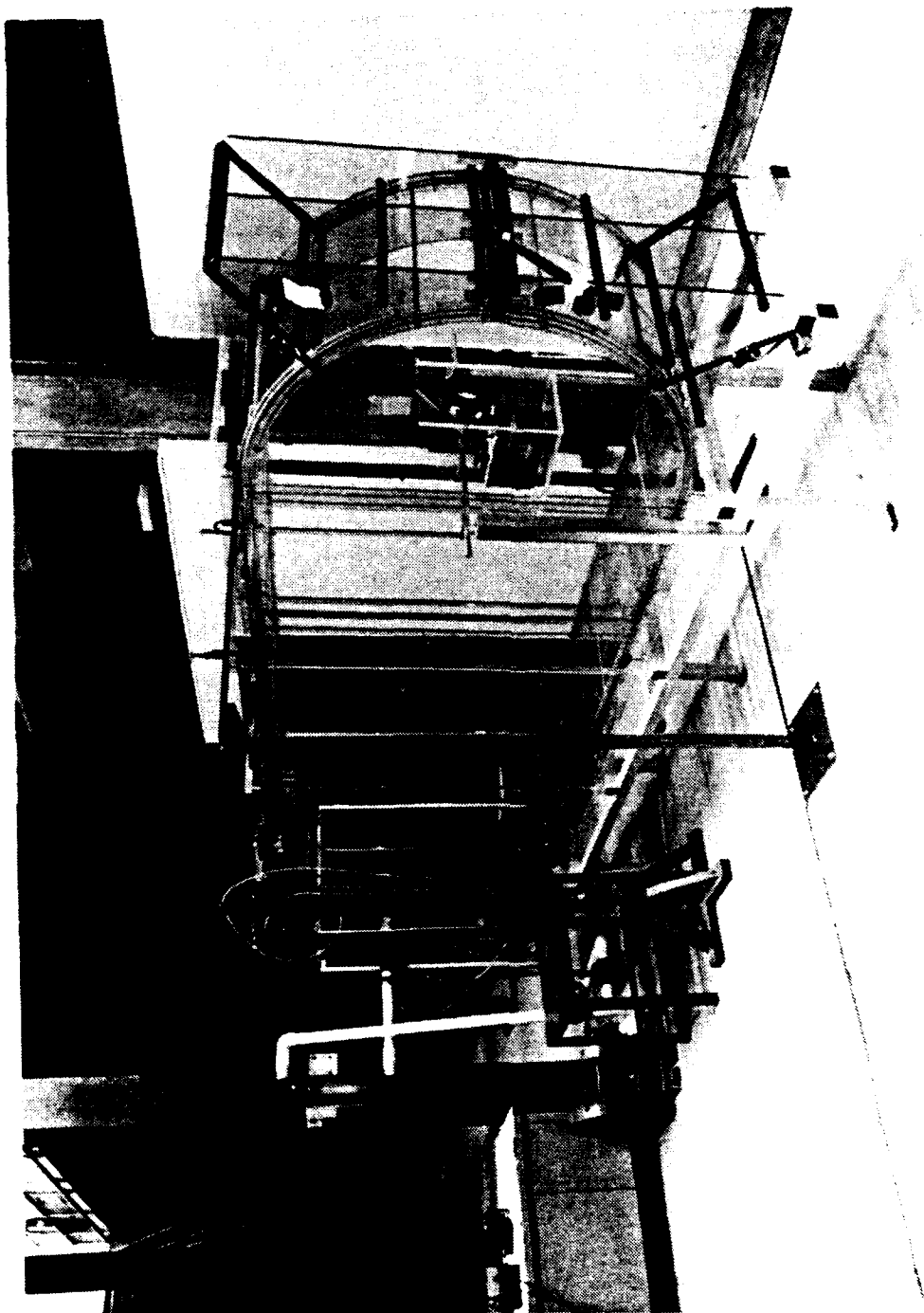


Figure 4. Test Facility (Side View)

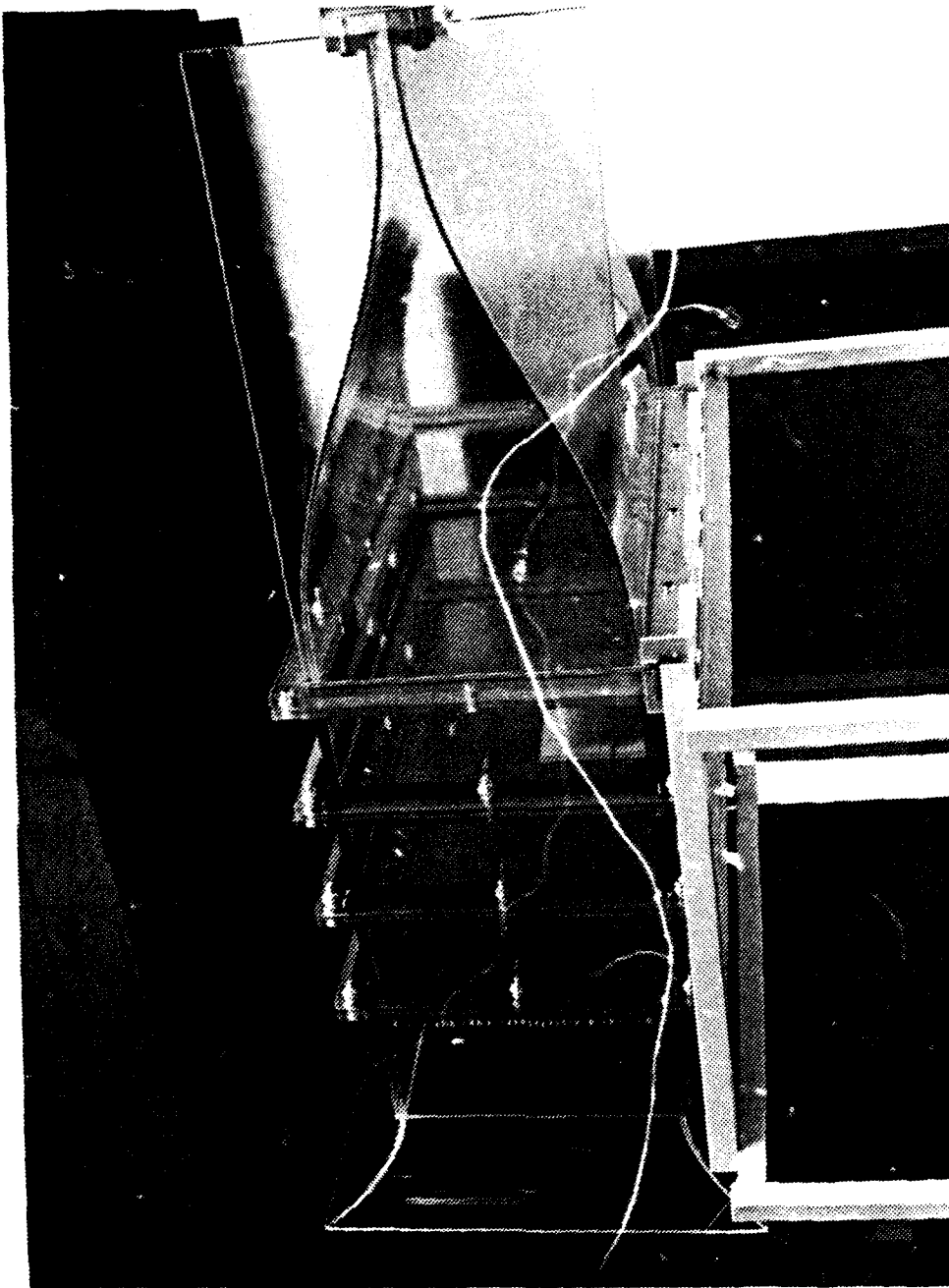


Figure 5. Channel Inlet and Nozzle

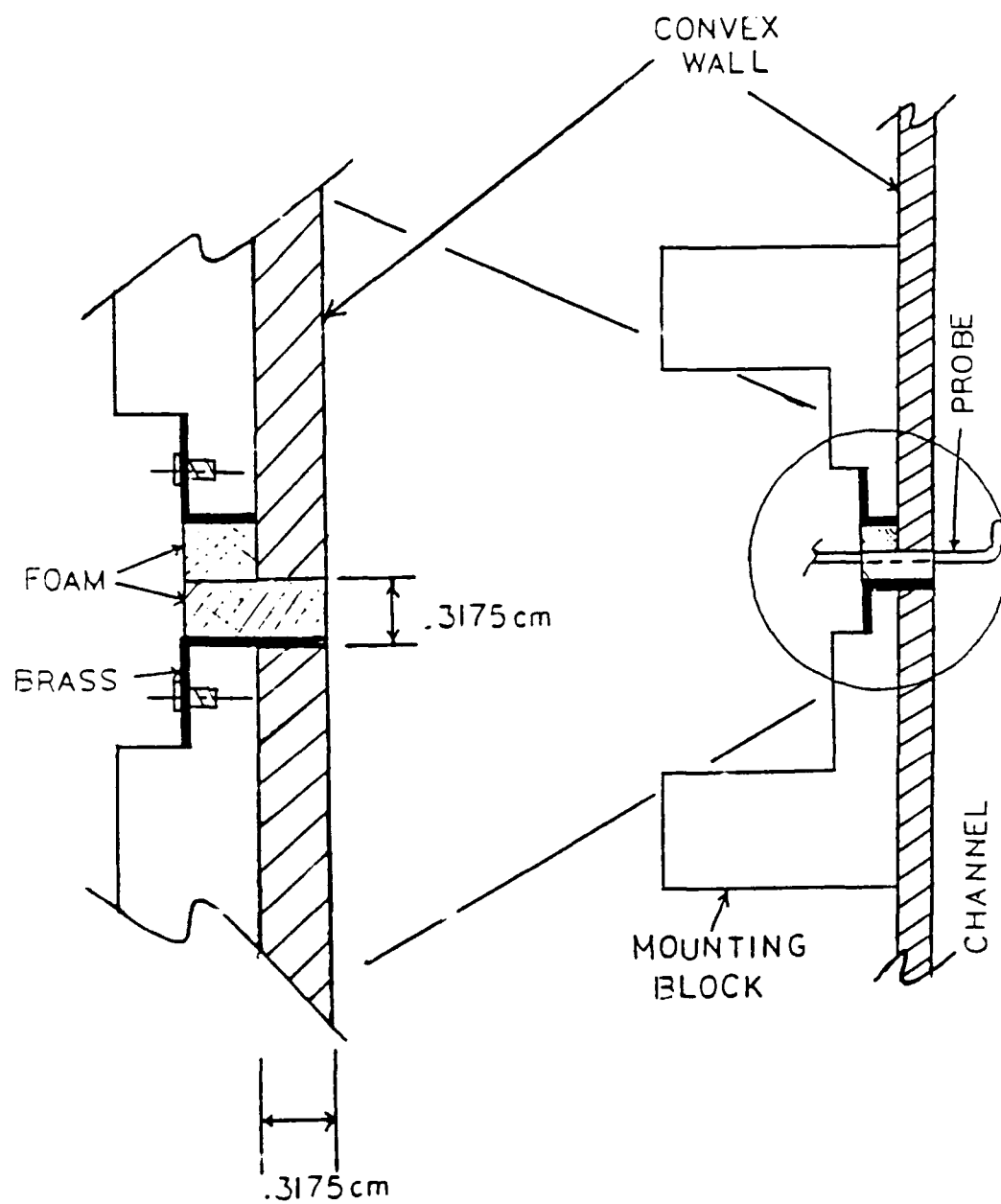


Figure 6. Schematic of Support Block

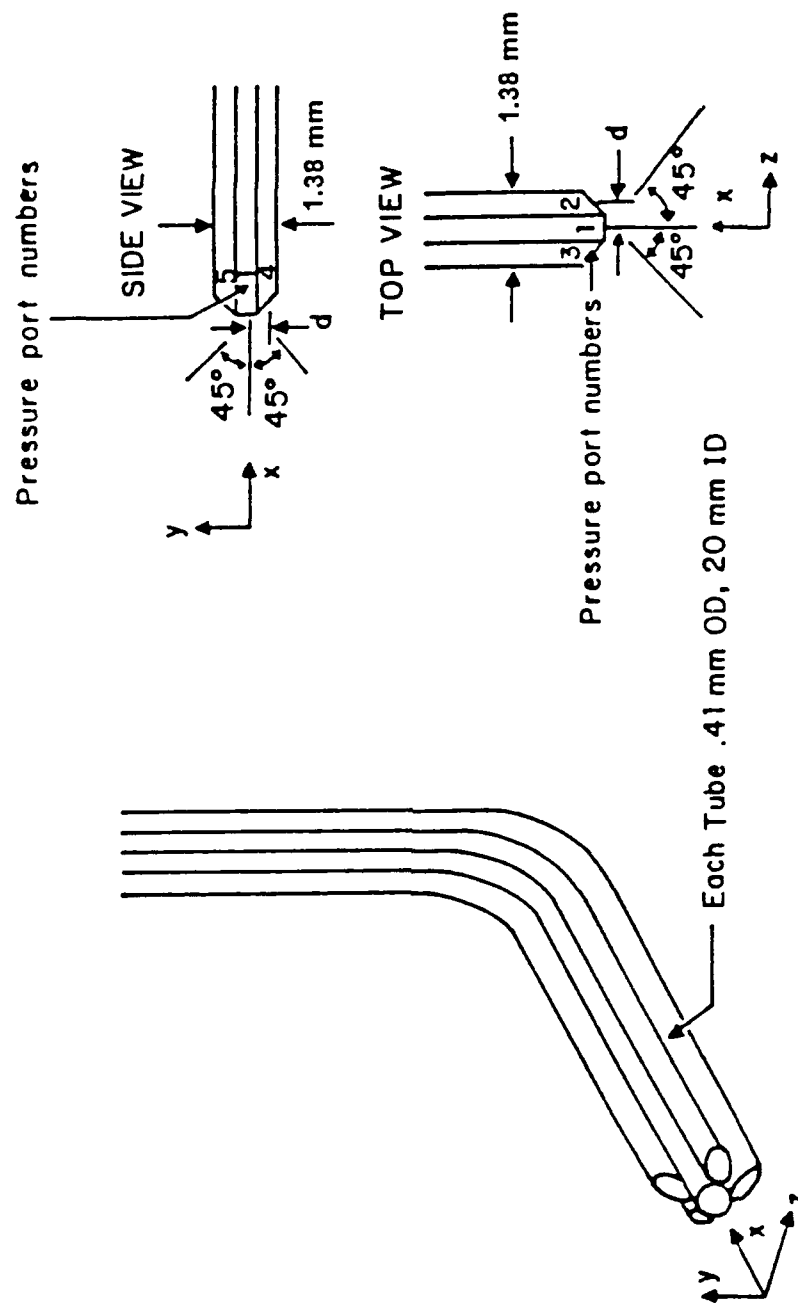


Figure 7. Five-Hole Pressure Probe Geometry

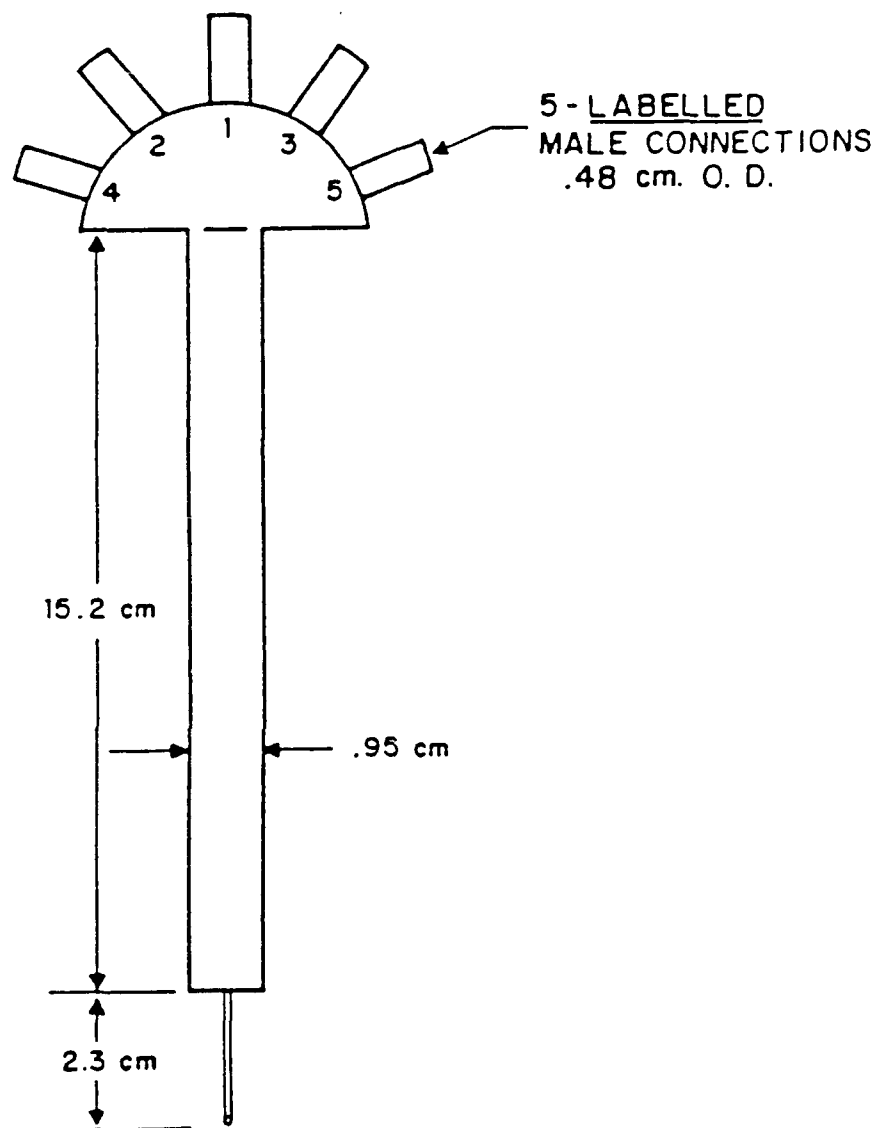


Figure 8. Five-Hole Pressure Probe

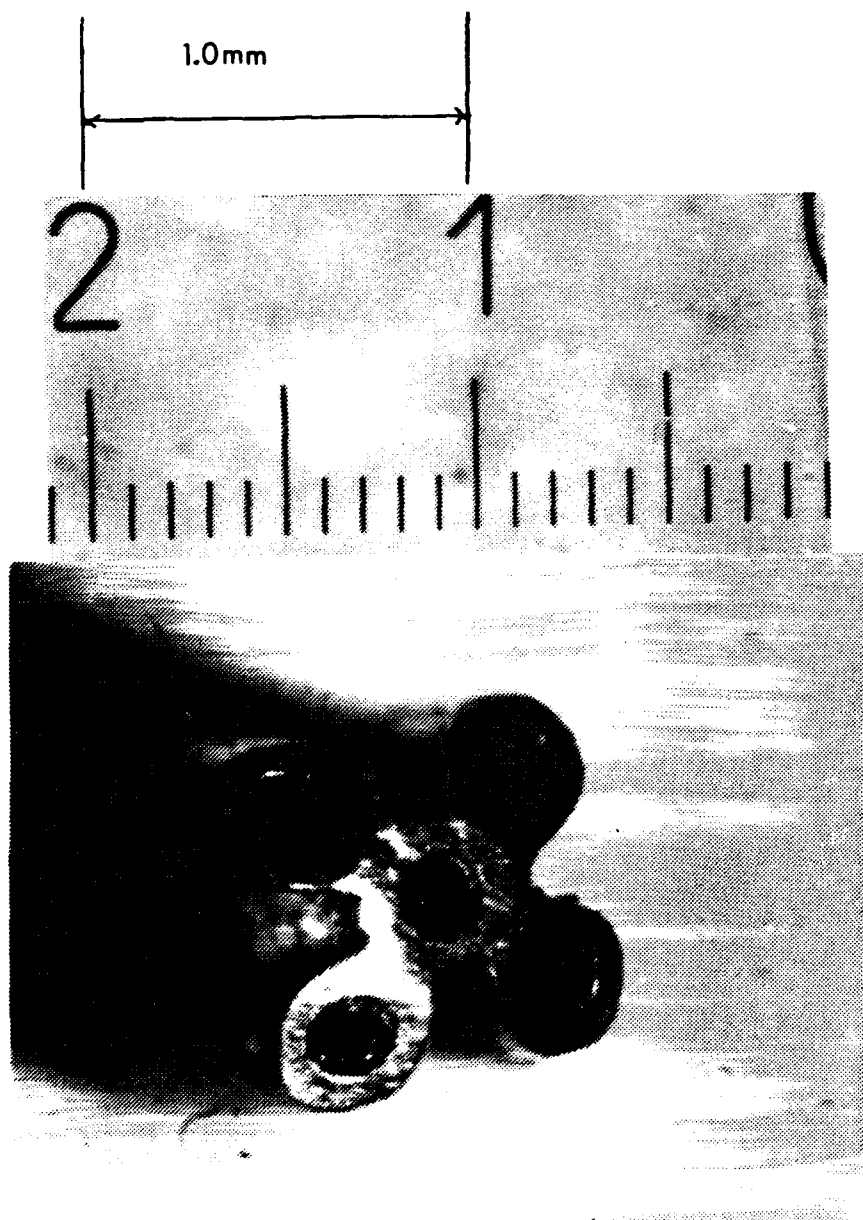


Figure 9. Five-Hole Pressure Probe (100μ between scale markings)

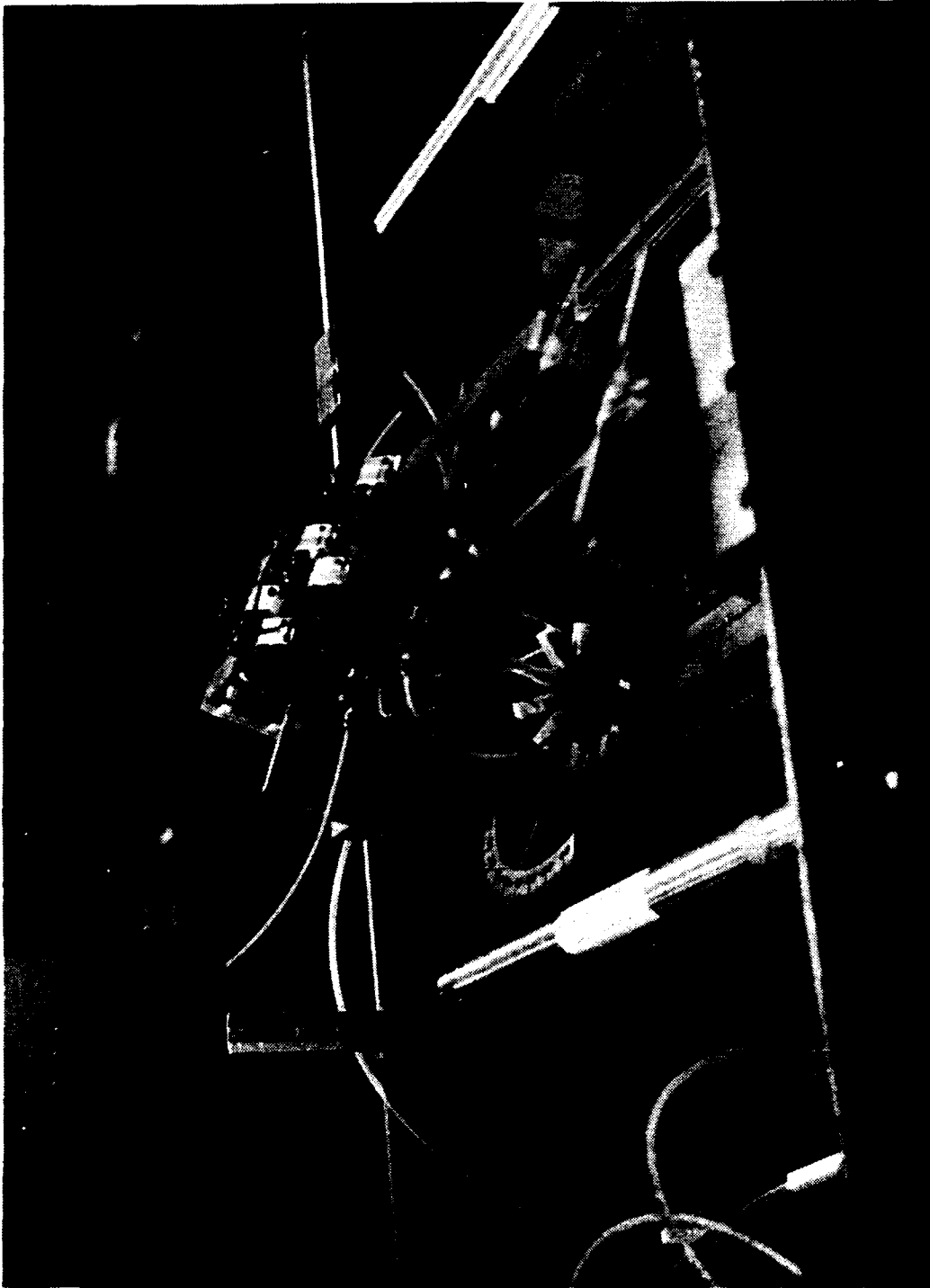


Figure 10. Pressure Probe Calibration Sled

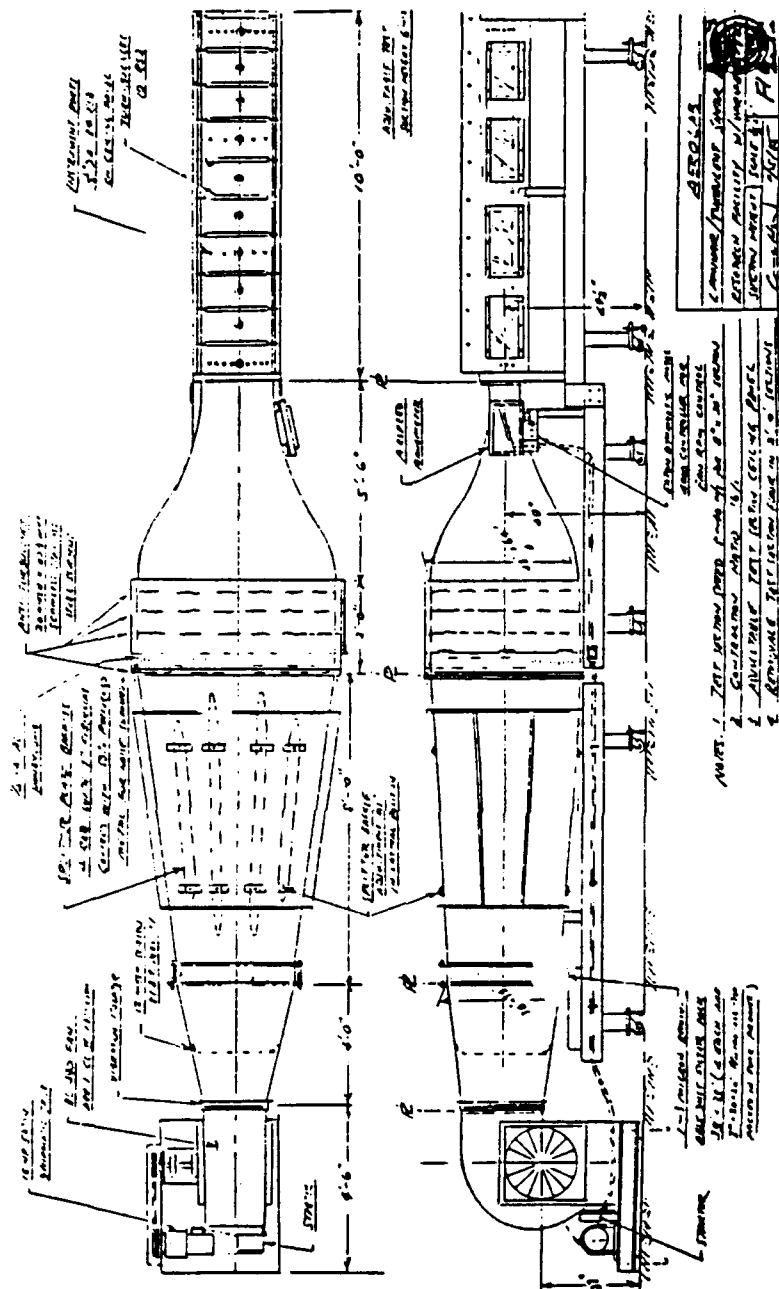


Figure 11. Wind Tunnel Used For Probe Calibration

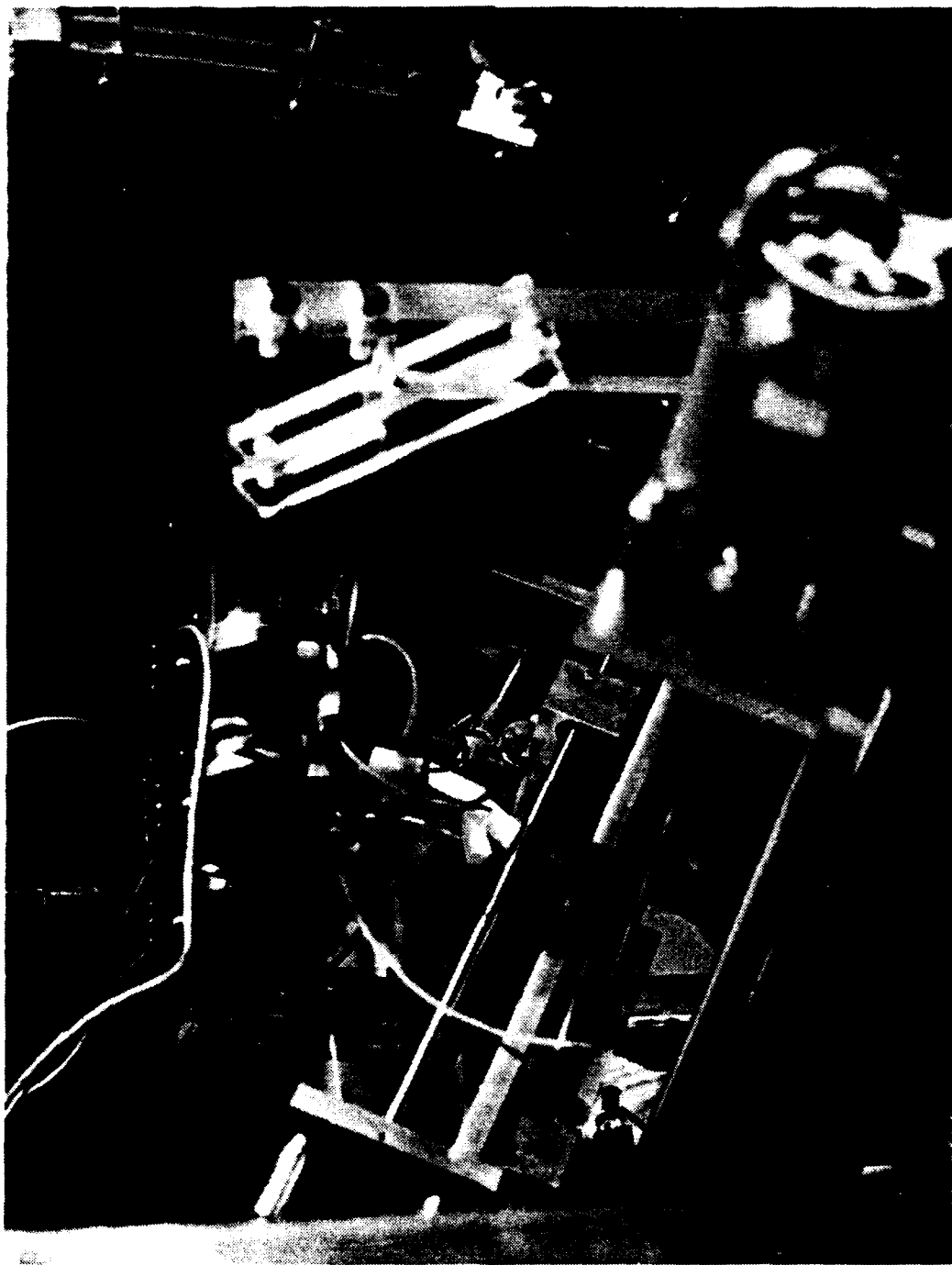


Figure 12. Curved Channel Traversing Mechanism, Transducers, Probe and Mount

FIVE-HOLE PRESSURE PROBE

(CALIBRATION PLOT)

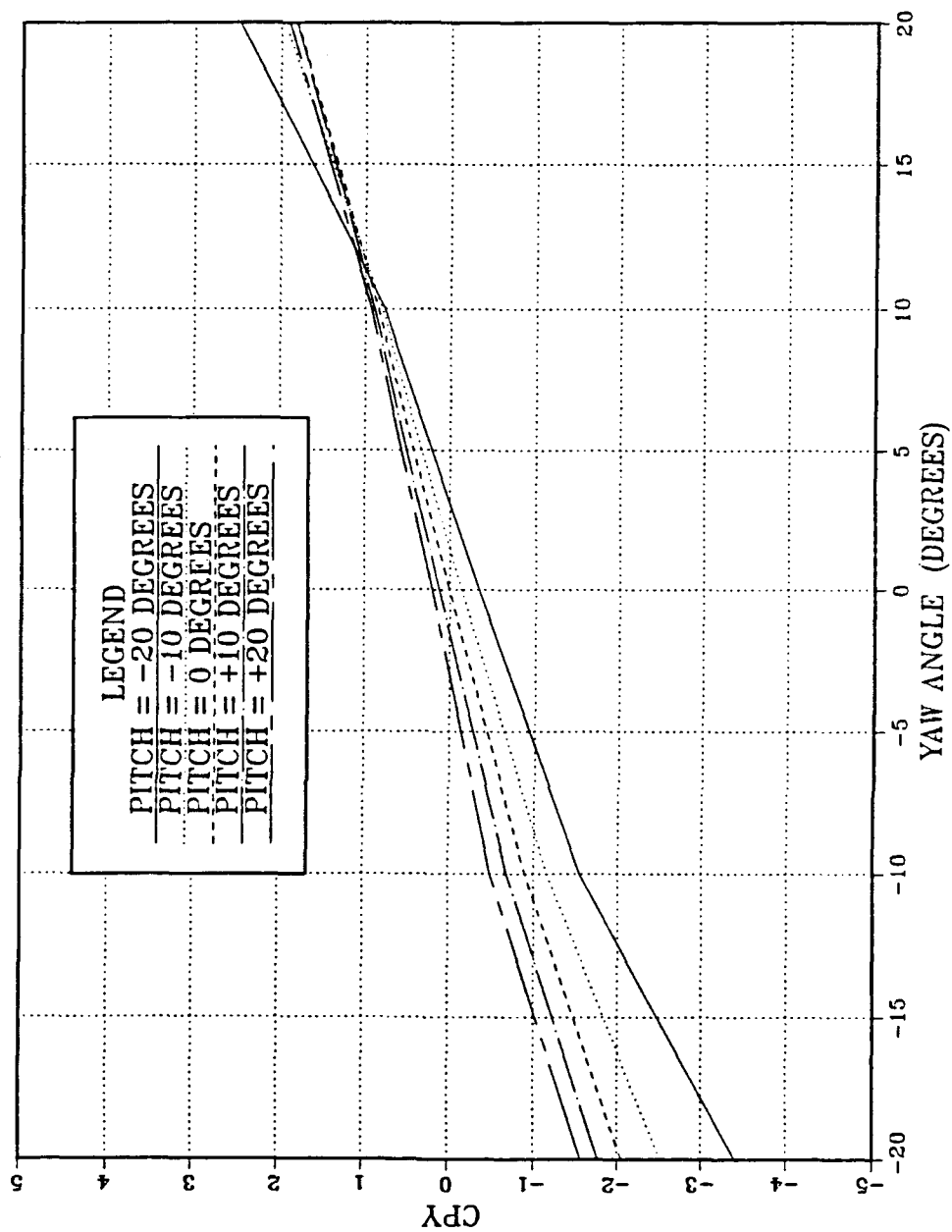


Figure 13. C_{py} vs. Yaw Angle, 3.9 m/s

FIVE-HOLE PRESSURE PROBE

(CALIBRATION PLOT)

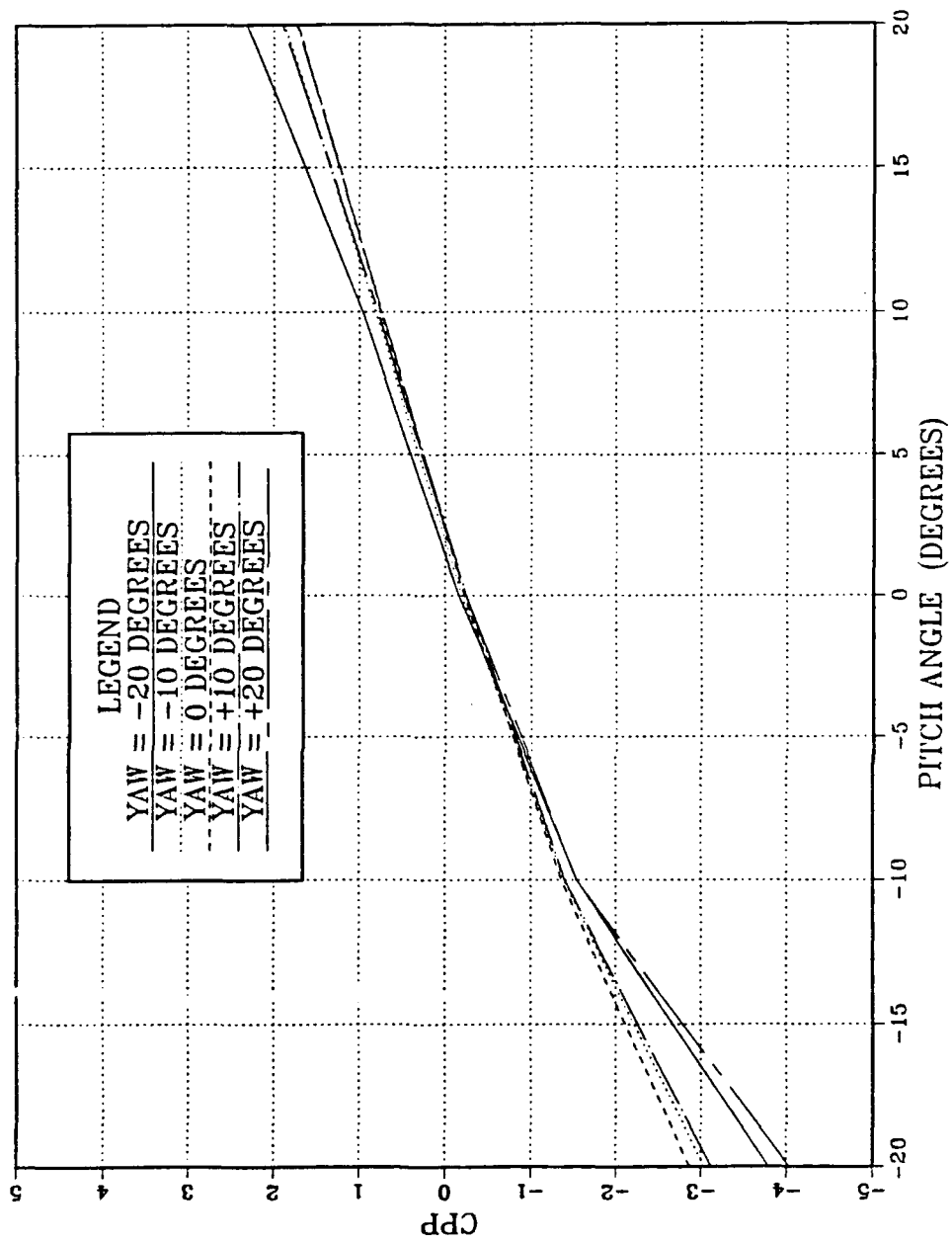


Figure 14. C_{pp} vs. Pitch Angle, 3.9 m/s

FIVE-HOLE PRESSURE PROBE

(CALIBRATION PLOT)

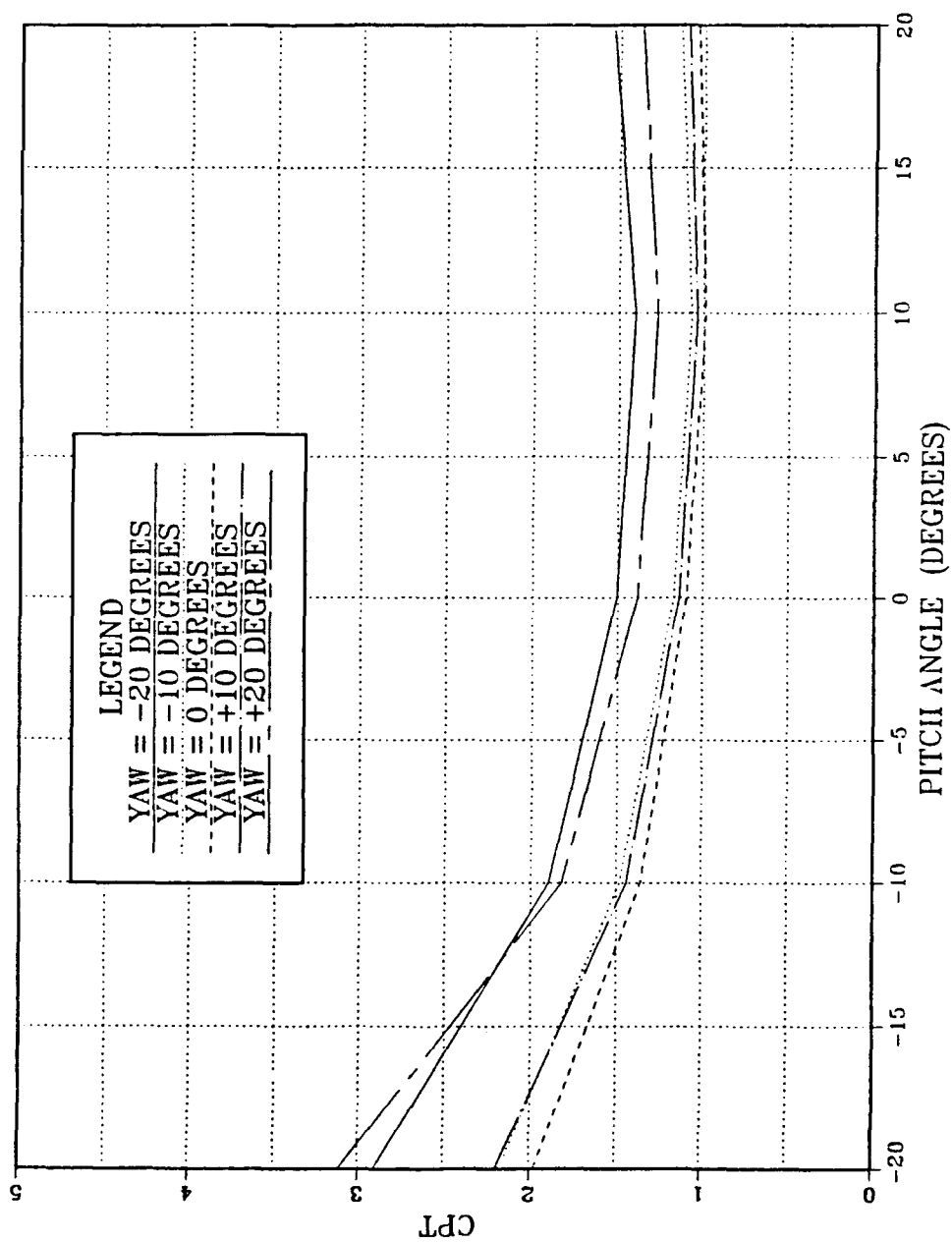


Figure 15. $C_{p'}$ vs. Pitch Angle, 3.9 m/s

FIVE-HOLE PRESSURE PROBE

(CALIBRATION PLOT)

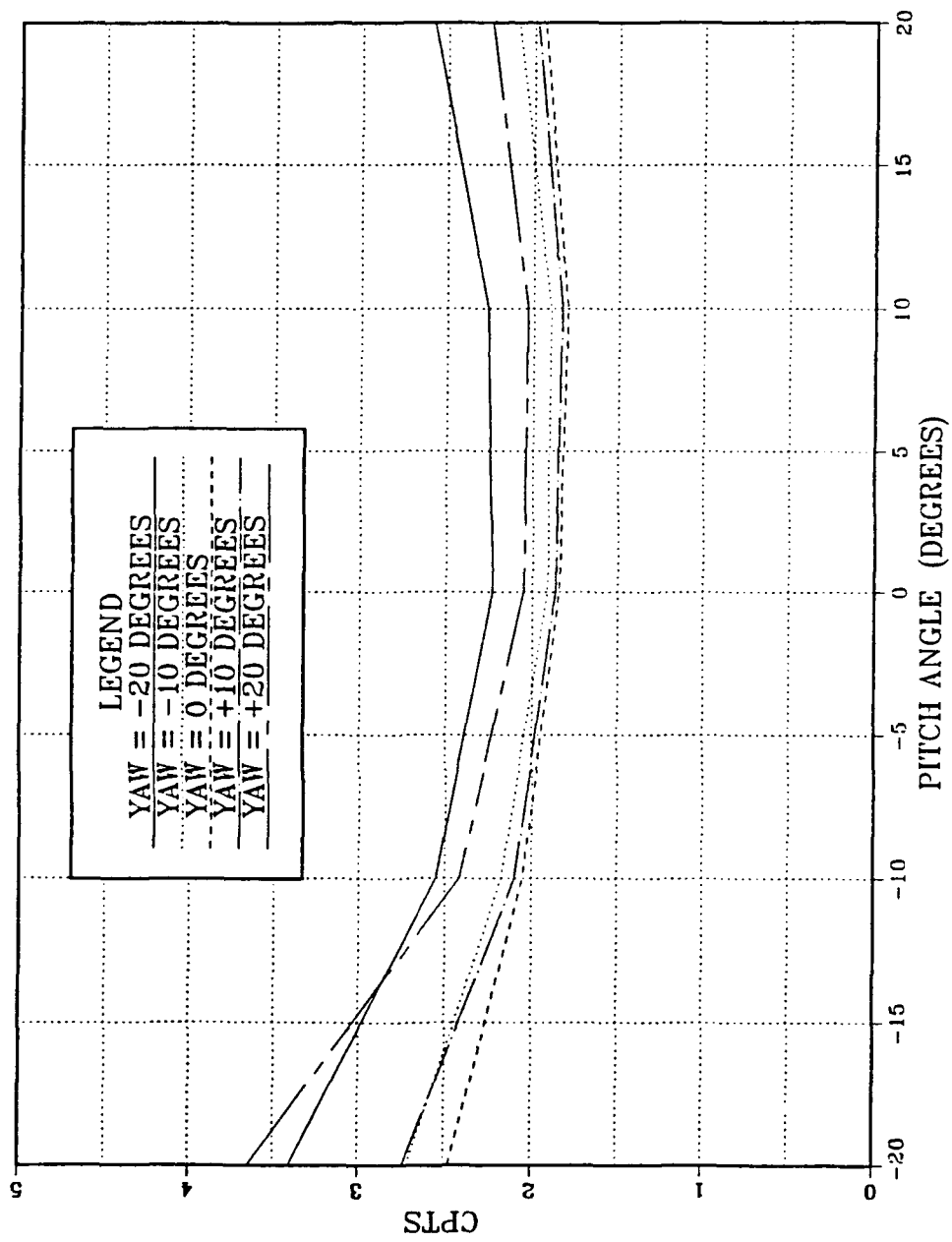


Figure 16. C_{pu} vs. Pitch Angle, 3.9 m/s

FIVE-HOLE PRESSURE PROBE

(CALIBRATION PLOT)

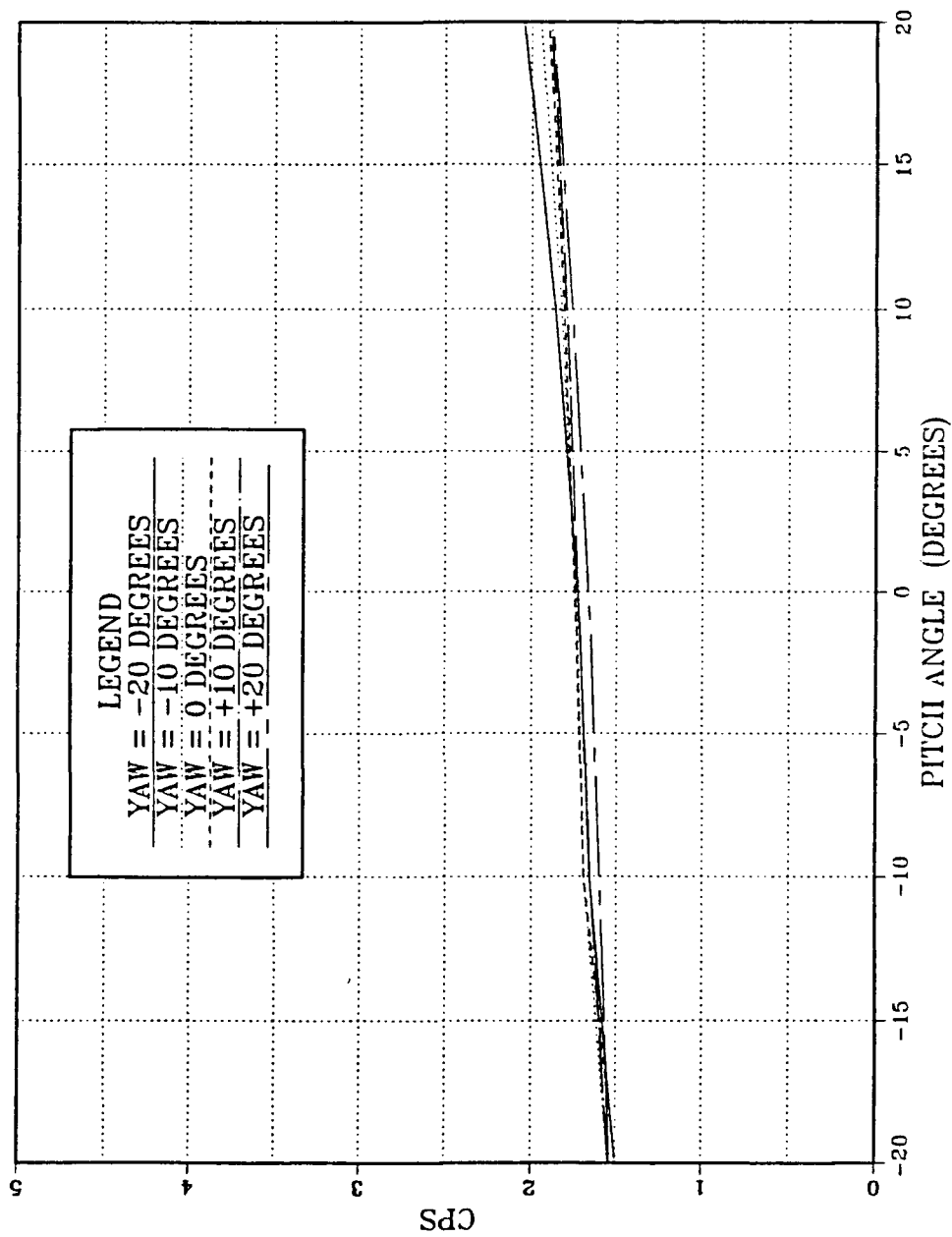


Figure 17. C_p vs. Pitch Angle, 3.9 m/s

KIEL PROBE TOTAL PRESSURE CONTOURS $P_{kiel} - P_{ambient}$ (inches H₂O) AVERAGE DEAN NUMBER = 51.81

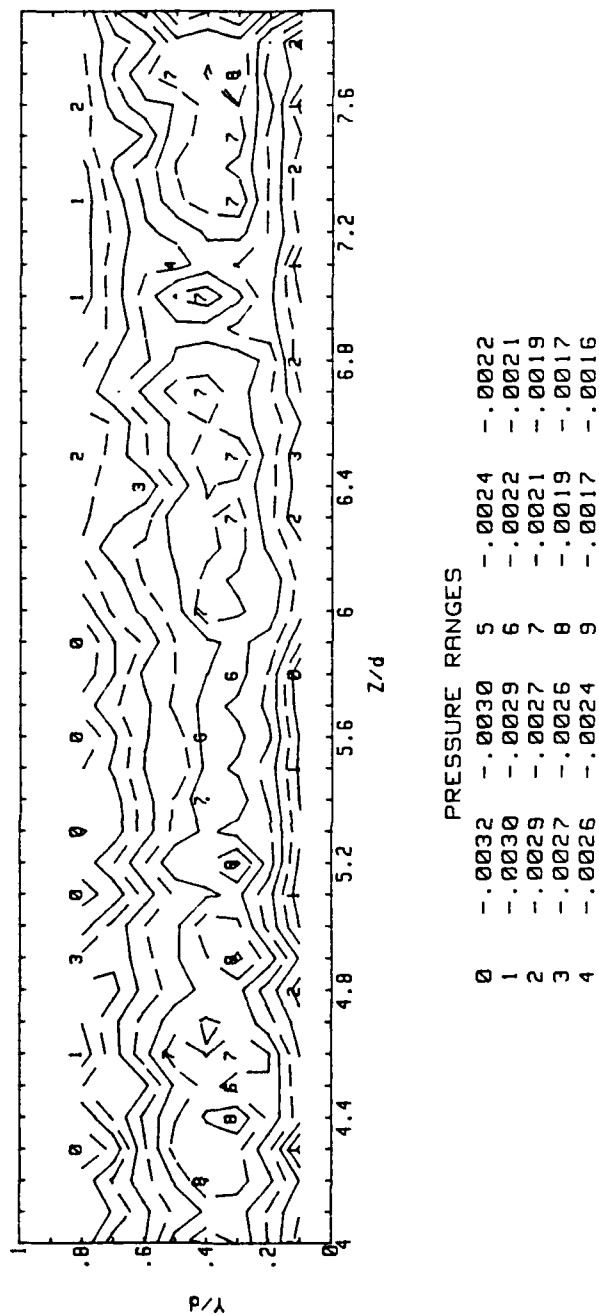


Figure 18. Kiel Probe Total Pressure Contour, $De = 51.81$

KIEL PROBE TOTAL PRESSURE CONTOURS Pkiel-Pambient (inches H2O)

AVERAGE DEAN NUMBER = 77.47

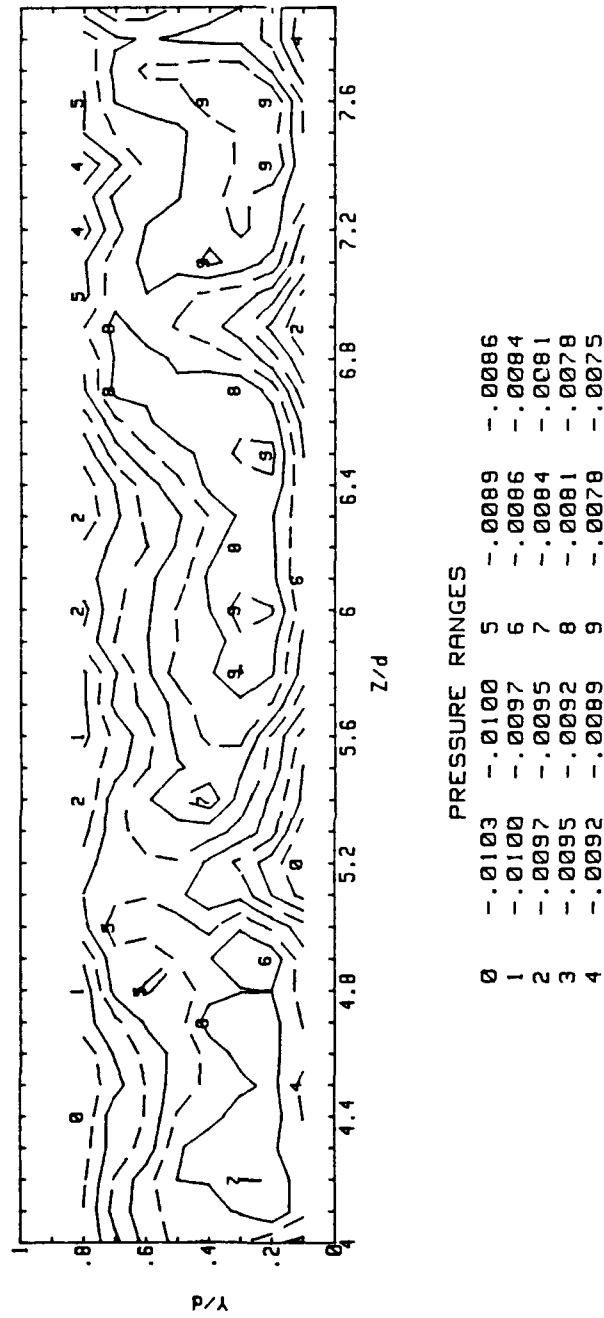


Figure 19. Kiel Probe Total Pressure Contour, $De = 77.47$

KIEL PROBE TOTAL PRESSURE CONTOURS
 Pkiel-Pambient (inches H2O)
 AVERAGE DEAN NUMBER =103.59

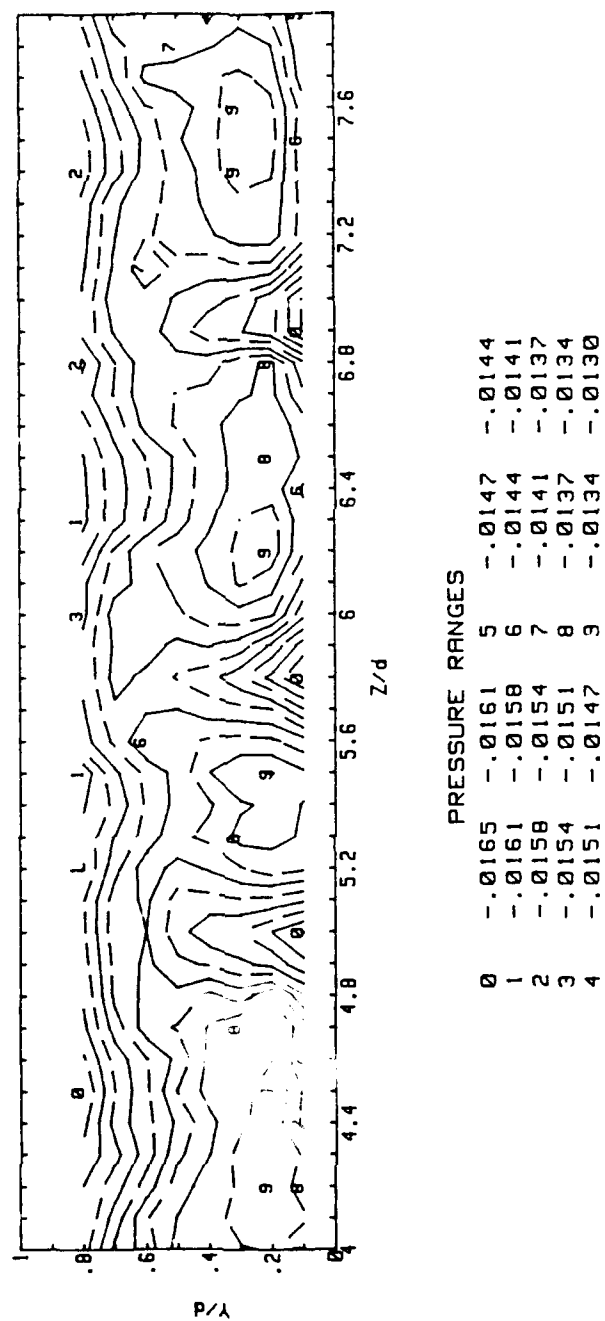
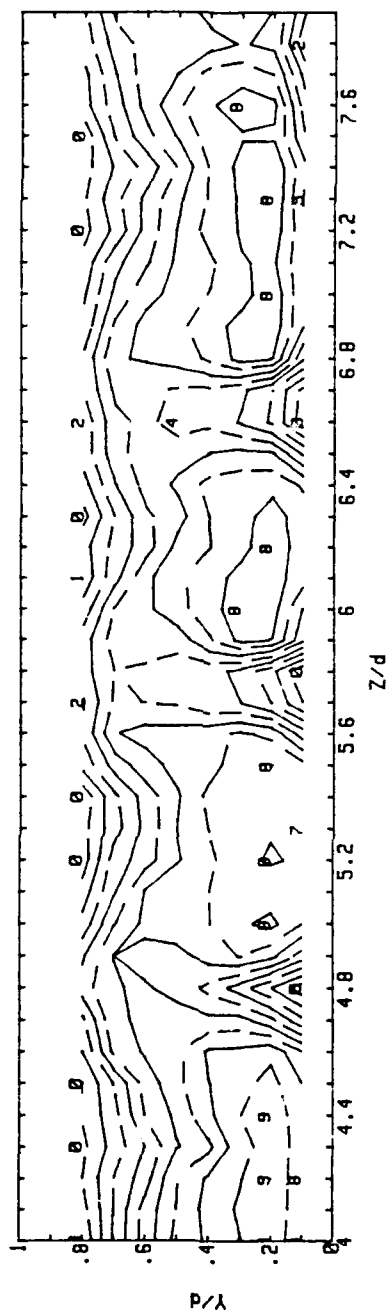


Figure 20. Kiel Probe Total Pressure Contour, $De = 103.6$

KIEL PROBE TOTAL PRESSURE CONTOURS Pkiel-Pambient (inches H2O)

AVERAGE DEAN NUMBER =126.23



PRESSURE RANGES				
0	-.0233	-.0228	5	-.0209
1	-.0228	-.0223	6	-.0204
2	-.0223	-.0218	7	-.0199
3	-.0218	-.0214	8	-.0194
4	-.0214	-.0209	9	-.0190
				-.0185

Figure 21. Kiel Probe Total Pressure Contour, $De = 126.2$

KIEL PROBE TOTAL PRESSURE CONTOURS $P_{kiel} - P_{ambient}$ (inches H₂O) AVERAGE DEAN NUMBER = 149.60

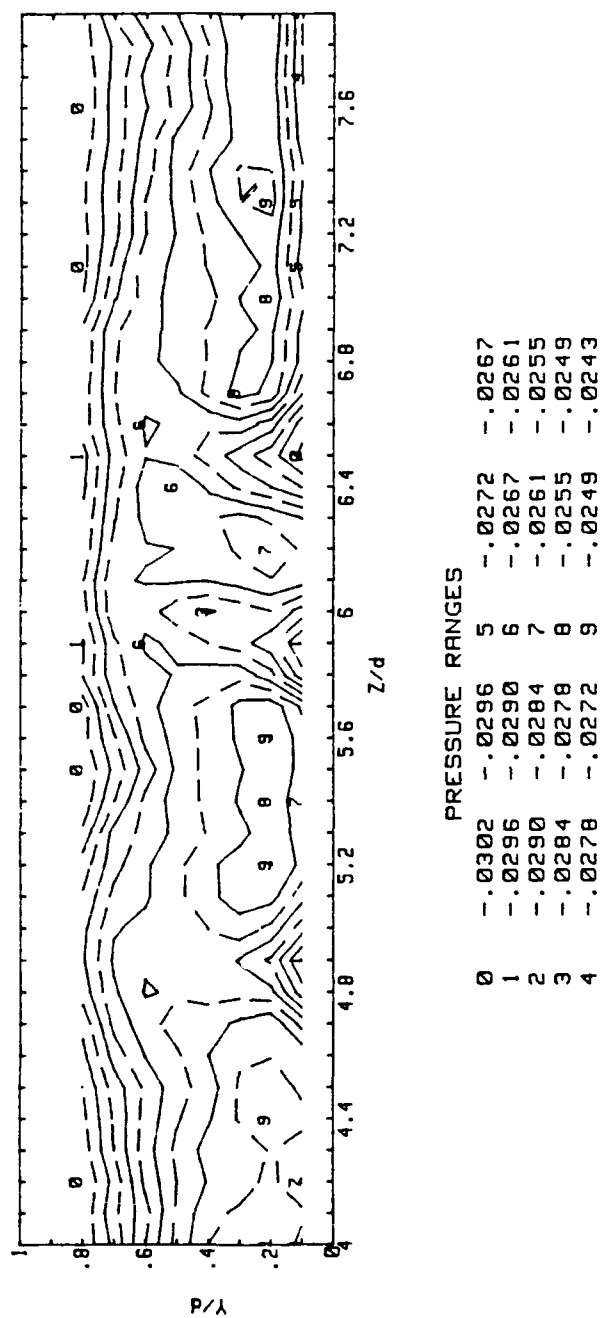


Figure 22. Kiel Probe Total Pressure Contour, $De = 149.6$

KIEL PROBE TOTAL PRESSURE CONTOURS $P_{kiel} - P_{ambient}$ (inches H₂O) AVERAGE DEAN NUMBER = 177.50

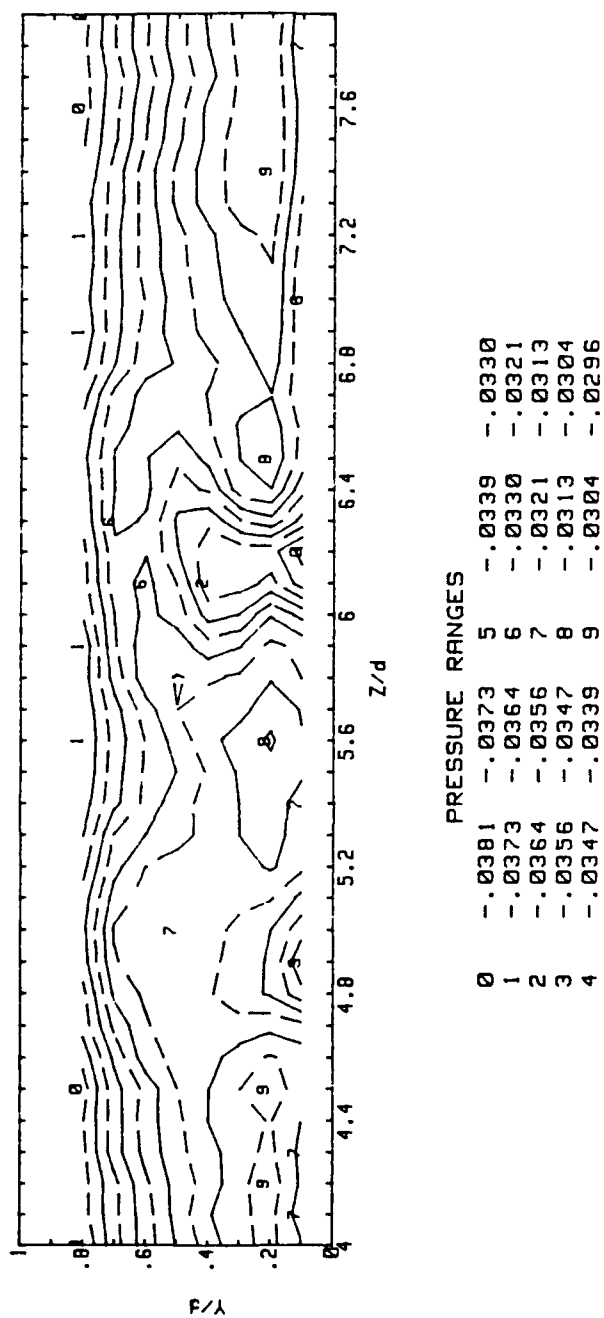


Figure 23. Kiel Probe Total Pressure Contour, $De = 177.5$

KIEL PROBE TOTAL PRESSURE CONTOURS $P_{kiel} - P_{ambient}$ (inches H₂O)

AVERAGE DEAN NUMBER = 202.73

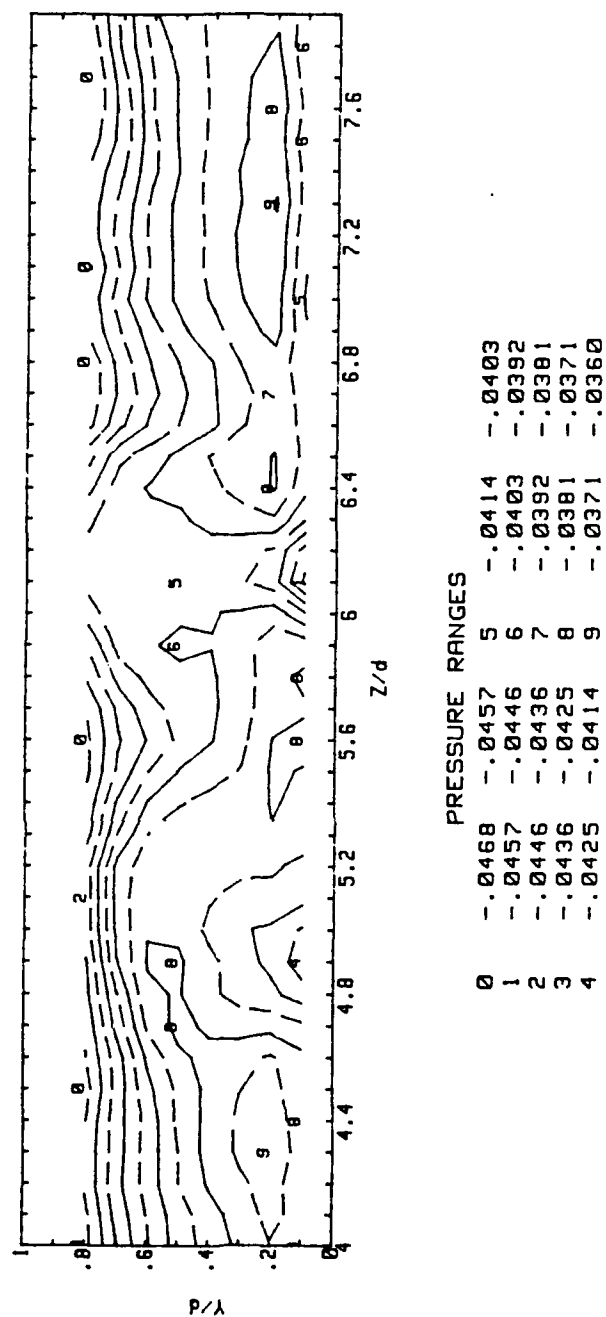


Figure 24. Kiel Probe Total Pressure Contour, $De = 202.7$

KIEL PROBE TOTAL PRESSURE CONTOURS $P_{kiel} - P_{ambient}$ (inches H₂O) AVERAGE DEAN NUMBER = 226.79

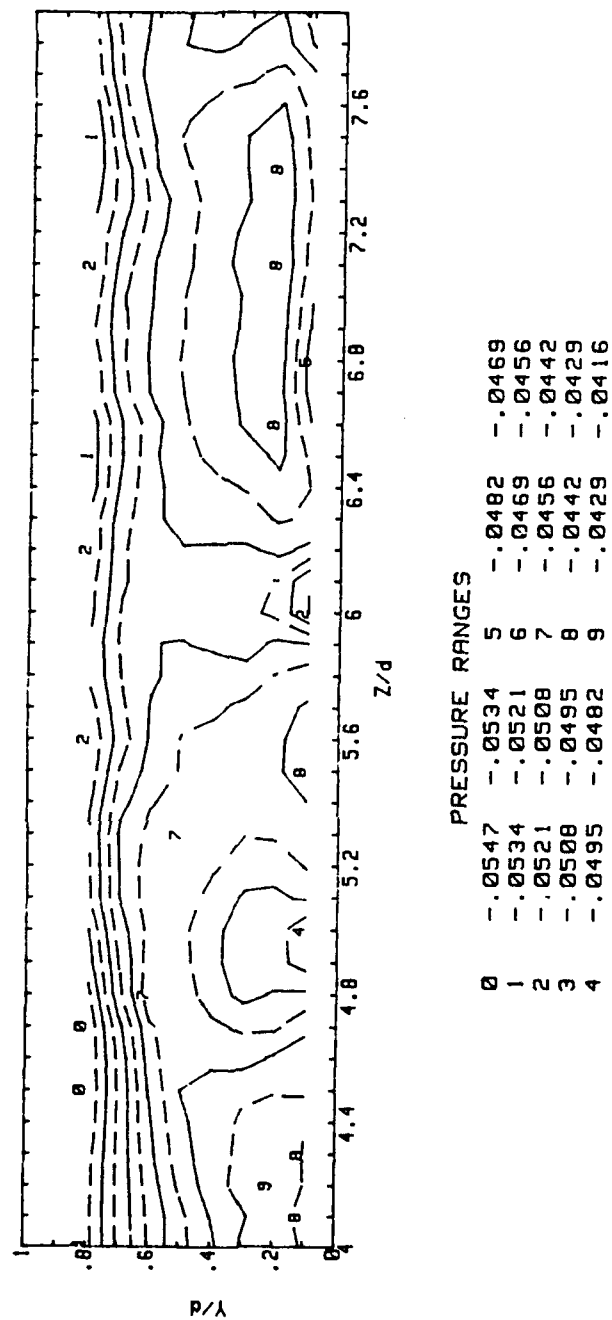


Figure 25. Kiel Probe Total Pressure Contour, $De = 226.8$

KIEL PROBE TOTAL PRESSURE CONTOURS Pkiel-Pambient (inches H2O) AVERAGE DEAN NUMBER =252.35

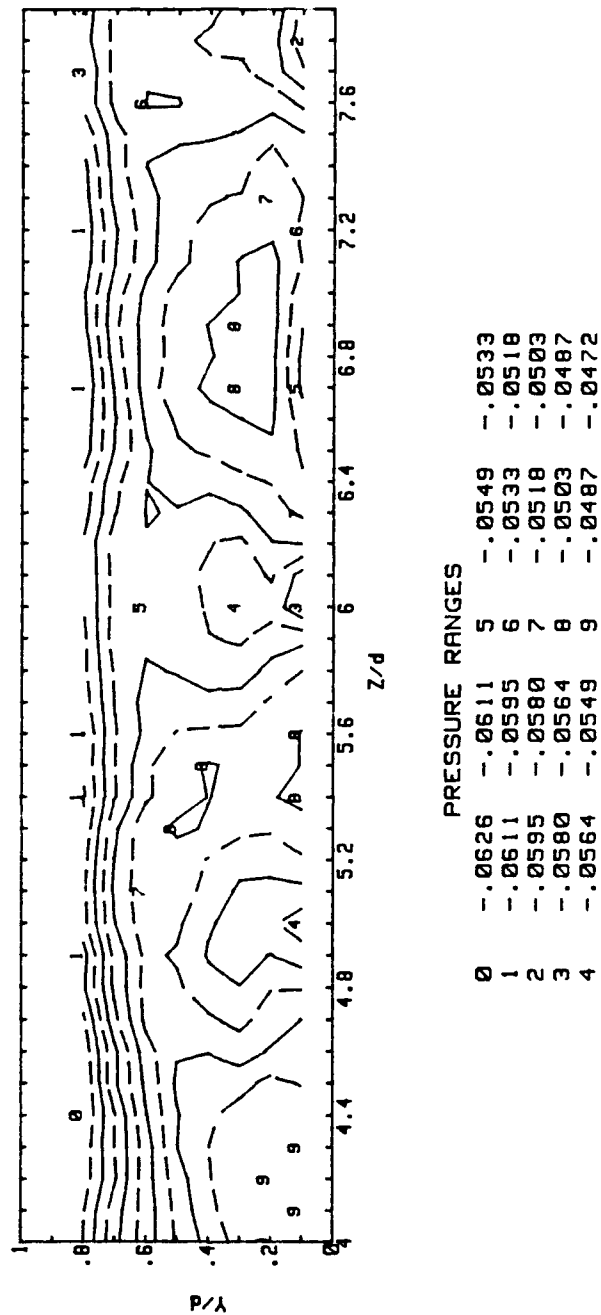


Figure 26. Kiel Probe Total Pressure Contour, $De = 252.4$

KIEL PROBE TOTAL PRESSURE CONTOURS $P_{kiel} - P_{ambient}$ (inches H₂O)

AVERAGE DEAN NUMBER = 274.45

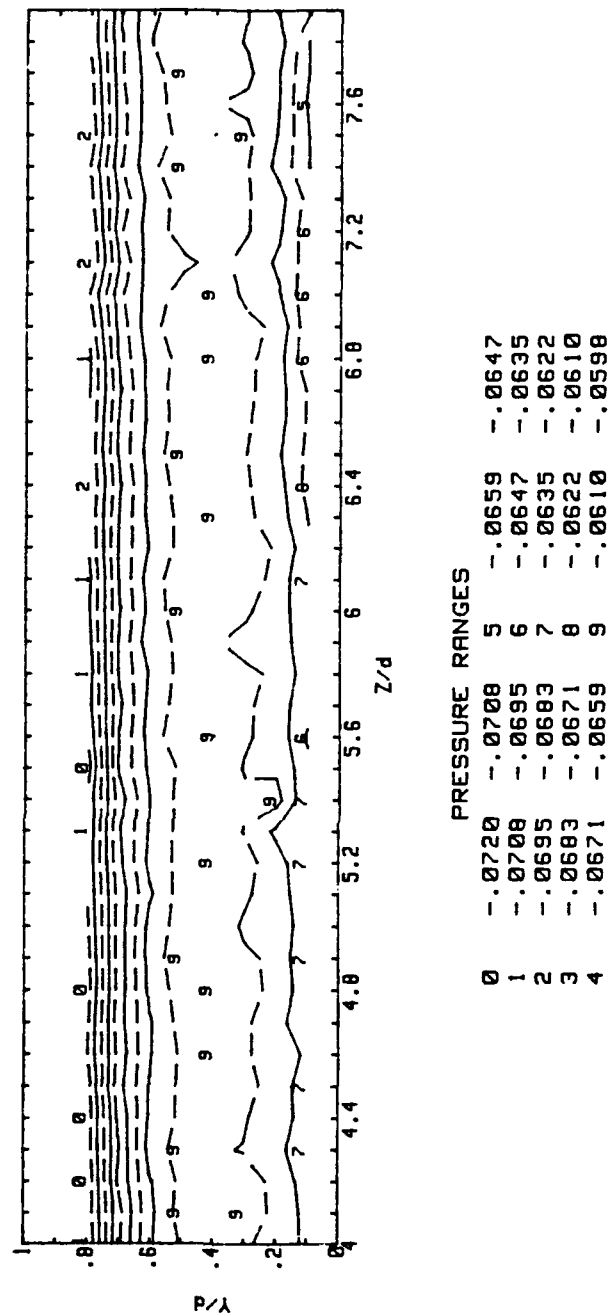


Figure 27. Kiel Probe Total Pressure Contour, $De = 274.5$

KIEL PROBE TOTAL PRESSURE CONTOURS $P_{kiel} - P_{ambient}$ (inches H₂O)

AVERAGE DEAN NUMBER = 301.95

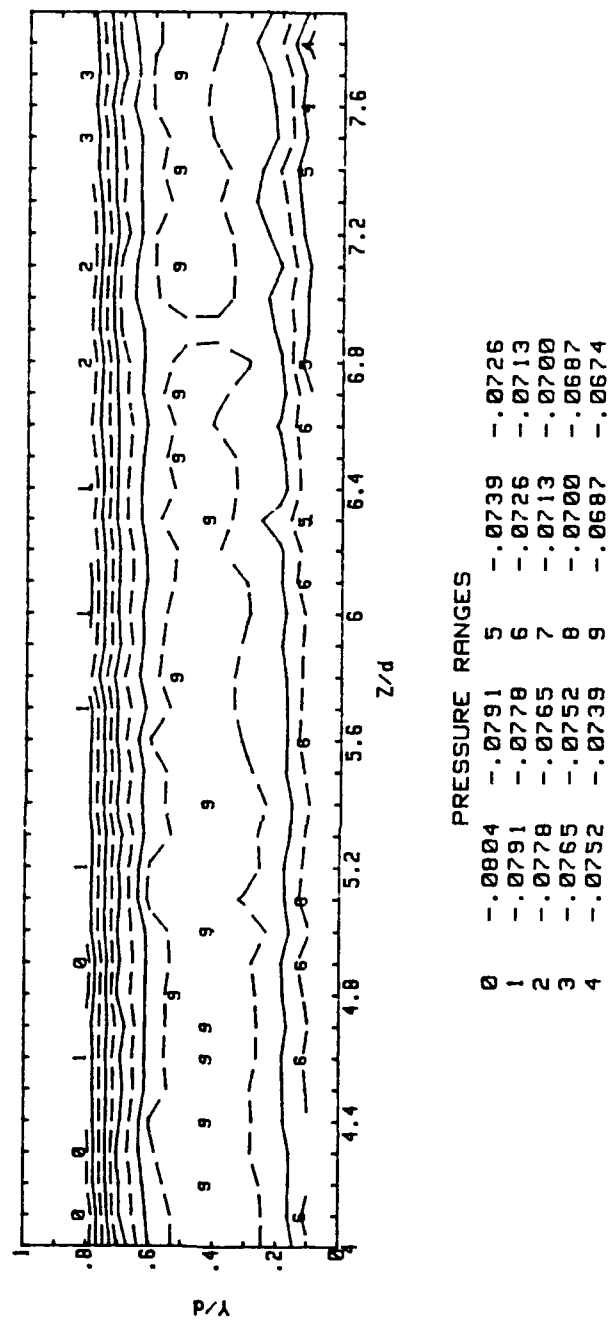


Figure 28. Kiel Probe Total Pressure Contour, $De = 302.0$

KIEL PROBE TOTAL PRESSURE CONTOURS $P_{kiel} - P_{ambient}$ (inches H₂O) AVERAGE DEAN NUMBER = 327.52

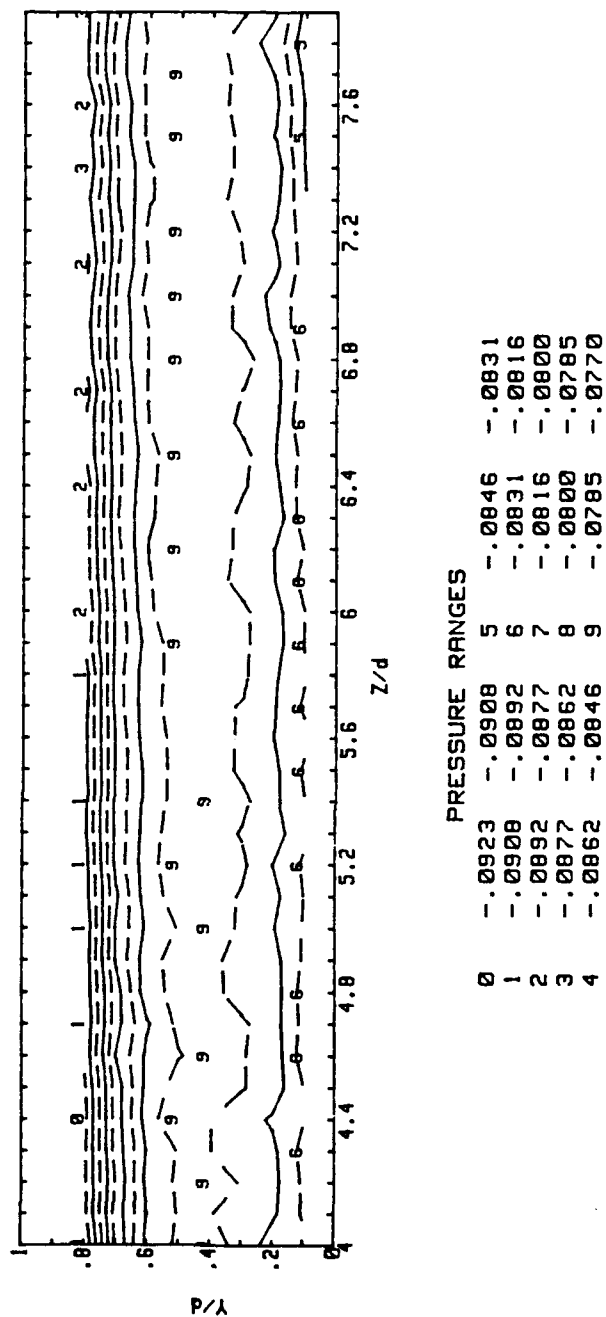


Figure 29. Kiel Probe Total Pressure Contour, $De = 327.5$

KIEL PROBE TOTAL PRESSURE CONTOURS $P_{kiel} - P_{ambient}$ (inches H₂O) AVERAGE DEAN NUMBER = 350.72

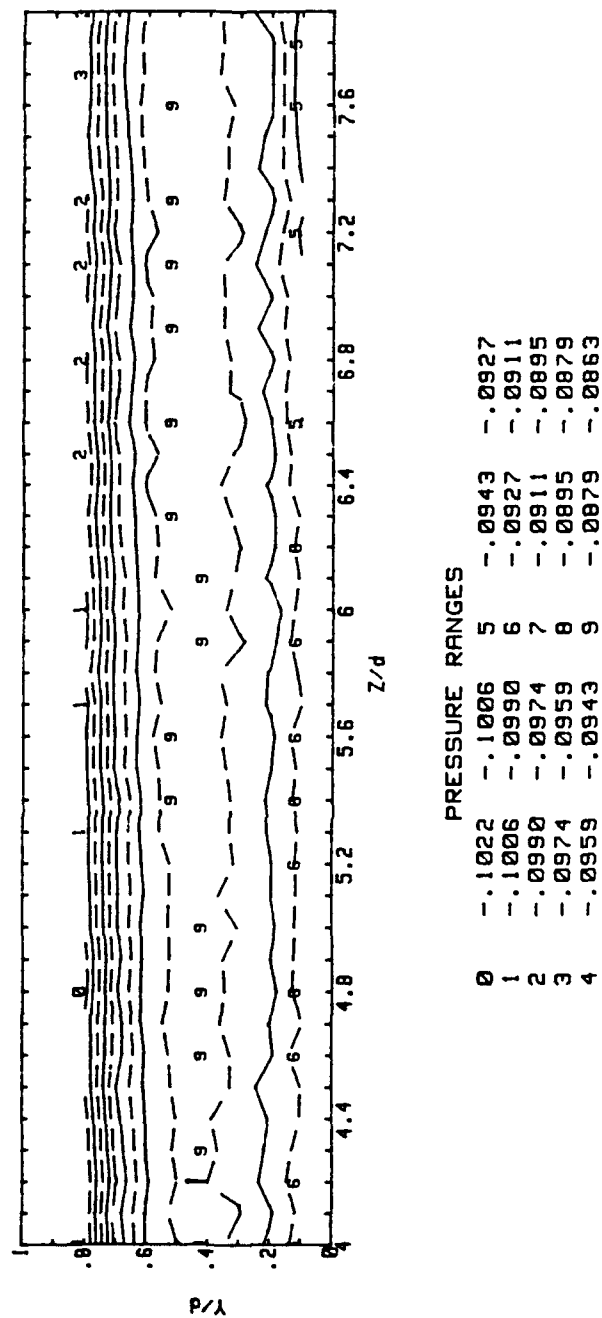


Figure 30. Kiel Probe Total Pressure Contour, $De = 350.7$

KIEL PROBE TOTAL PRESSURE CONTOURS $P_{kiel} - P_{ambient}$ (inches H₂O)

AVERAGE DEAN NUMBER = 375.85

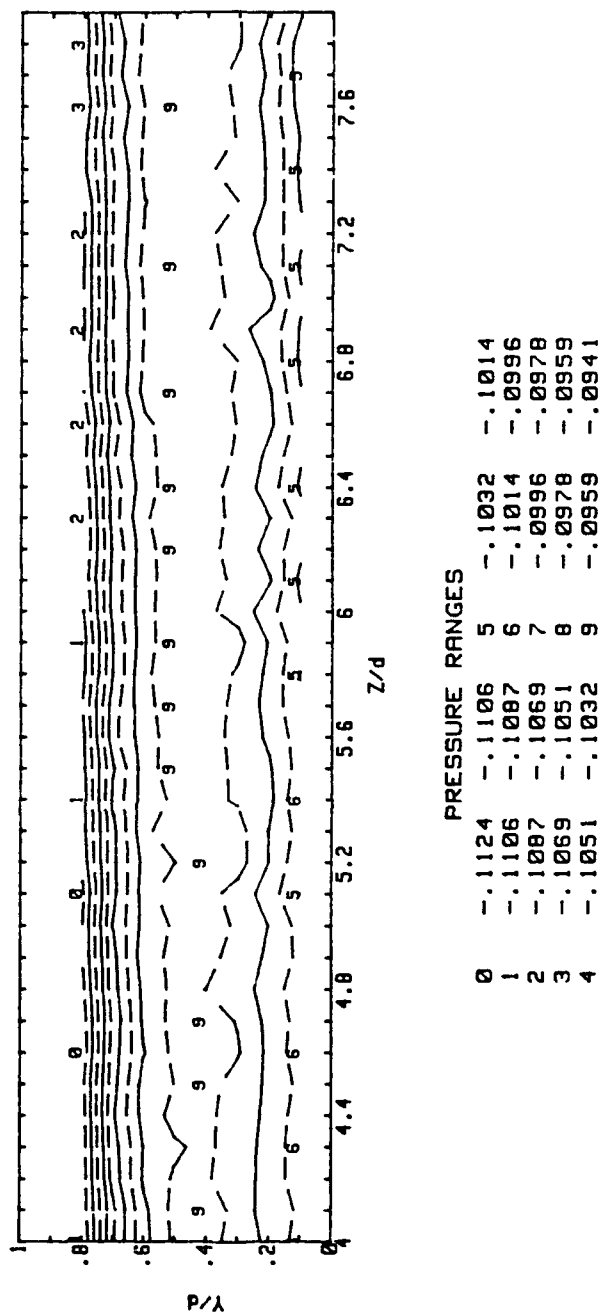
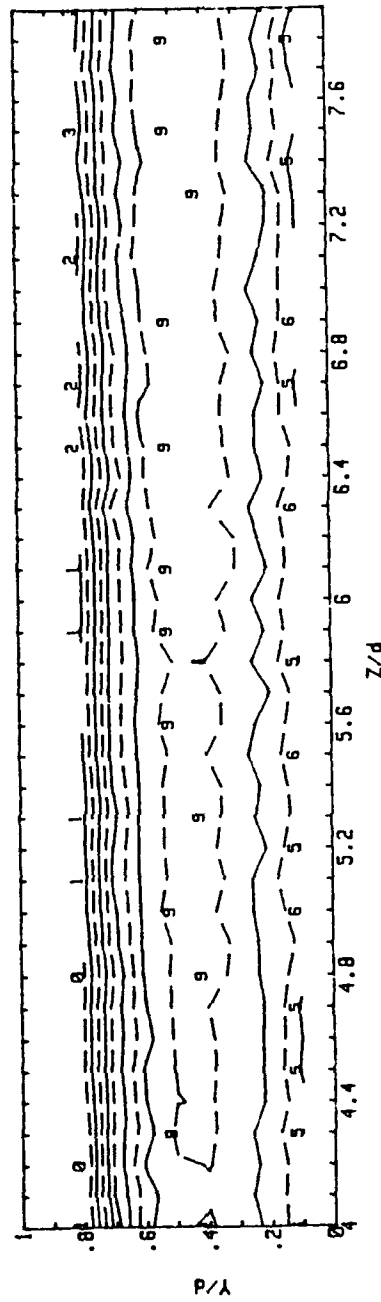


Figure 31. Kiel Probe Total Pressure Contour, $De = 375.9$

KIEL PROBE TOTAL PRESSURE CONTOURS Pkiel-Pambient (inches H2O)

AVERAGE DEAN NUMBER =402.77



PRESSURE RANGES				
0	-.1250	-.1230	5	-.1149
1	-.1230	-.1210	6	-.1129
2	-.1210	-.1189	7	-.1109
3	-.1189	-.1169	8	-.1088
4	-.1169	-.1149	9	-.1068

Figure 32. Kiel Probe Total Pressure Contour, $De = 402.8$

KIEL PROBE TOTAL PRESSURE CONTOURS $P_{kiel} - P_{ambient}$ (inches H₂O) AVERAGE DEAN NUMBER = 425.76

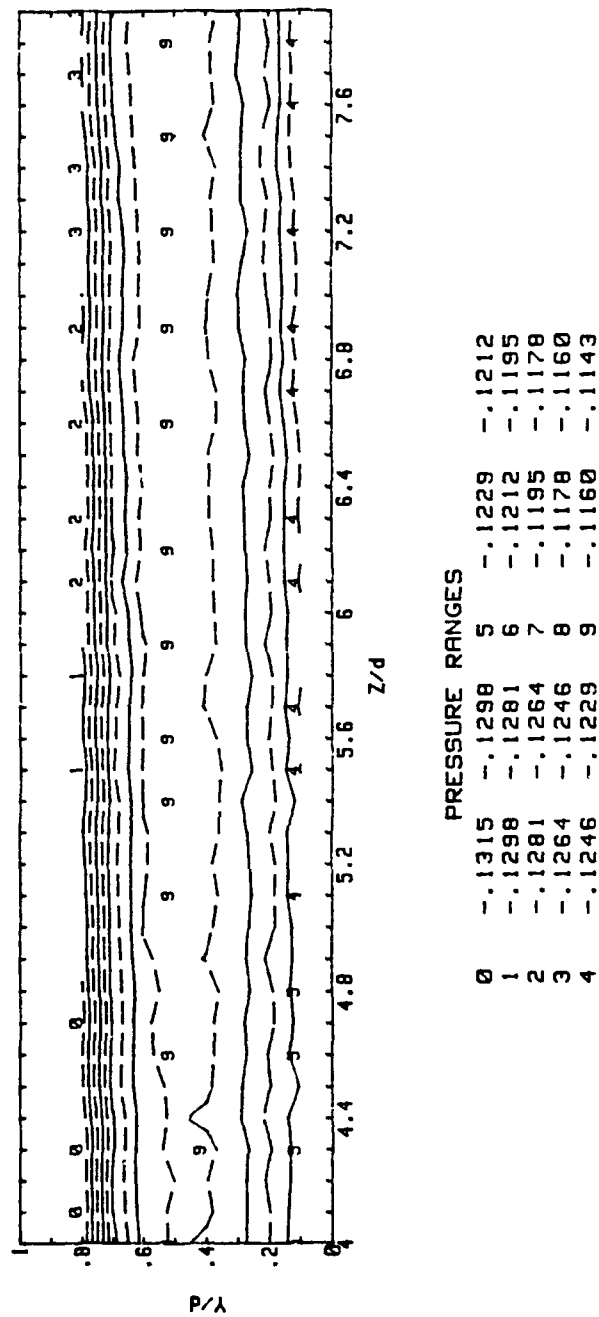


Figure 33. Kiel Probe Total Pressure Contour, $De = 425.8$

KIEL PROBE TOTAL PRESSURE CONTOURS Pkiel-Pambient (inches H2O) AVERAGE DEAN NUMBER =450.17

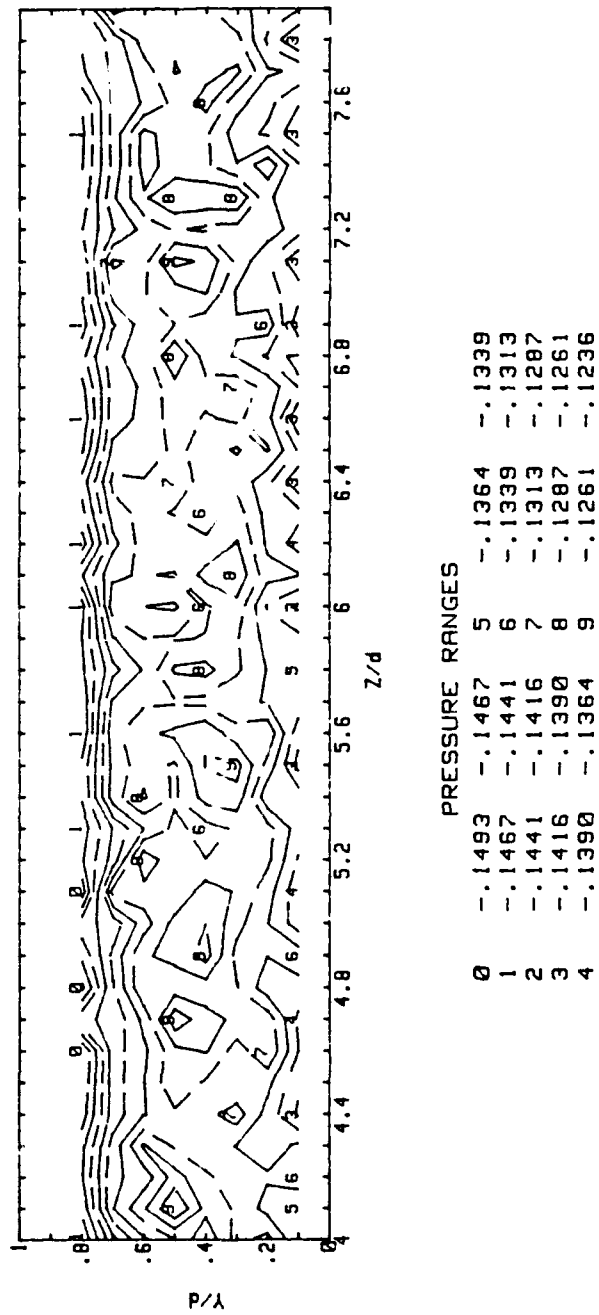


Figure 34. Kiel Probe Total Pressure Contour, De = 450.2

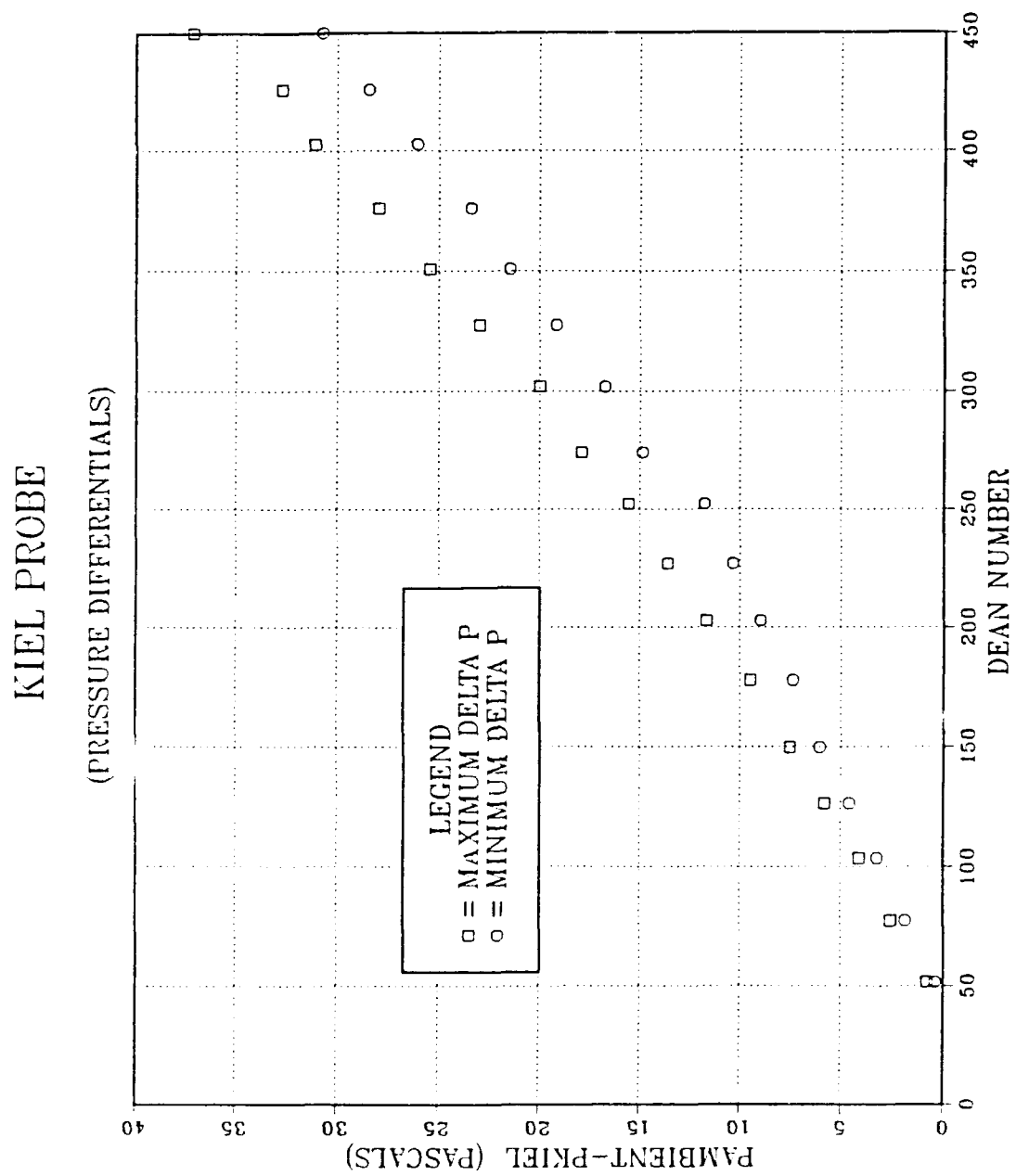


Figure 35. Kiel Probe Pressure Differentials

Pamb-Ptotal
RANGES IN PASCALS

- 0: 0.88 TO 0.91
- 1: 0.91 TO 0.94
- 2: 0.94 TO 0.97
- 3: 0.97 TO 1.00
- 4: 1.00 TO 1.03
- 5: 1.03 TO 1.06
- 6: 1.06 TO 1.09
- 7: 1.09 TO 1.12
- 8: 1.12 TO 1.16

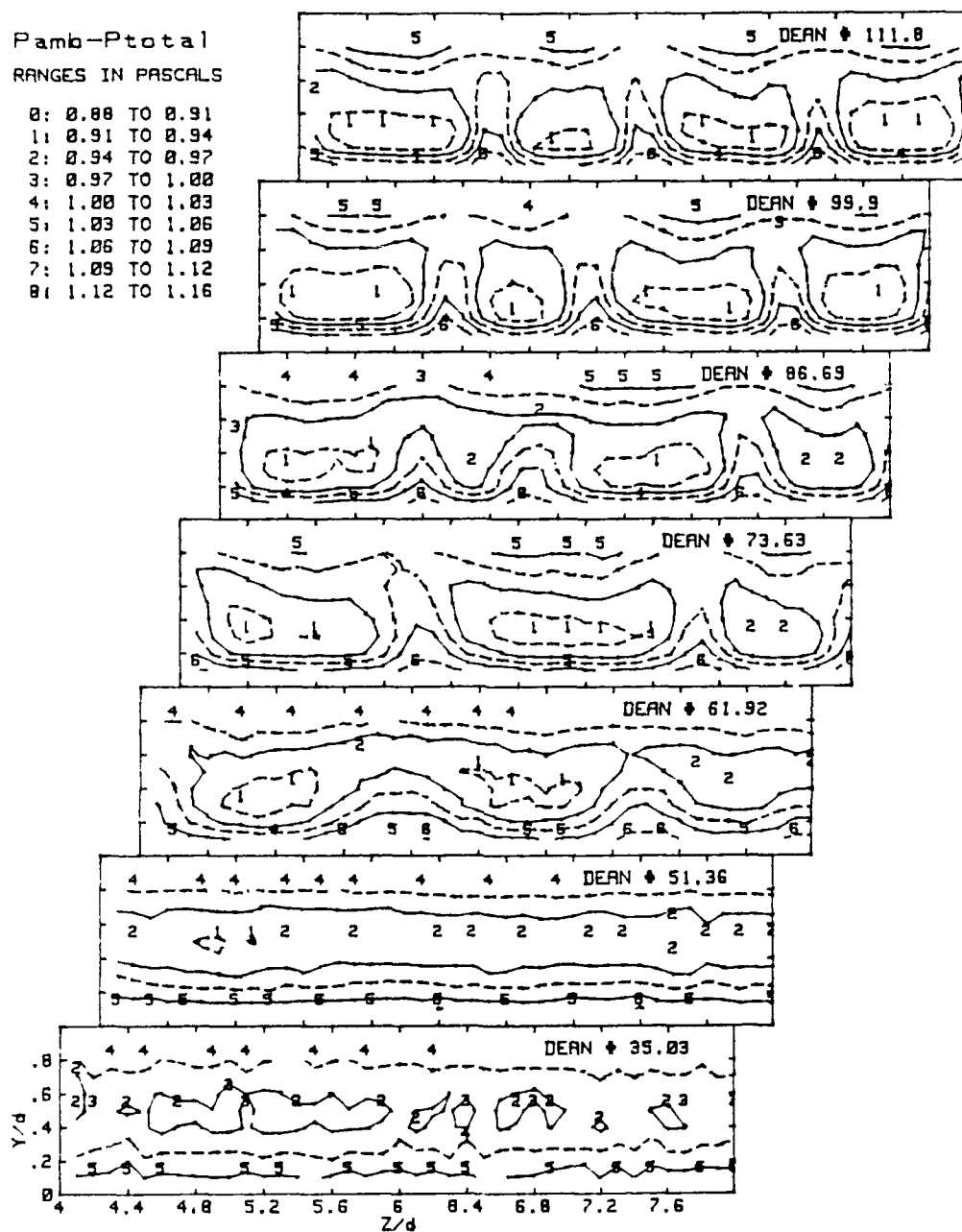


Figure 36. Five-Hole Probe Total Pressure Contours, $De = 35.0$ to $De = 111.8$

Pamb-Ptotal
RANGES IN PASCALS

- 0: 0.88 TO 0.91
- 1: 0.91 TO 0.94
- 2: 0.94 TO 0.97
- 3: 0.97 TO 1.00
- 4: 1.00 TO 1.03
- 5: 1.03 TO 1.06
- 6: 1.06 TO 1.09
- 7: 1.09 TO 1.12
- 8: 1.12 TO 1.16

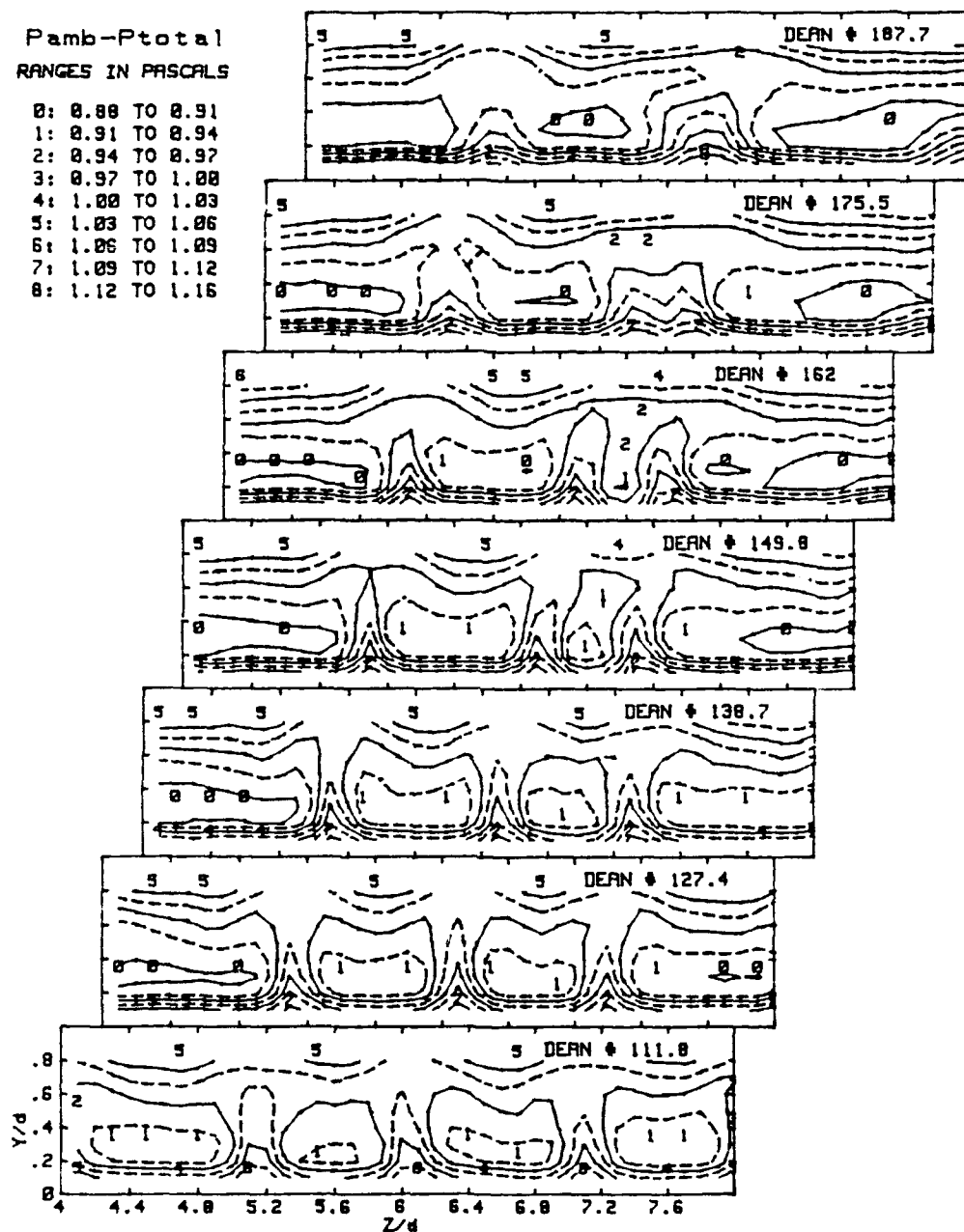


Figure 37. Five-Hole Probe Total Pressure Contours, $De = 111.8$ to $De = 187.7$

$P_{amb} - P_{total}$
RANGES IN PASCALS

- 0: 0.88 TO 0.91
- 1: 0.91 TO 0.94
- 2: 0.94 TO 0.97
- 3: 0.97 TO 1.00
- 4: 1.00 TO 1.03
- 5: 1.03 TO 1.06
- 6: 1.06 TO 1.09
- 7: 1.09 TO 1.12
- 8: 1.12 TO 1.16

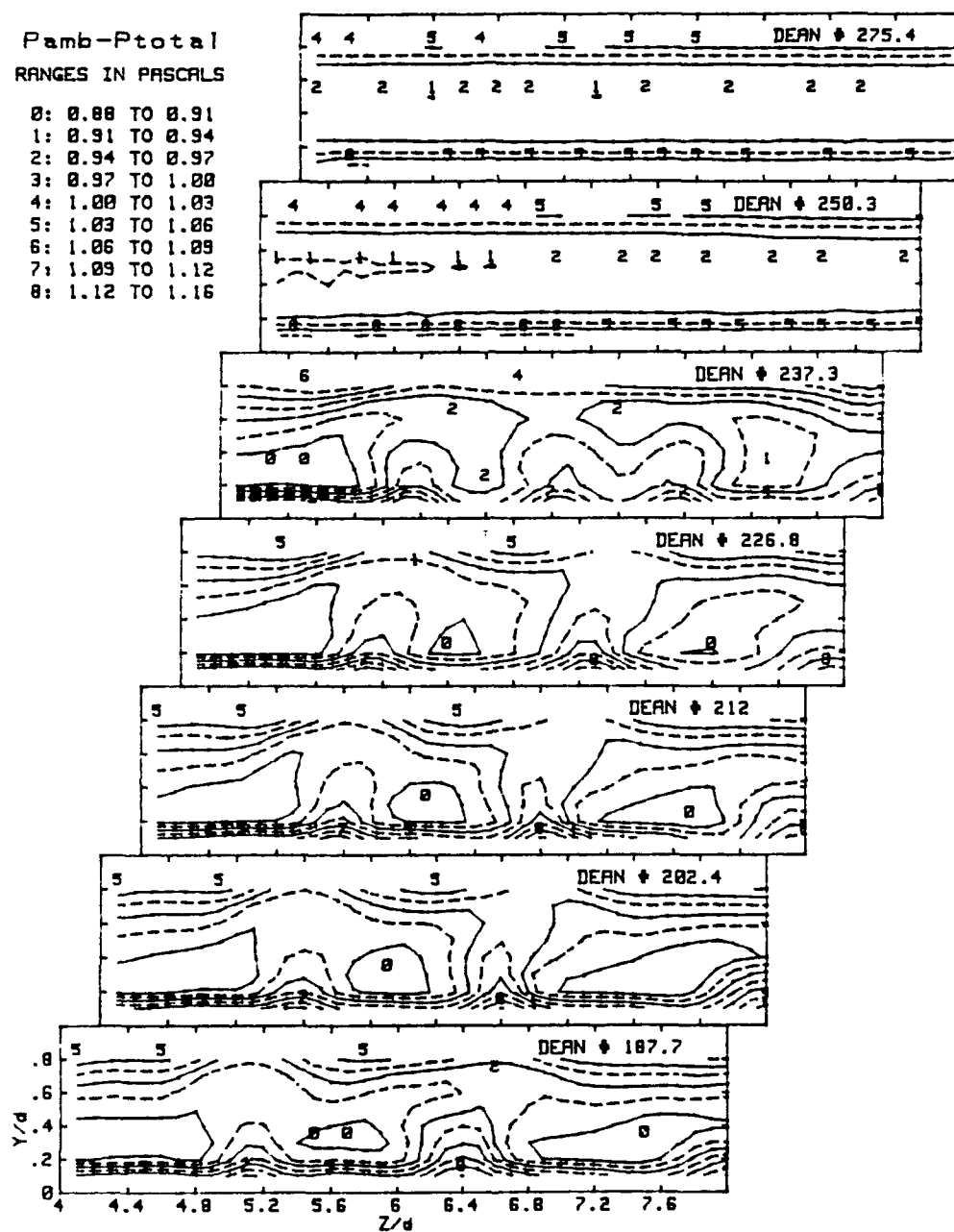


Figure 38. Five-Hole Probe Total Pressure Contours, $De = 187.7$ to $De = 275.4$

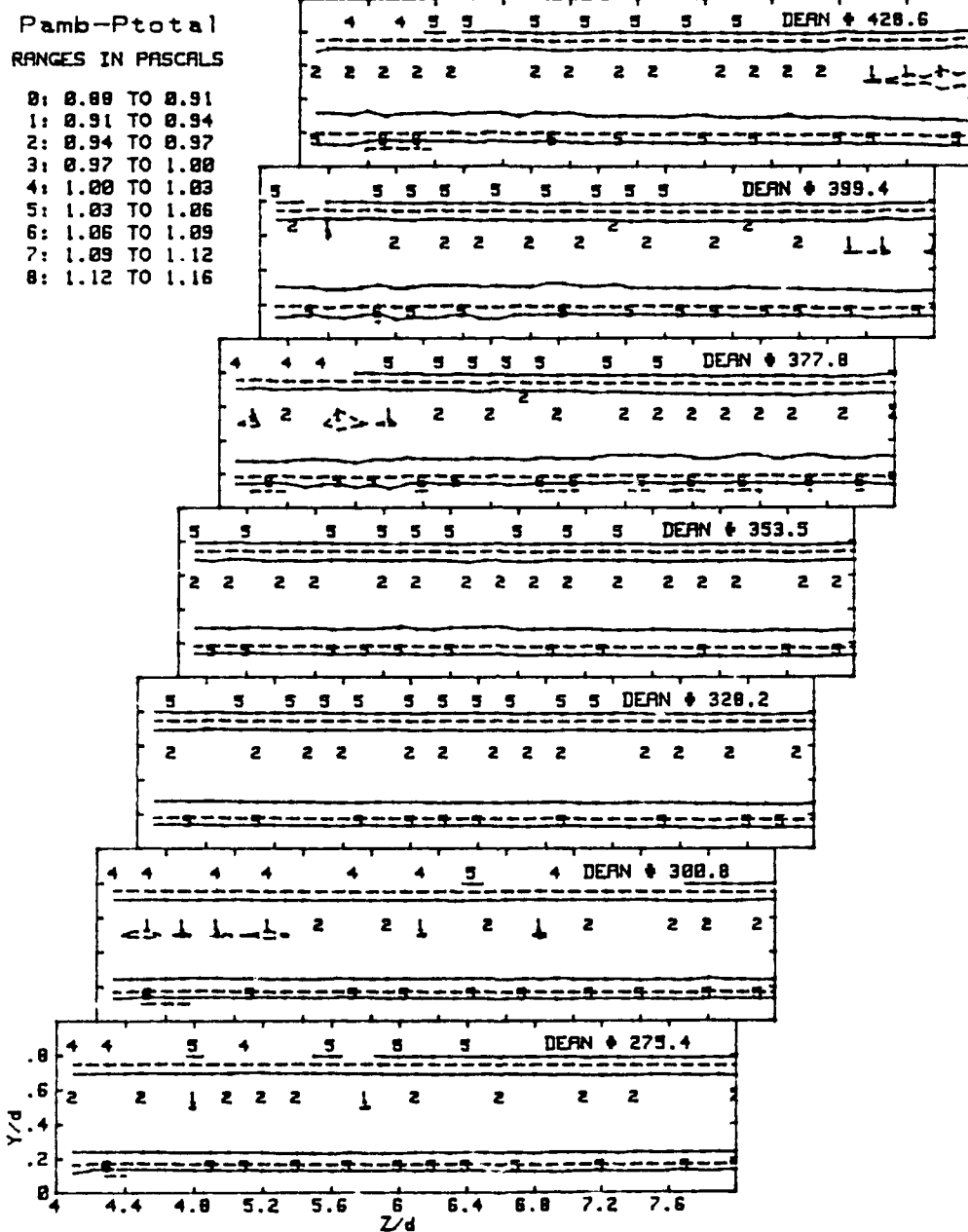


Figure 39. Five-Hole Probe Total Pressure Contours, $De = 275.4$ to $De = 428.6$

FIVE-HOLE PRESSURE PROBE

(PRESSURE DIFFERENTIALS)

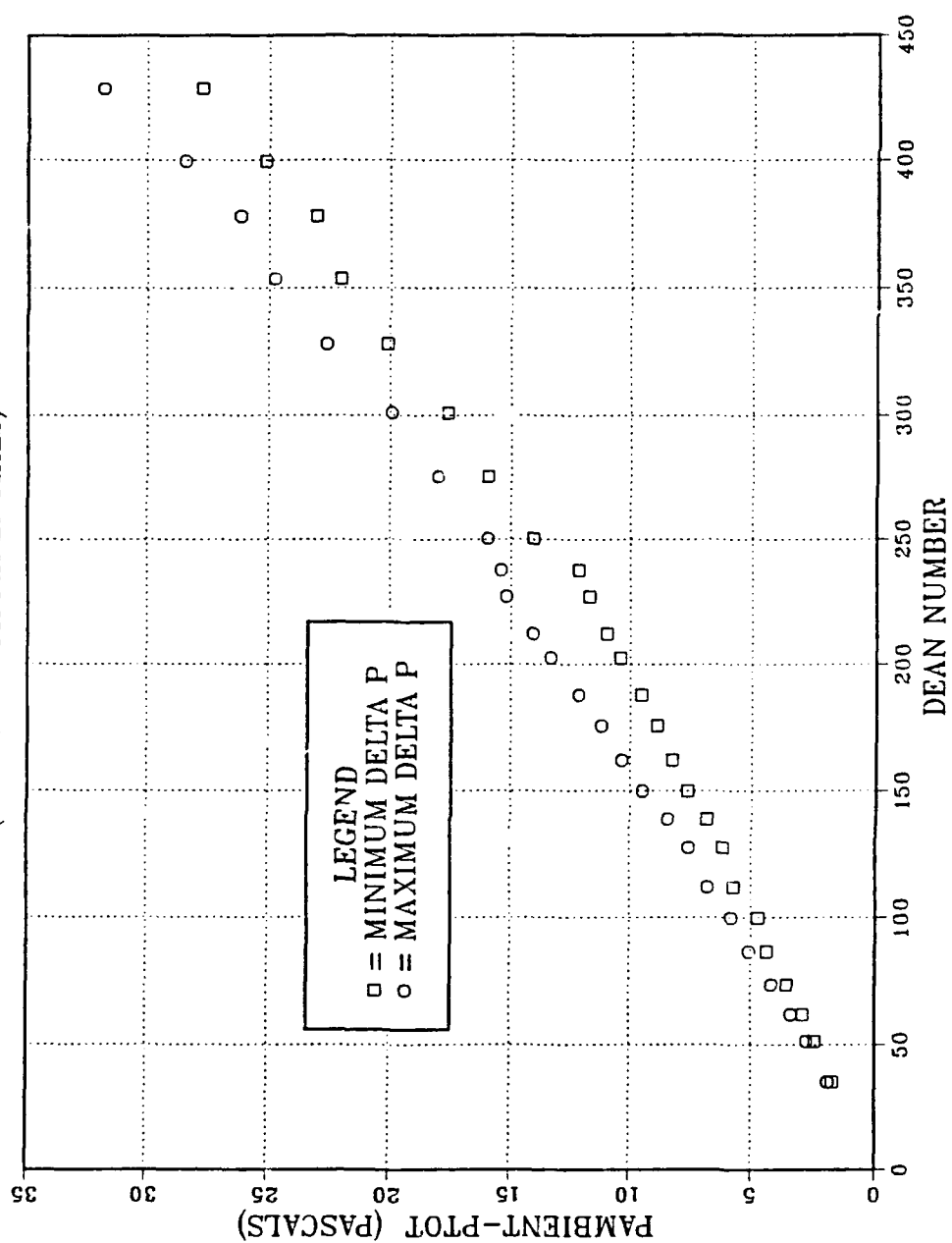


Figure 40. Five-Hole Probe Pressure Differentials

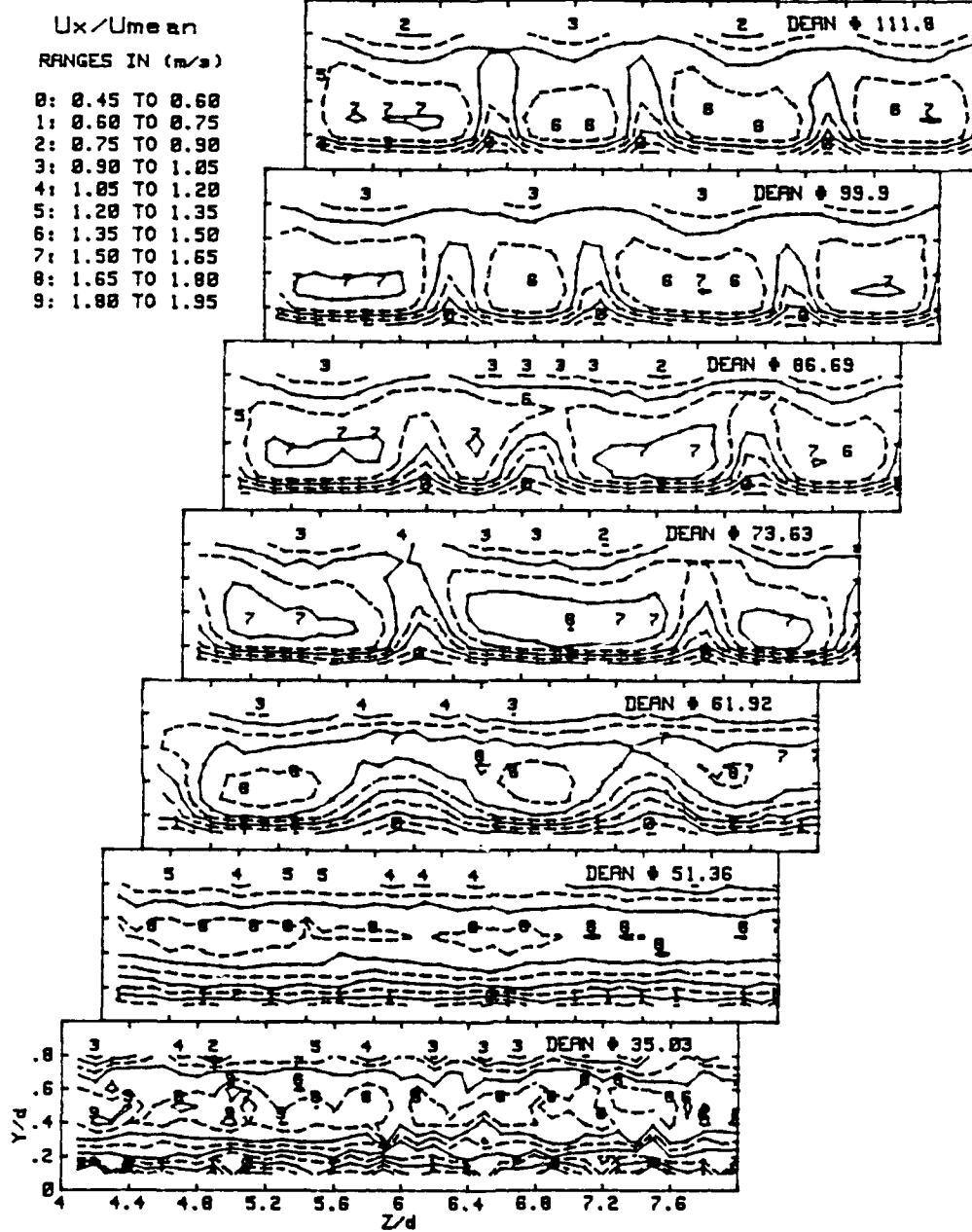


Figure 41. Streamwise Velocity Contours, $De = 35.0$ to $De = 111.8$

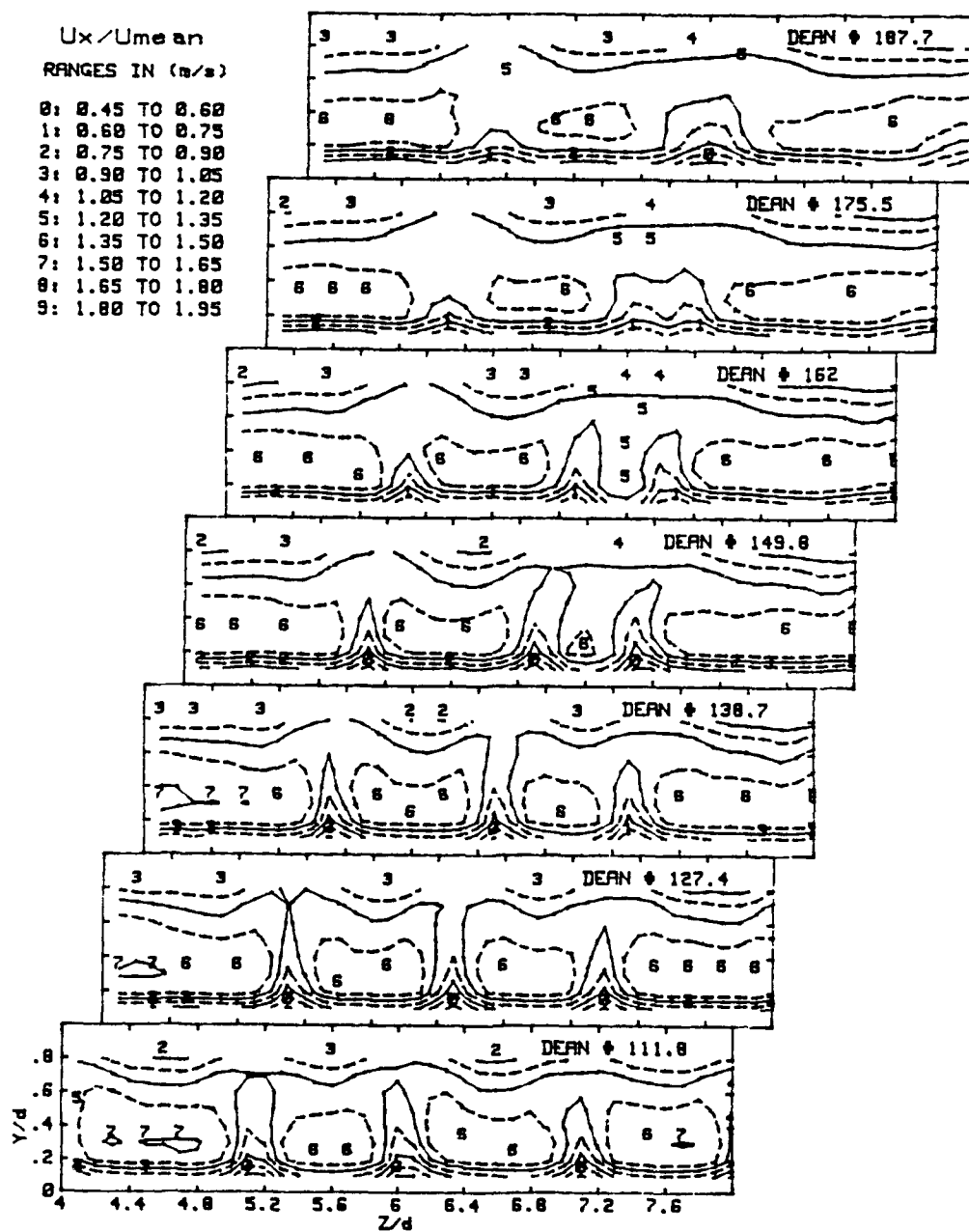


Figure 42. Streamwise Velocity Contours, $De = 111.8$ to $De = 187.7$

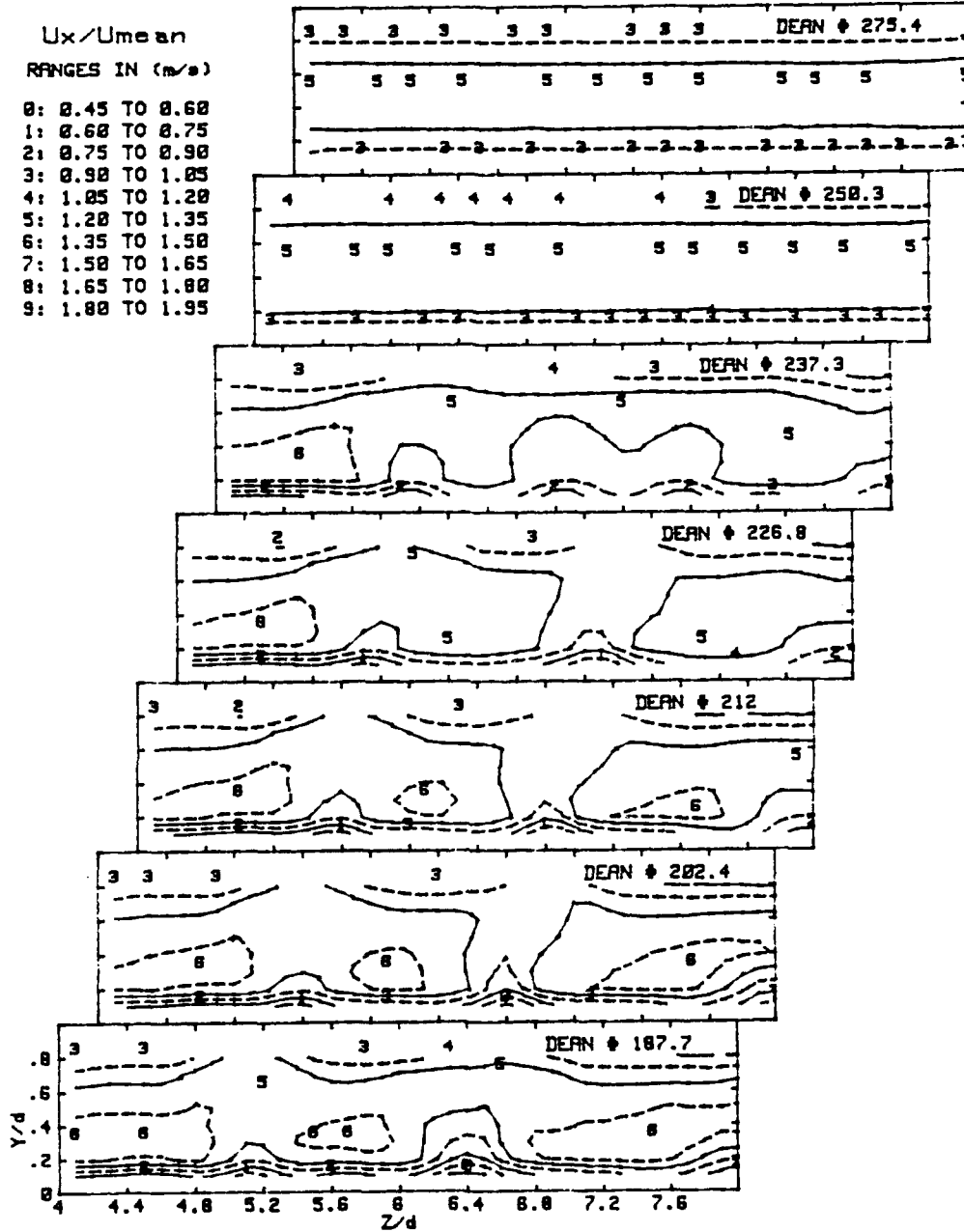


Figure 43. Streamwise Velocity Contours, $De = 187.7$ to $De = 275.4$

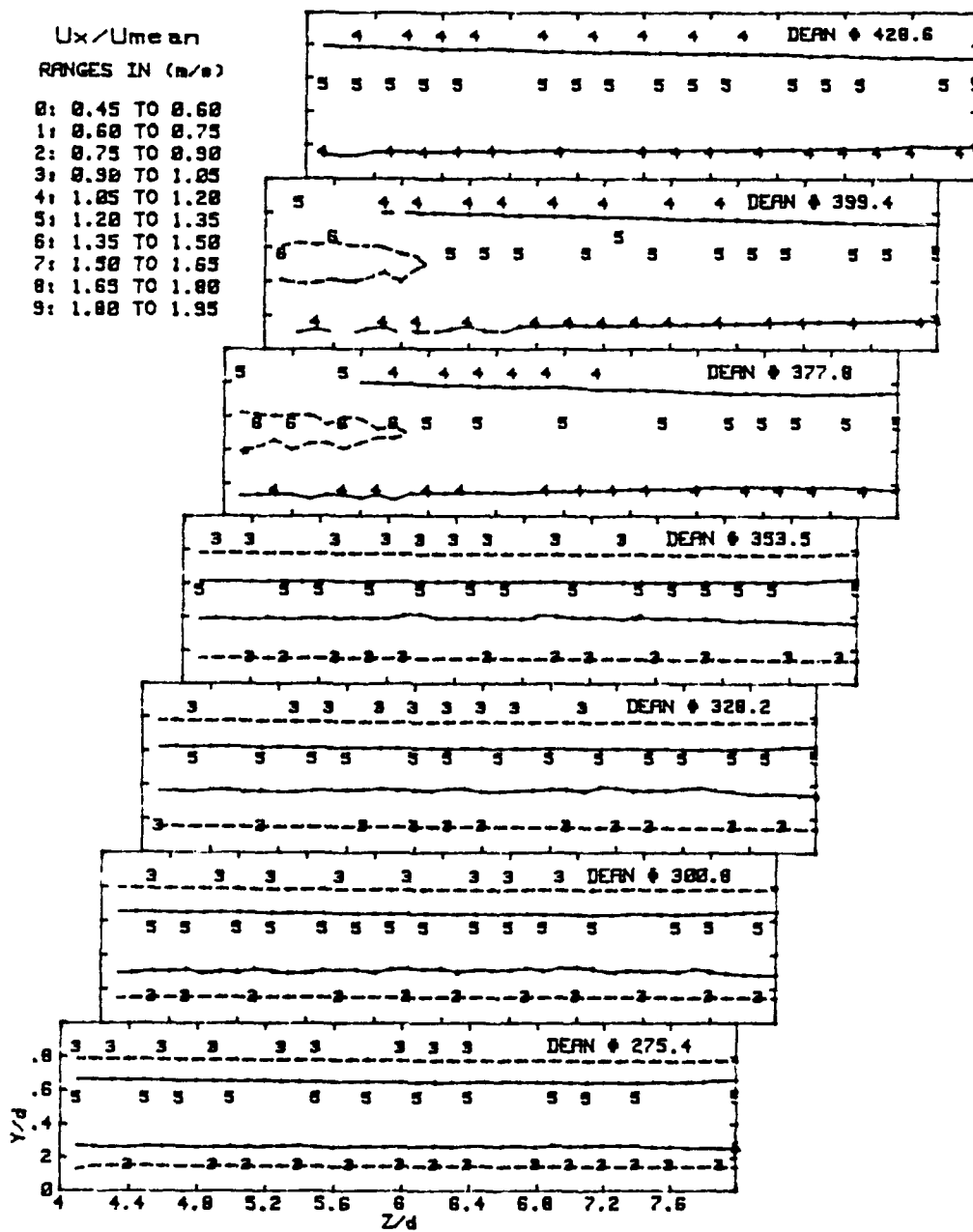


Figure 44. Streamwise Velocity Contours, $De = 275.4$ to $De = 428.6$

VELOCITY VECTORS IN CURVED CHANNEL FLOW

— .103M/S

DEAN = 86.69 RUN # 60890.2201

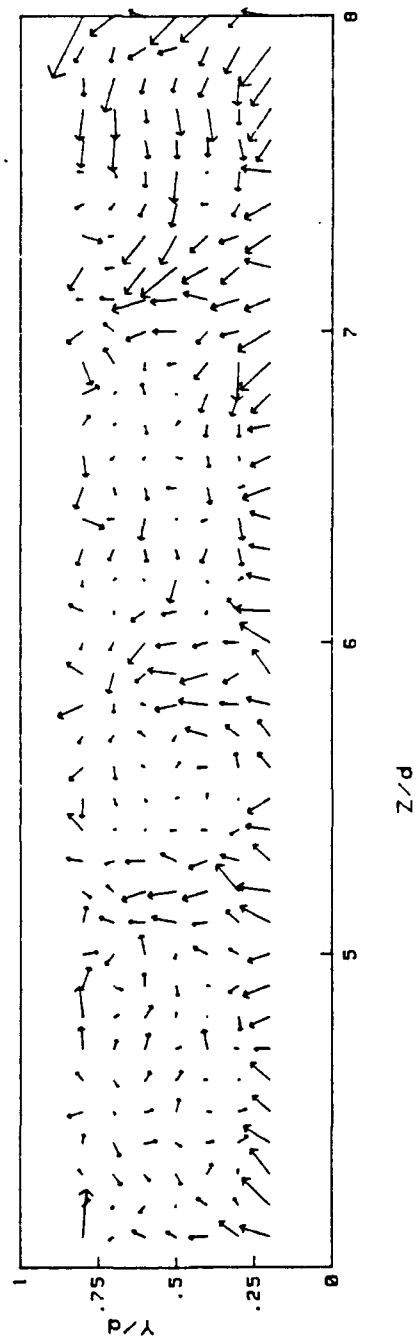


Figure 45. Plot of Velocity Vectors for $De = 86.69$

VELOCITY VECTORS IN CURVED CHANNEL FLOW

— .0752M/S

DEAN = 99.9 RUN # 52690.1331

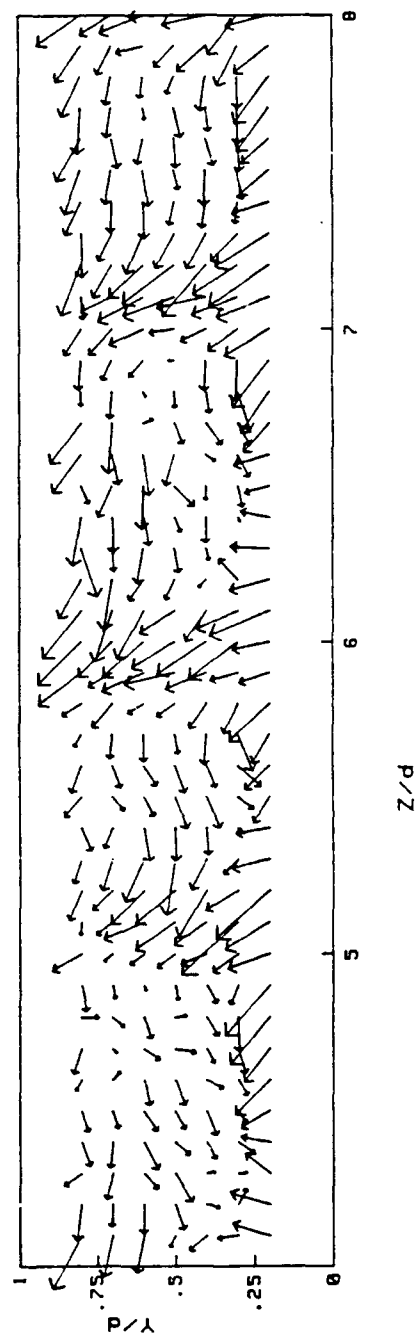


Figure 46. Plot of Velocity Vectors for $De = 99.9$

VELOCITY VECTORS IN CURVED CHANNEL FLOW
 .0948M/S
 DEAN = 149.8 RUN # 52790.0901

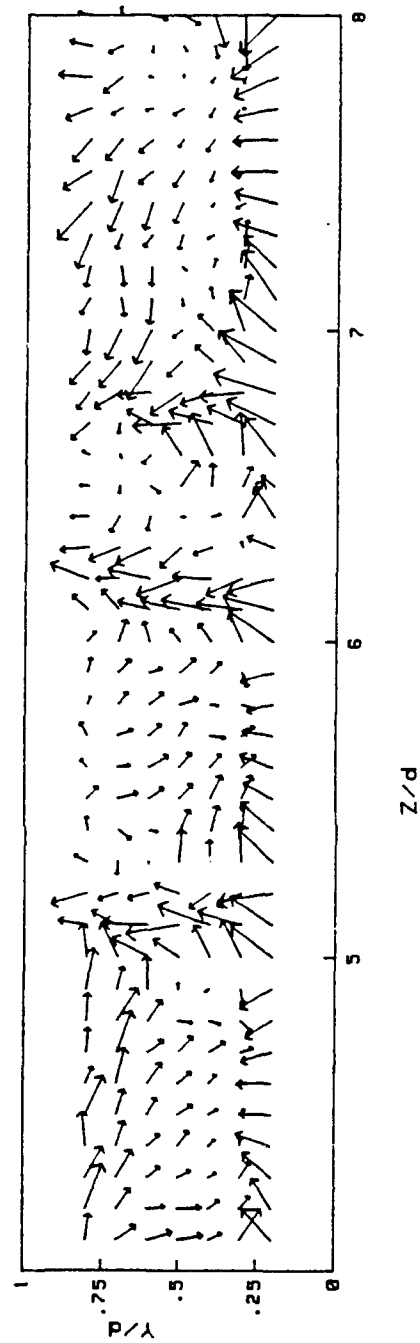


Figure 47. Plot of Velocity Vectors for $De = 149.8$

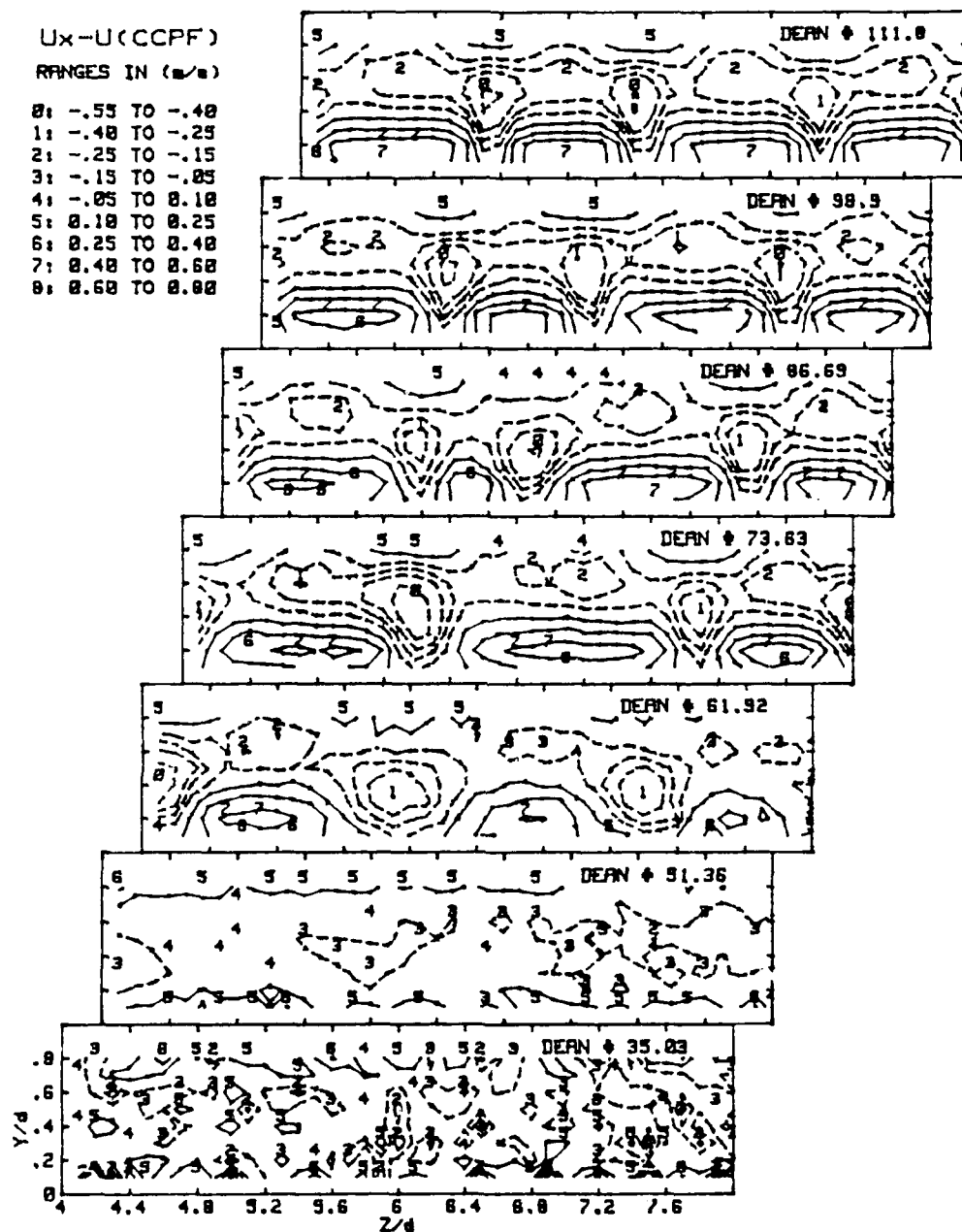


Figure 48. Velocity Perturbation Contours, $De = 35.0$ to $De = 111.8$

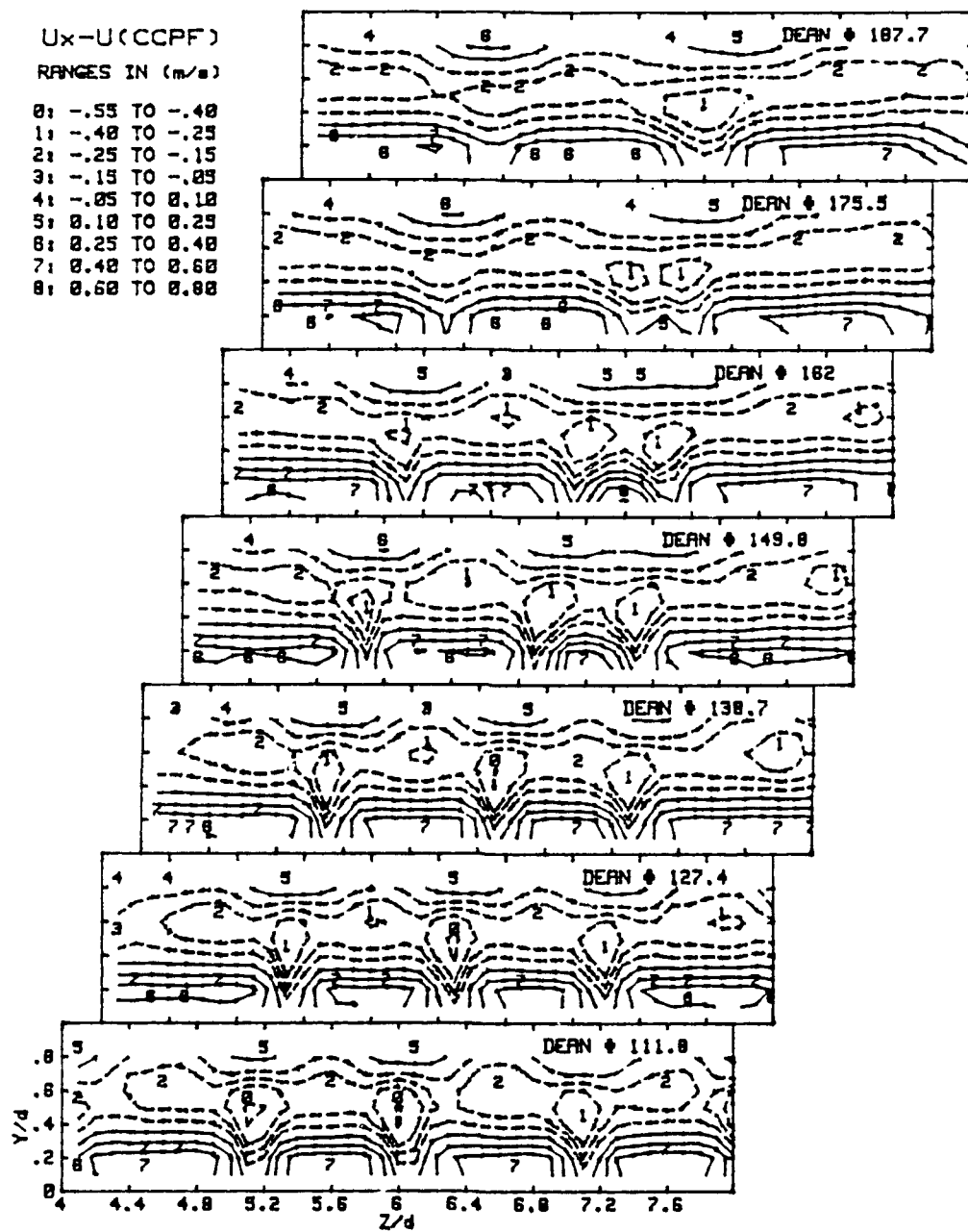


Figure 49. Velocity Perturbation Contours, $De = 111.8$ to $De = 187.7$

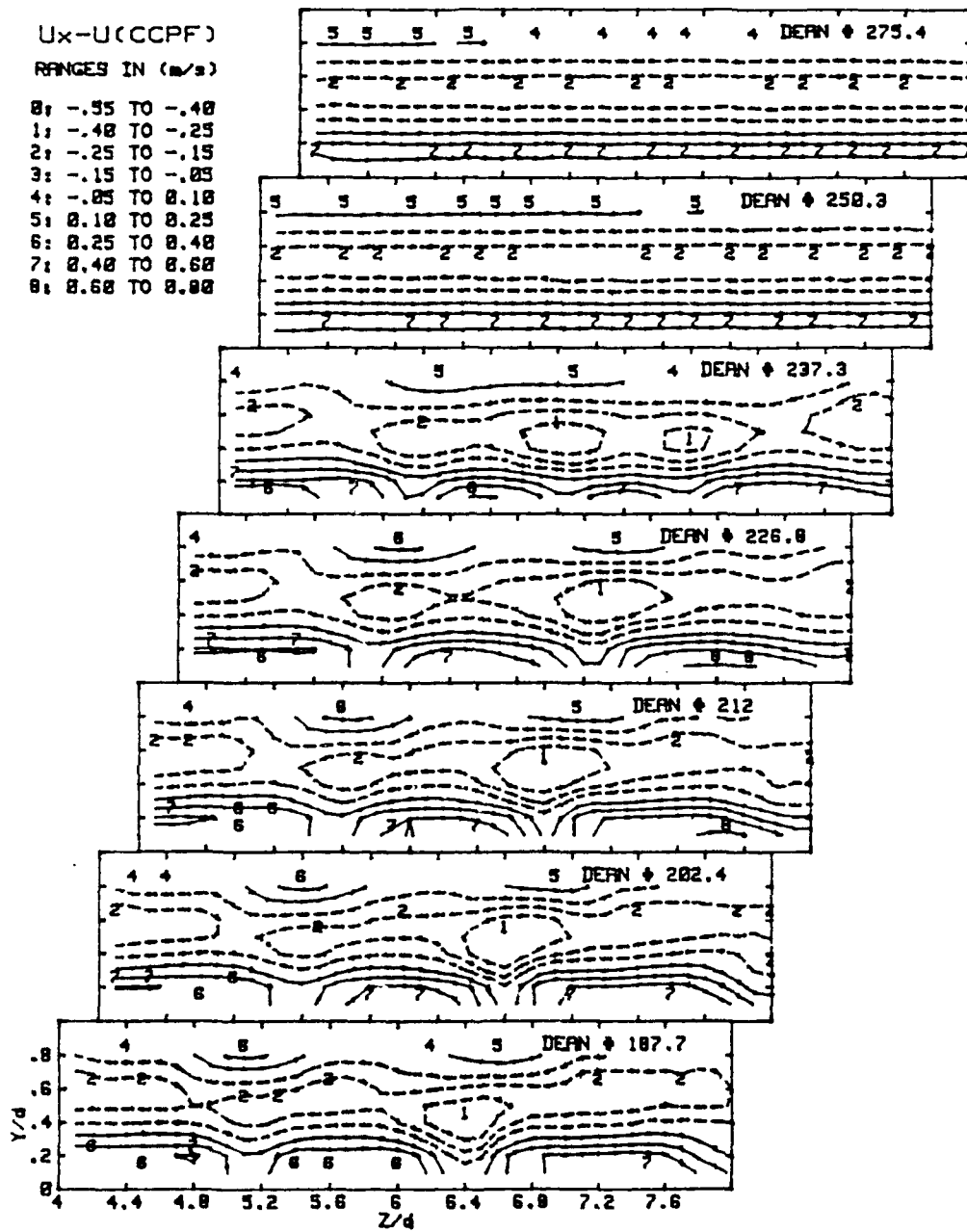


Figure 50. Velocity Perturbation Contours, $De = 187.7$ to $De = 275.4$

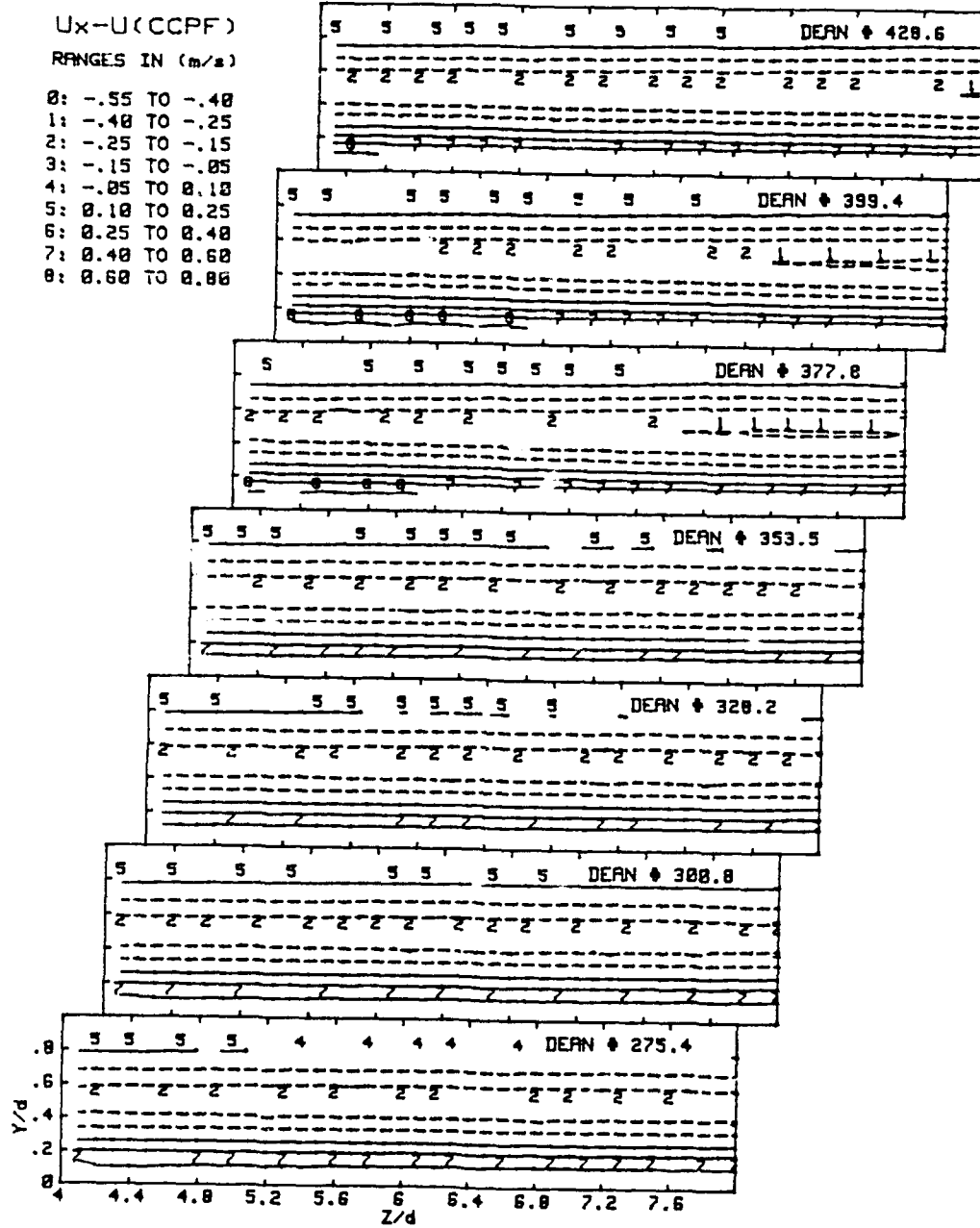


Figure 51. Velocity Perturbation Contours, $De = 275.4$ to $De = 428.6$

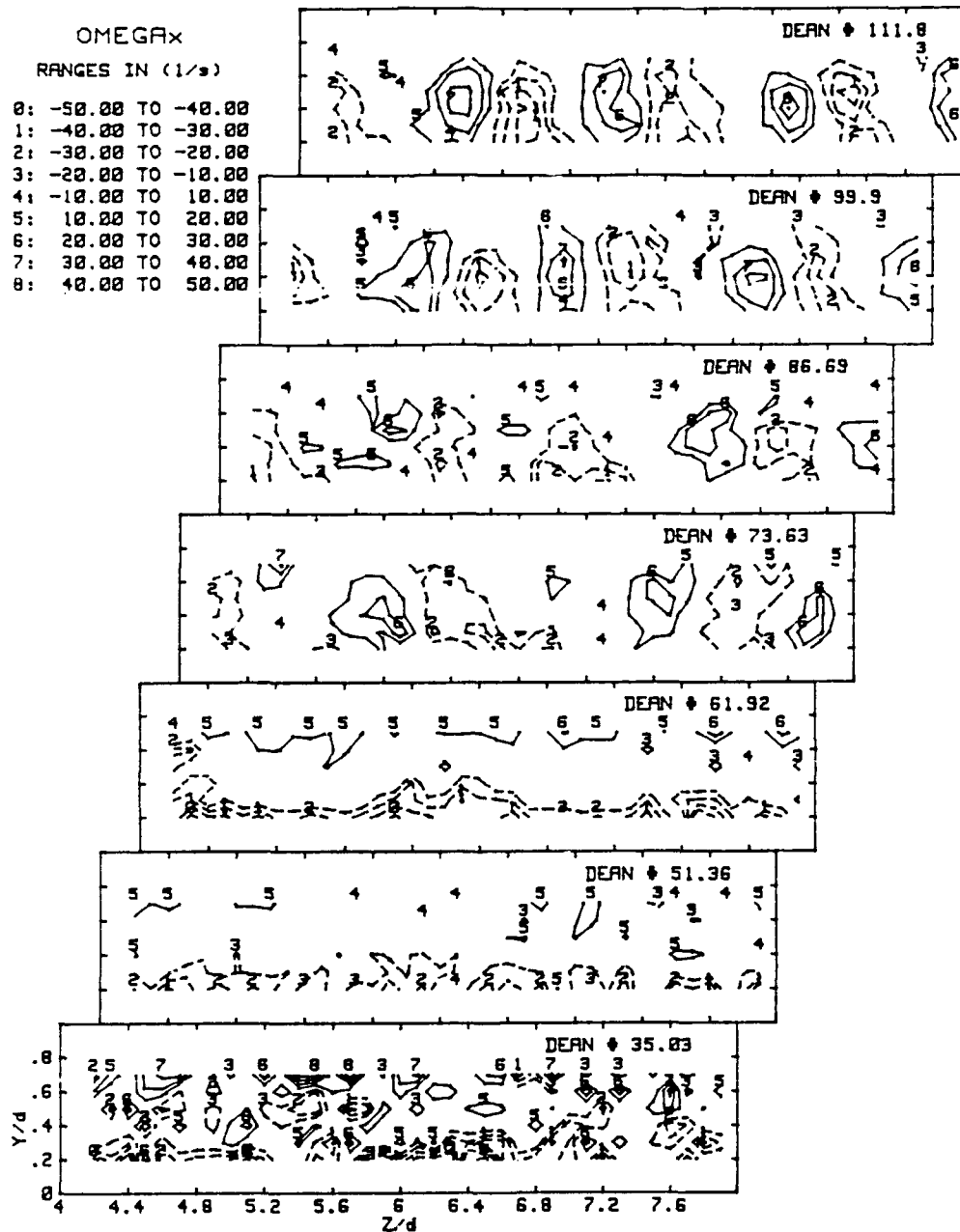


Figure 52. Streamwise Vorticity Contours, $De = 35.0$ to $De = 111.8$

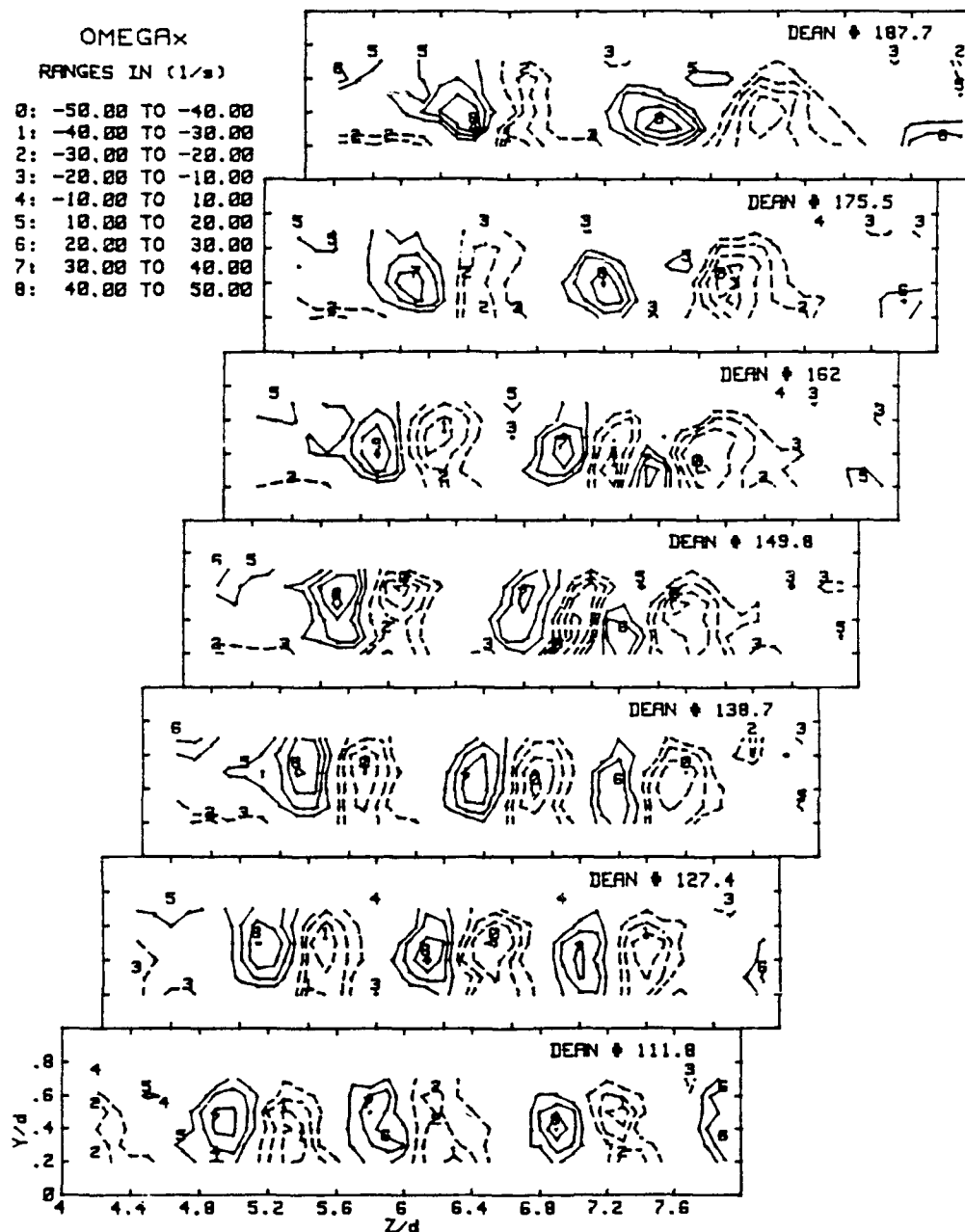


Figure 53. Streamwise Vorticity Contours, $De = 111.8$ to $De = 187.7$

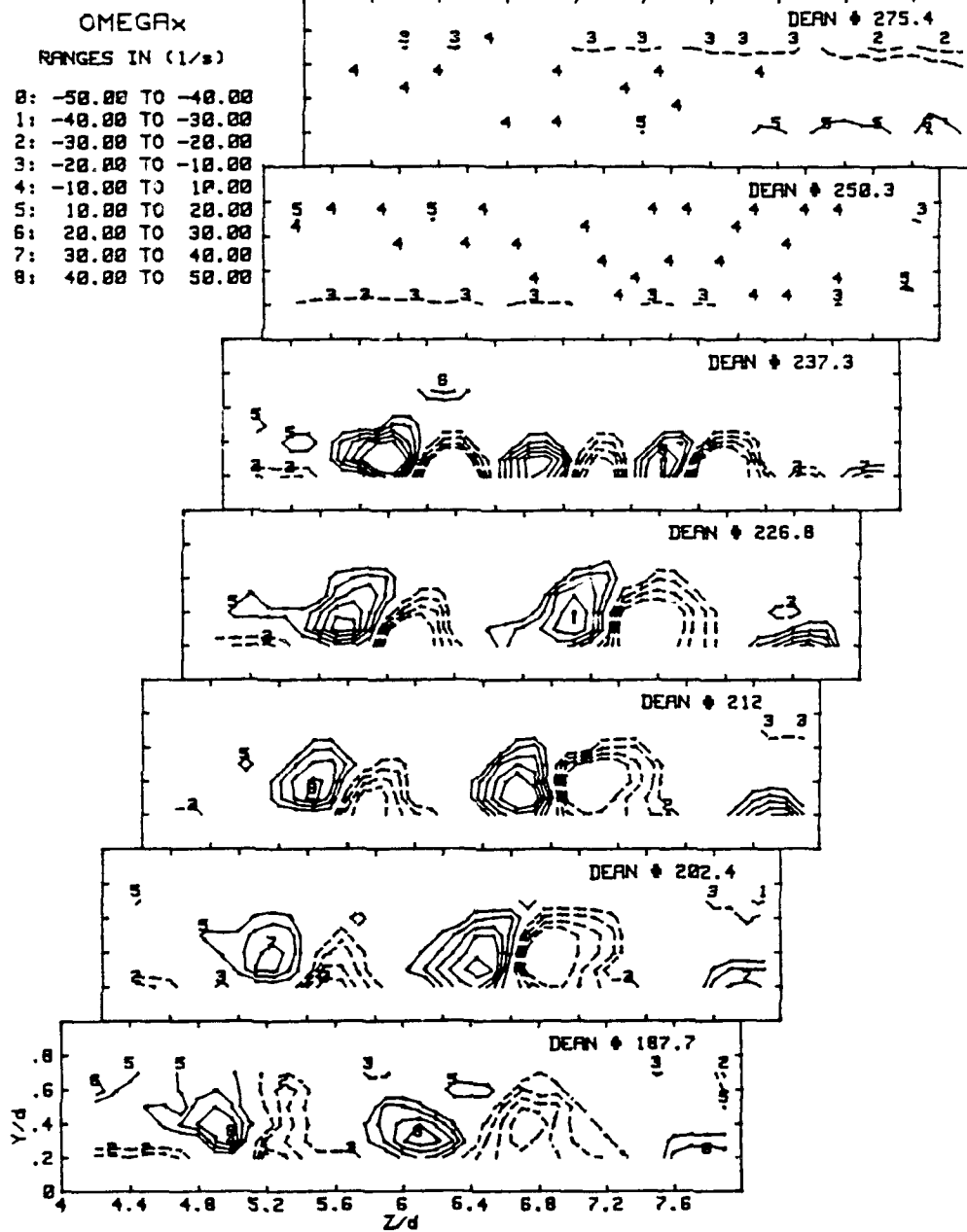


Figure 54. Streamwise Vorticity Contours, $De = 187.7$ to $De = 275.4$

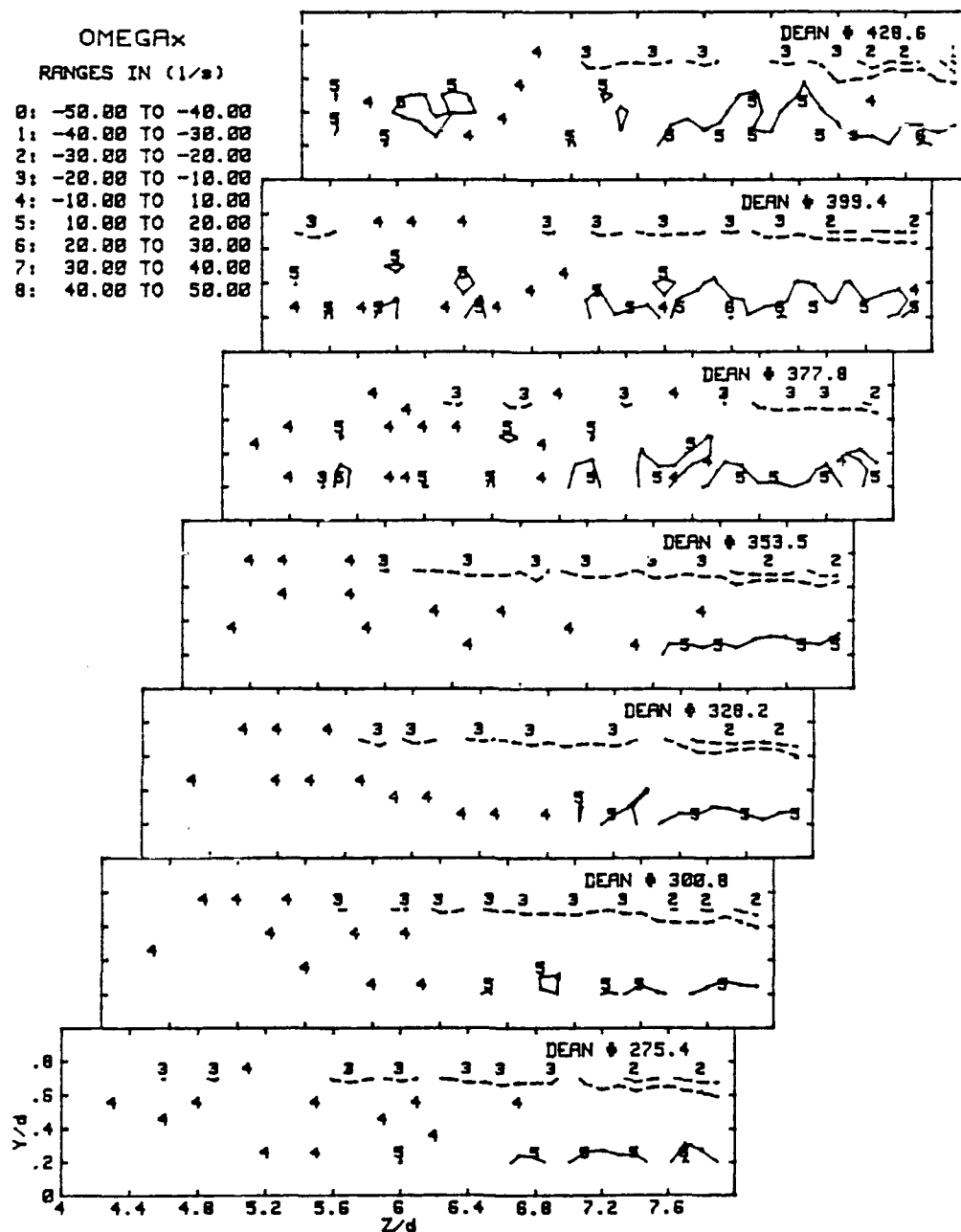


Figure 55. Streamwise Vorticity Contours, $De = 275.4$ to $De = 428.6$

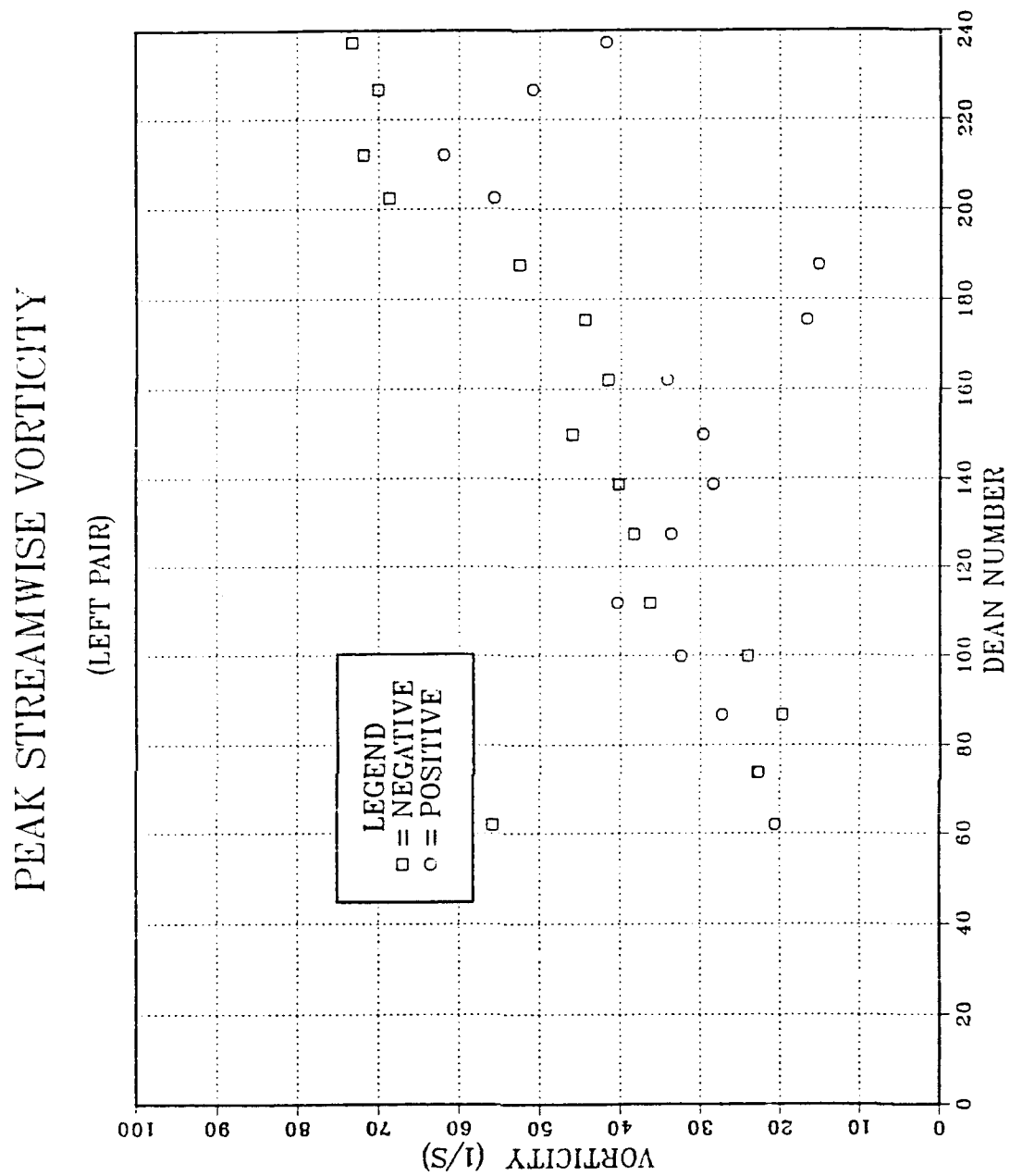


Figure 56. Peak Streamwise Vorticity vs. Dean Number, Left Vortex Pair

PEAK STREAMWISE VORTICITY

(MIDDLE PAIR)

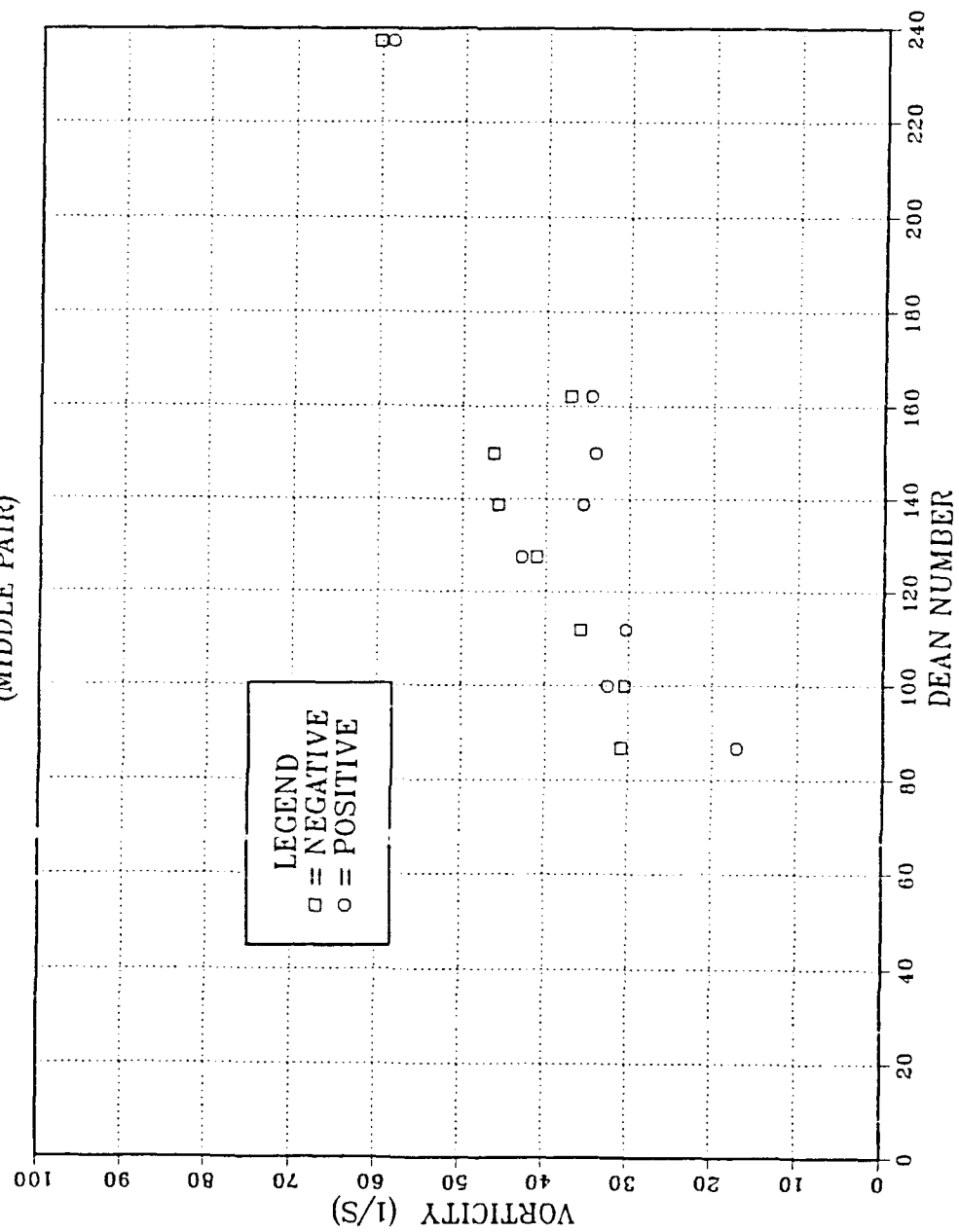


Figure 57. Peak Streamwise Vorticity vs. Dean Number, Middle Vortex Pair

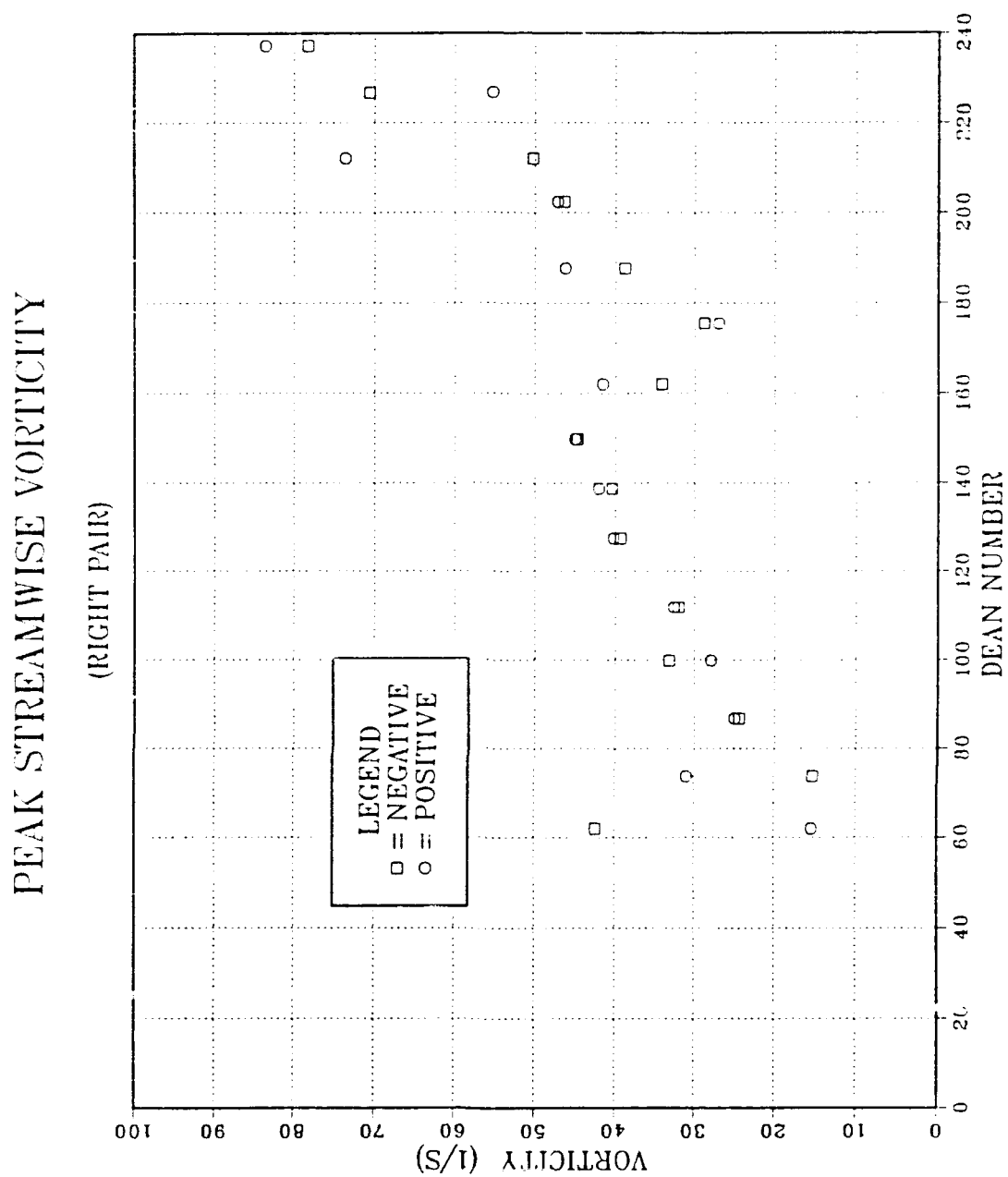


Figure 58. Peak Streamwise Vorticity vs. Dean Number, Right Vortex Pair

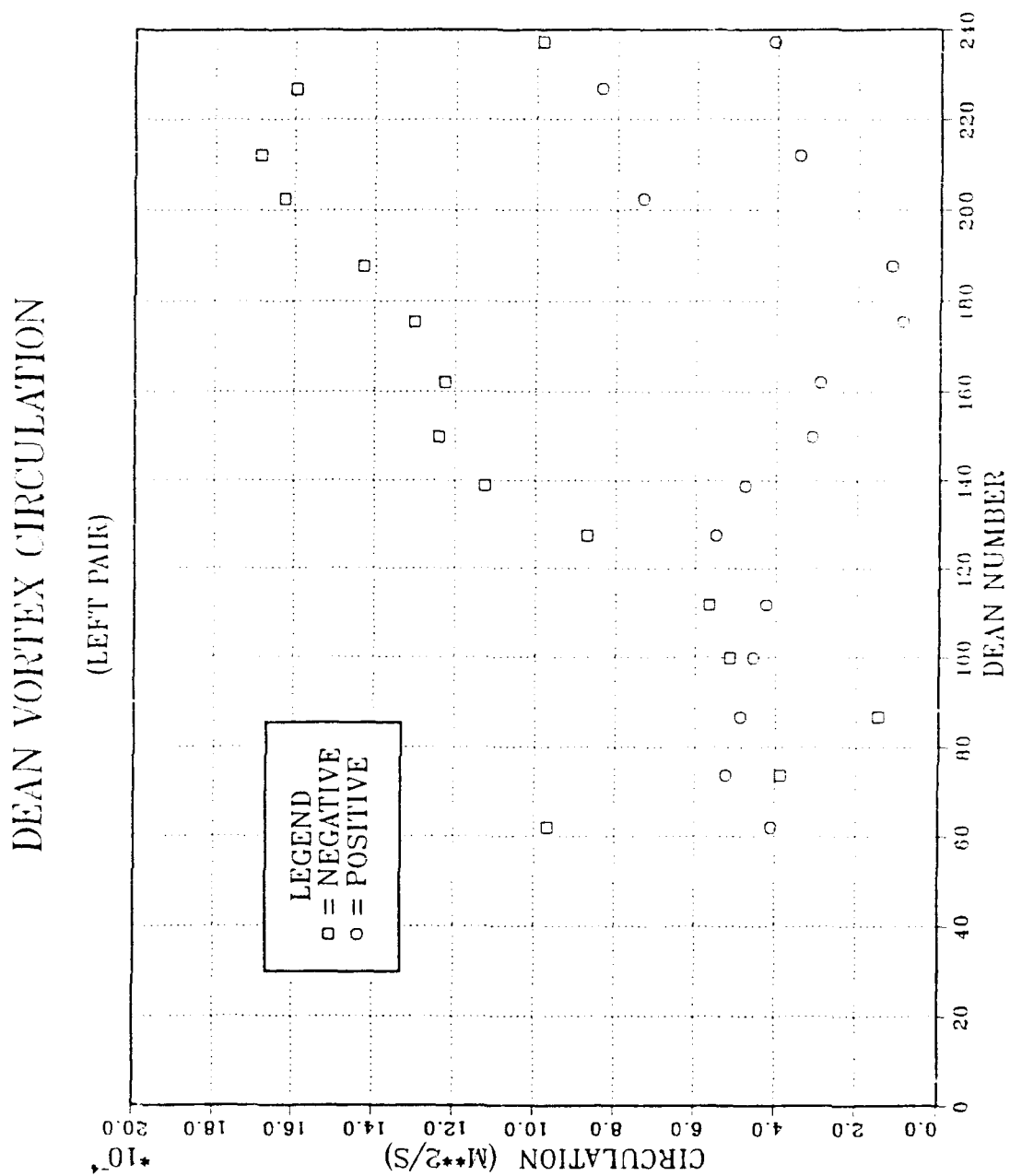


Figure 59. Vortex Circulation vs. Dean Number, Left Vortex Pair

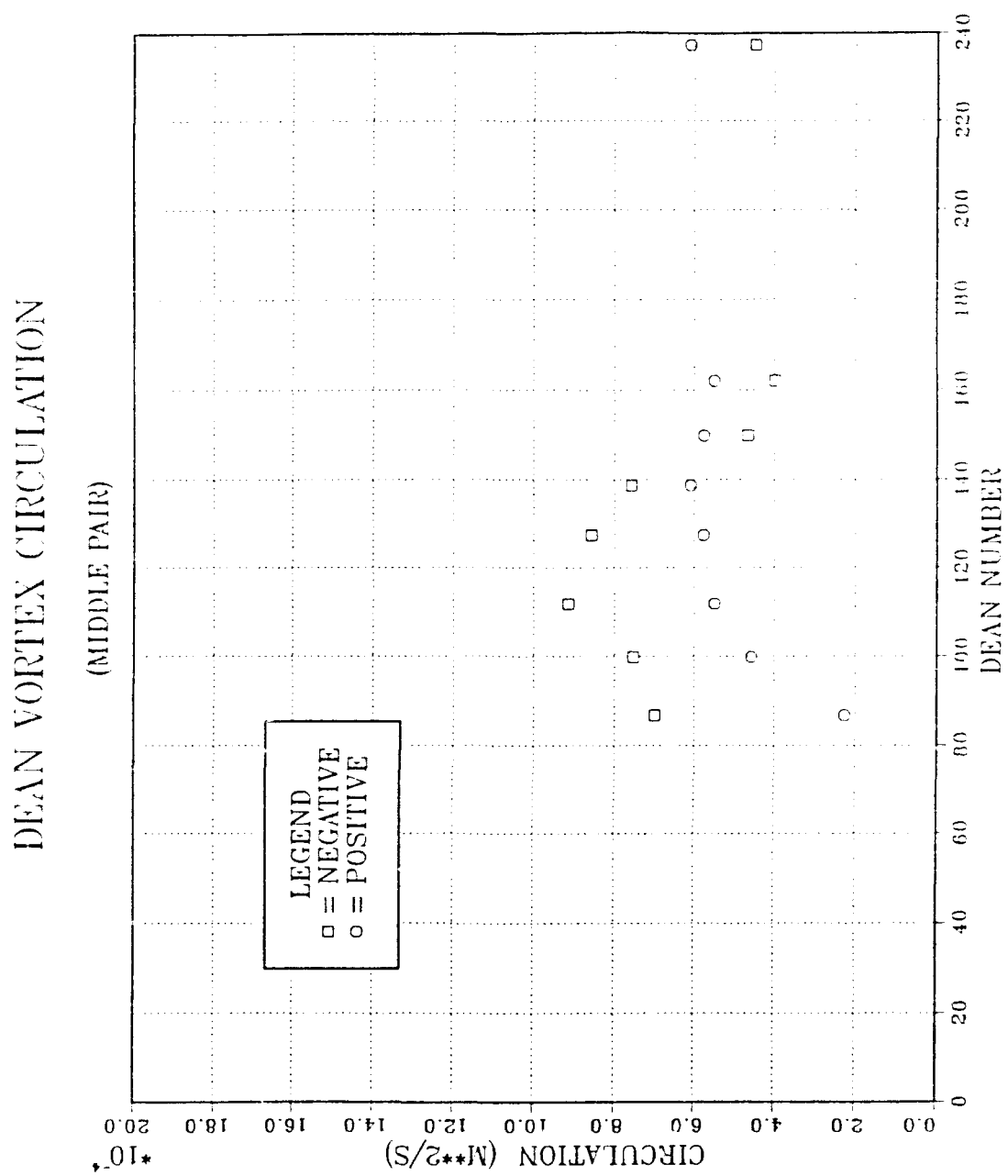


Figure 60. Vortex Circulation vs. Dean Number, Middle Vortex Pair

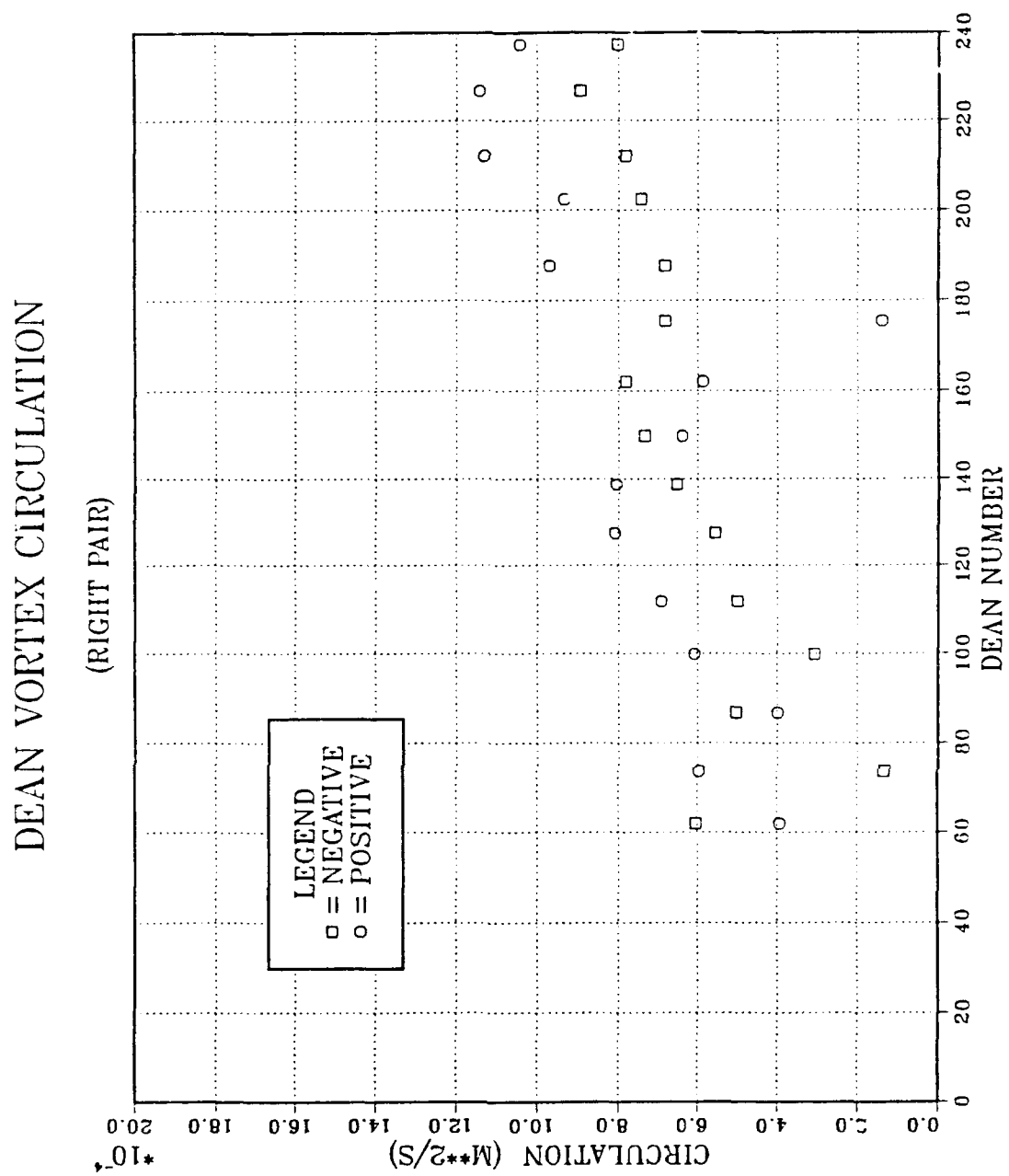


Figure 61. Vortex Circulation vs. Dean Number, Right Vortex Pair

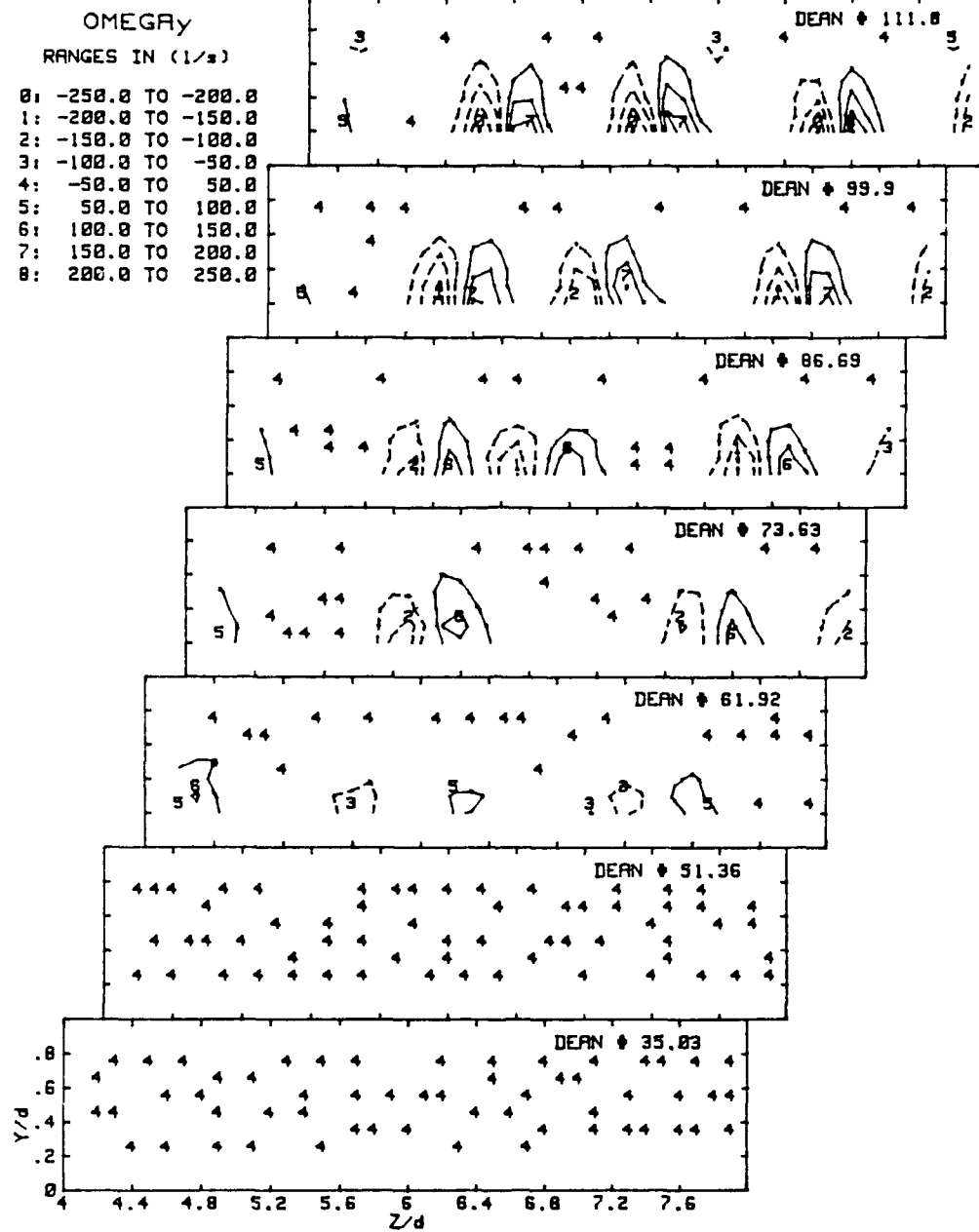


Figure 62. Radial Vorticity Contours, $De = 35.0$ to $De = 111.8$

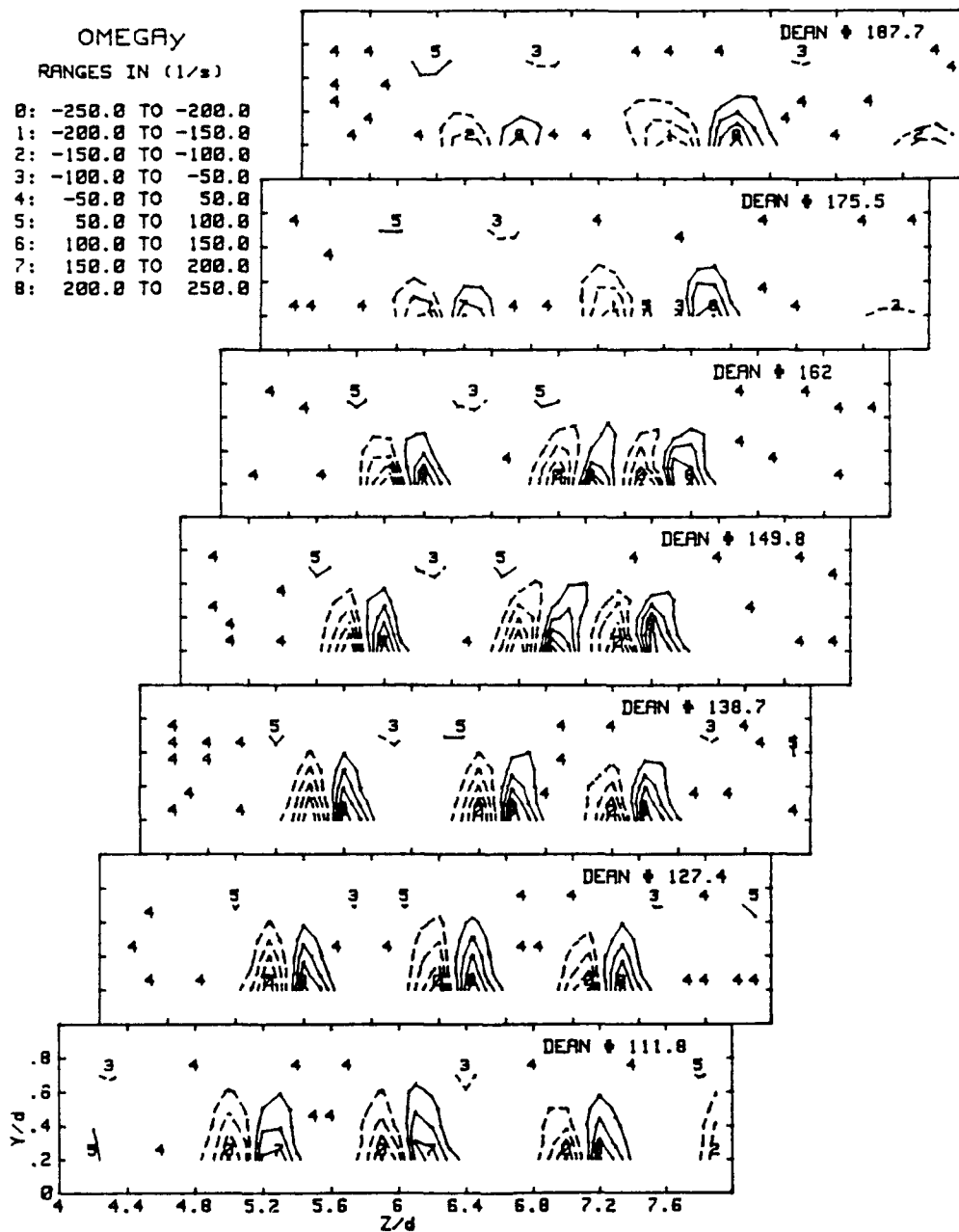


Figure 63. Radial Vorticity Contours, $De = 111.8$ to $De = 187.7$

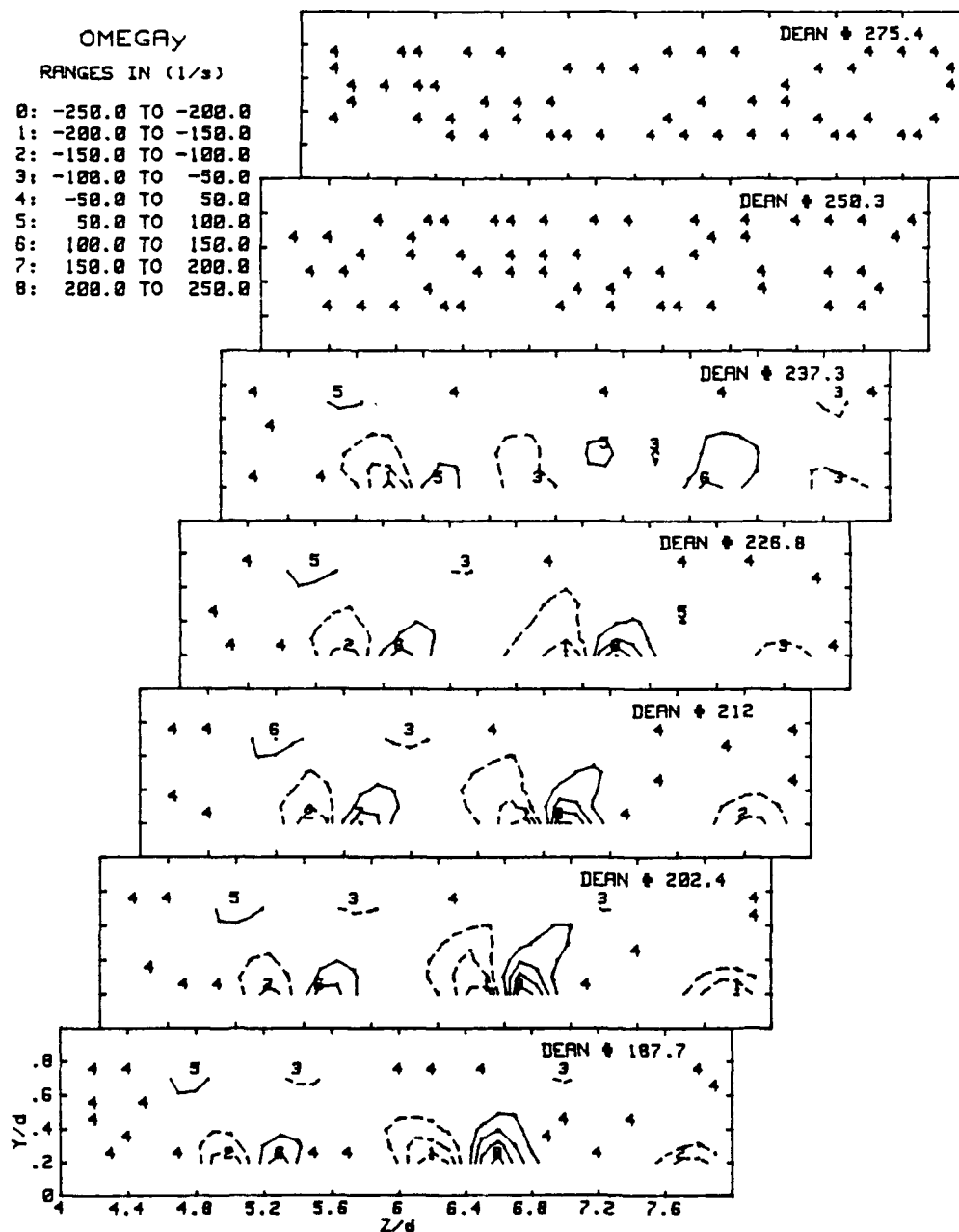


Figure 64. Radial Vorticity Contours, $De = 187.7$ to $De = 275.4$

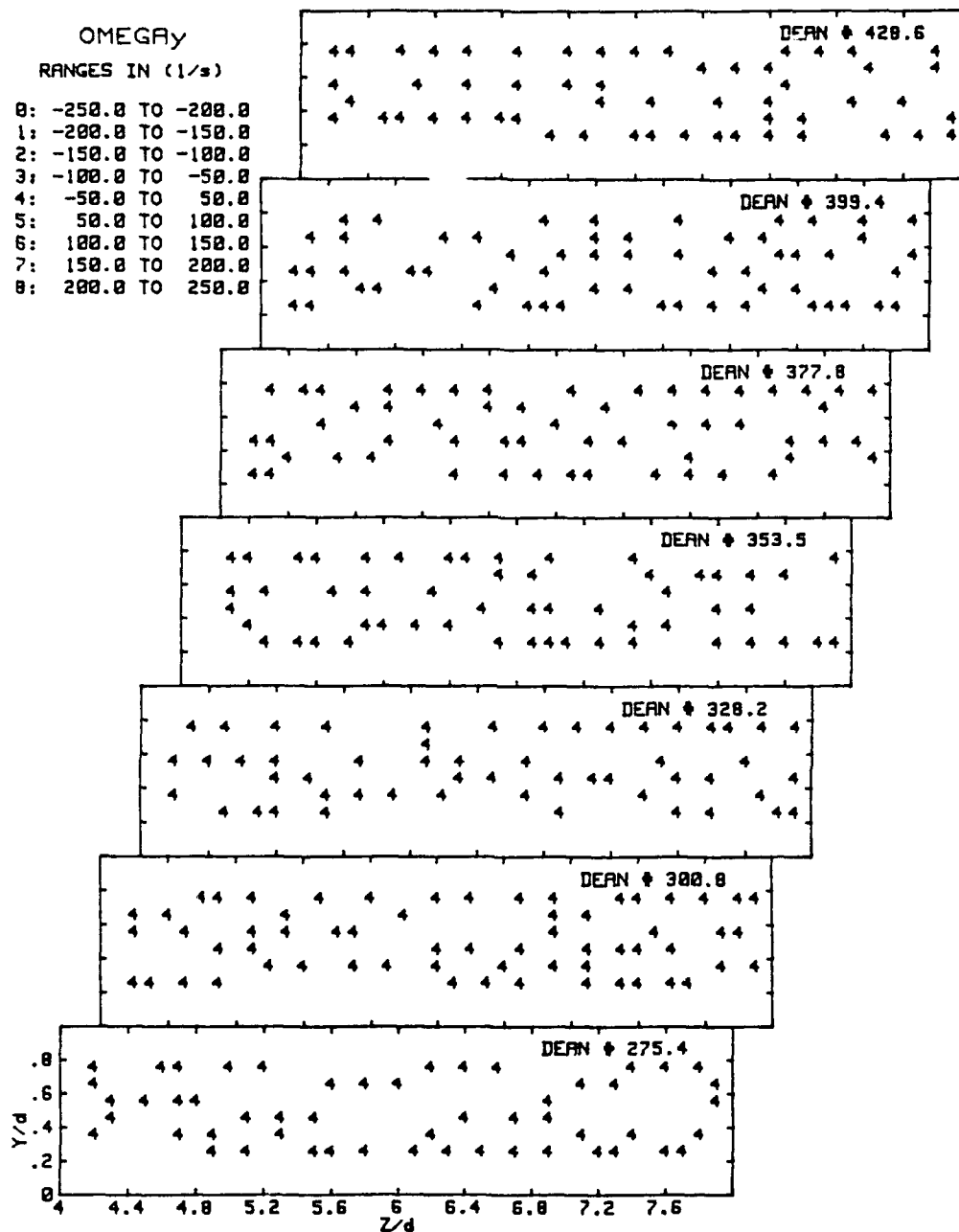


Figure 65. Radial Vorticity Contours, $De = 275.4$ to $De = 428.6$

PEAK RADIAL VORTICITY

(LEFT PAIR)

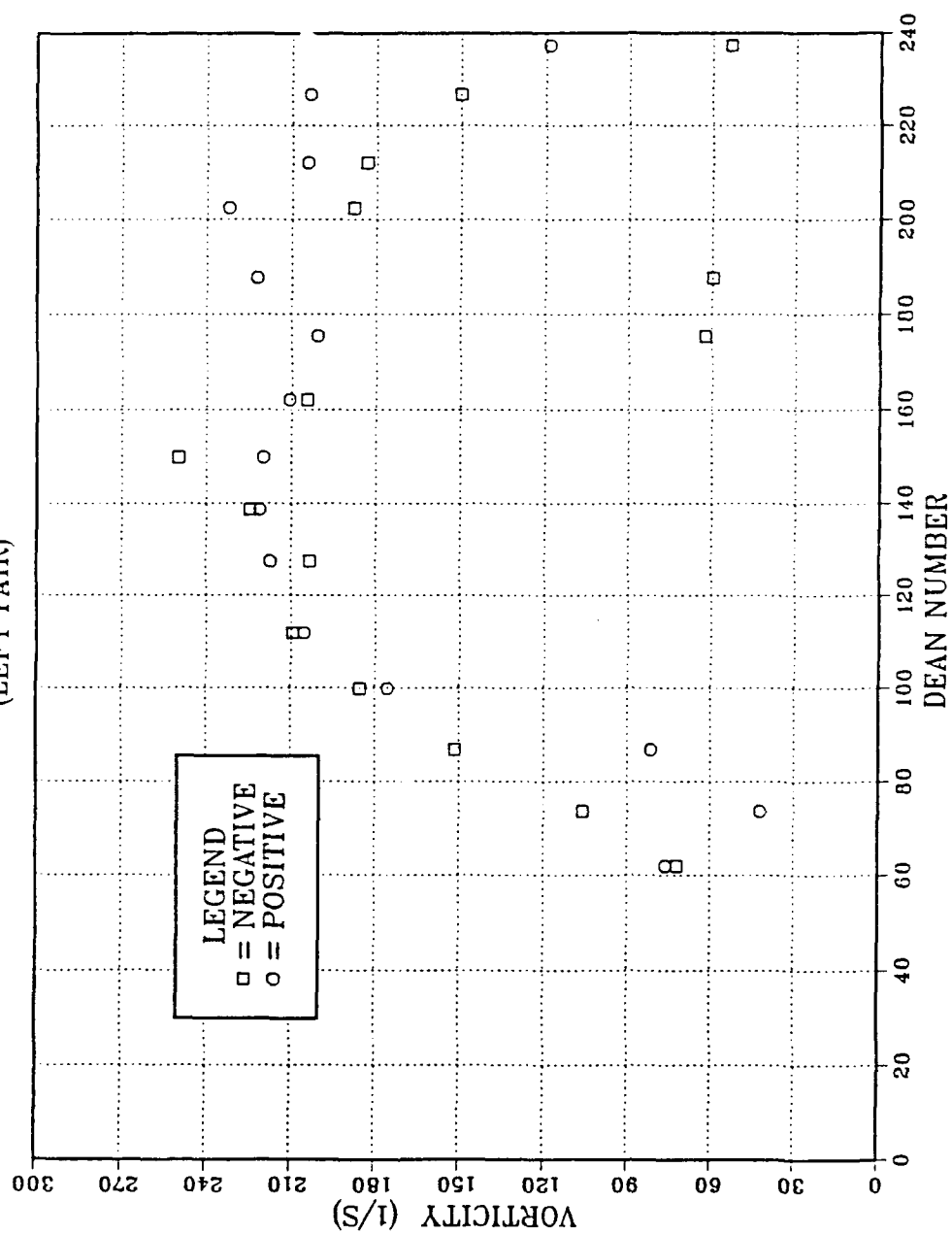


Figure 66. Peak Radial Vorticity vs. Dean Number, Left Vortex Pair

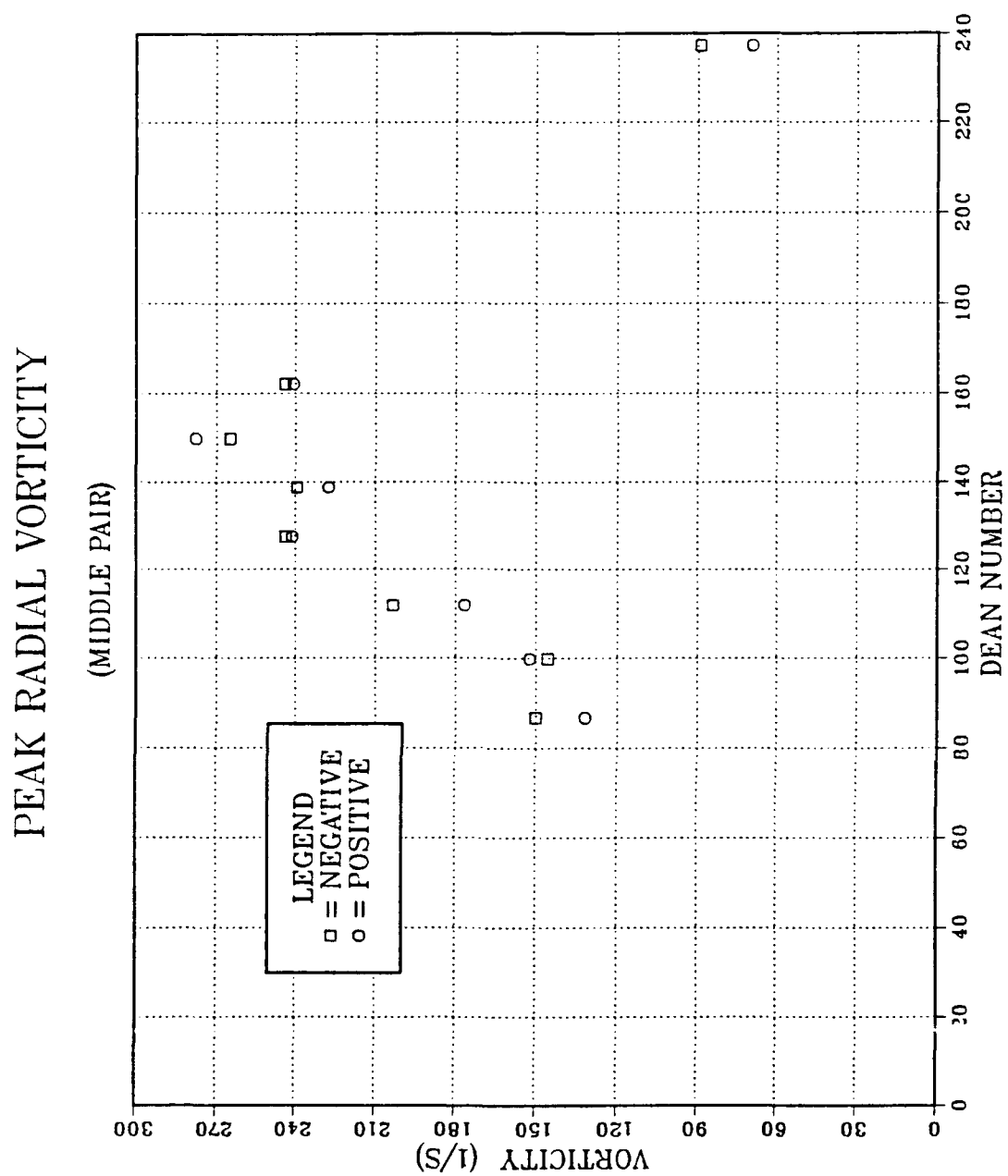


Figure 67. Peak Radial Vorticity vs. Dean Number, Middle Vortex Pair

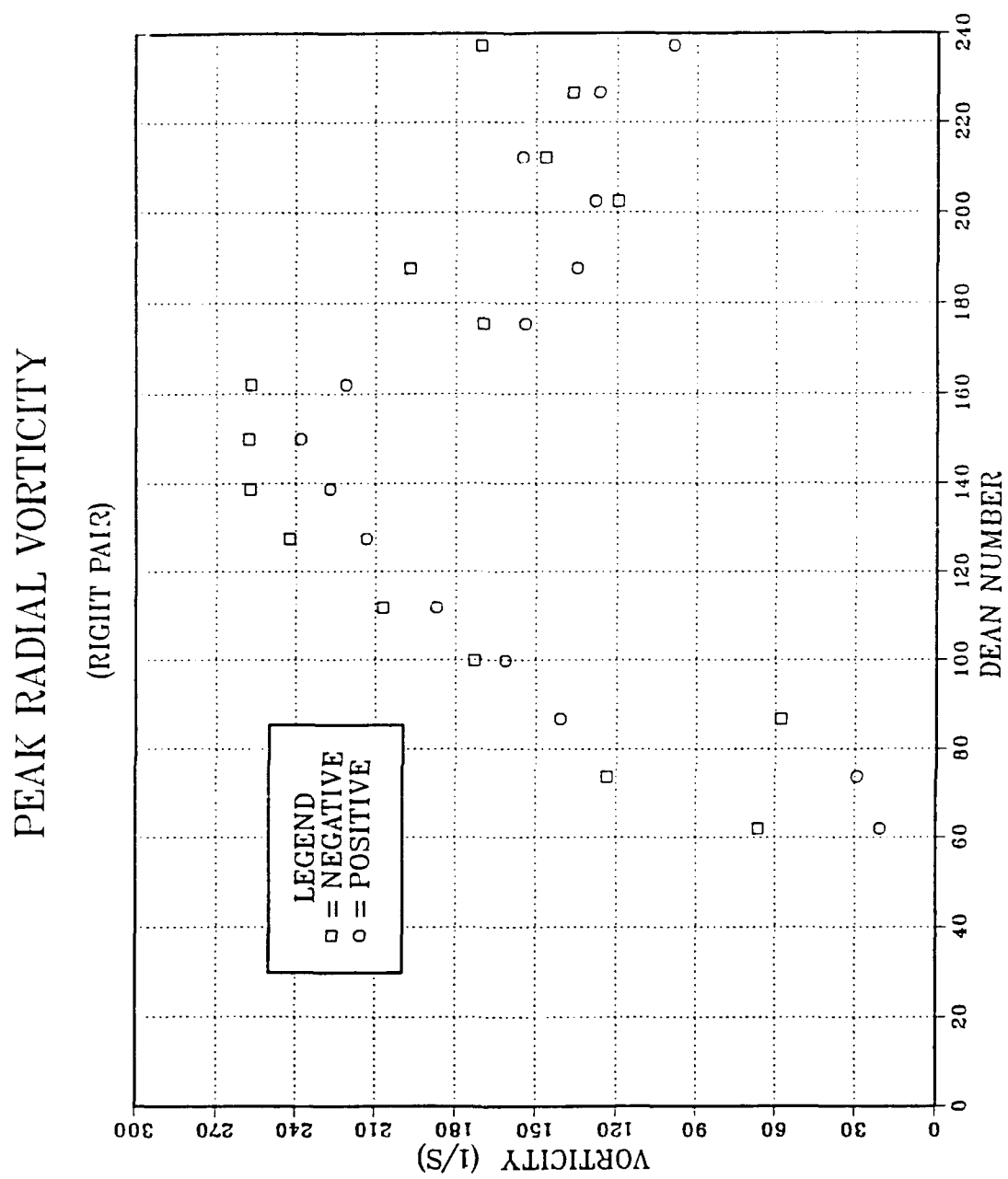


Figure 68. Peak Radial Vorticity vs. Dean Number, Right Vortex Pair

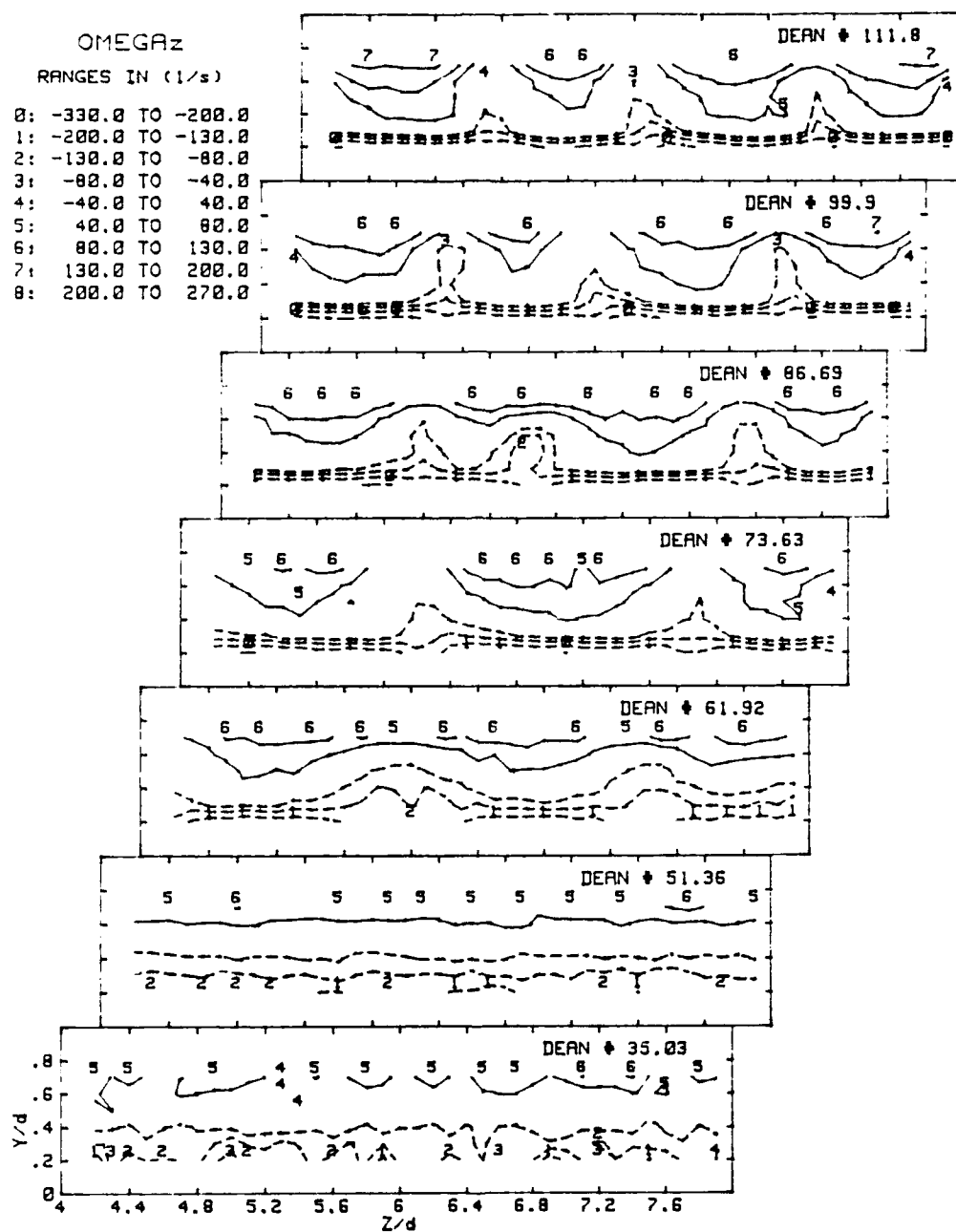


Figure 69. Spanwise Vorticity Contours, $De = 35.0$ to $De = 111.8$

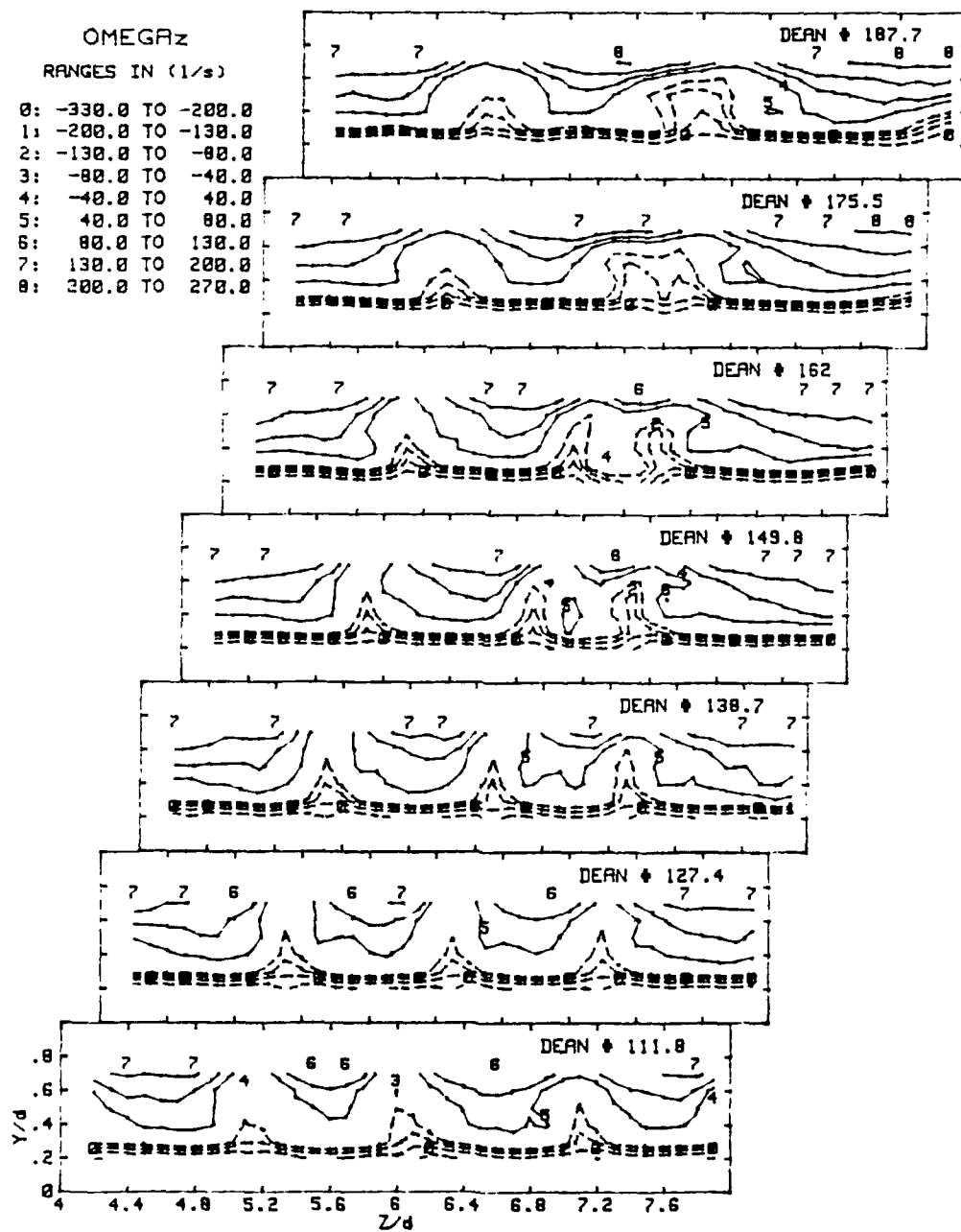


Figure 70. Spanwise Vorticity Contours, $De = 111.8$ to $De = 187.7$

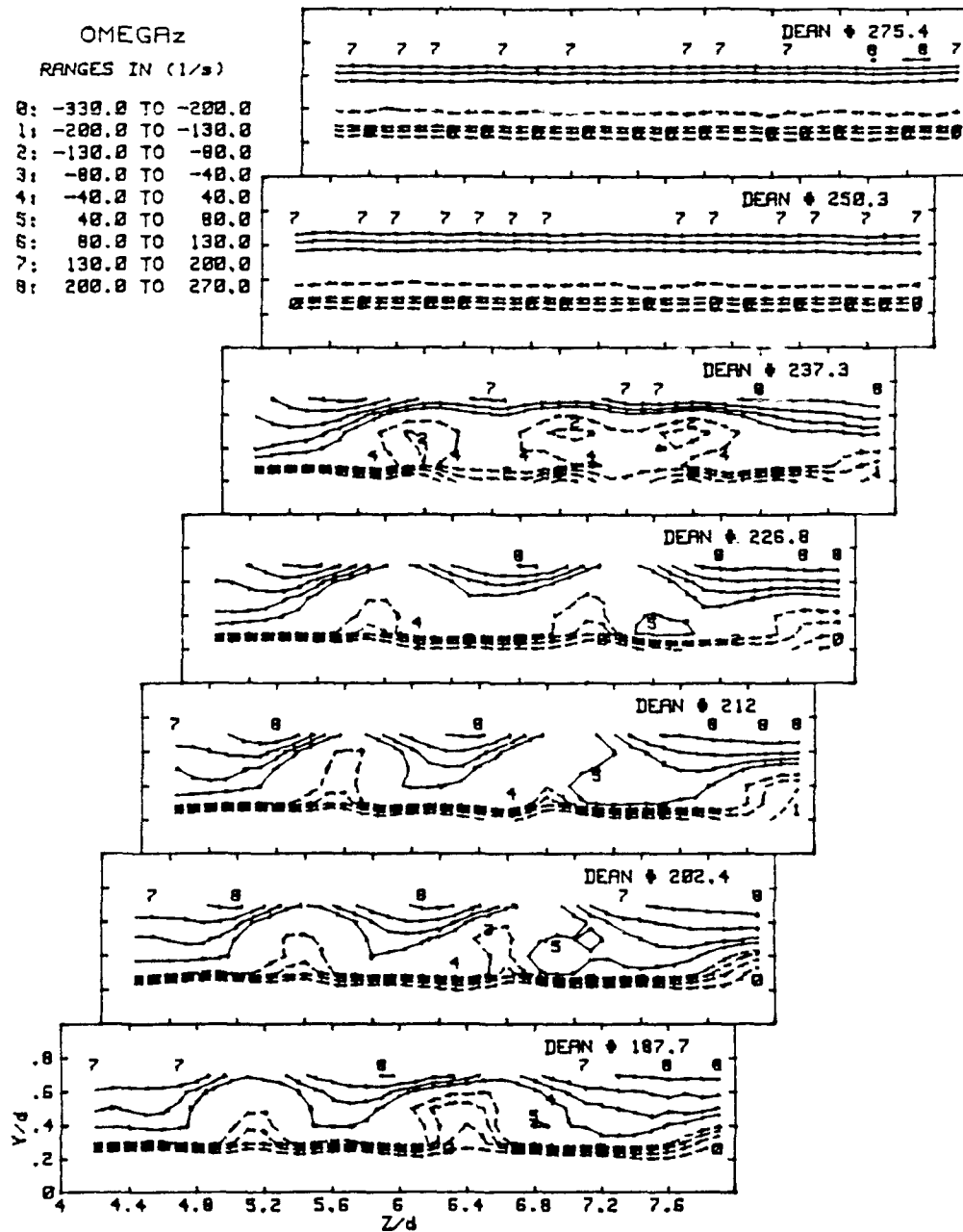


Figure 71. Spanwise Vorticity Contours, $De = 187.7$ to $De = 275.4$

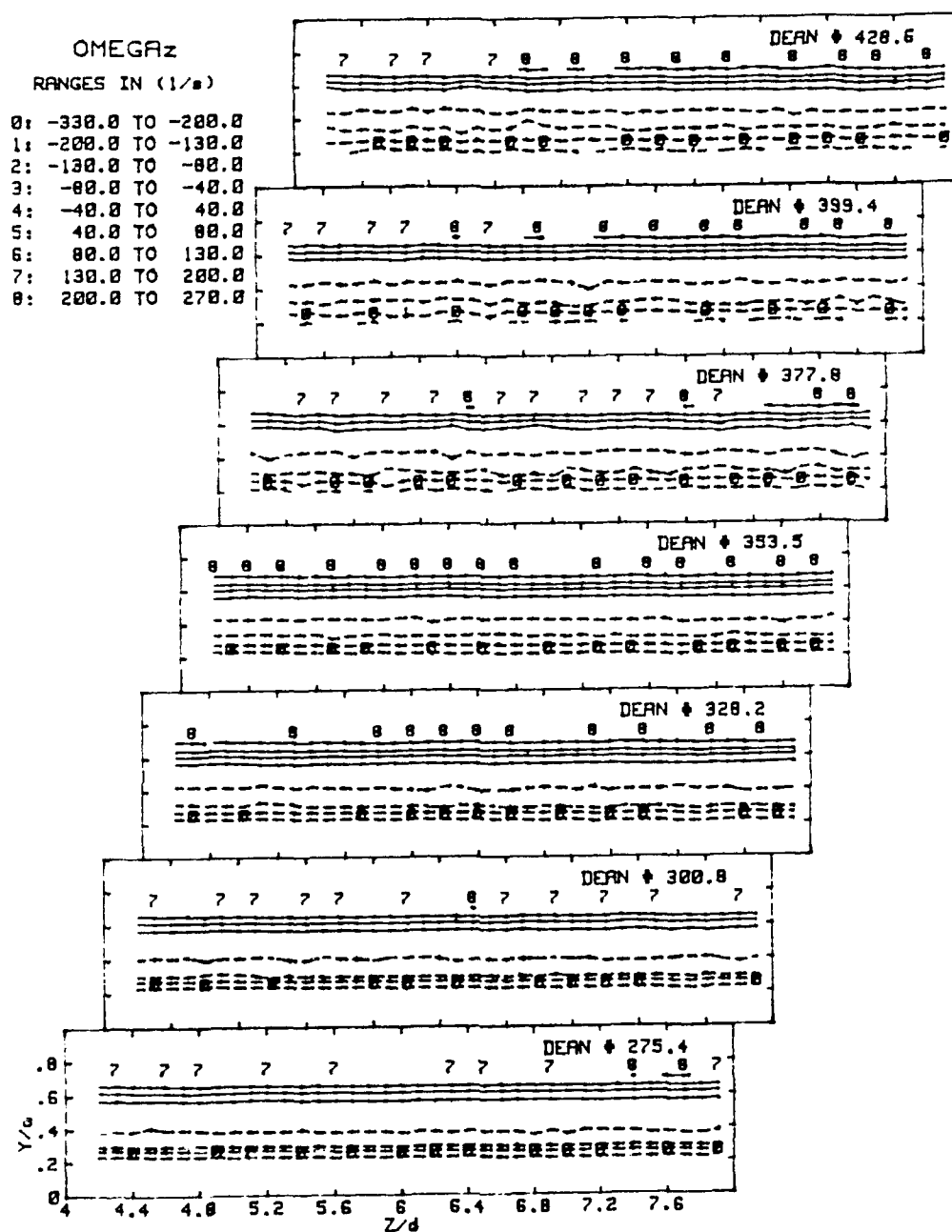


Figure 72. Spanwise Vorticity Contours, $De = 275.4$ to $De = 428.6$

FIVE-HOLE PROBE PROFILES

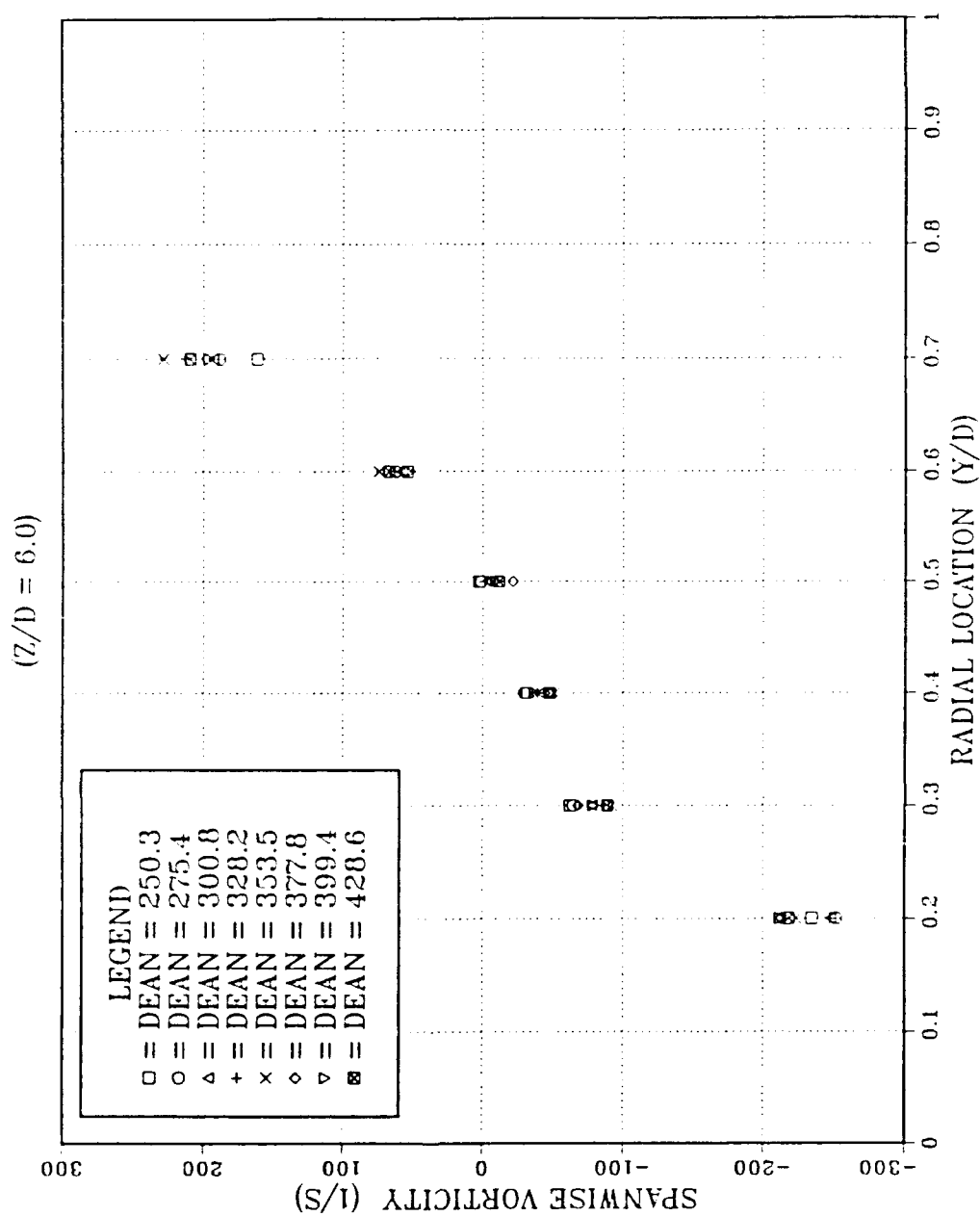


Figure 73. Spanwise Vorticity vs. Radial Location

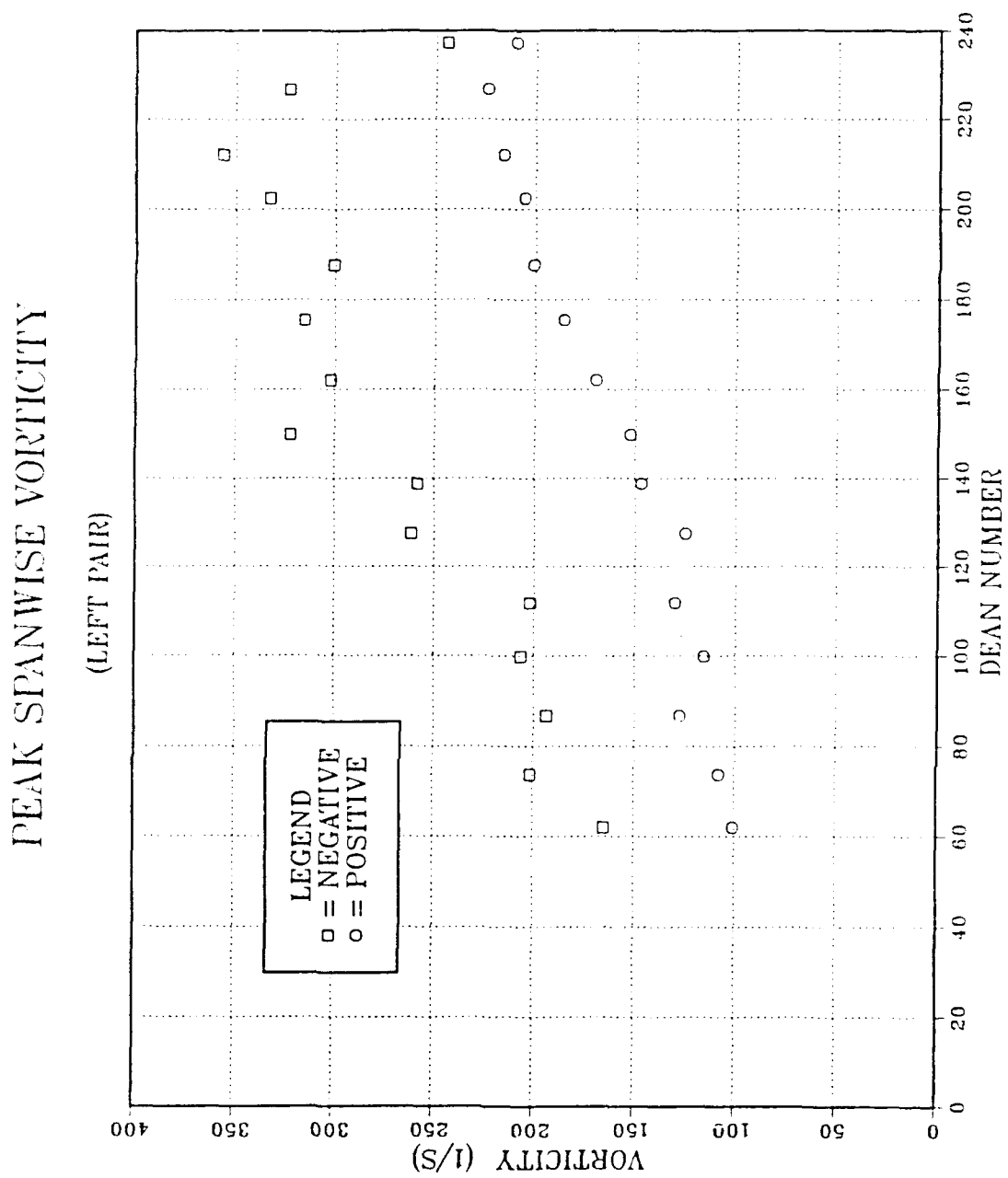


Figure 74. Peak Spanwise Vorticity vs. Dean Number, Left Vortex Pair

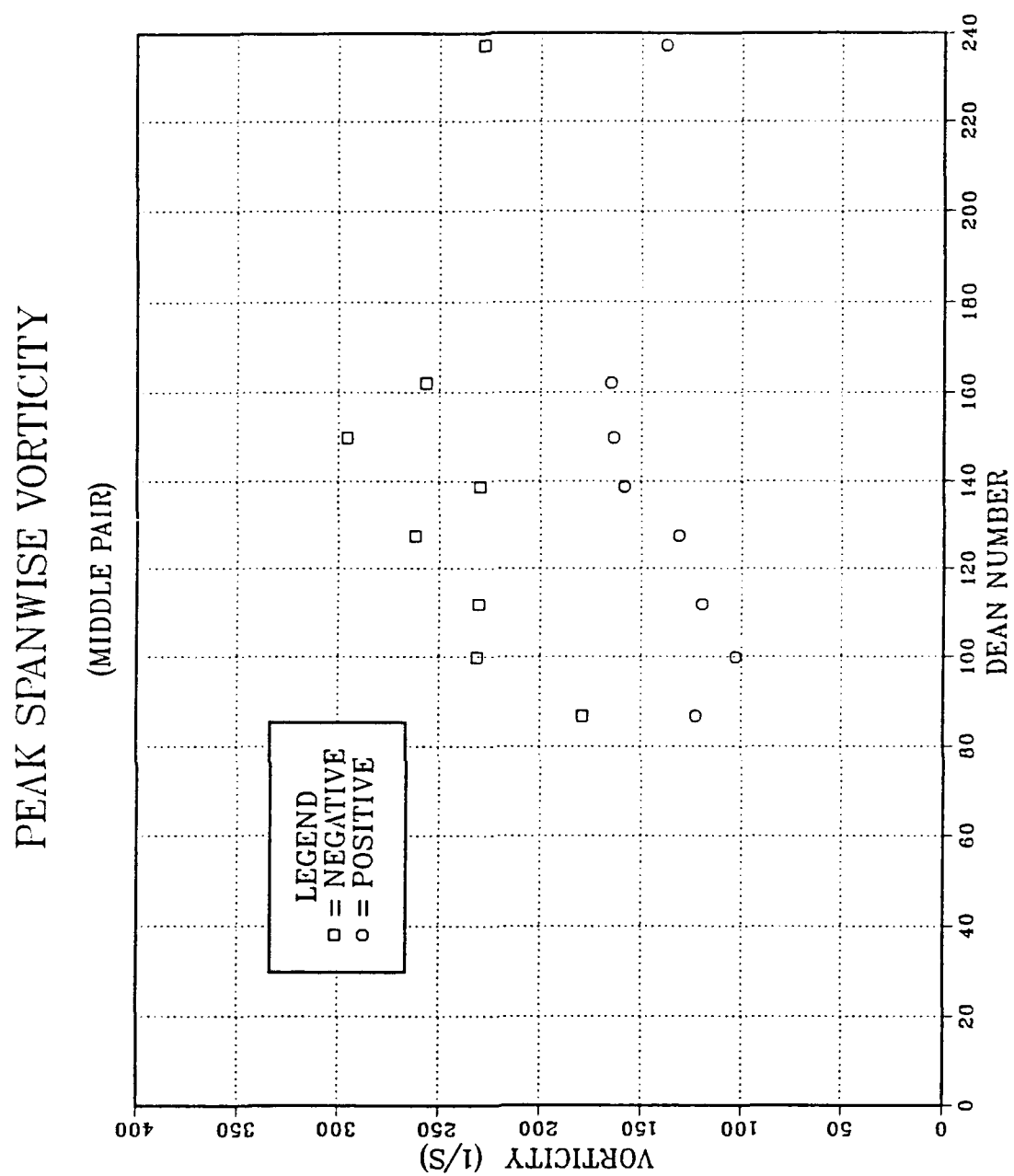


Figure 75. Peak Spanwise Vorticity vs. Dean Number, Middle Vortex Pair

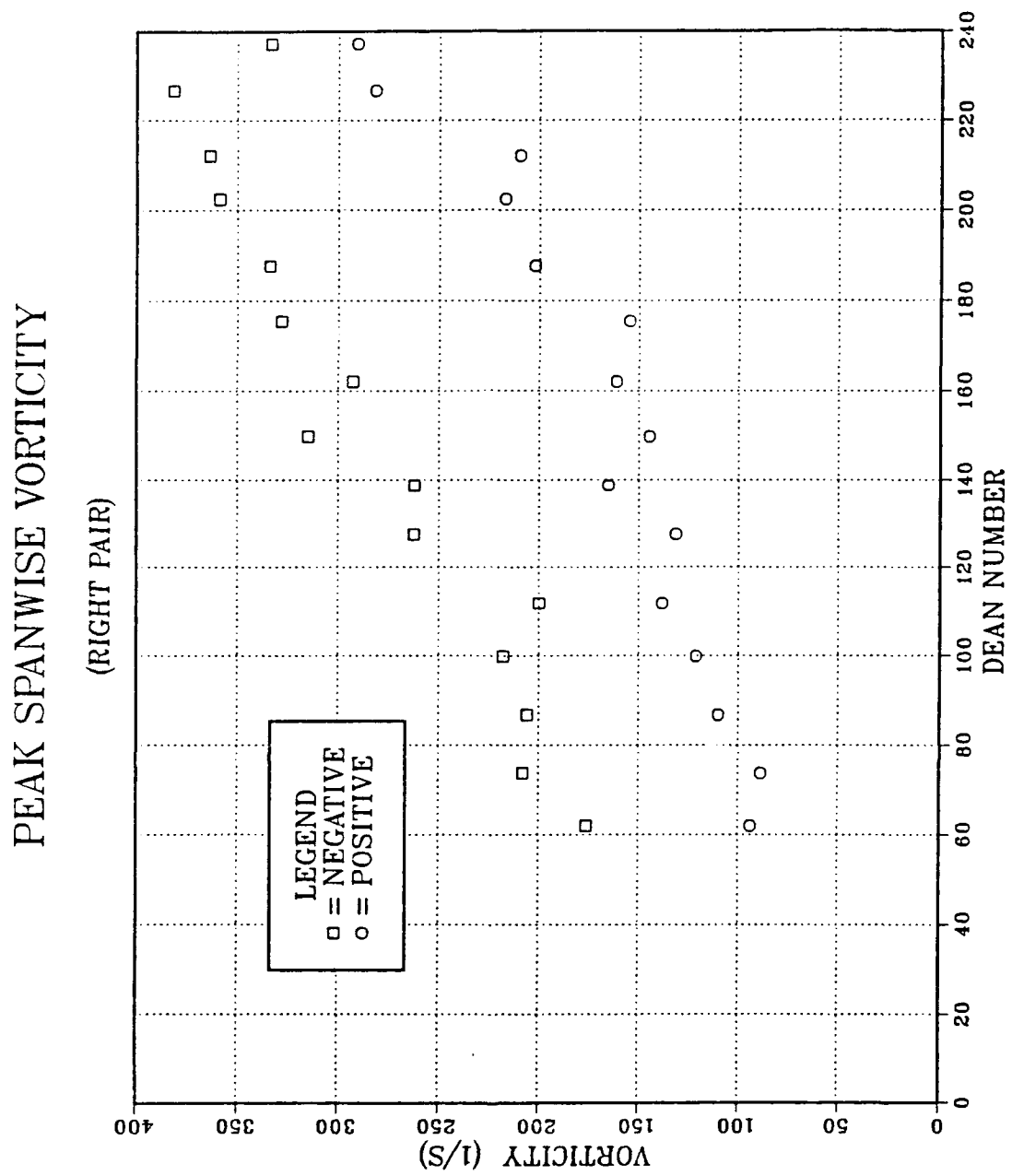


Figure 76. Peak Spanwise Vorticity vs. Dean Number, Right Vortex Pair

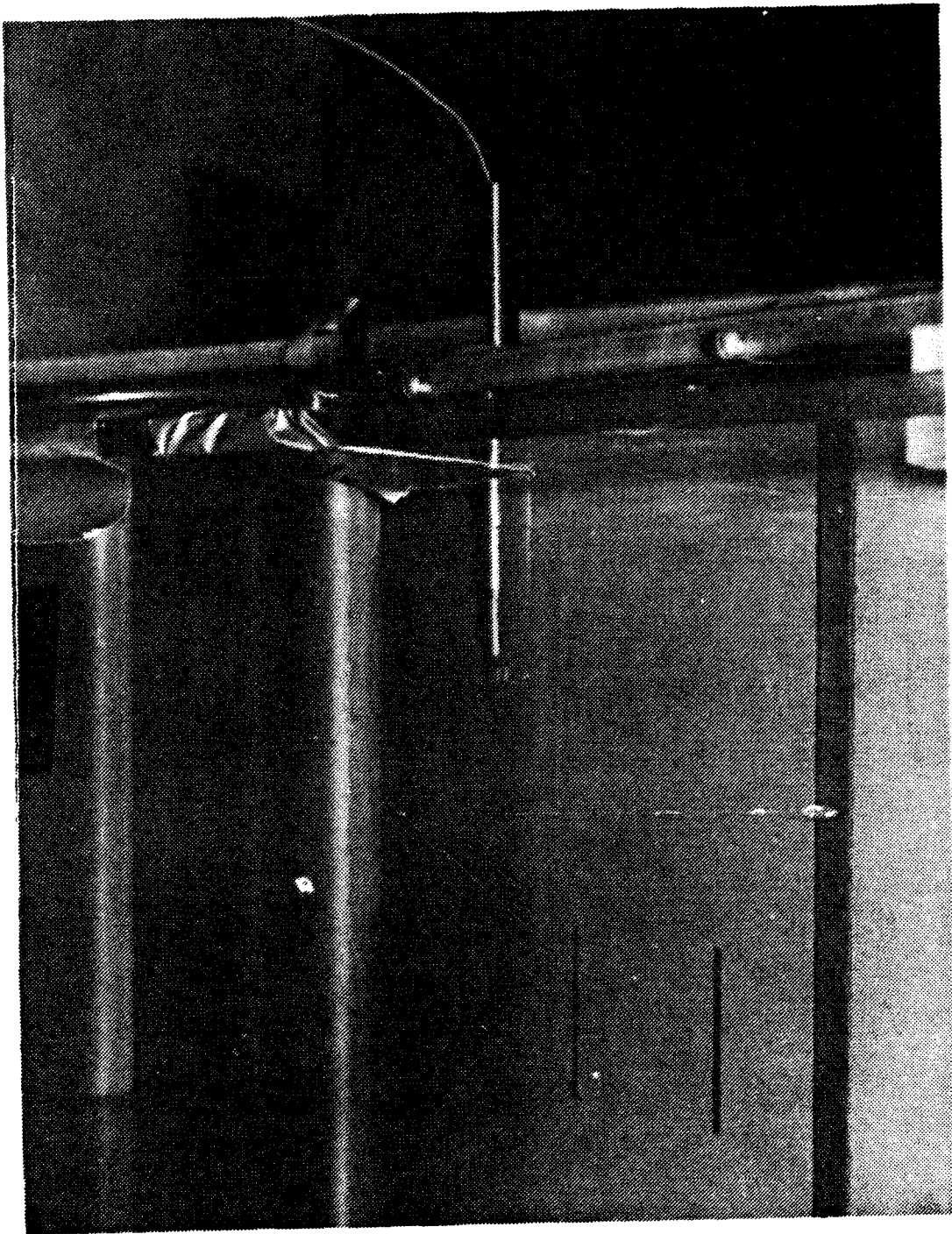


Figure 77. Hot-wire Probe Mounting

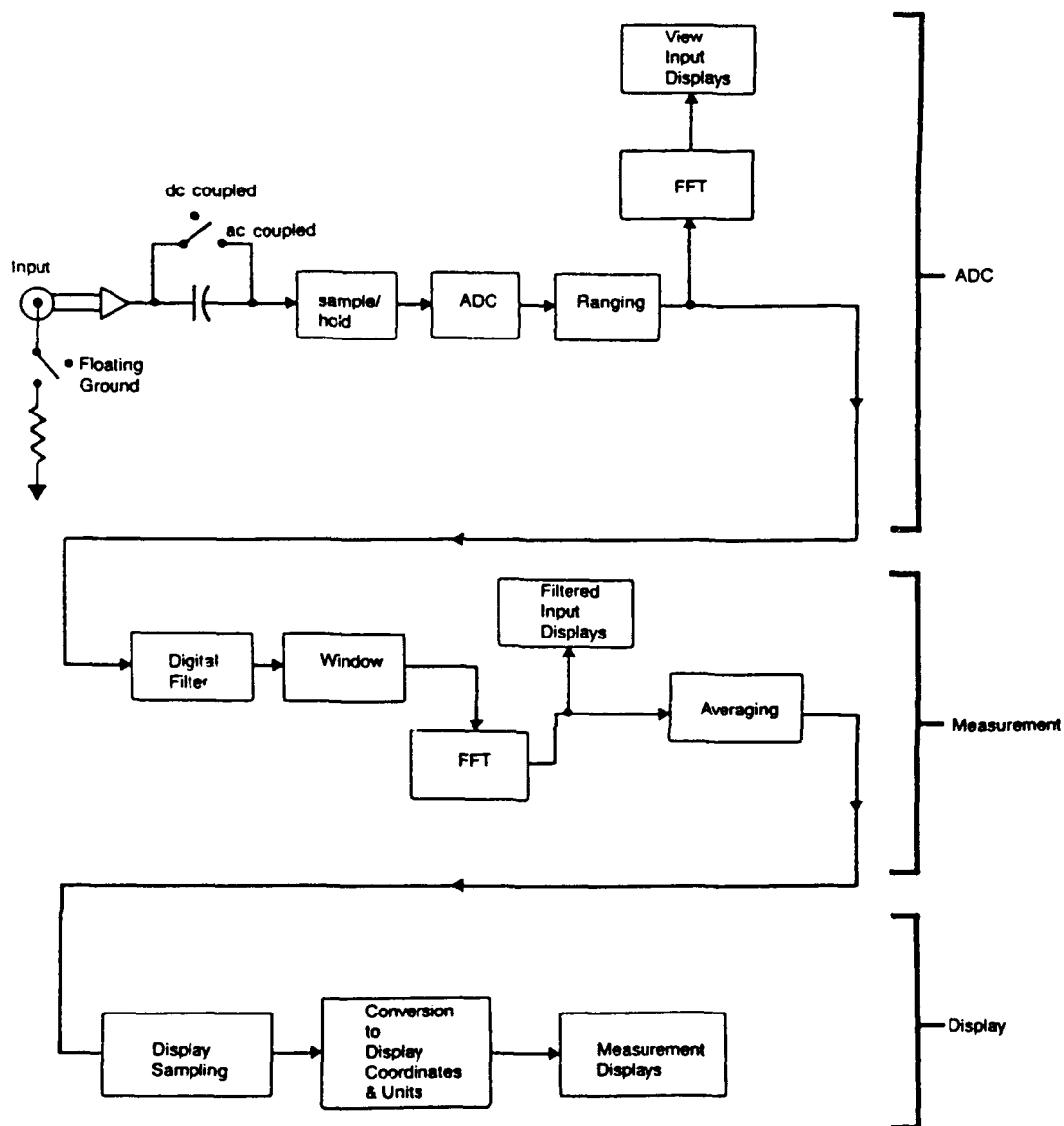


Figure 78. Overview of the HP 3562A Signal Analyzer Measurement Process

Linear Resolution

MEASURE:	CHAN 1 Power Spec	CHAN 2 Power Spec			
WINDOW:	CHAN 1 Hanning	CHAN 2 Hanning			
AVERAGE:	TYPE Stable	# AVG 7	OVERLAP 0%	TIME AVG Off	
FREQ:	CENTER 50 Hz		SPAN 100 Hz	BW 187mHz	
	REC LGTH 8.0 S	Δt 3.91mS			
TRIGGER:	TYPE FreeRun	LEVEL 0.0 Vpk	SLOPE Pos	PREVIEW Off	
INPUT:	RANGE 4.47 Vpk	ENG UNITS 1.0 V/EU	COUPLING DC (Fit)	DELAY 0.0 S	
	CH 2 502mVpk	1.0 V/EU	DC (Fit)	0.0 S	
SOURCE:	TYPE Off		LEVEL 0.0 Vpk	OFFSET 0.0 Vpk	

Figure 79. Typical Settings Used on the HP 3562A Signal Analyzer

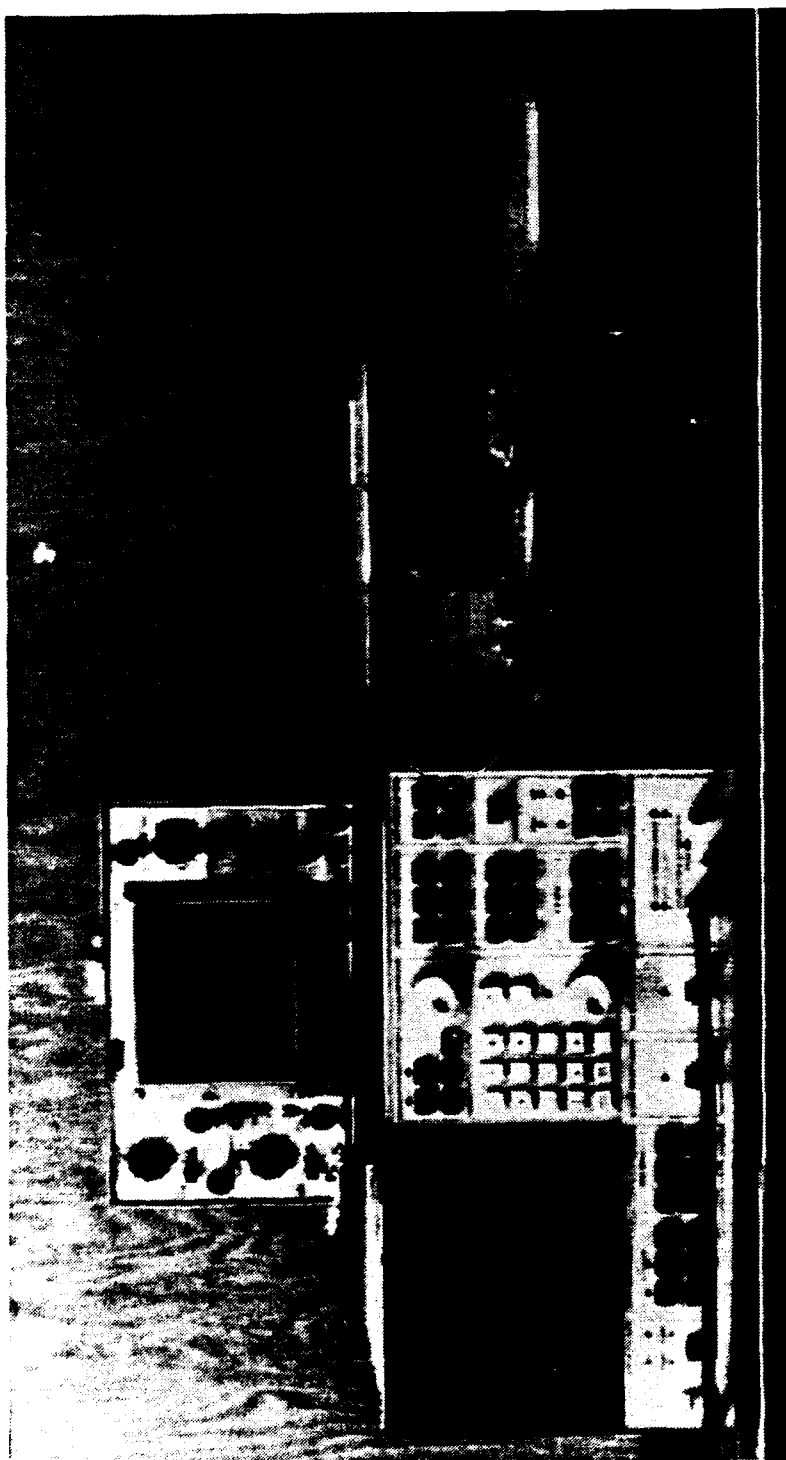


Figure 80. Hot-wire Measurement Setup

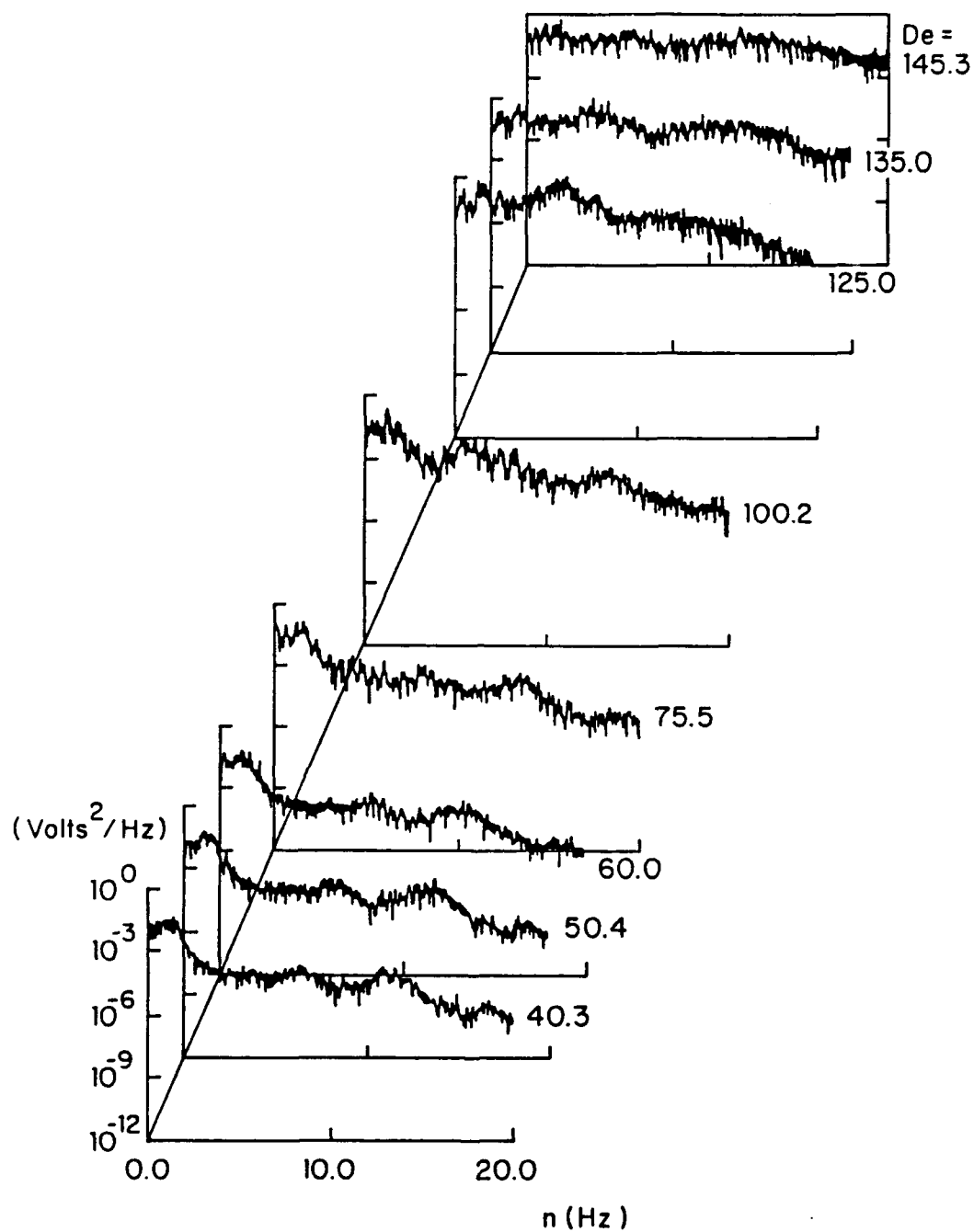


Figure 81. Conventional Hot-wire Probe Spectra, $De = 40.3$ to $De = 145.3$

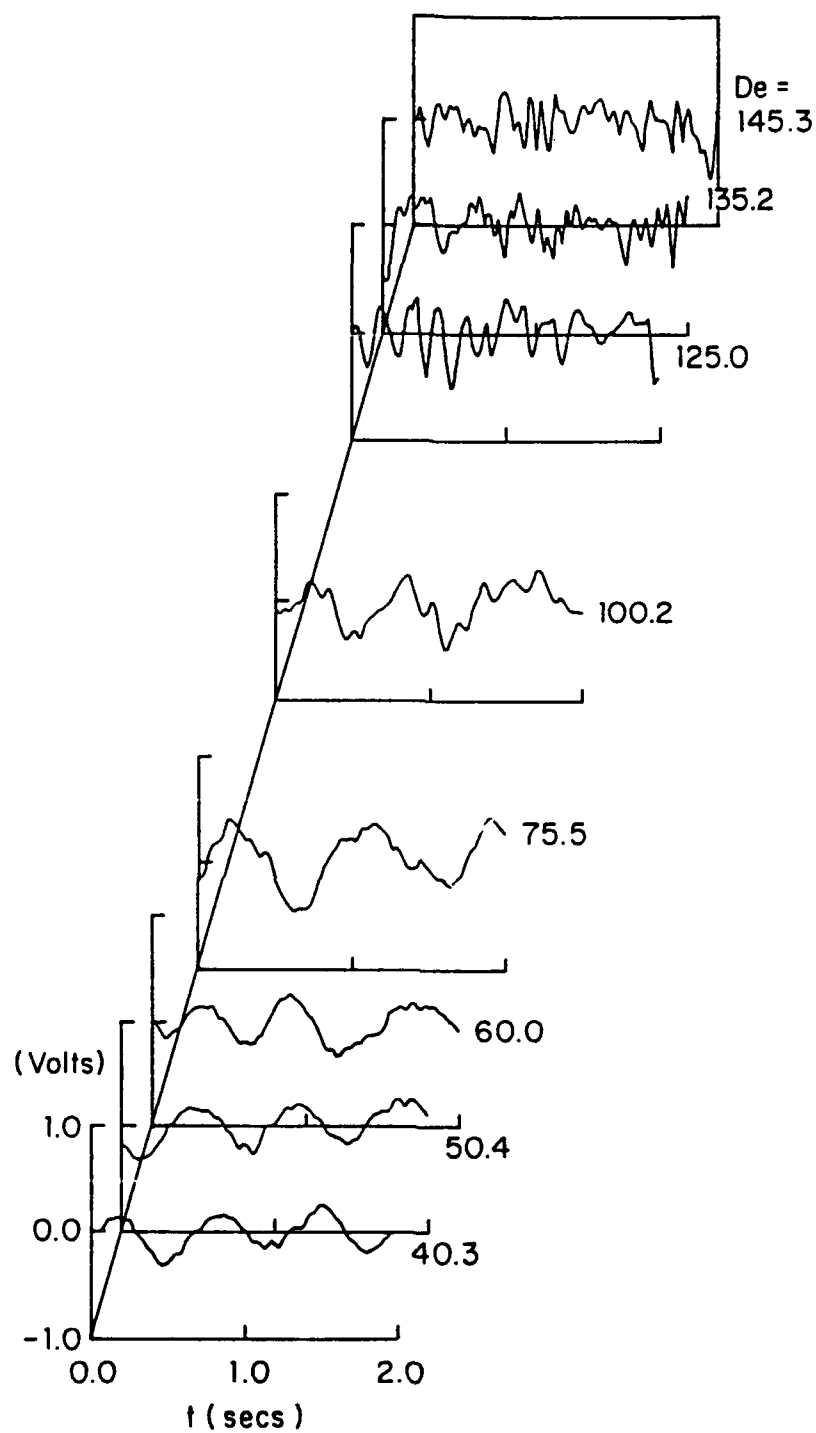


Figure 82. Conventional Hot-wire Probe Time Traces, $De = 40.3$ to $De = 145.3$

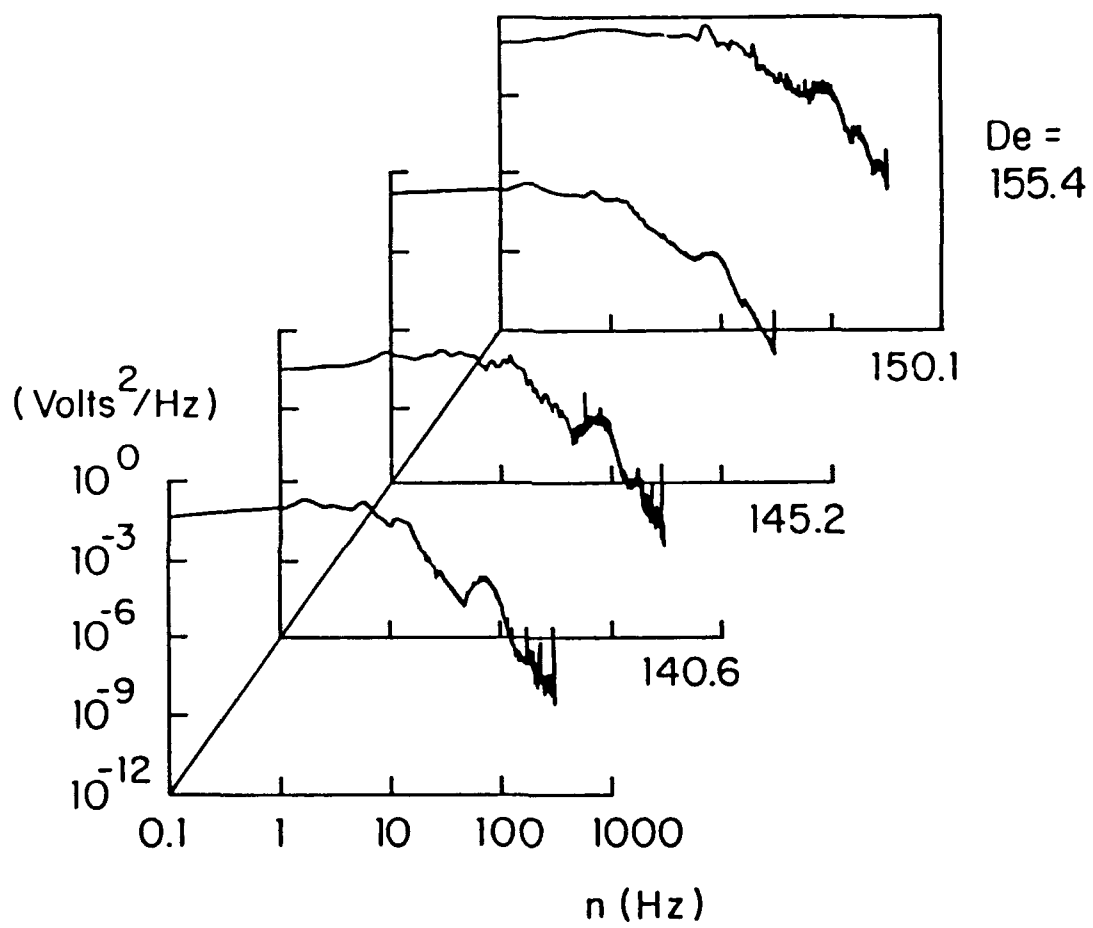


Figure 83. Conventional Hot-wire Probe Spectra, $De = 140.6$ to $De = 155.4$

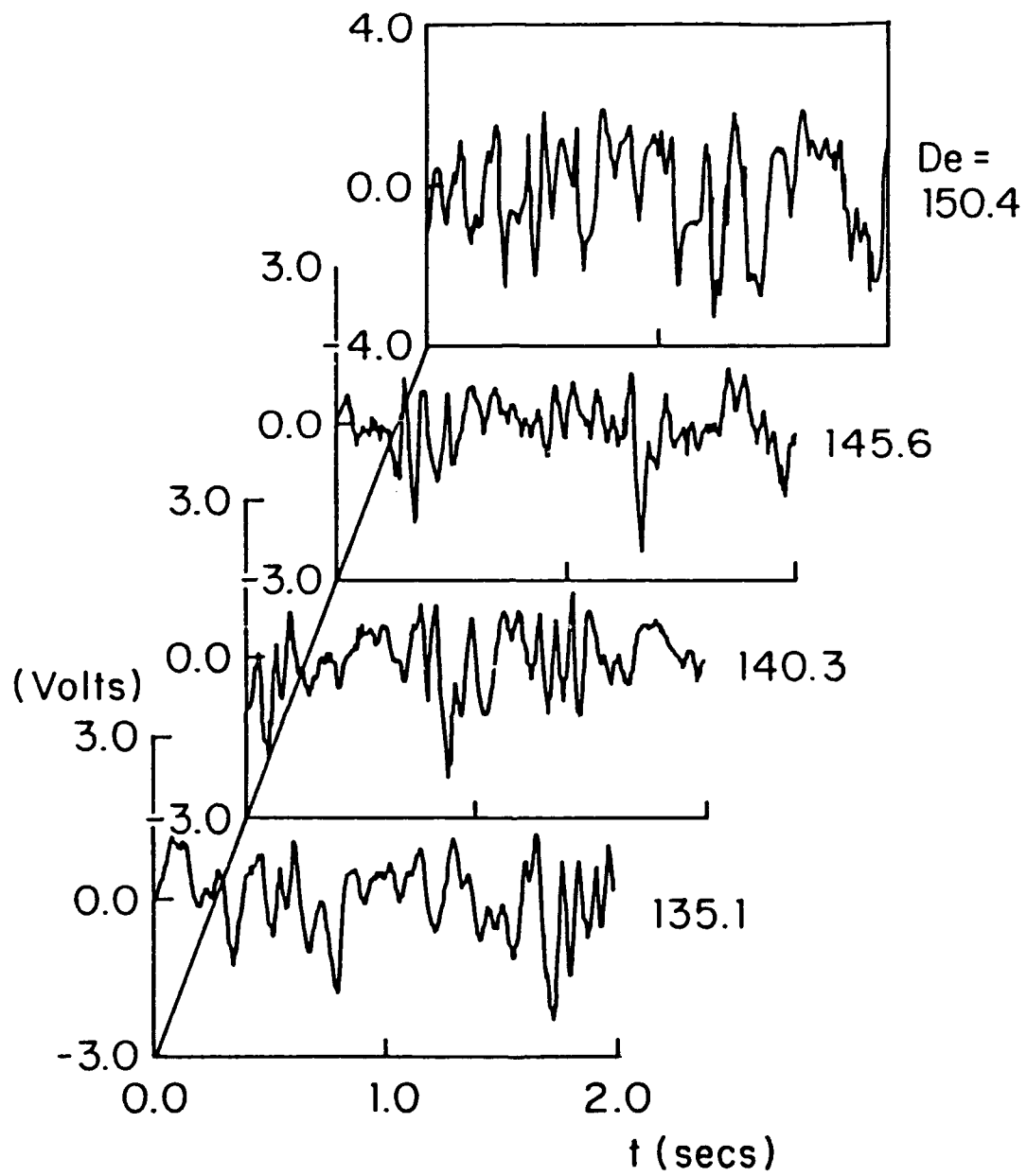


Figure 84. Conventional Hot-wire Probe Time Traces, $De = 135.1$ to $De = 150.4$

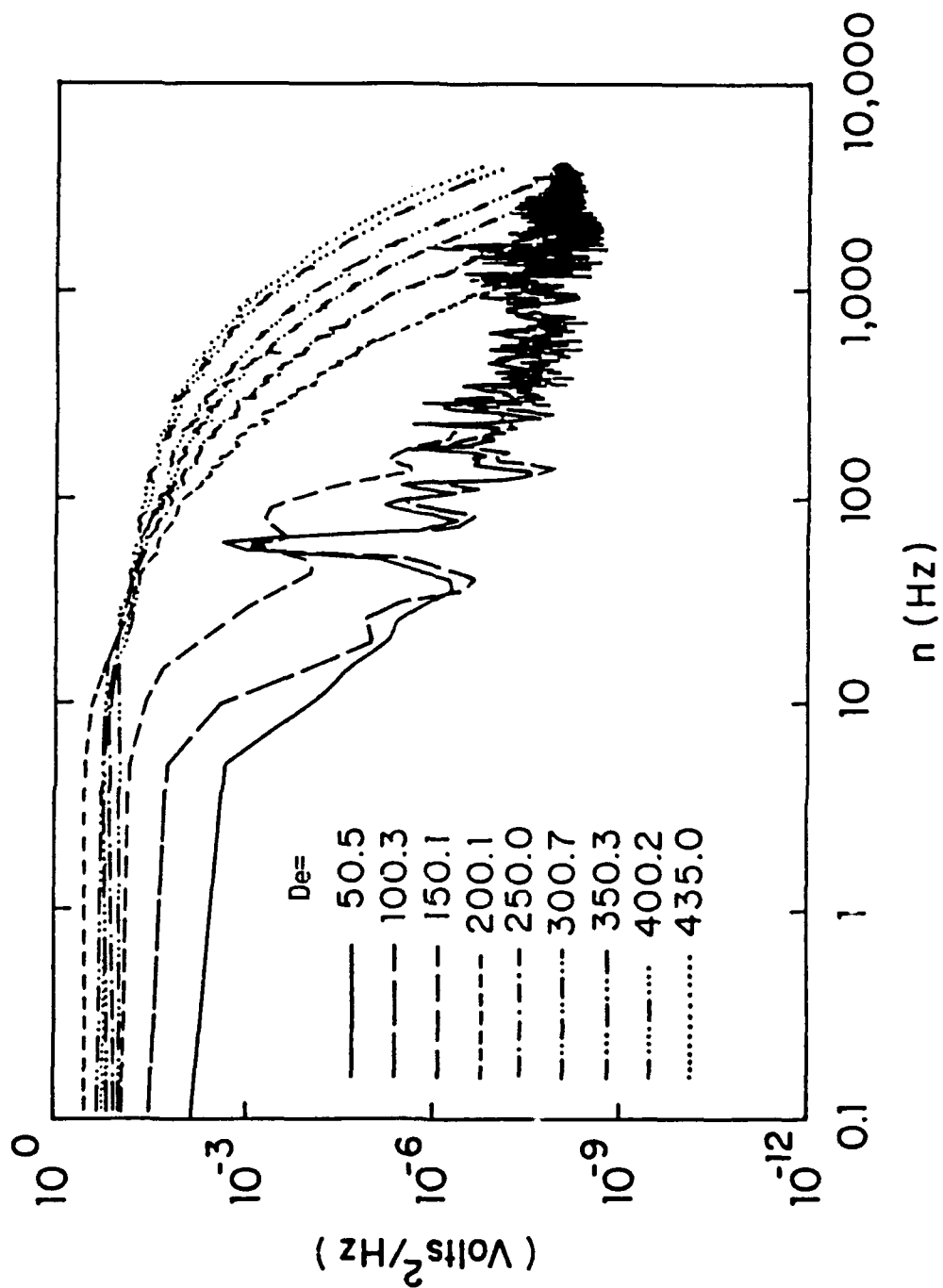


Figure 85. Conventional Hot-wire Probe Spectra, $De = 50.5$ to $De = 435.0$

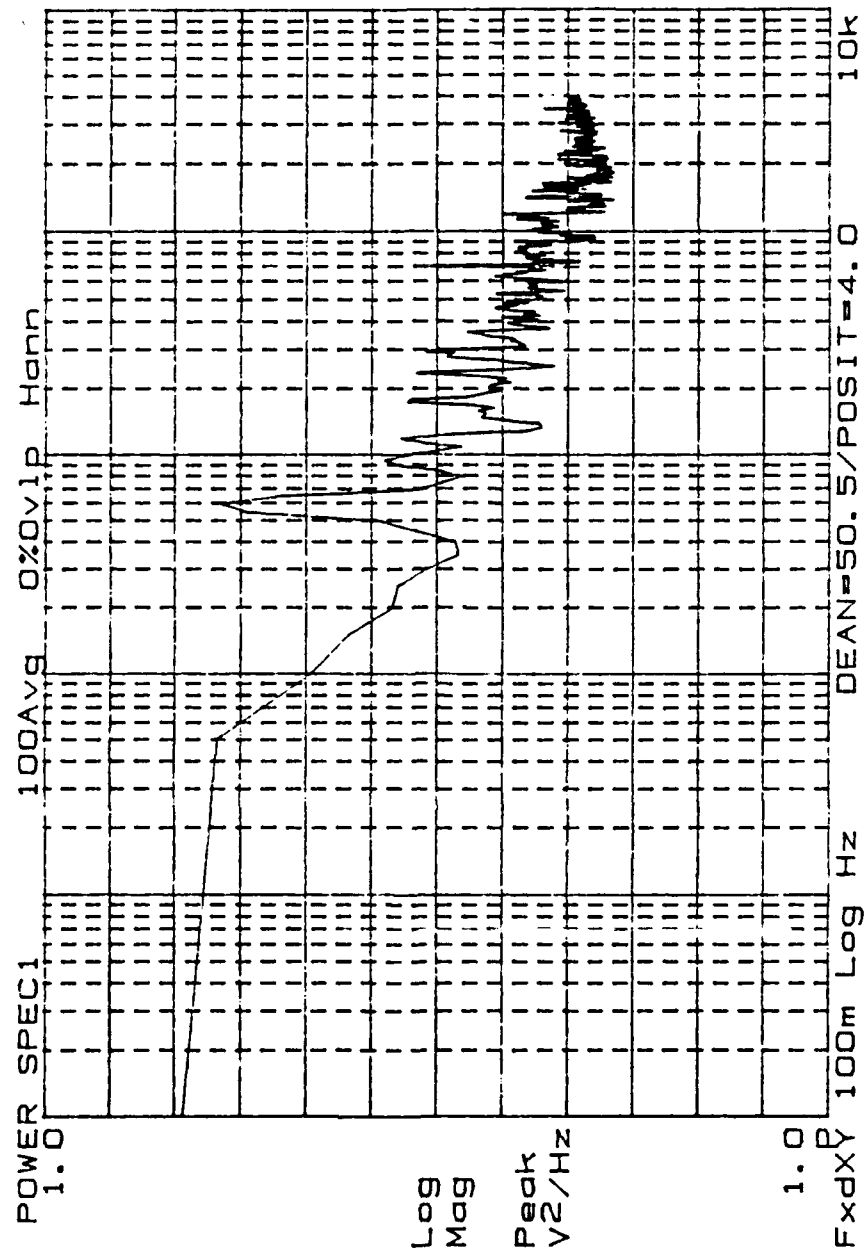


Figure 86. Conventional Hot-wire Probe Spectrum, $De = 50.5$



XXXX

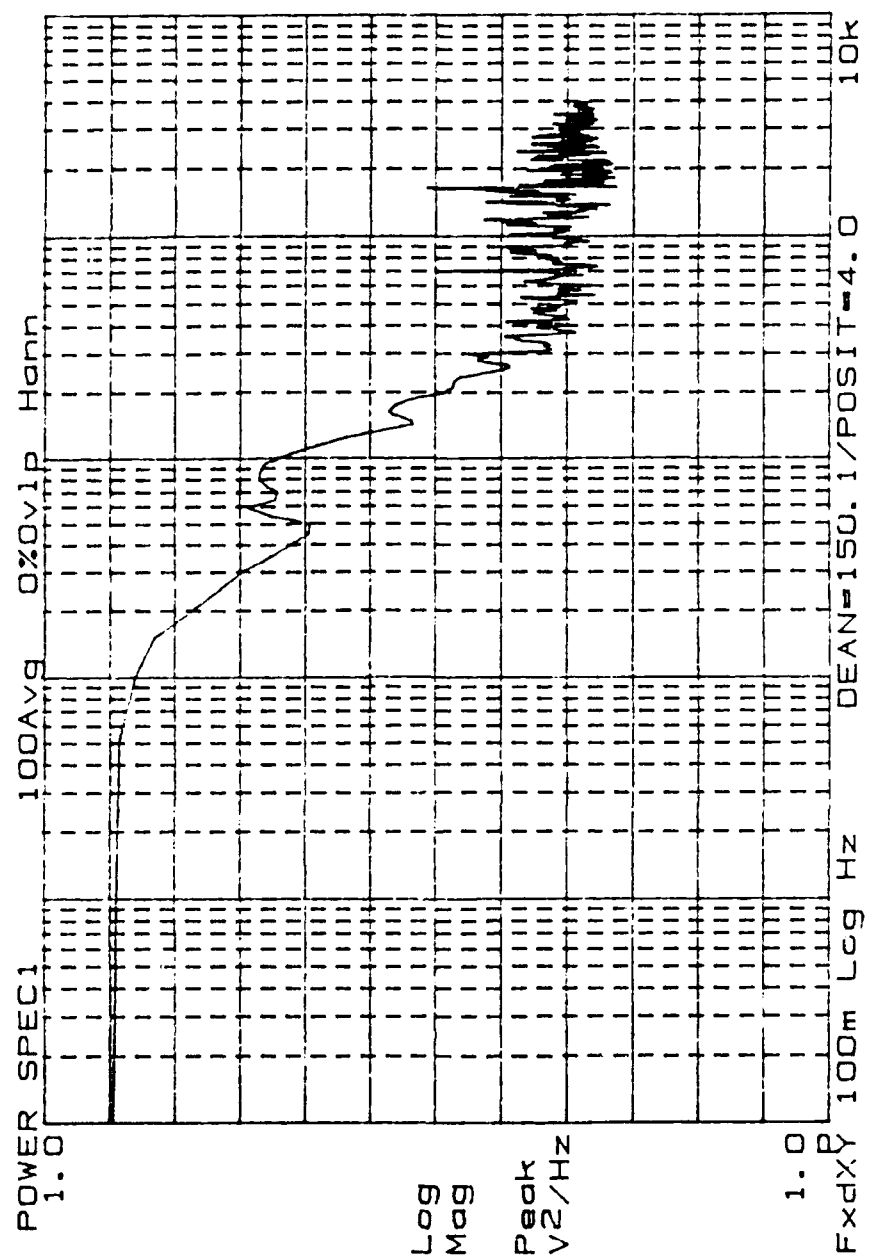


Figure 88. Conventional Hot-wire Probe Spectrum, $De = 150.1$

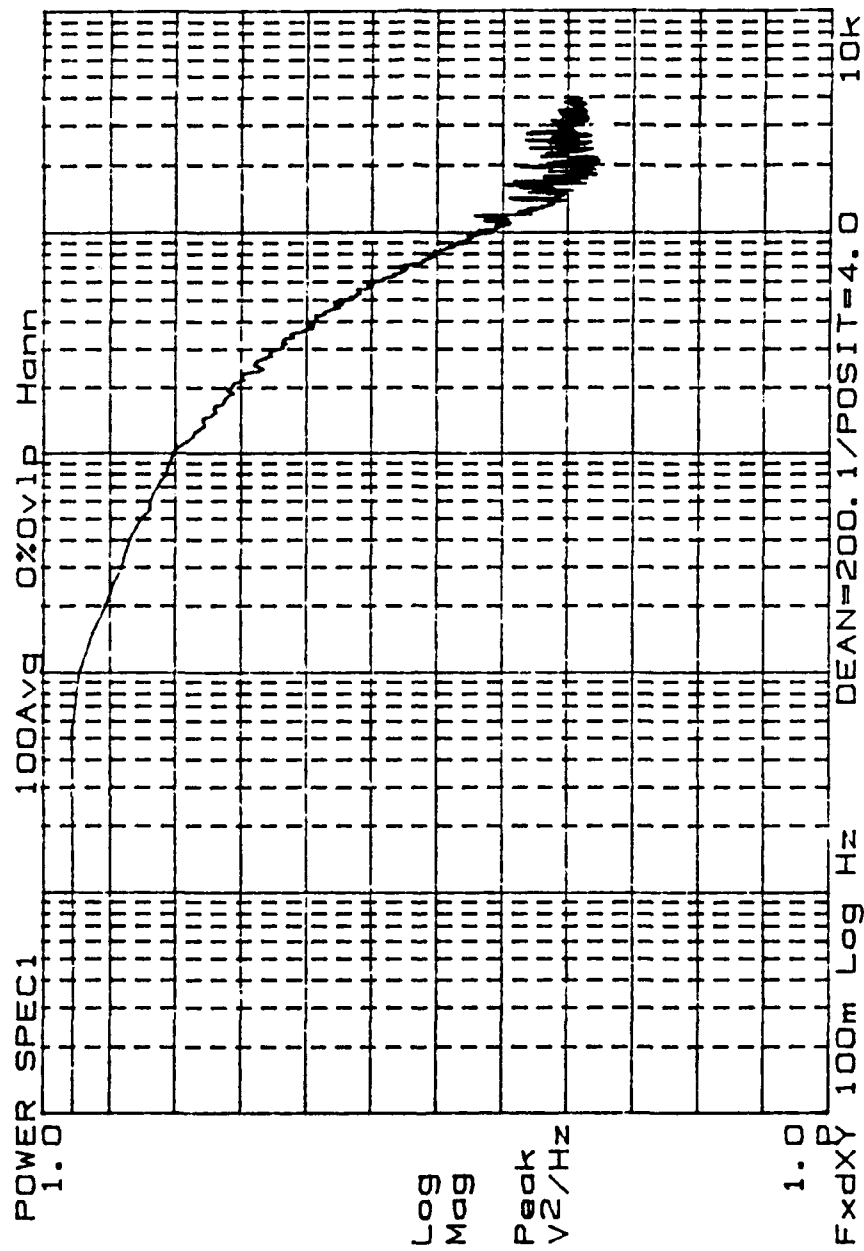


Figure 89. Conventional Hot-wire Probe Spectrum, $De = 200.1$

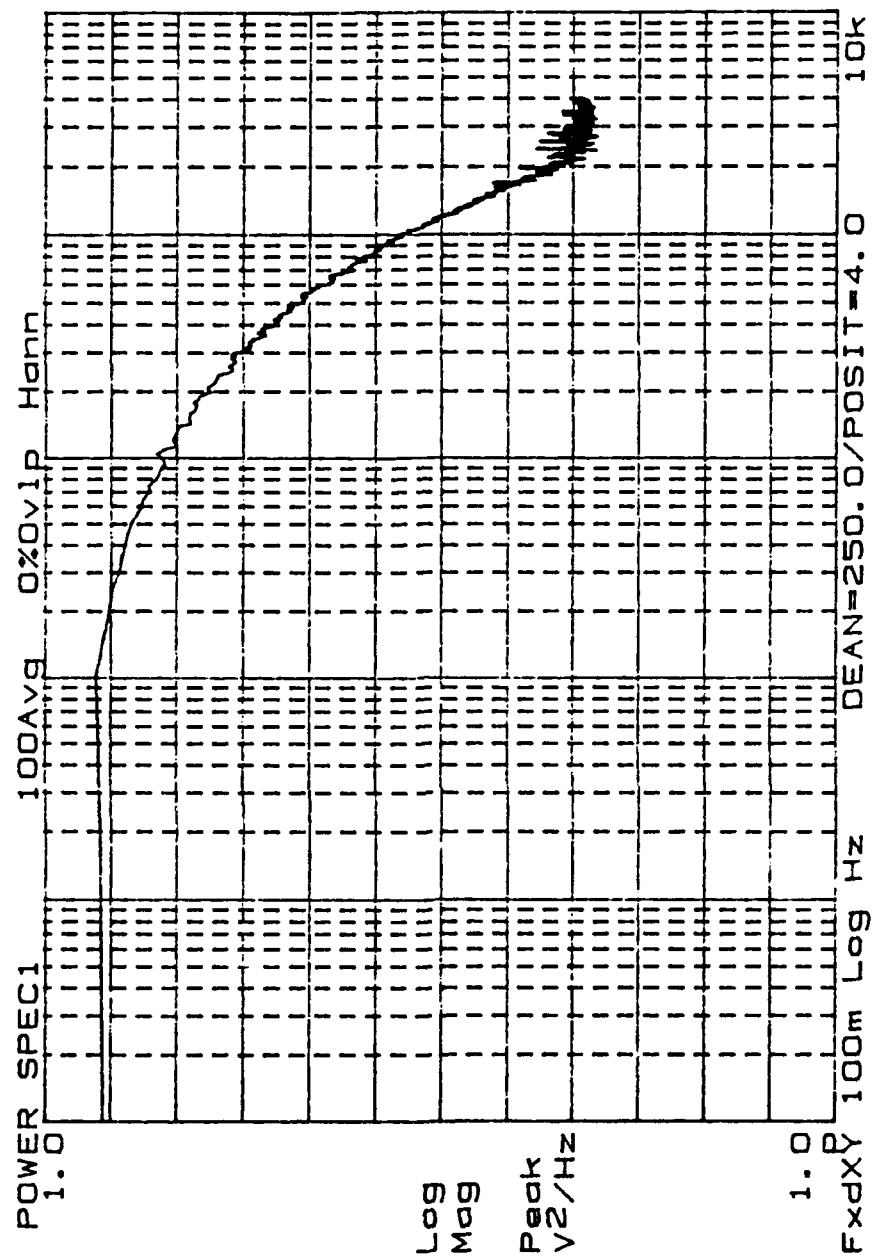


Figure 90. Conventional Hot-wire Probe Spectrum, $De = 250.0$

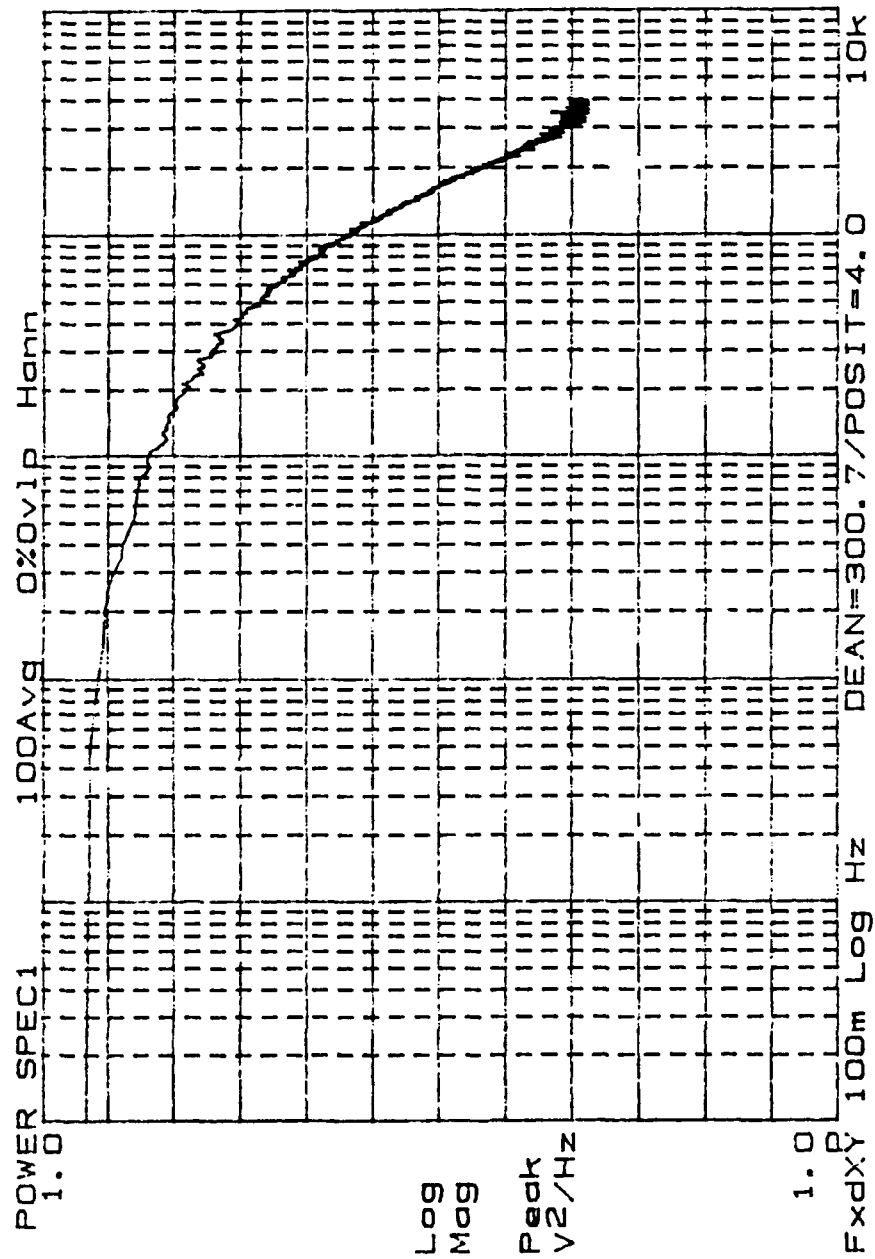


Figure 91. Conventional Hot-wire Probe Spectrum, $De = 300.7$

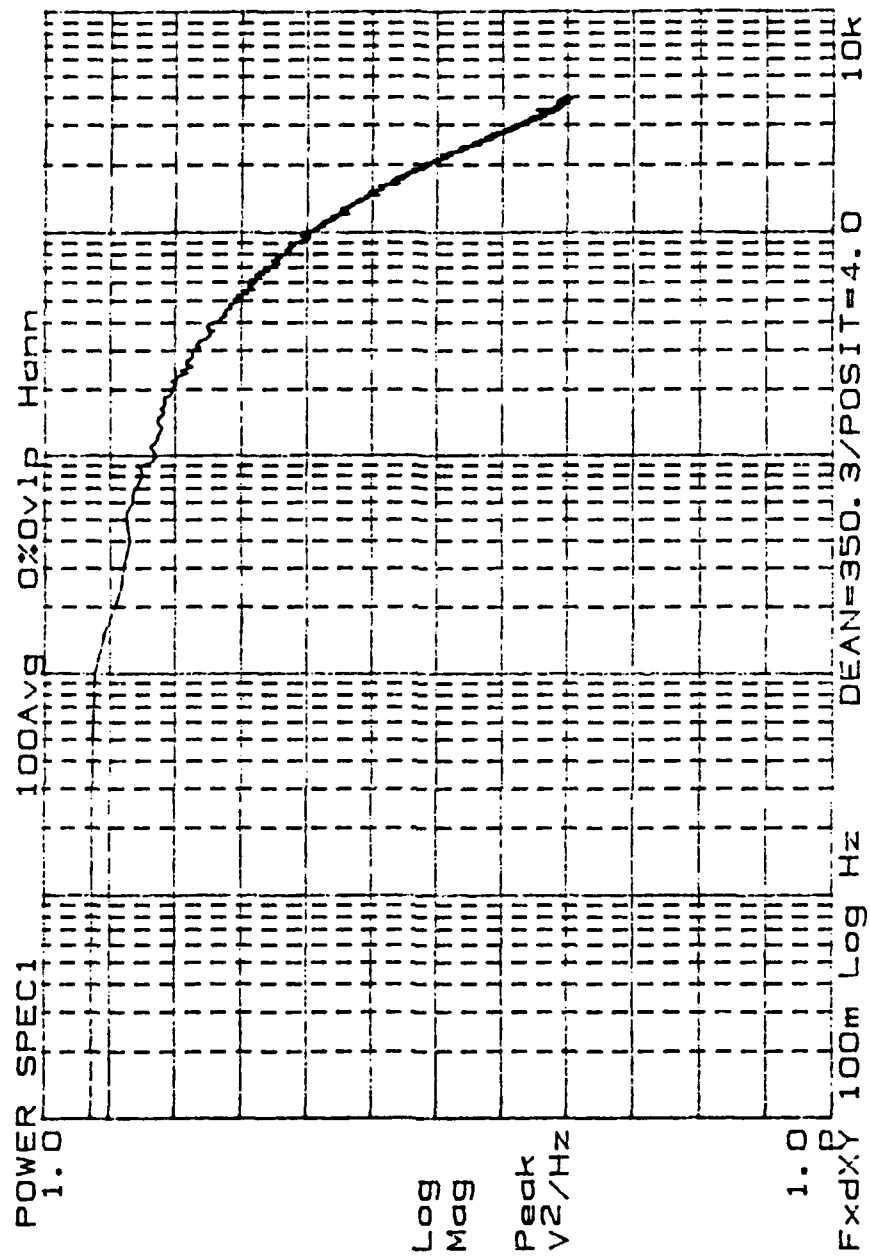


Figure 92. Conventional Hot-wire Probe Spectrum, $De = 350.3$

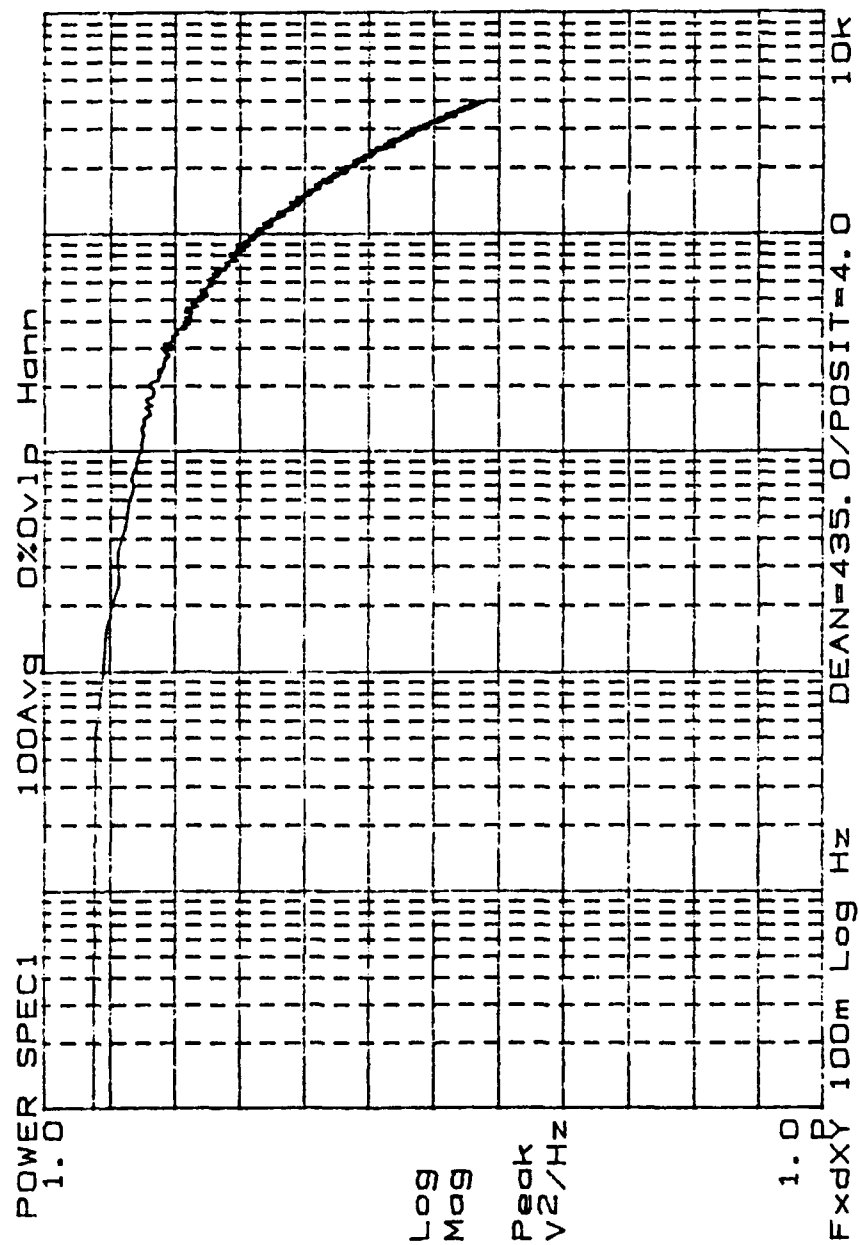


Figure 94. Conventional Hot-wire Probe Spectrum, $De = 435.0$

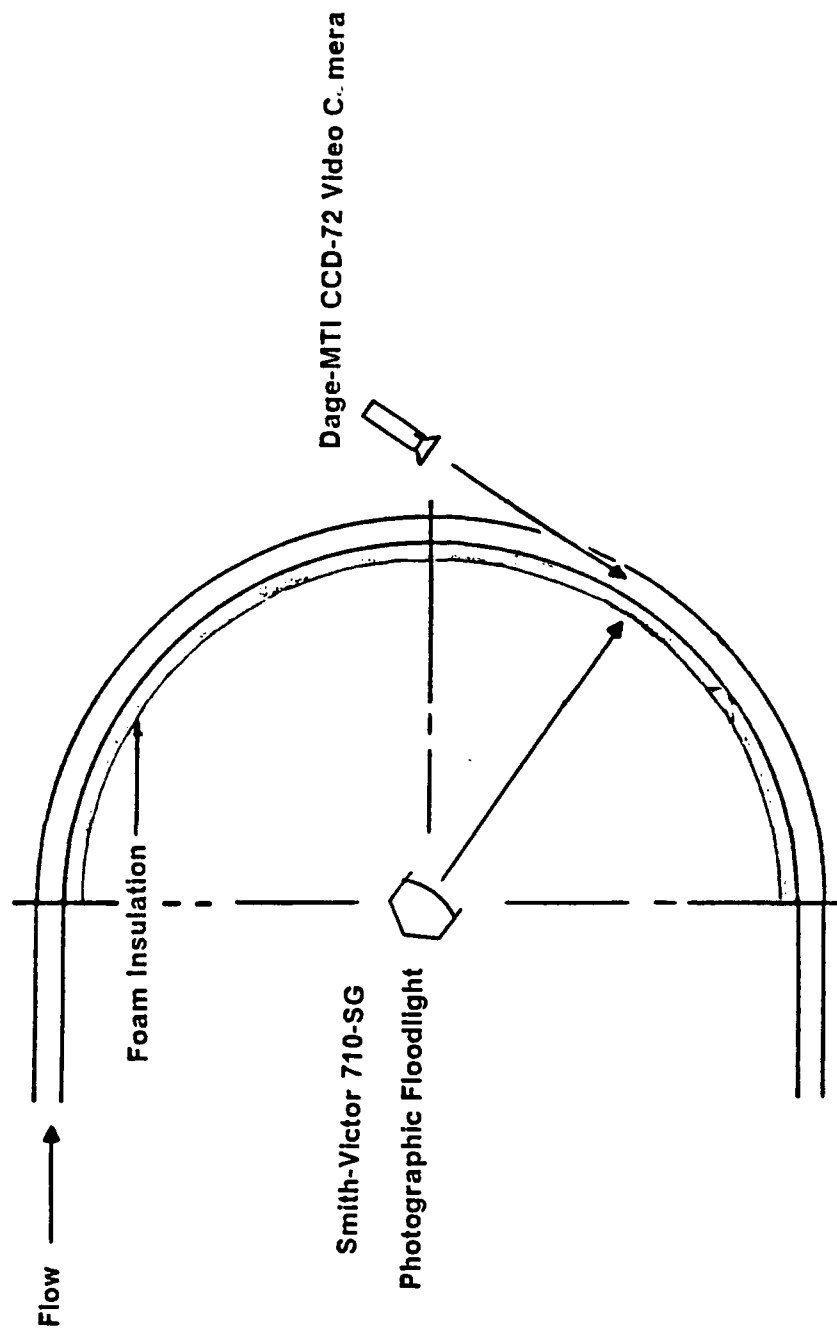


Figure 95. Flow Visualization Radial/Spanwise Plane

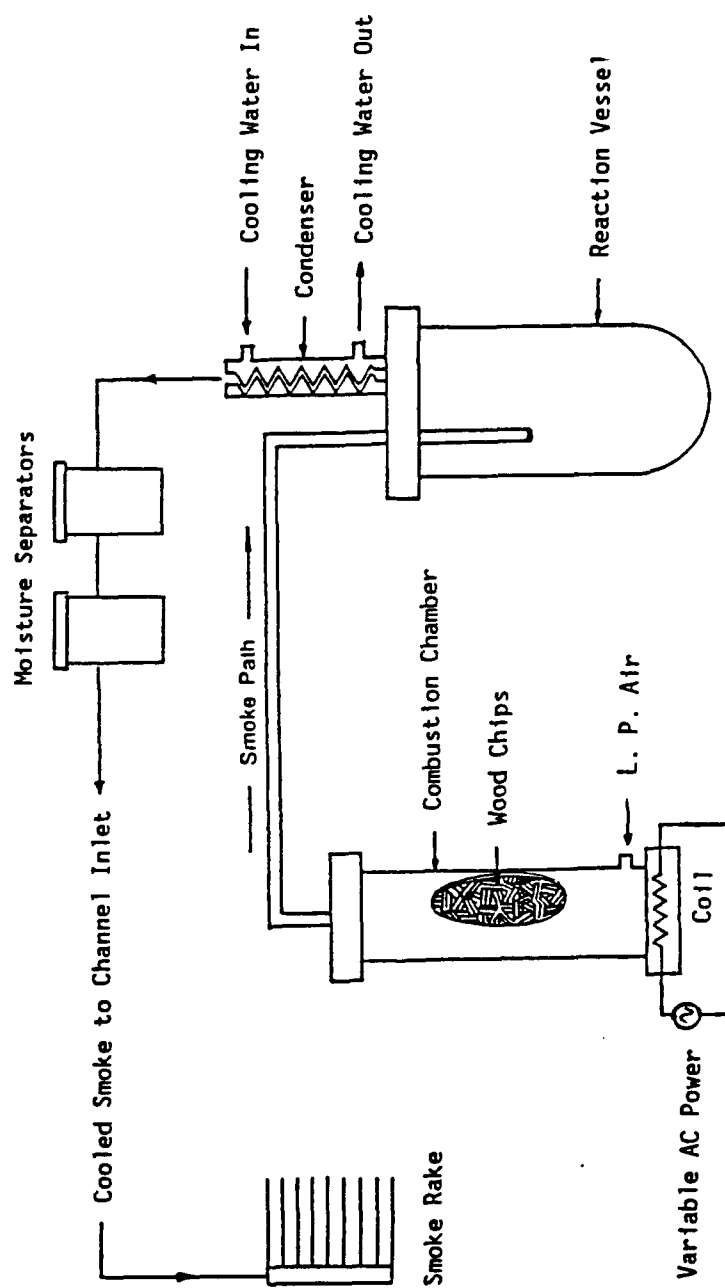


Figure 96. Schematic of Smoke Generator and Smoke Rake

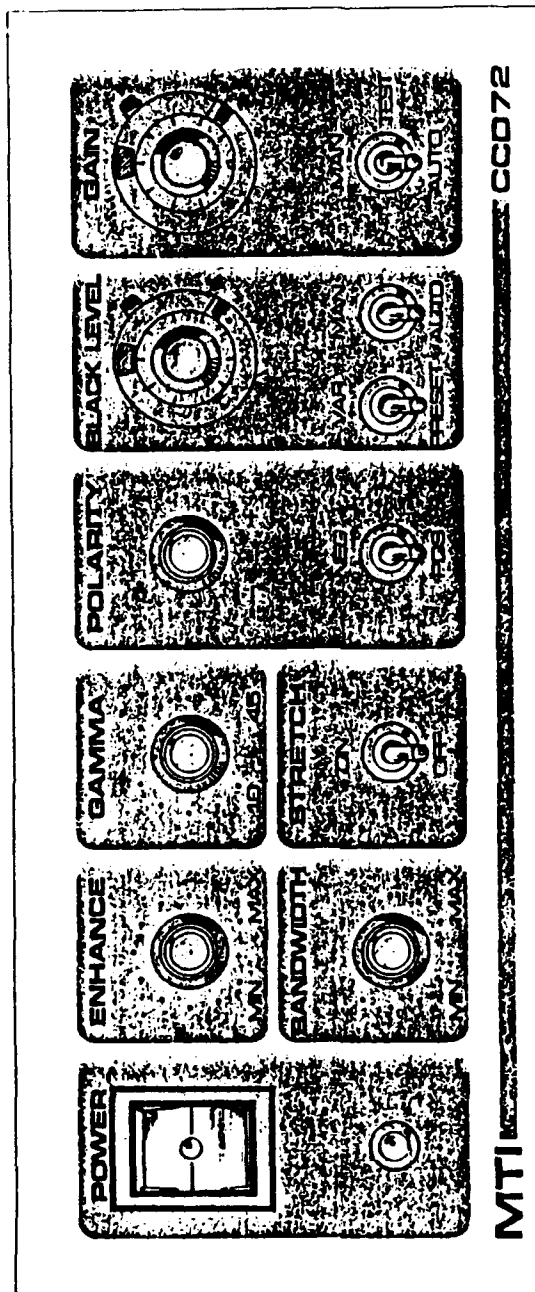


Figure 97. Camera Control Unit (CCU) Front Panel

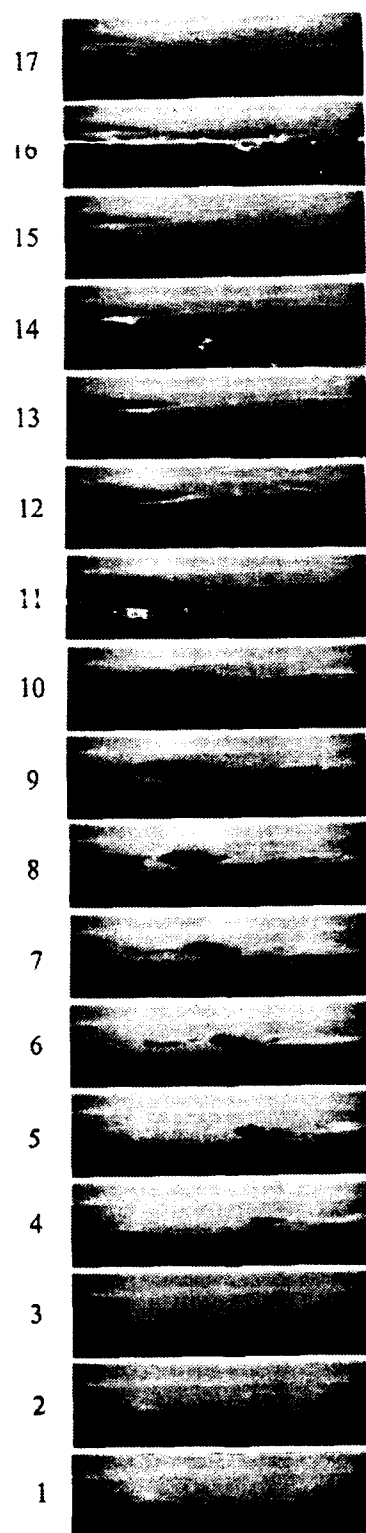


Figure 98. Flow Visualization, $De = 50.9$, $\theta = 40^\circ$ (inside), 1/15 Second Intervals

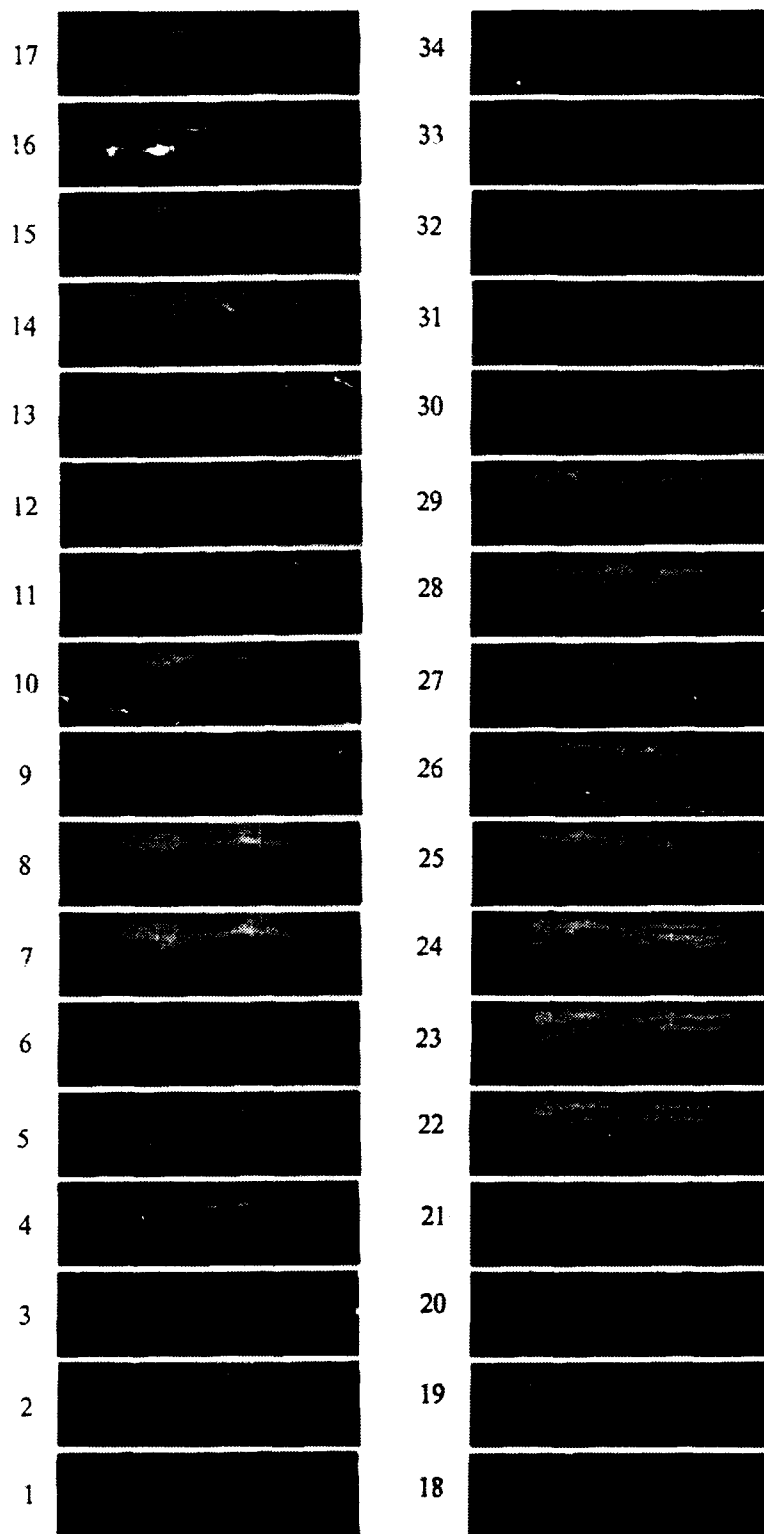


Figure 99. Flow Visualization, $De = 100.1$, $\theta = 40^\circ(\text{inside})$, 1/15 Second Intervals

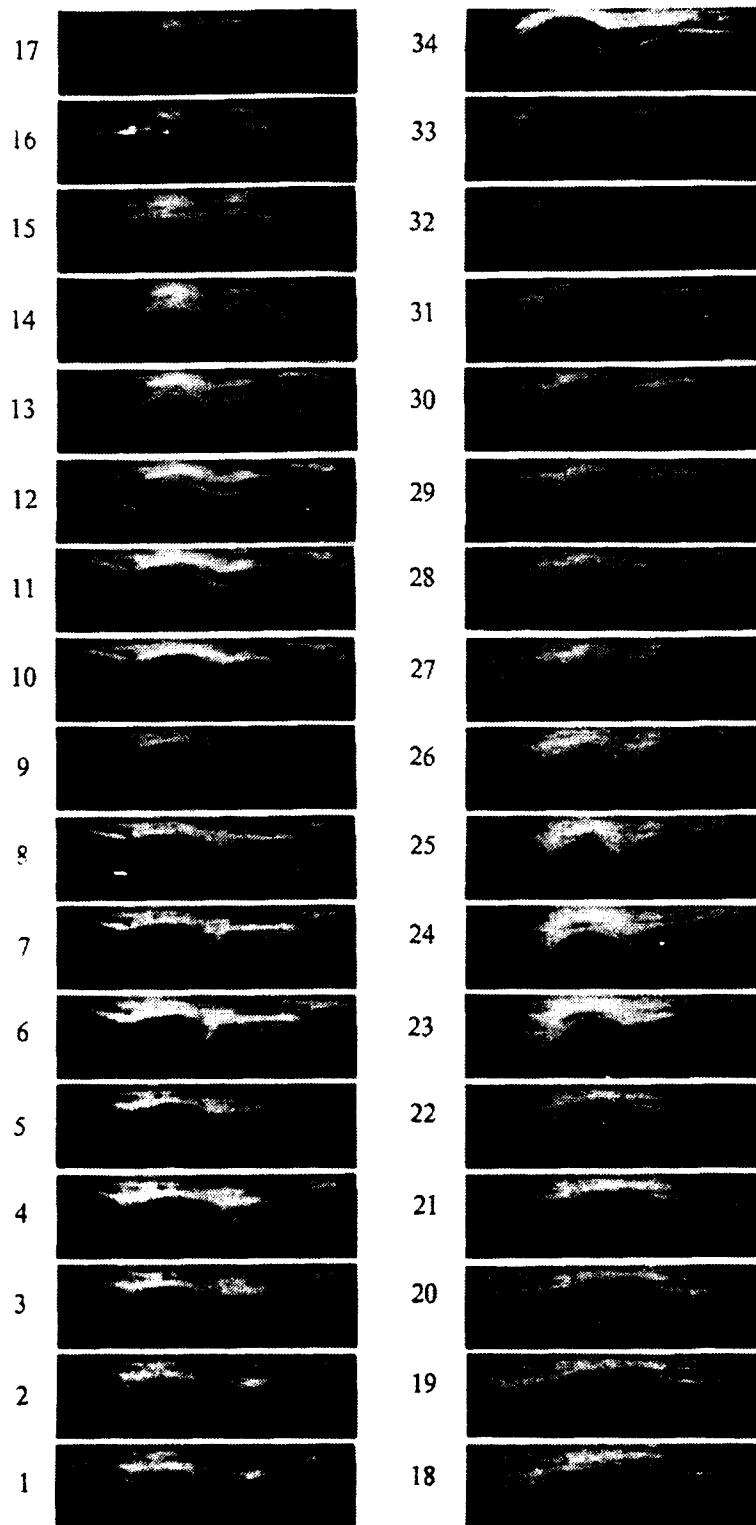


Figure 100. Flow Visualization, $De = 150.7$, $\theta = 40^\circ$ (inside), 1/15 Second Intervals

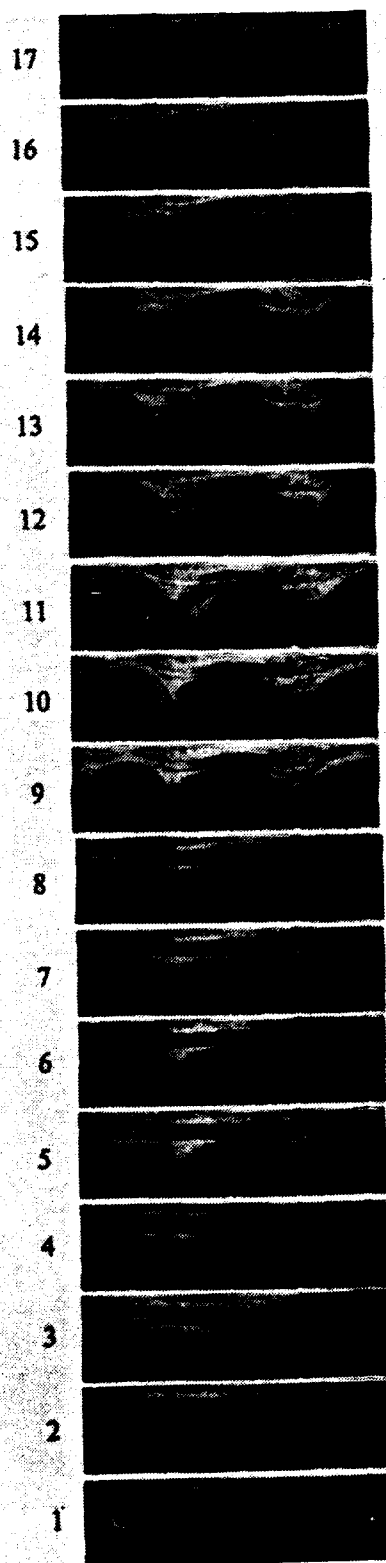


Figure 101. Flow Visualization, $De = 200.5$, $\theta = 40^\circ$ (*inside*), 1/30 Second Intervals

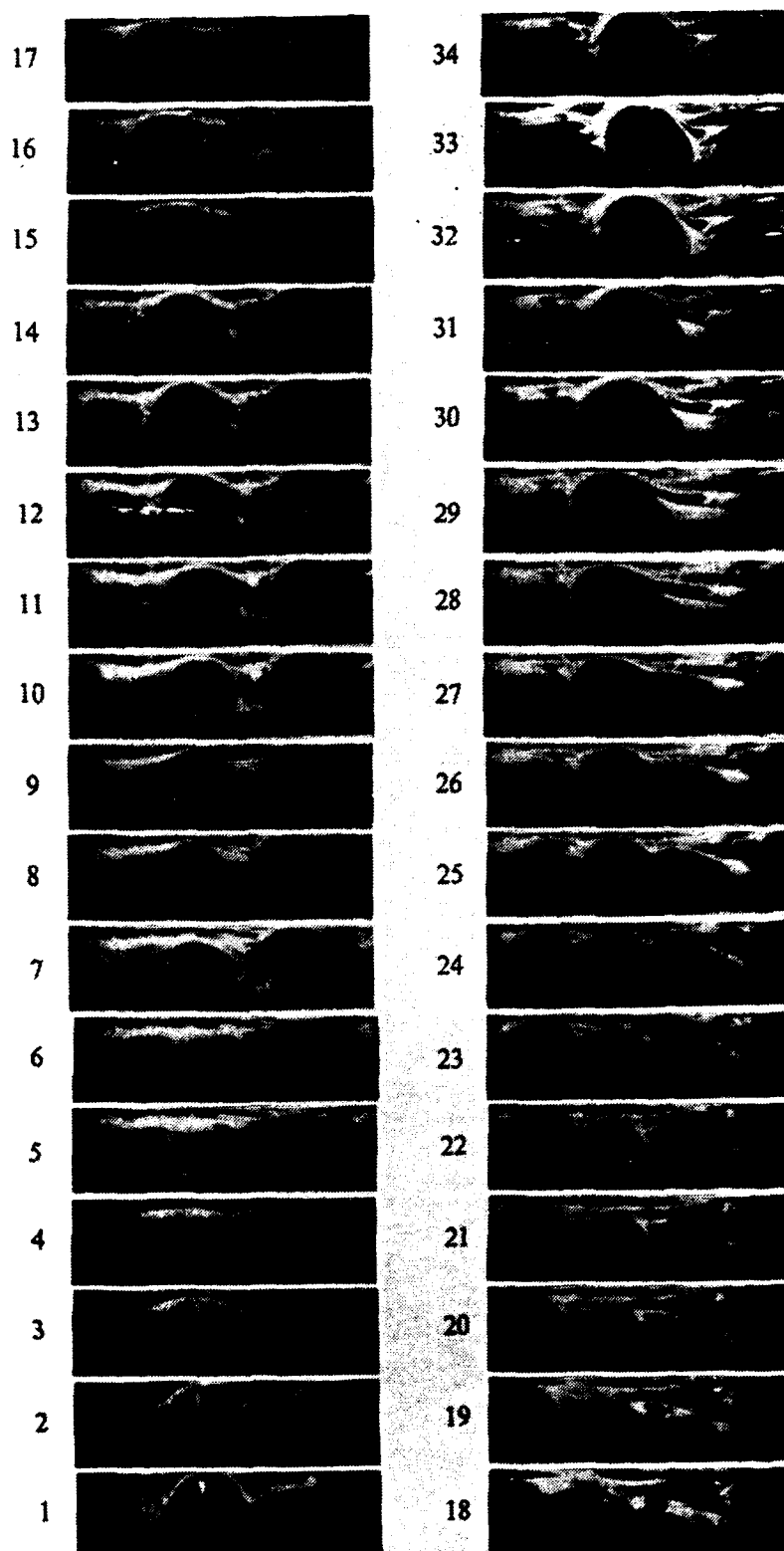


Figure 102. Flow Visualization, $De = 250.8$, $\theta = 40^\circ$ (inside), 1/60 Second Intervals

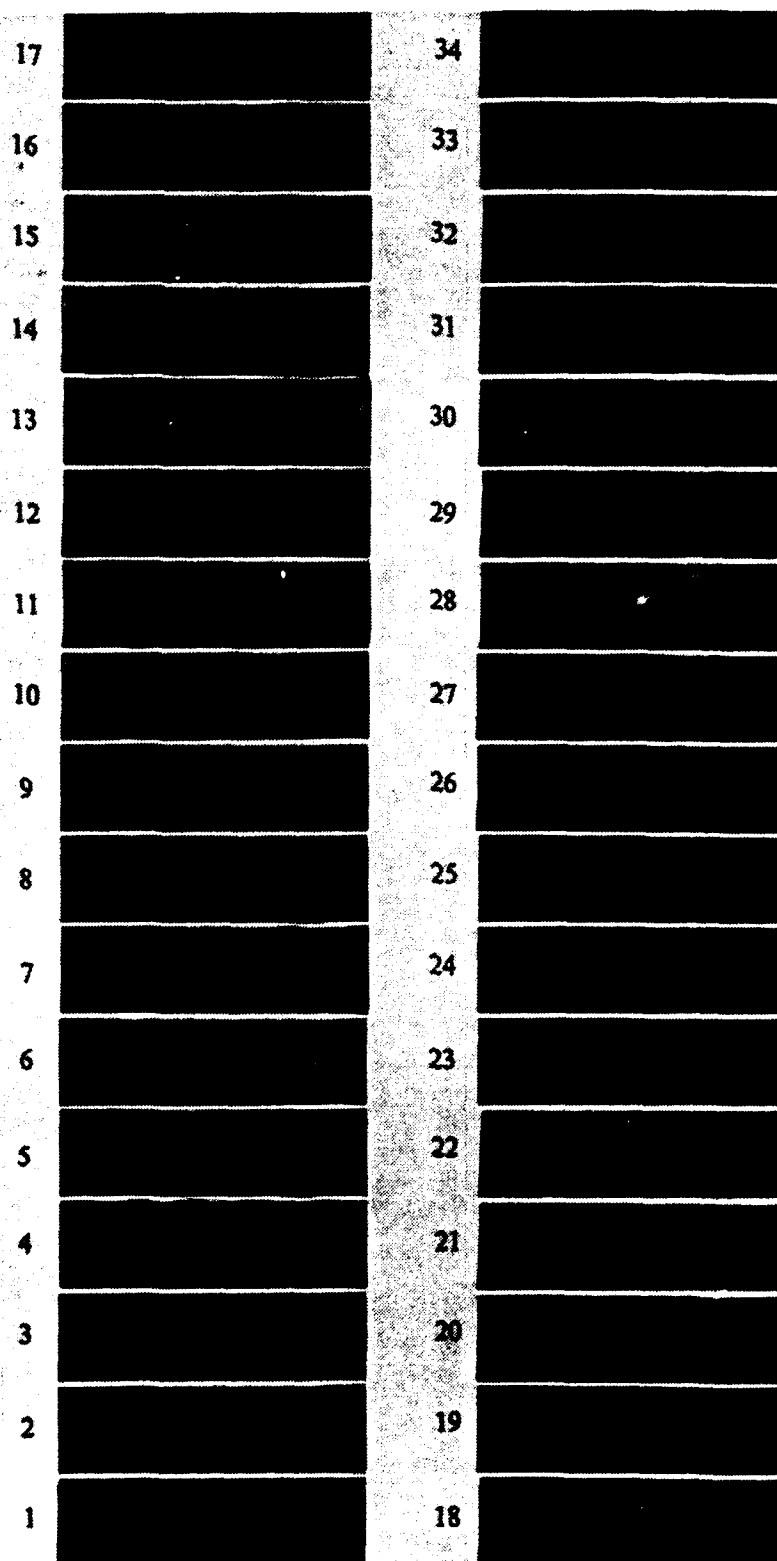


Figure 103. Flow Visualization, $De = 300.3$, $\theta = 40^\circ$ (*inside*), $1/60$ Second Intervals

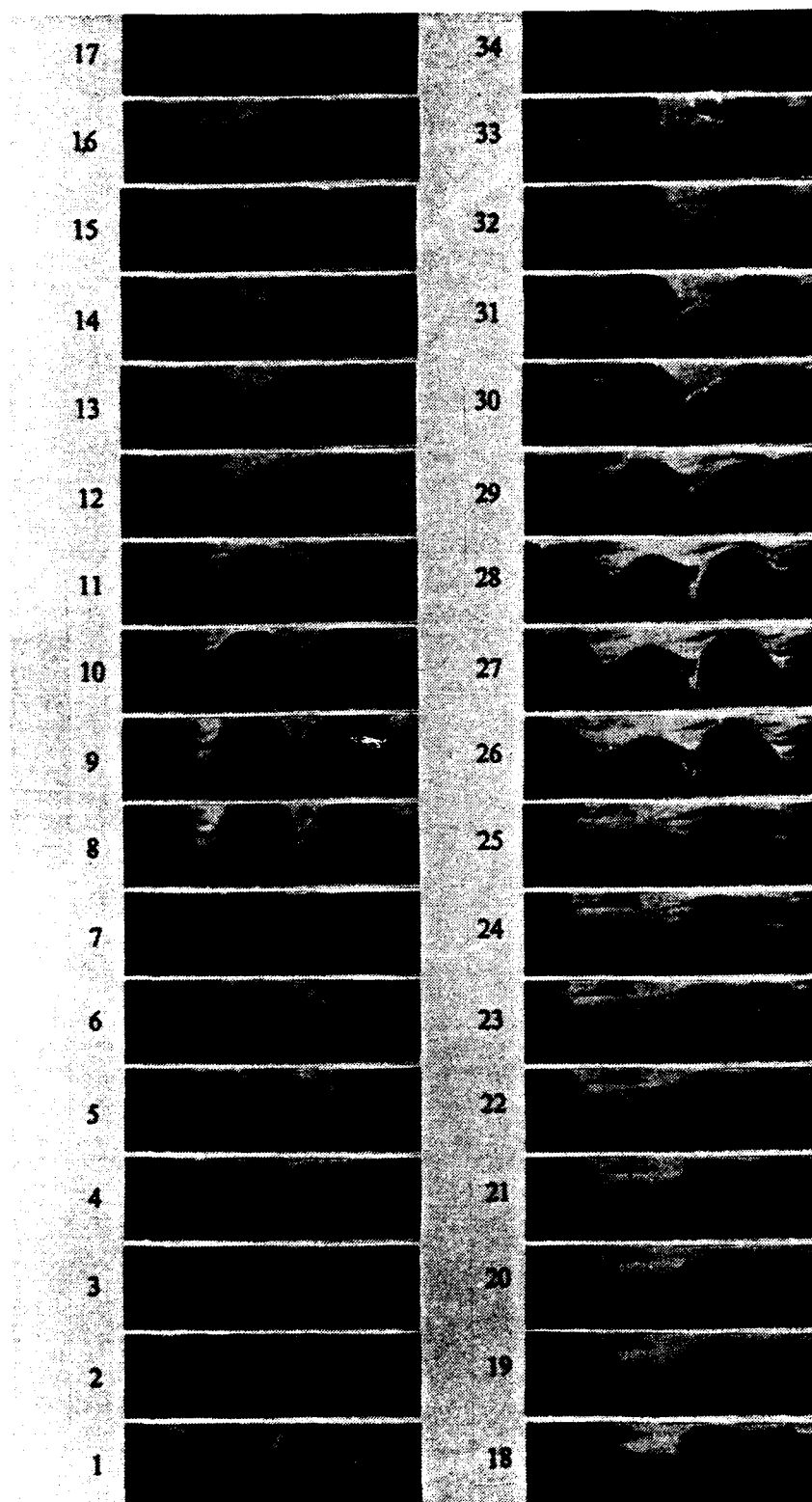


Figure 104. Flow Visualization, $De = 350.3$, $\theta = 40^\circ$ (inside), 1/60 Second Intervals

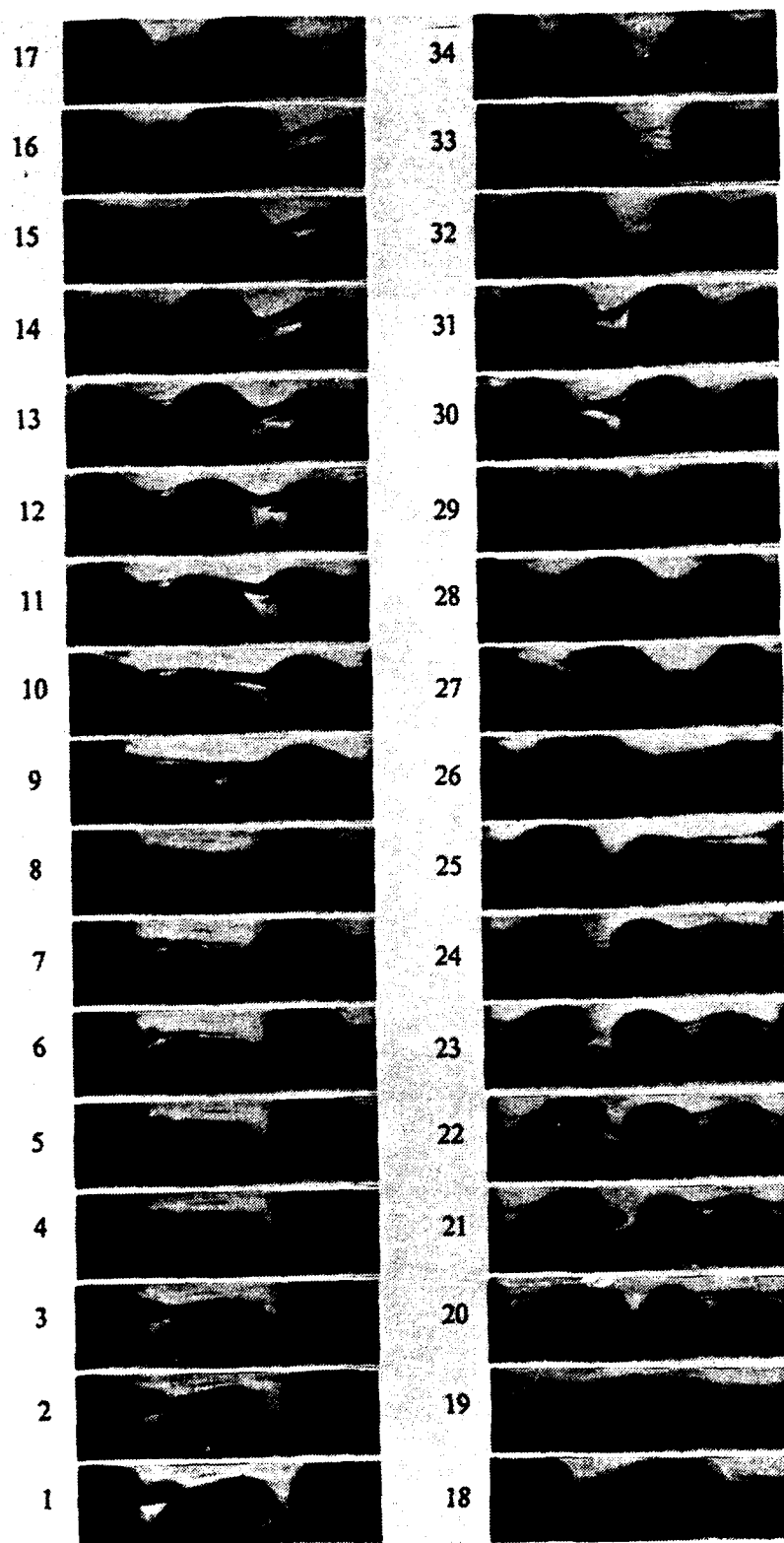


Figure 105. Flow Visualization, $De = 400.4$, $\theta = 40^\circ$ (inside), 1/60 Second Intervals

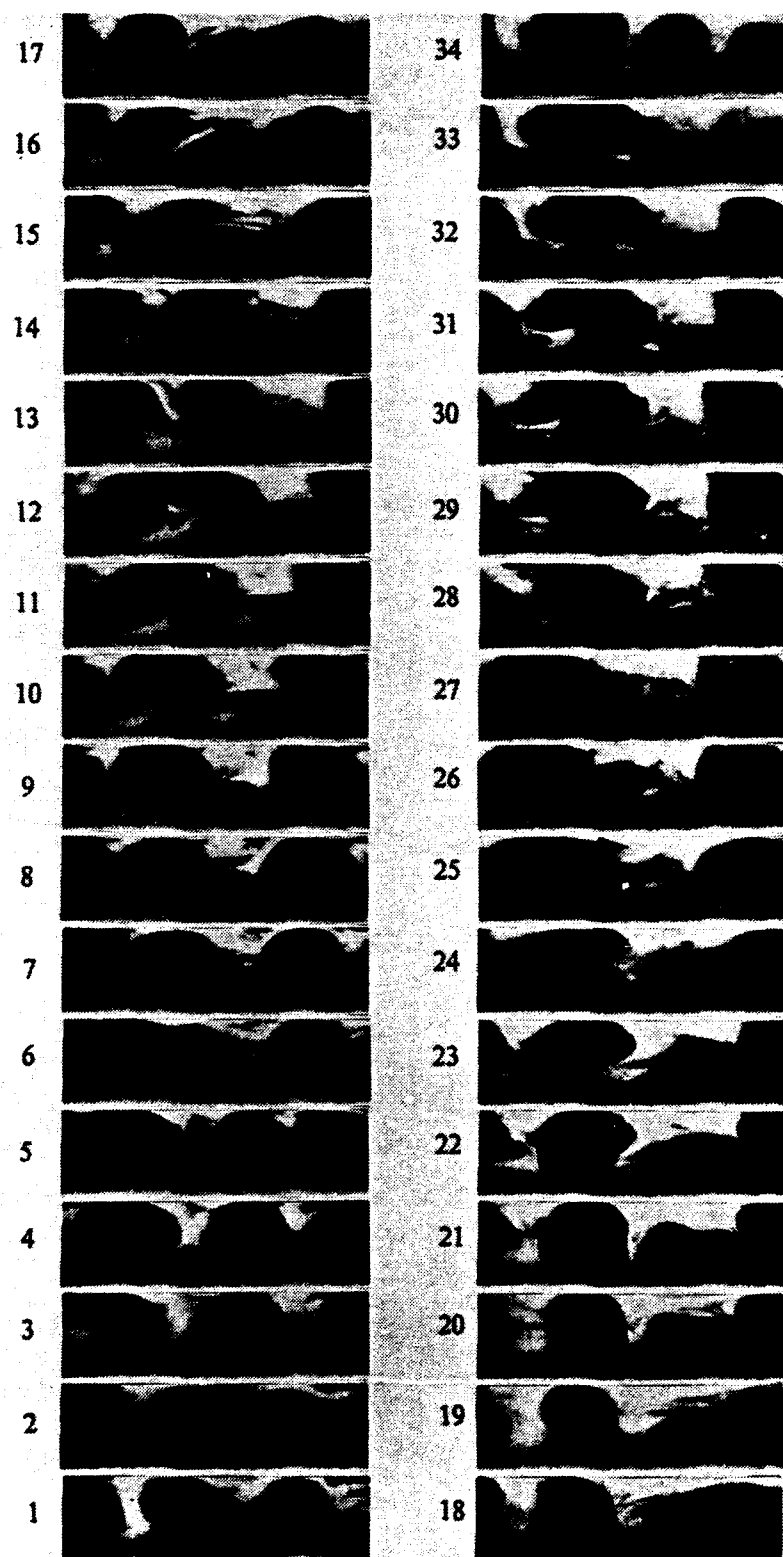


Figure 106. Flow Visualization, $De = 425.0$, $\theta = 40^\circ$ (inside), 1/60 Second Intervals

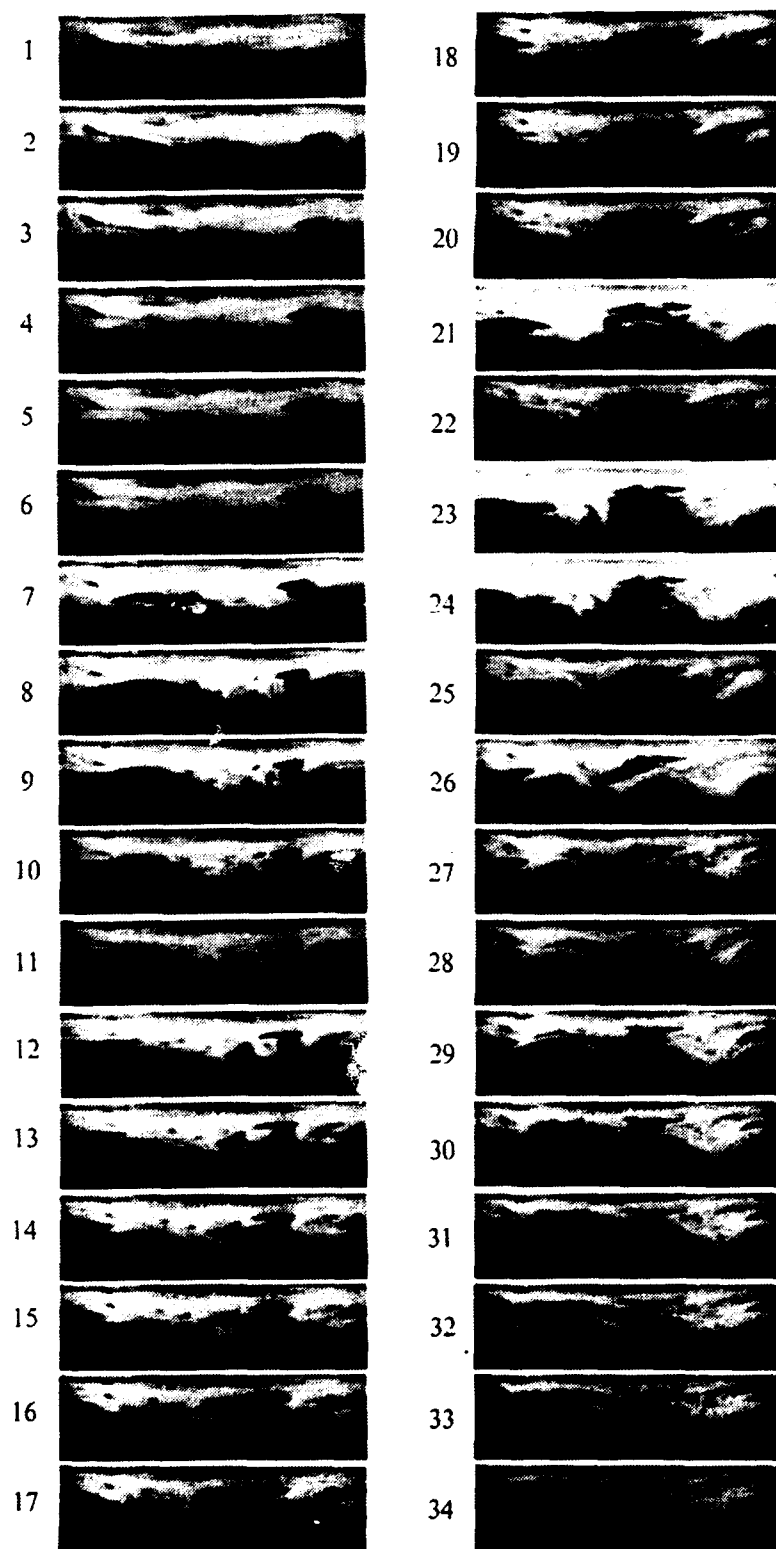


Figure 107. Flow Visualization, $De = 50.9$, $\theta = 40^\circ$ (outside), 1/20 Second Intervals

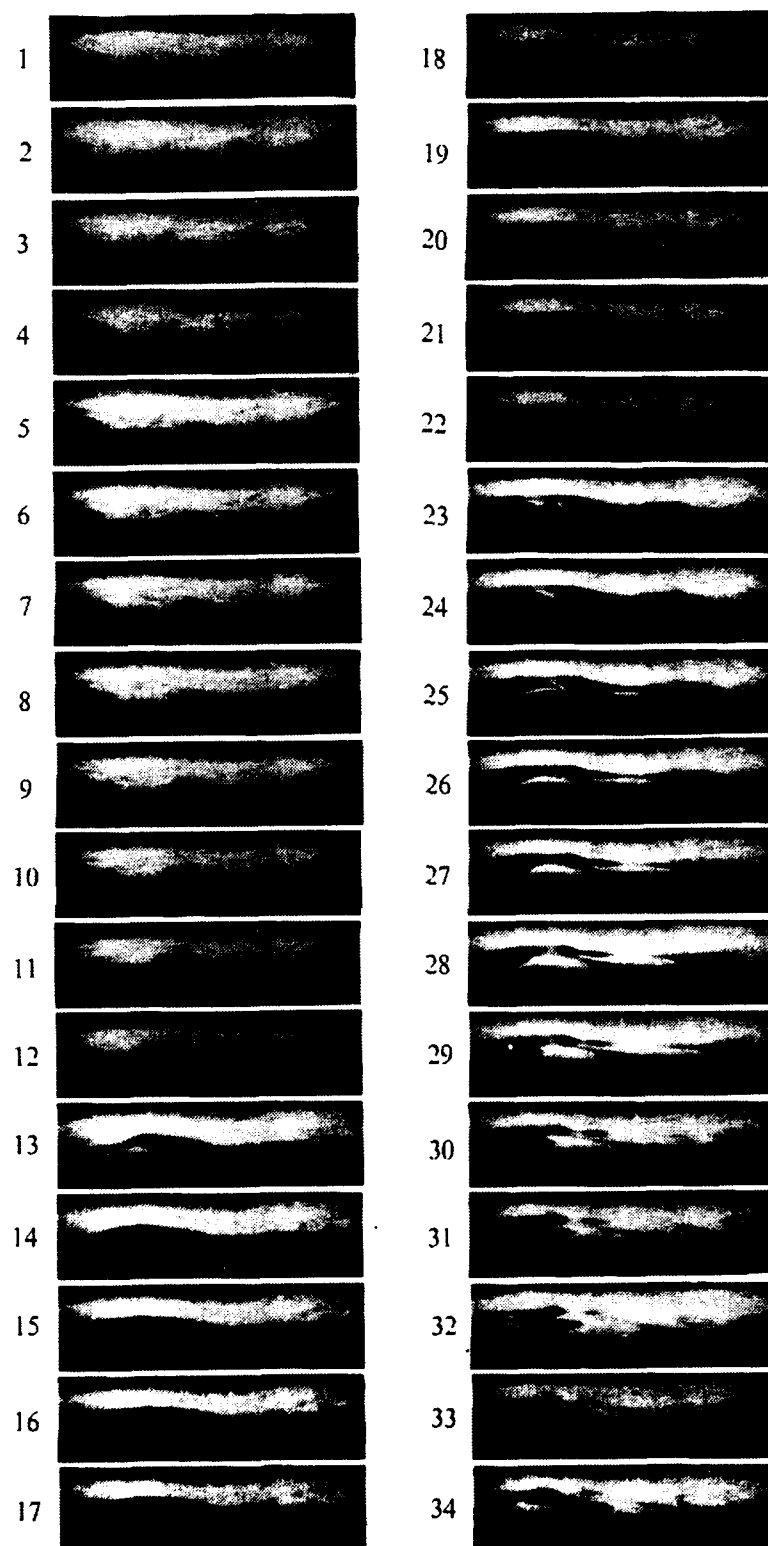


Figure 108. Flow Visualization, $De = 100.0$, $\theta = 40^\circ$ (outside), 1/30 Second Intervals

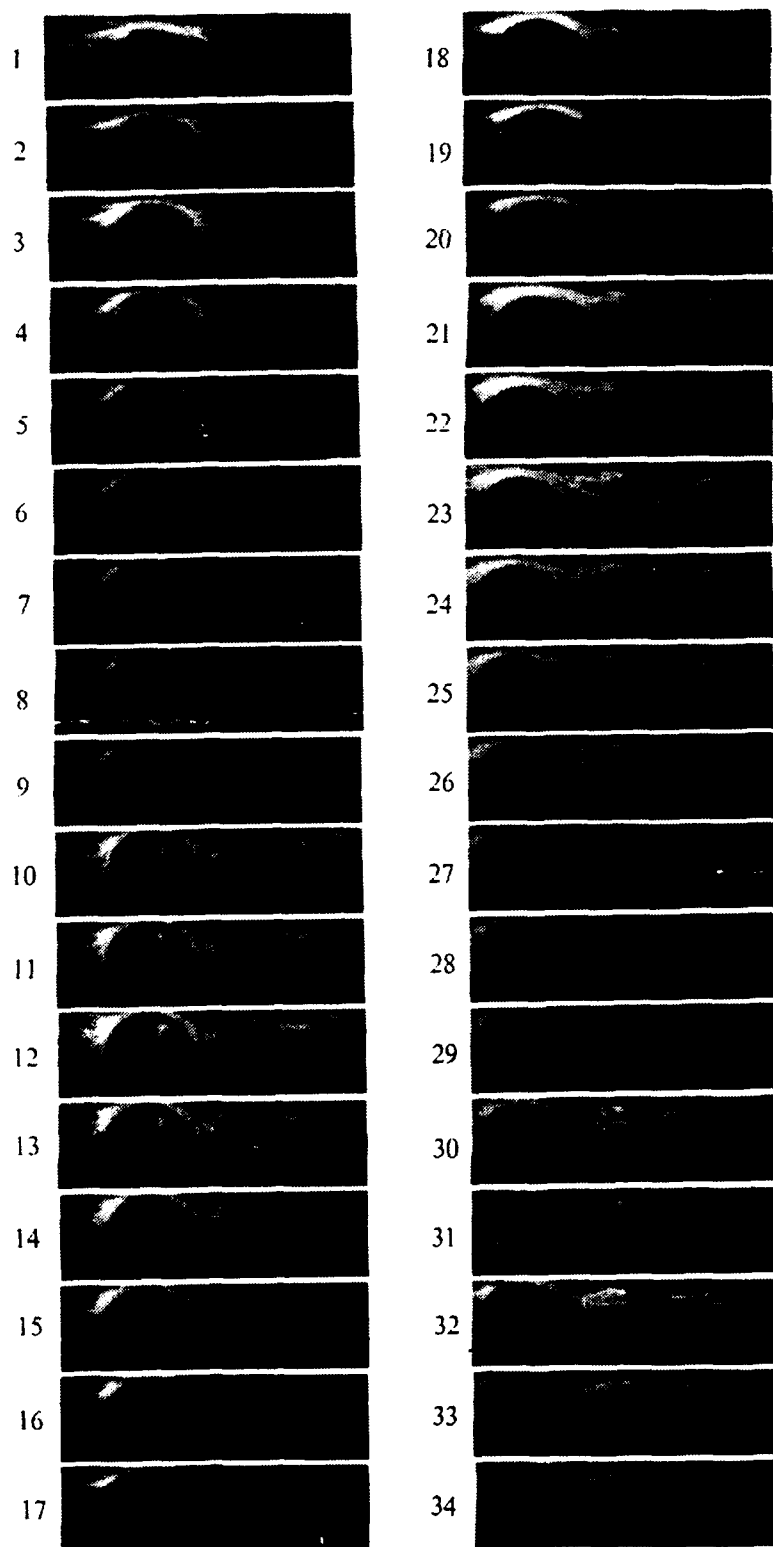


Figure 109. Flow Visualization, $De = 150.5$, $\theta = 40^\circ(\text{outside})$, 1/60 Second Intervals

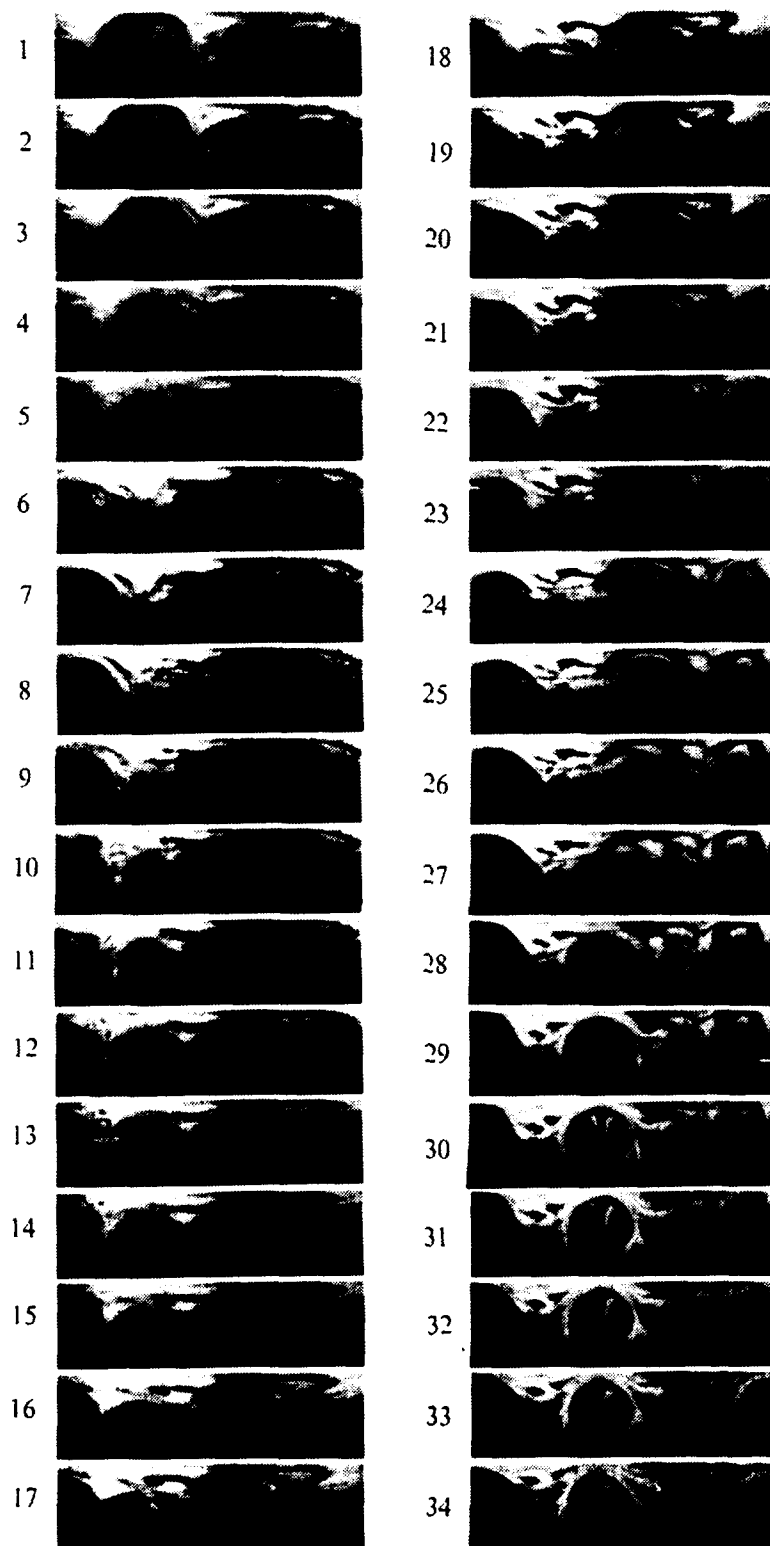


Figure 110. Flow Visualization, $De = 200.3$, $\theta = 40^\circ$ (outside), 1/60 Second Intervals

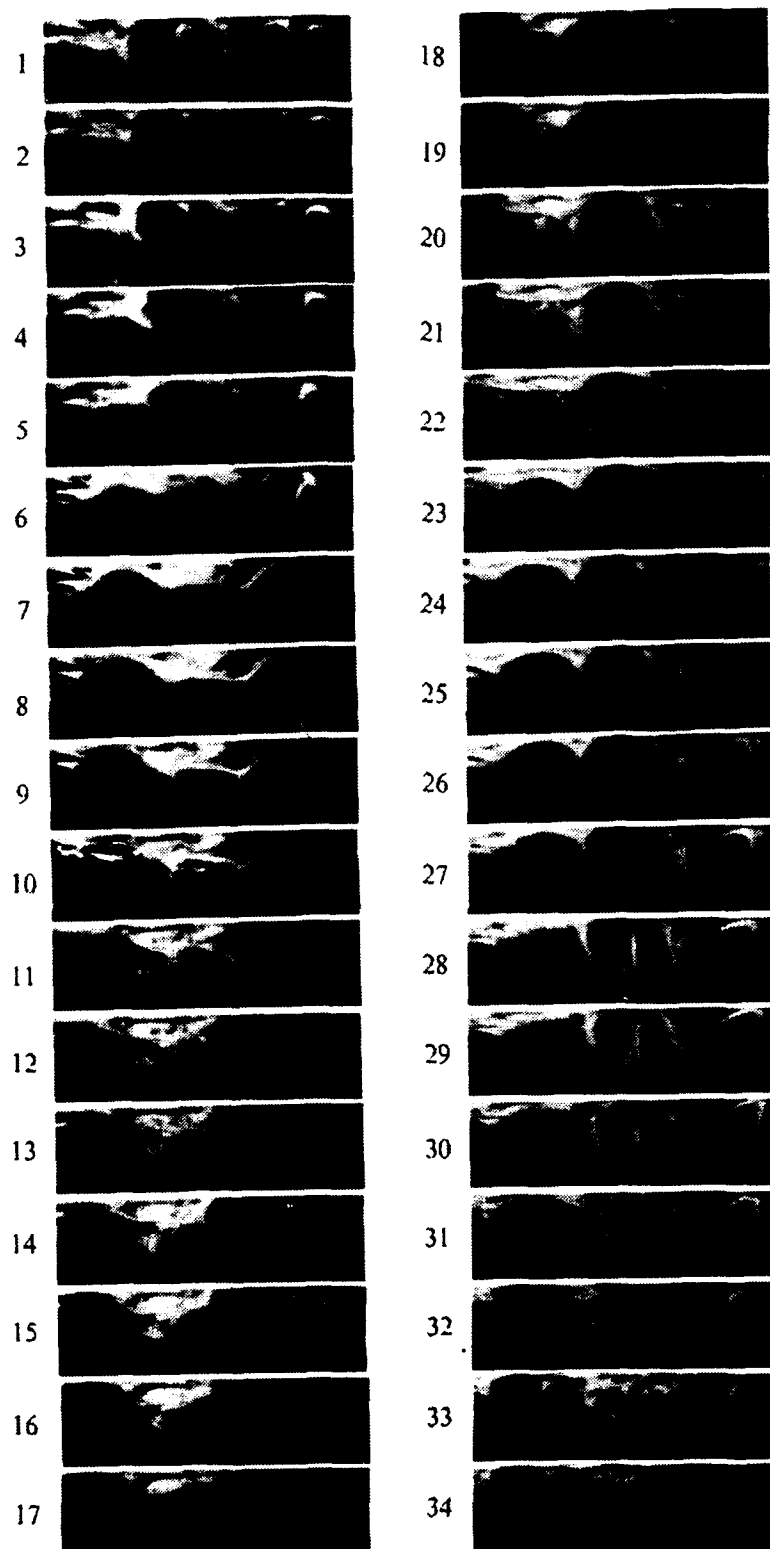


Figure 111. Flow Visualization, $De = 250.6$, $\theta = 40^\circ$ (outside), 1/60 Second Intervals

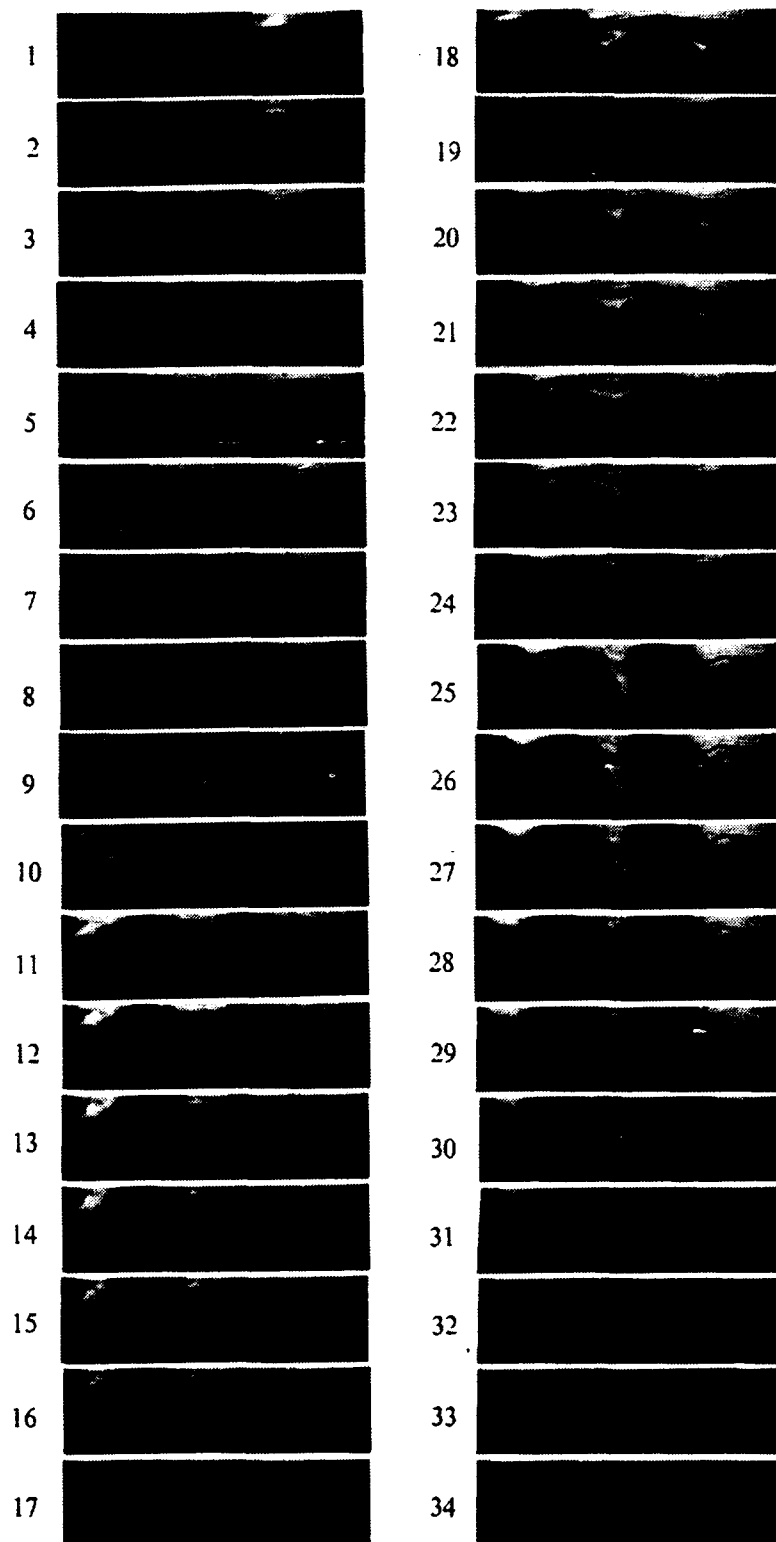


Figure 112. Flow Visualization, $De = 300.7$, $\theta = 40^\circ$ (*outside*), 1/60 Second Intervals

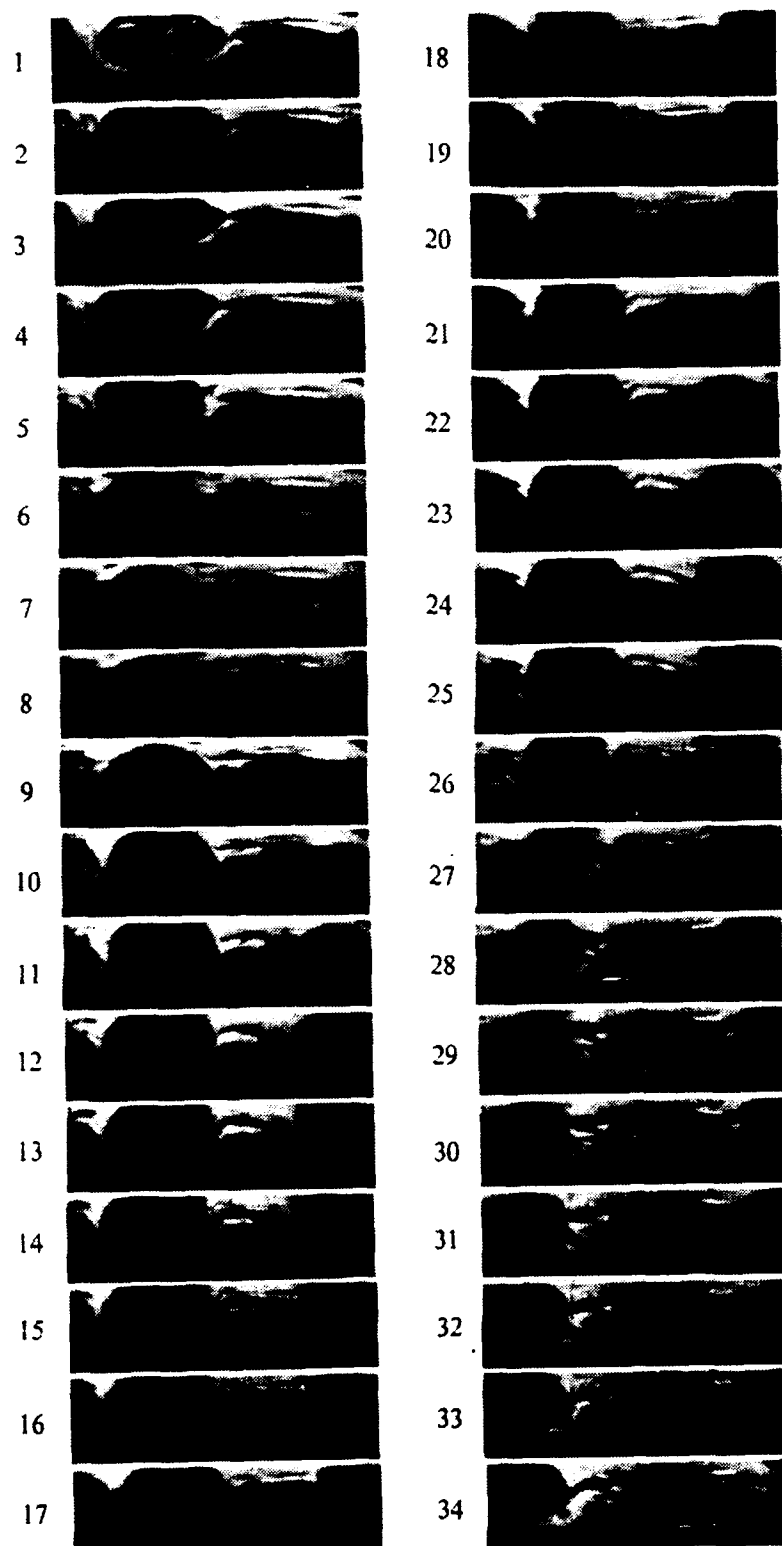


Figure 113. Flow Visualization, $De = 350.7$, $\theta = 40^\circ(\text{outside})$, $1/60$ Second Intervals

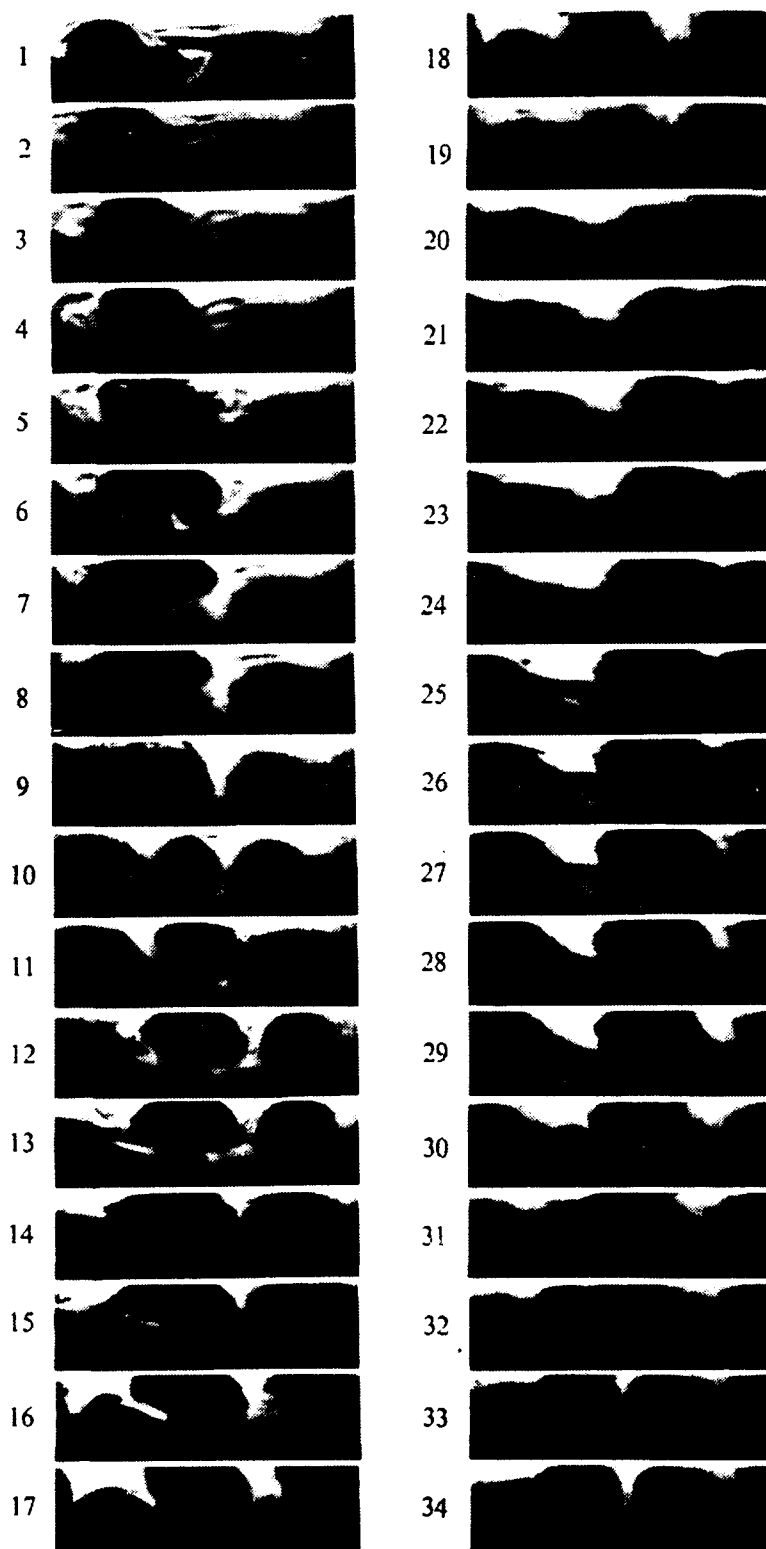


Figure 114. Flow Visualization, $De = 400.9$, $\theta = 40^\circ$ (outside), 1/60 Second Intervals

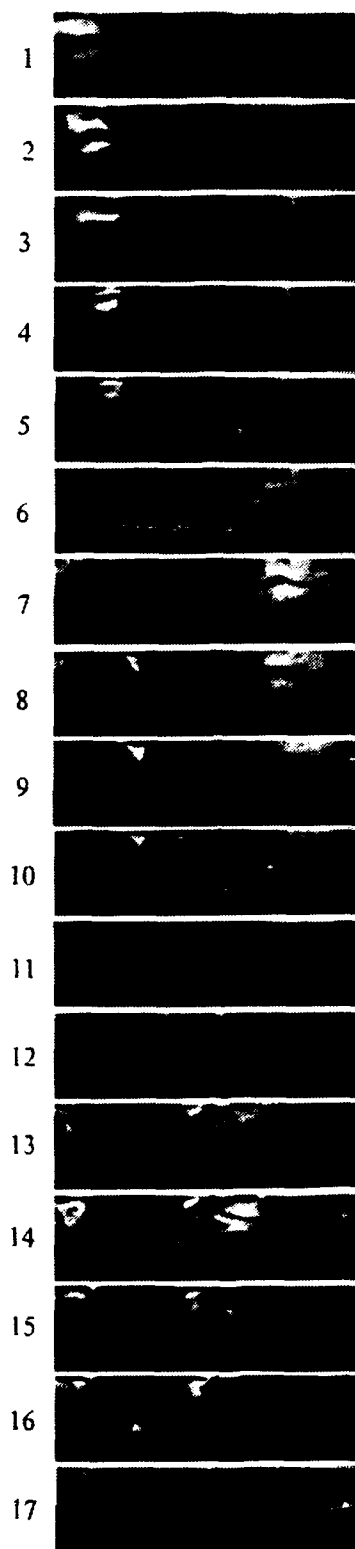


Figure 115. Flow Visualization, $De = 425.3$, $\theta = 40^\circ$ (outside), 1/60 Second Intervals

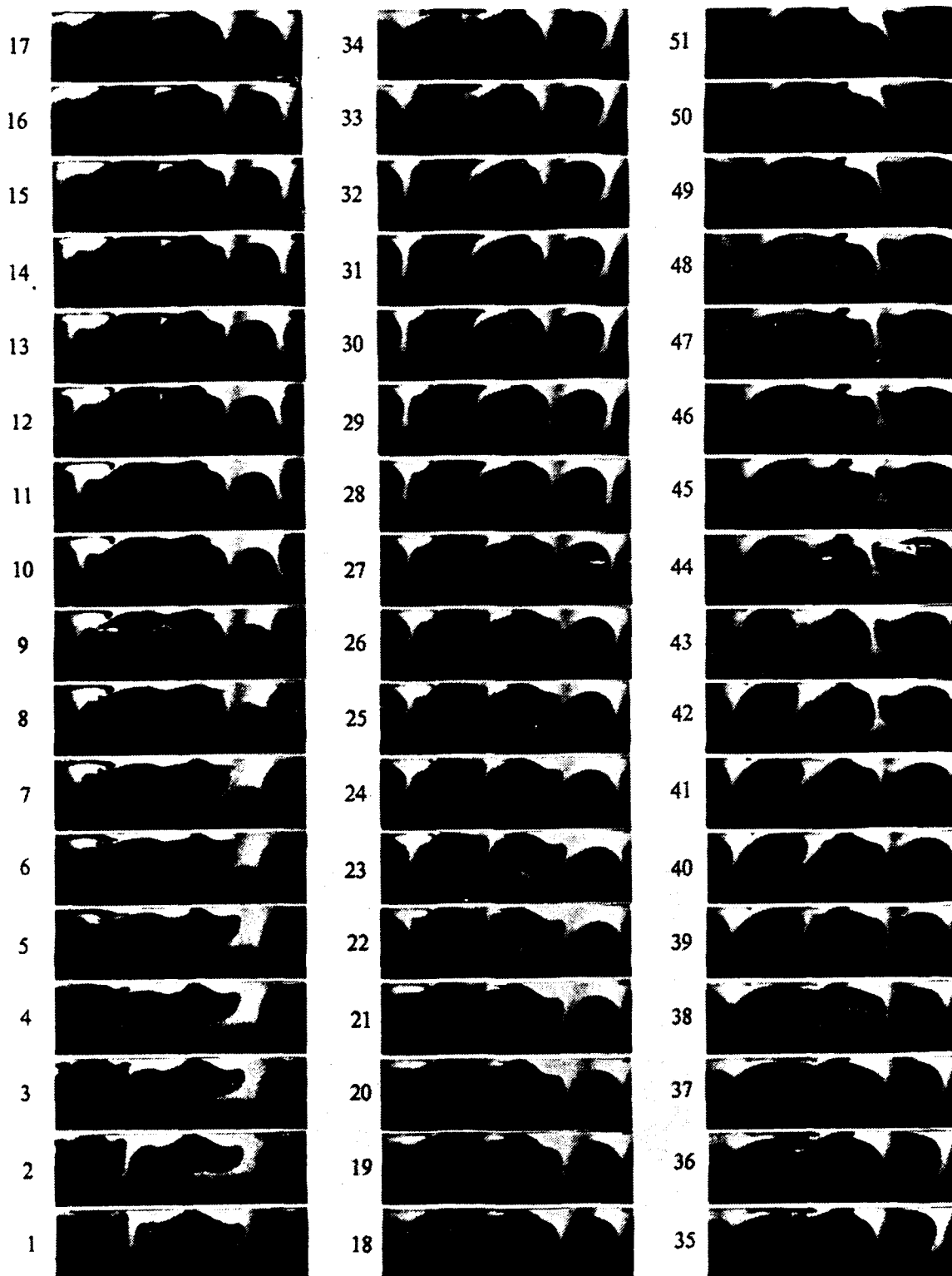


Figure 116. Flow Visualization, $De = 200.4$, $\theta = 80^\circ$ (inside), 1/60 Second Intervals

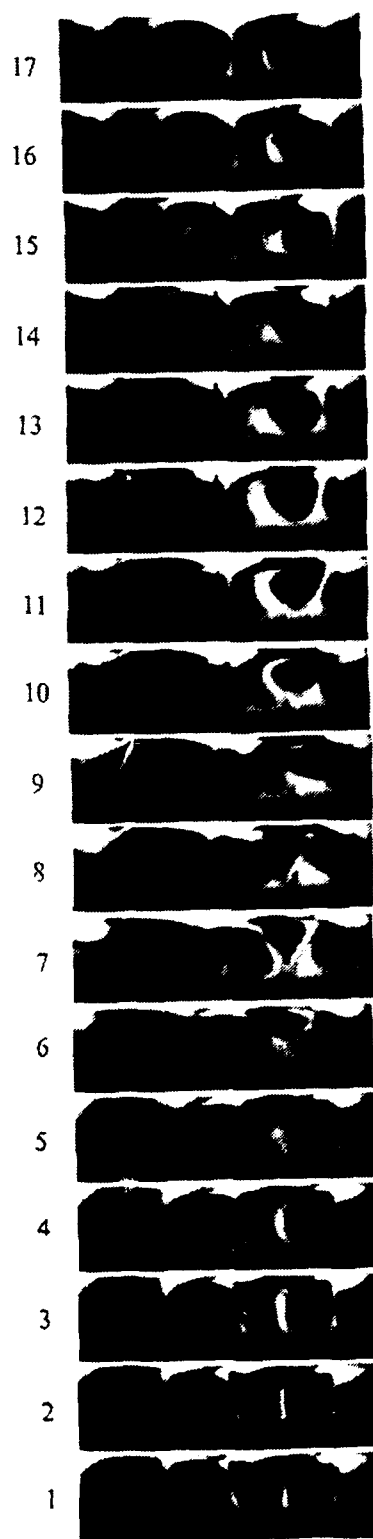


Figure 117. Flow Visualization, $De = 250.3$, $\theta = 80^\circ$ (inside), 1/60 Second Intervals

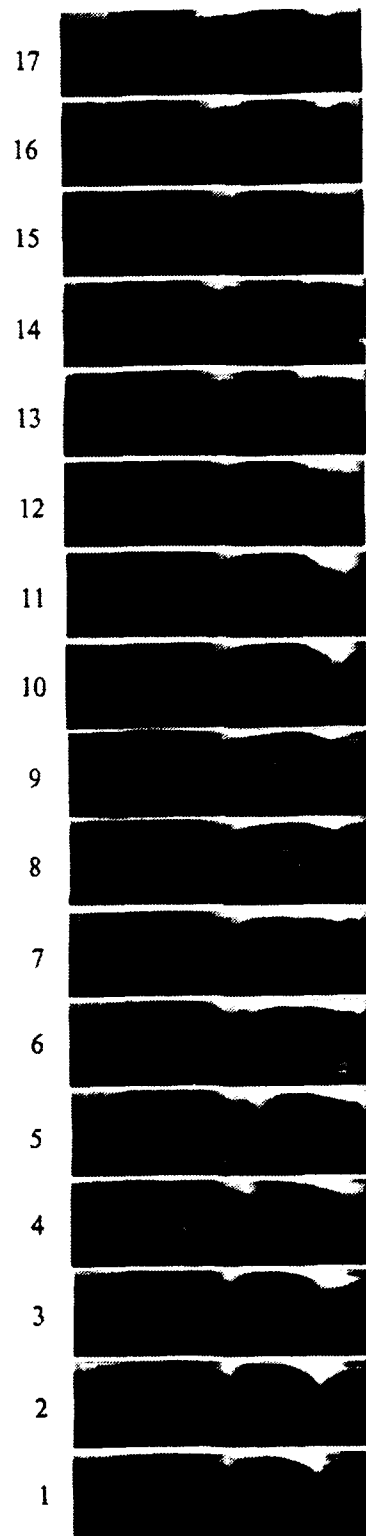


Figure 118. Flow Visualization, $De = 300.3$, $\theta = 80^\circ$ (inside), 1/60 Second Intervals

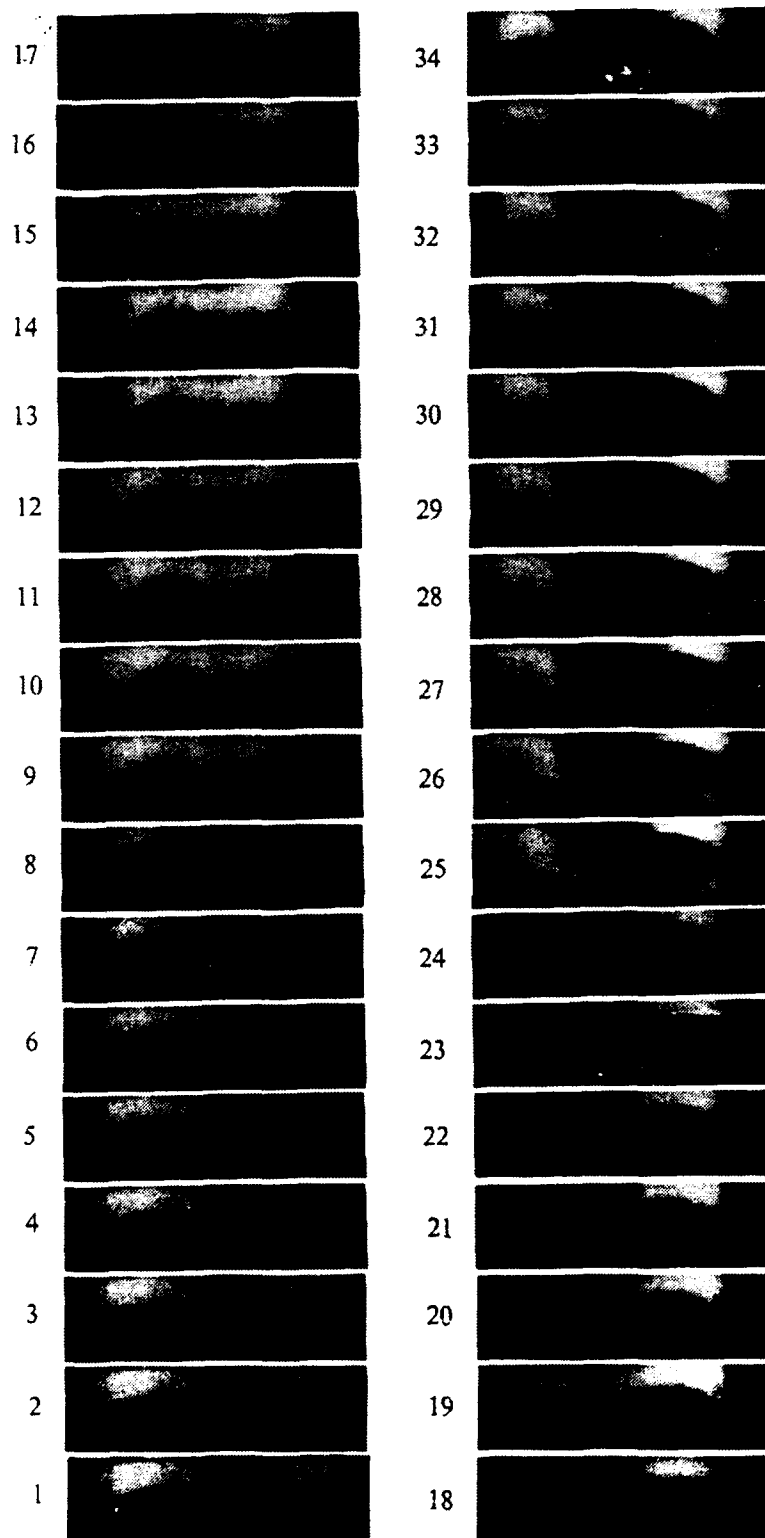


Figure 119. Flow Visualization, $De = 50.9$, $\theta = 120^\circ$ (inside), 1/30 Second Intervals

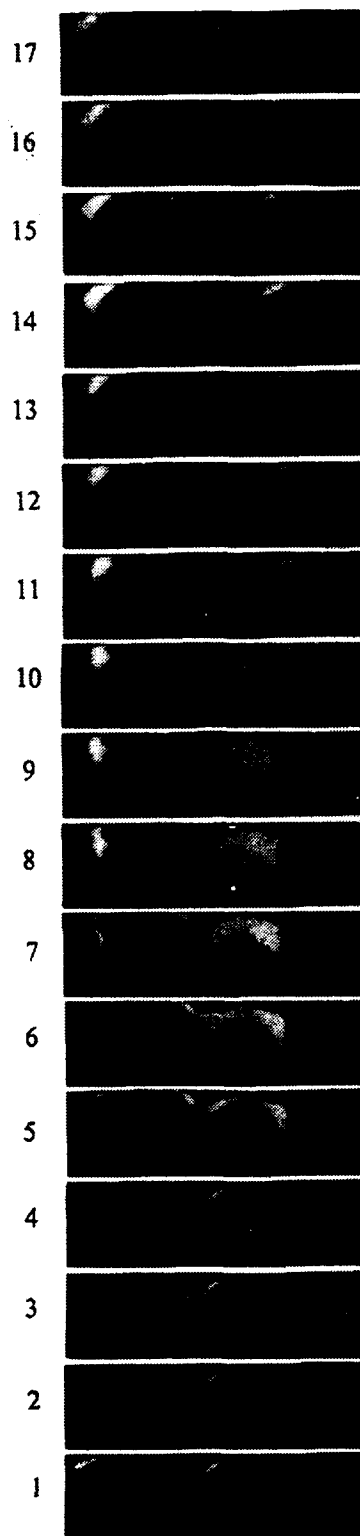


Figure 120. Flow Visualization, $De = 75.5$, $\theta = 120^\circ$ (inside), 1/30 Second Intervals

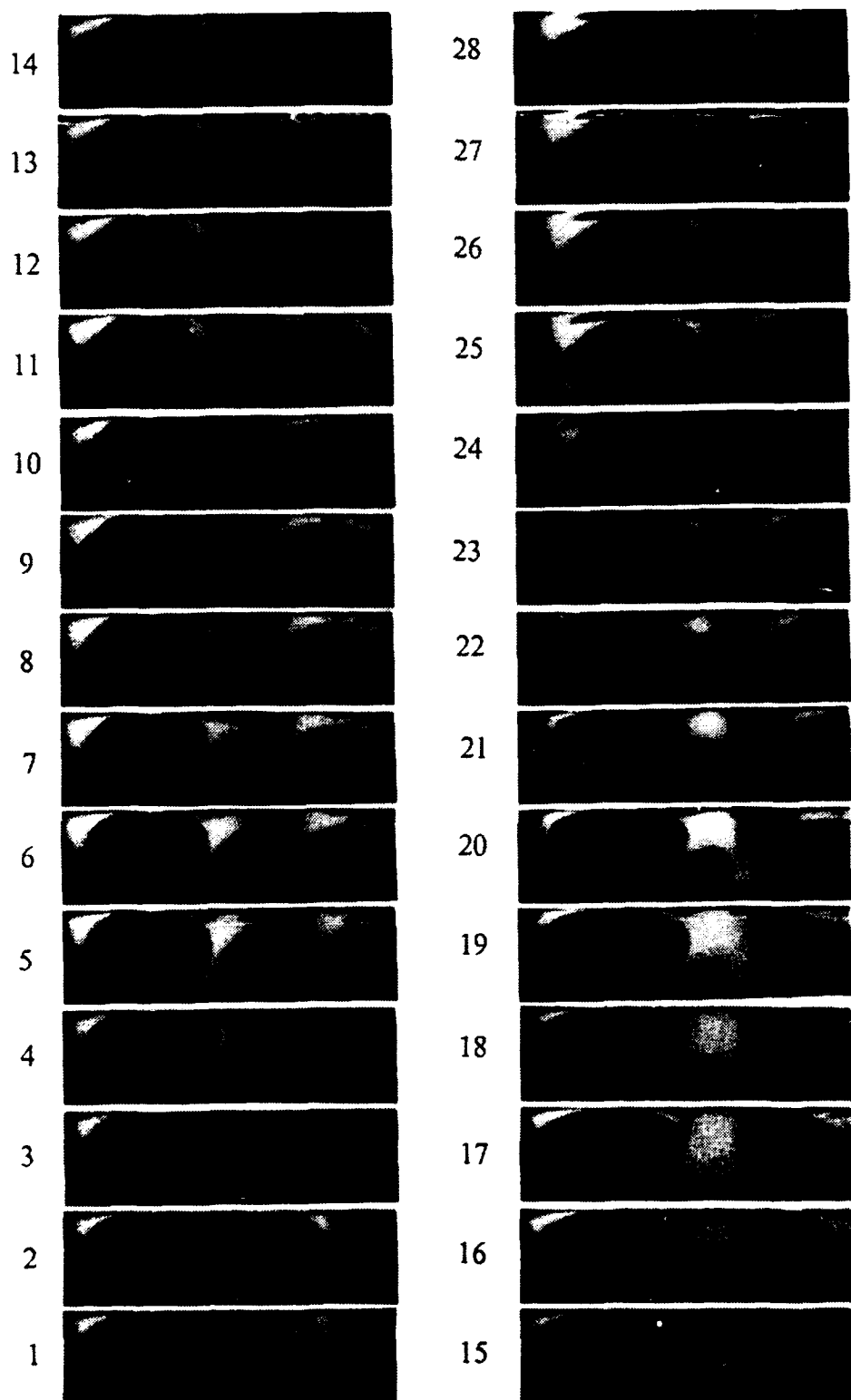


Figure 121. Flow Visualization, $De = 75.5$, $\theta = 120^\circ$ (inside), 1/30 Second Intervals

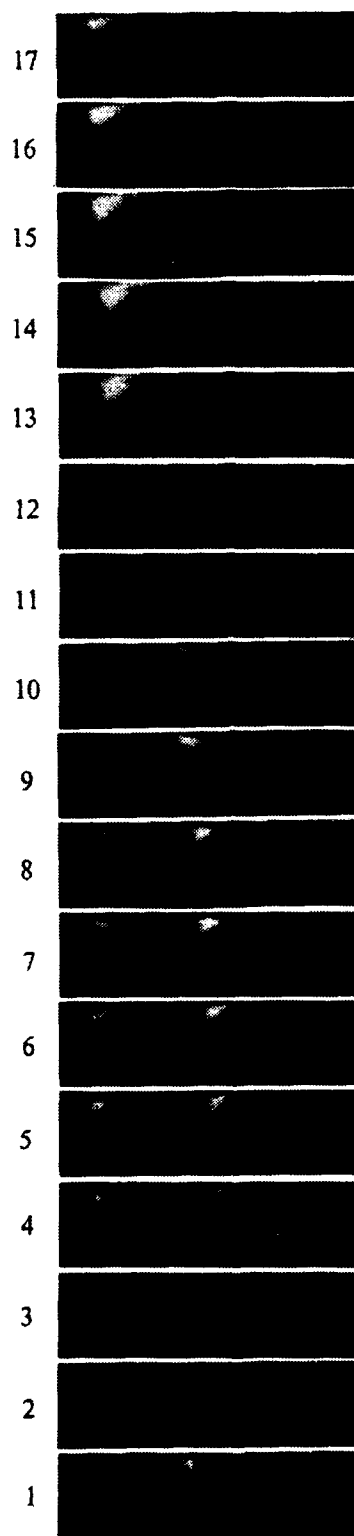


Figure 122. Flow Visualization, $De = 75.5$, $\theta = 120^\circ$ (inside), 1/30 Second Intervals

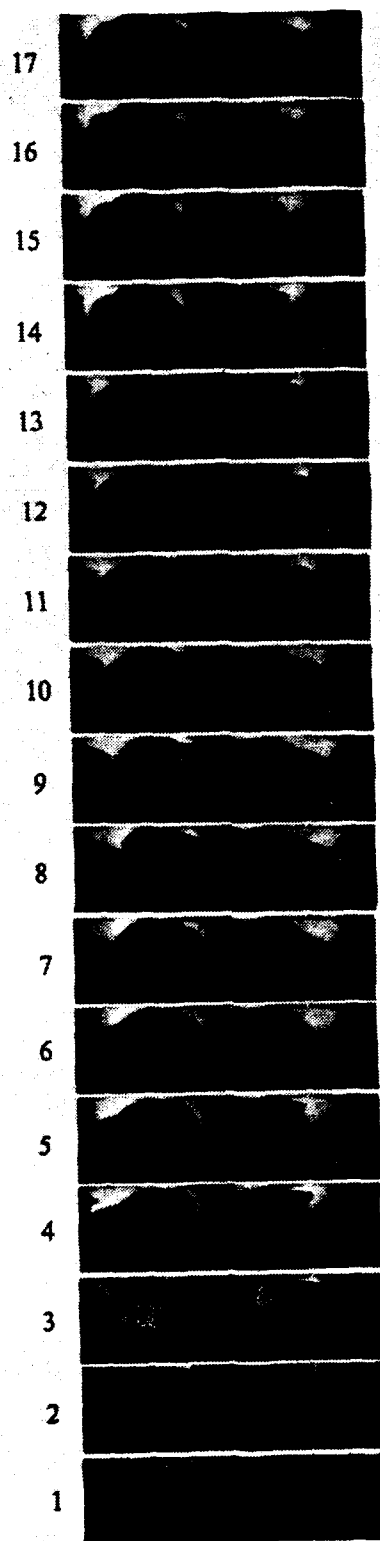


Figure 123. Flow Visualization, $De = 100.6$, $\theta = 120^\circ$ (inside), 1/30 Second Intervals

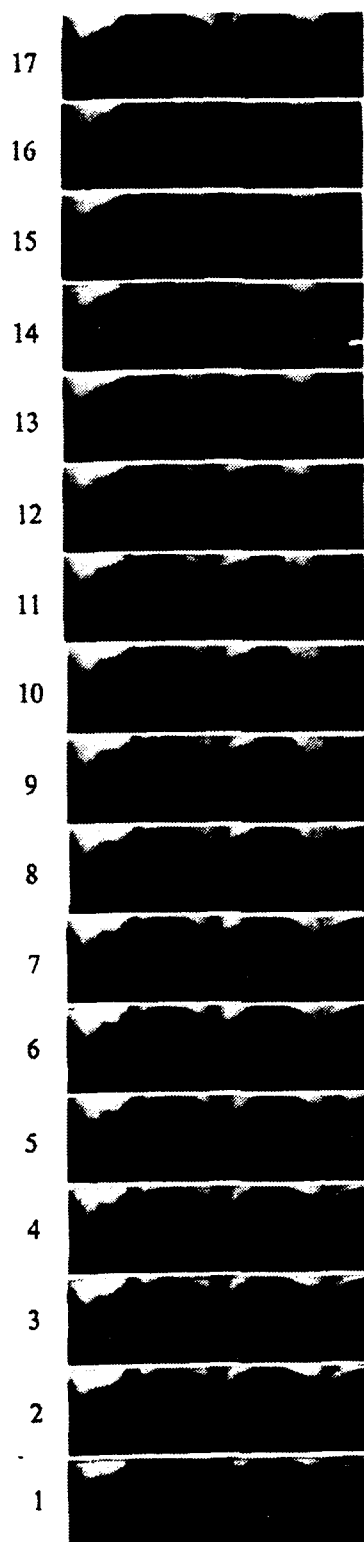


Figure 124. Flow Visualization, $De = 125.5$, $\theta = 120^\circ$ (inside), 1/30 Second Intervals

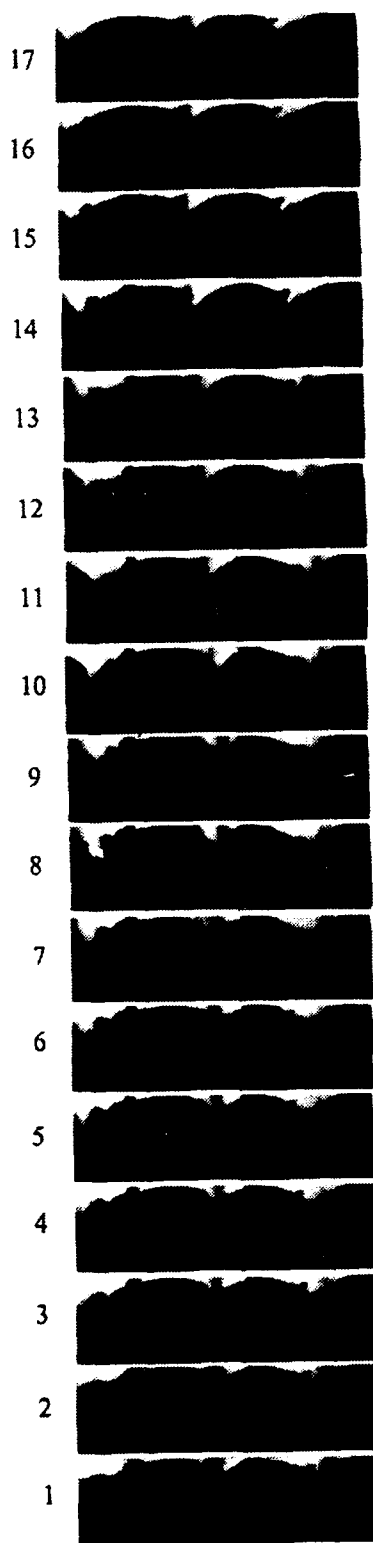


Figure 125. Flow Visualization, $De = 150.5$, $\theta = 120^\circ$ (inside), 1/30 Second Intervals

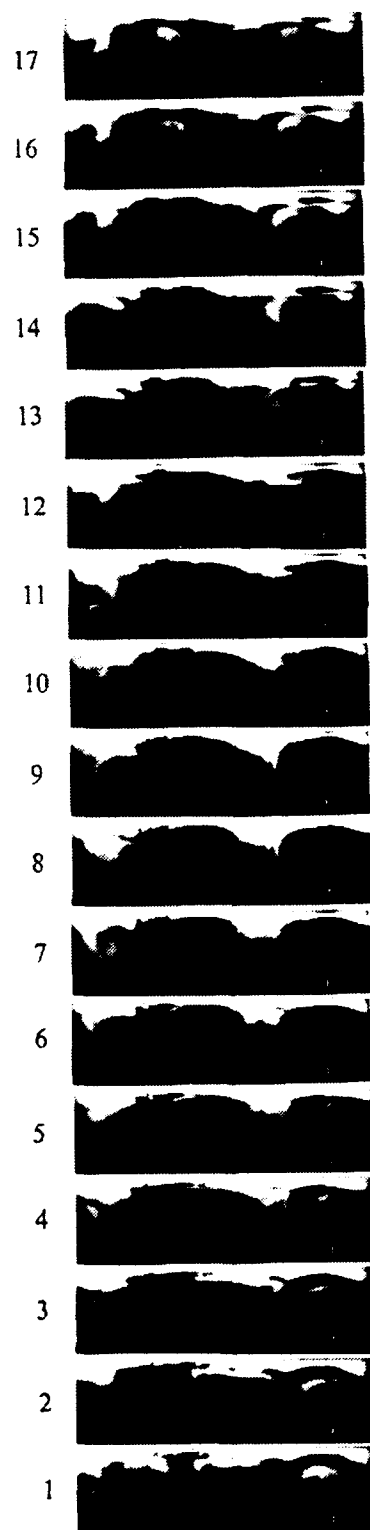


Figure 126. Flow Visualization, $De = 200.8$, $\theta = 120^\circ$ (inside), 1/60 Second Intervals

APPENDIX B. UNCERTAINTY ANALYSIS

The uncertainty analysis presented below is taken from Baun [Ref. 17]. The present study deals with flow situations similar to those explored by Baun, and utilizes the same facilities and equipment.

A. DEAN NUMBER UNCERTAINTY

The uncertainty associated with the calculation of the Dean number is derived from the uncertainty in determining the pressure drop across the ASME orifice plate. Values of uncertainty for $De \approx 150$ are listed below.

1. CELESCO TRANSDUCER CALIBRATION UNCERTAINTY

$$\delta P_{\text{manometer}} = \pm 0.002 \text{ in. } H_2O$$

$$\delta \bar{E} = \pm 0.0007 \text{ Volts}$$

$$\delta \bar{C} = \pm 0.0012 \text{ in. } H_2O/\text{Volt}$$

2. PRESSURE DROP UNCERTAINTY

$$\delta \bar{E} = \pm 0.047 \text{ Volts}$$

$$\delta \Delta P_{\text{or}} = \pm 0.005 \text{ in. } H_2O$$

3. MASS FLOW RATE UNCERTAINTY

$$\delta A_{\text{or}} = \pm 0.012 \text{ in}^2$$

$$\delta K = \pm 0.001$$

$$\delta Y = \pm 0.02$$

$$\delta \rho = \pm 0.002 \text{ lbm/ft}^3$$

$$\delta \dot{m} = \pm 0.0004 \text{ lbm/sec (95\% confidence level)}$$

$$\delta A_{\text{ch}} = \pm 0.0052 \text{ in}^2$$

$$\delta De = \pm 4.4 \text{ (95\% confidence level)}$$

B. FIVE-HOLE PROBE VELOCITY MEASUREMENT UNCERTAINTY

The uncertainties associated with the five-hole probe velocity components are derived from the uncertainty in probe calibration as well as the uncertainty with the pressures measured with the five-hole probe. Values of uncertainty for $De=100.3$, $y/d=0.5$, $z/d=6.0$ are listed below. The probe calibration uncertainty is for $yaw = -10^\circ$, $pitch = 0^\circ$.

1. VALIDYNE TRANSDUCER CALIBRATION UNCERTAINTY

$$\delta P_{manometer} = \pm 0.001 \text{ in. } H_2O$$

$$\delta \bar{E} = \pm 0.0007 \text{ Volts}$$

$$\delta \bar{C} = \pm 0.000072 \text{ in. } H_2O/Volt \text{ (bias error is disregarded since it will cancel out}$$

when pressure differentials are calculated)

2. PROBE CALIBRATION UNCERTAINTY

$$\delta \bar{E} = \pm 0.0004 \text{ Volts}$$

$$\delta P_1 = \pm 0.0006 \text{ in. } H_2O$$

$$\delta P_2 = \pm 0.0001 \text{ in. } H_2O$$

$$\delta P_3 = \pm 0.0005 \text{ in. } H_2O$$

$$\delta P_4 = \pm 0.0002 \text{ in. } H_2O$$

$$\delta P_5 = \pm 0.0003 \text{ in. } H_2O$$

$$\delta P_6 = \pm 0.00004 \text{ in. } H_2O$$

$$\delta P_7 = \pm 0.0007 \text{ in. } H_2O$$

$$\delta P = \pm 0.00015 \text{ in. } H_2O$$

$$\delta C_{\rho\rho} = \pm 0.025$$

$$\delta C_{\rho\rho} = \pm 0.011$$

$$\delta C_{\rho n} = \pm 0.045$$

$$\delta K_y = \pm 0.004 \text{ degrees}^{-1}$$

$$\delta K_p = \pm 0.004 \text{ degrees}^{-1}$$

$$\delta K_n = \pm 0.003 \text{ degrees}^{-1}$$

3. CURVED CHANNEL MEASUREMENT UNCERTAINTY

$$\delta \bar{E} = \pm 0.0007 \text{ Volts}$$

$$\delta \bar{C} = \pm 0.000072 \text{ in. } H_2O/Volt$$

$$\delta P_1 = \pm 0.0002 \text{ in. } H_2O$$

$$\delta P_2 = \pm 0.0002 \text{ in. } H_2O$$

$$\delta P_3 = \pm 0.0002 \text{ in. } H_2O$$

$$\delta P_4 = \pm 0.0002 \text{ in. } H_2O$$

$$\delta P_5 = \pm 0.0002 \text{ in. } H_2O$$

$$\delta \bar{P} = \pm 0.0001 \text{ in. } H_2O$$

$$\delta C_{py} = \pm 0.134$$

$$\delta C_{pp} = \pm 0.141$$

$$\delta Yaw = \pm 1.33^\circ$$

$$\delta Pitch = \pm 1.4^\circ$$

$$\delta (P_i - P_j) = \pm 0.0004 \text{ in. } H_2O$$

$$\delta U = \pm 0.063 \text{ m/s}$$

$$\delta U_\theta = \pm 0.062 \text{ m/s}$$

$$\delta U_r = \pm 0.062 \text{ m/s}$$

$$\delta U_z = \pm 0.030 \text{ m/s}$$

APPENDIX C. SOFTWARE DIRECTORY

This appendix lists the various programs used in this study. Accompanying each program listed, is a general summary of what the program does, user inputs, program outputs and additional features. Programs are listed alphabetically by usage: Kiel probe, five-hole pressure probe, and plotting routines. All programs are written/modified in BASIC 4.0 for use on the HP 300 Model 9000 computer.[Ref. 17]

A. KIEL PROBE PROGRAMS

KIEL15: This program is used to control Kiel probe positioning and data acquisition in the curved channel. It interfaces with the MITAS controller to control the probe position and is similar to the program FIVHOLE but obtains data for a single pressure. The *15* in the program name refers to the 1.5 inch orifice plate used between the outlet and blower plenums.

user input

- estimated Dean number.
- number of spanwise and radial locations at which data is to be taken.
- spanwise and radial resolution.
- initial position of the probe.
- number of samples to be taken per channel.
- number of standard deviations.
- number of consecutive runs.
- transducer calibration coefficient.
- ambient pressure.
- time to delay the start of the experiment.

program output

- all information input by the user.
- data file of raw pressures: y , z , P_1 , De .
- average Dean number.

additional features

- reads temperature and calculates ambient density and Dean number for each measurement location.
- allows user to calibrate transducer or input the calibration coefficient.

B. FIVE-HOLE PRESSURE PROBE PROGRAMS

ALIGN: This program aligns the five-hole pressure probe in the curved channel at zero yaw and zero pitch. It also interfaces with the MITAS controller to position the probe at a desired location and repositions the probe to the original position upon completion of the program.

user input

- number of samples per channel.
- number of standard deviations.
- ambient pressure.
- transducer calibration coefficients.
- original position of the probe.
- desired position of the probe.

program output

- mean velocity.
- P_1, P_2, P_3, P_4, P_5 .
- C_{py}, C_{pp} .

additional features

- allows the user to realign the probe between measurement sequences.
- allows user to calibrate transducers or input their calibration coefficients.

CCPF1: This program calculates the Curved Channel Poiseuille Flow (CCPF) at a given Dean number.

user input

- data file of velocities as output by the program VELOCITY1.

program output

- data file of streamwise velocities: $y, z, U_{CCPF}, U_x - U_{CCPF}$.

additional features

- none.

CIRC1: This program calculates the peak vorticity levels and circulation values from a particular set of vorticity data, using user defined boundaries.

user input

- data file of vorticity as output by the program VORTICITY.
- threshold limits, as a percentage, for omitting data points when circulation is calculated. For example, a 20 percent threshold will cause the program to omit all vorticity values less than 20 percent of peak vorticity.
- spanwise (z/d) locations that define boundaries of the areas of interest.

program output

- hard copy and/or binary data file of y/d and z/d limits, peak vorticity and circulation for each vortex pair defined by the user.

additional features

- none.

DEAN15: This program samples the orifice pressure drop and calculates the Dean number as discussed in Chapter II. The 15 in the program name refers to the 1.5 inch orifice plate used between the outlet and blower plenums.

user input

- ambient pressure.
- transducer calibration coefficient.

program output

- transducer calibration coefficient if calculated.
- expansion coefficient, Y.
- flow coefficient, K.
- orifice pressure drop.
- mass flow rate.
- channel Reynolds number.
- Dean number.

additional features

- allows user to adjust the system throttle valve (flow rate) and then calculate another Dean number.
- allows user to calibrate transducer or input the calibration coefficient.

FIVHOLE: This program is used to control the five-hole probe positioning and data acquisition in the curved channel. It interfaces with the MITAS controller to control the probe position.

user input

- estimated Dean number.
- orifice size.
- number of spanwise and radial locations at which data is to be taken.
- spanwise and radial resolution.
- initial position of the probe.
- time required for pressure reading to stabilize.
- number of samples to be taken per channel.
- number of standard deviations.
- transducer calibration coefficients.
- ambient pressure.
- time to delay the start of the experiment.

program output

- all information input by the user.
- data file of raw pressures: $y, z, P_1, P_2, P_3, P_4, P_5, \bar{P}, De$.
- data file of uncorrected pressure coefficients: y, z, C_{py}, C_{pp} .
- average Dean number.

additional features

- reads temperature and calculates ambient density and Dean number for each measurement location.
- allows user to calibrate transducers or input their calibration coefficients.

ORIENT: This program is used to orient the five-hole probe in the calibration wind tunnel before calibration begins.

user input

- number of samples to be taken per channel.
- number of standard deviations.
- transducer calibration coefficients.

program output

- mean velocity.
- P_1, P_2, P_3, P_4, P_5 .
- C_{py}, C_{pp} .

additional features

- allows user to continue through the program adjusting the probe calibration sled until satisfactory C_{py} and C_{pp} are attained.
- allows user to calibrate transducers or input their calibration coefficients.

PADJUST: This program implements the spatial resolution correction as described by Ligrani *et al.* [Ref. 16]. Chapter III of this study briefly describes this correction procedure.

user input

- distance between port 1 and the center of the other pressure ports, y_{len} and z_{len} . For the miniature five-hole pressure probe used in this study, both y_{len} and z_{len} are equal to 0.018 in.
- data file of the raw pressure data as output by the program FIVHOLE.

program output

- file of corrected pressure coefficients: $y, z, C_{py}, C_{pp}, P_1, \bar{P}, De$.

additional features

- can be used with a survey of one spanwise location, i.e., a profile.

PROCAL: This program is used for the calibration of the five-hole pressure probe in the calibration wind tunnel.

user input

- number of yaw points.
- number of pitch points.
- number of samples to be taken per channel.
- number of standard deviations.
- transducer calibration coefficients.
- yaw and pitch angle resolution.

program output

- data file of calibration coefficients: pitch, yaw, $C_{py}, C_{pp}, C_{pt}, C_{pt}, C_{pts}$.
- data file of pressures: pitch, yaw, P_1, P_2, P_3, P_4, P_5 .
- P_c, P_r .

additional features

- allows user to calibrate transducers or input their calibration coefficients.
- allows user to vary yaw at constant pitch or vary pitch at constant yaw.

- can accommodate up to seven transducers.
- allows for simultaneous printout of data if desired.

VELOCITY1: This program computes the three mean velocity components from pressure data that has been corrected for spatial resolution.

user input

- data files of calibration coefficients and pressure data as output from program PROCAL.
- number of yaw points.
- number of pitch points.
- data file of pressure coefficients as output by program PADJUST.
- values of y and z direction downwash velocity correction, $dely$ and $delz$. In this study, a value of 0.011 is used for both $dely$ and $delz$.

program output

- data file of pressures and velocities for each measurement location: $y, z, P, U, U_\theta, U_r, U_z$.

additional features

- can be used with a survey of one spanwise location, i.e., a profile.

VORTICITY: This program calculates the three mean components of vorticity at each measurement location. Methods used for calculating vorticity are presented in Chapter III.

user input

- data file of velocities as output by the program VELOCITY1.

program output

- data file of vorticity as follows: $y, z, \omega_\theta, \omega_r, \omega_z$.

additional features

- can be used with a survey of one spanwise location, i.e., a profile.

C. DATA PROCESSING

CONTOUR: This program is a general contour plotting routine that has been adapted for specific plotting purposes. It plots contour lines between predetermined levels.

user input

- number of data files to be averaged.
- plot option: average values, average of deviations from mean value, or average of standard deviations from mean value.
- number of contour levels to plot.

program output

- contour plot and table of levels.
- maximum and minimum values.
- average Dean number.

additional features

- none.

PROFILE1: This program is a modified version of PLTRAV used by Baun [Ref. 17]. It has been modified to print out specific parameters for five-hole probe surveys conducted at one spanwise location, i.e., a profile.

user input

- data file of pressures and velocities as output by the program VELOCITY1.
- column number of dependent variable.

program output

- spanwise location.
- specified parameters with corresponding radial position.

additional features

- none.

3DPLOT1: This program plots up to seven contour plots from curved channel measurements in a *three dimensional* format. An example of this format is presented in Figure 36.

user input

- type of data plot desired: vorticity, streamwise velocity, total pressure, or $U_x - UCCPF$.
- appropriate data files.

program output

- *three-dimensional* presentation of specified contour plots.
- table of levels.

additional features

- none.

VECTOR1: This program plots secondary flow vectors present in the flow field.

user input

- data file of velocities as output by the program VELOCITY1.

program output

- plot of secondary flow vectors.
- average Dean number.
- actual length of largest vector and its corresponding velocity.

additional features

- allows user to zero velocity vectors present in the bottom row.
- allows user to zero velocity vectors present at specific locations.

LIST OF REFERENCES

1. Dean, W.R., "Fluid Motion in a Curved Channel," *Proceedings of The Royal Society of London*, Series A, v. 121, pp. 402-420, 01 November 1928.
2. Reid, W.H., "On the Stability of Viscous Flow in a Curved Channel," *Proceedings of The Royal Society of London*, Series A, v. 244, pp. 186-198, 11 March 1958.
3. Hawthorne, W.R., "Secondary Circulation in Fluid Flow," *Proceedings of The Royal Society of London*, Series A, v. 206, pp. 374-386, 07 May 1951.
4. Cheng, K.C., Nakayama, J., Akiyama, M., "Effect of Finite and Infinite Aspect Ratios on Flow Patterns in Curved Rectangular Channels," *Proceedings of the International Symposium on Flow Visualization*, pp 181-186, 1977.
5. McKee, R.J., *An Experimental Study of Taylor-Goertler Vortices in a Curved Rectangular Channel*, M.E. Thesis, Naval Postgraduate School, Monterey, California, June 1973.
6. Flentie, D.L., *An Experimental Study of Taylor-Goertler Vortices in a Curved Rectangular Channel*, M.S. Thesis, Naval Postgraduate School, Monterey, California, March 1975.

7. Kelleher, M.D., Flentie, D.L., and McKee, R.J., "An Experimental Study of the Secondary Flow in a Curved Rectangular Channel," *ASME Journal of Fluids Engineering*, v. 102, pp. 92-96, 1980.
8. Thermosciences Division, Department of Mechanical Engineering, Stanford University Report TF-30, *Instability and Transition in Curved Channel Flow*, by W.H. Finlay, J.B. Keller and J.H. Ferziger, Stanford, California, May 1987.
9. Finlay, W.H., Keller, J.B., and Ferziger, J.H., "Finite Amplitude Vortices in Curved Channel Flow," *Journal of Fluid Mechanics*, v. 194, pp. 417-456, September 1988.
10. Finlay, W.H., Ligrani, P.M., Bland, S.B., "Features of Wavy Vortices in a Curved Channel from Experimental and Numerical Studies," *Physics of Fluids A - Fluid Dynamics*, 1991.
11. Ligrani, P.M., Niver, R.D., "Flow Visualization of Dean Vortices in a Curved Channel with 40 to 1 Aspect Ratio," *Physics of Fluids A - Fluid Dynamics*, v. 31, pp. 3605-3617, December 1988.
12. Alfredsson, P.H., Persson, H., "Instabilities in Channel Flow with System Rotation," *Journal of Fluid Mechanics*, v. 202, pp. 543-557, May 1989.
13. Ligrani, P.M., Longest, J.E., "Appearance, Disappearance and Spanwise Wavenumber Selection of Dean Vortex Pairs in a Curved Channel," submitted for publication, 1990.

14. Niver, R.D., *Structural Characteristics of Dean Vortices in a Curved Channel*, M.S. Thesis, Naval Postgraduate School, Monterey, California, June 1987.
15. Longest, J.M., *Flow Visualization Studies in (1) A Curved Rectangular Channel with 40 to 1 Aspect Ratio and (2) A Straight Channel with Bulk Flow Unsteadiness*, M.S. Thesis, Naval Postgraduate School, Monterey, California, June 1989.
16. Ligrani, P.M., Singer, B.A., and Baun, L.R., "Miniature Five Hole Pressure Probe for Measurement of Three Mean Velocity Components in Low Speed Flows," *Journal of Physics E - Scientific Instruments*, v. 22, pp. 868-876, October 1989.
17. Baun, L.R., *The Development and Structural Characteristics of Dean Vortices in a Curved Rectangular Channel*, M.E. Thesis, Naval Postgraduate School, Monterey, California, September 1988.
18. Sieband, M.A., *A Flow Visualization Study of Laminar/Turbulent Transition in a Curved Channel*, M.S. Thesis, Naval Postgraduate School, Monterey, California, March 1987.
19. Holman, J.P., and Gajda, W.J., Jr., *Experimental Methods for Engineers*, 4th ed., pp. 238-247, McGraw-Hill, 1984.
20. ASME Power Test Committee, *ASME Power Test Codes, (Supplement on Instruments and Apparatus)*, part 5, chapter 4, p. 25, American Society of Engineers, 1959.

21. Ligrani, P.M., Singer, B.A., and Baun, L.R., "Spatial Resolution and Downwash Velocity Corrections for Multiple-Hole Pressure Probes in Complex Flows," *Experiments in Fluids*, v. 7, pp. 424-426, June 1989.
22. Treaster, A.L. and Yocum, A.M., "The Calibration and Application of Five Hole Probes," *Instrument Society of America (ISA) Transactions*, v. 18, no. 3, pp. 23-24, 1979.
23. Smol'yakov, A.V., Tkachenko V.M., *The Measurement of Turbulent Fluctuations*, pp. 65-67, Springer-Verlag, 1983.
24. Pao, R.H.F., *Fluid Mechanics*, p. 371, John Wiley and Sons, 1961.
25. Hewlett Packard 3562A Dynamic Signal Analyzer, *Operating Manual*, Appendix E, pp. 1-6, 1986.
26. Hewlett Packard 3562A Dynamic Signal Analyzer, *Operating Manual*, Chapter 1, pp. 28-33, 1986.
27. Morrison, G.A., *On The Use of Liquid Crystal Thermography as a Technique of Flow Visualization*, M.S. Thesis, Naval Postgraduate School, Monterey, California, June 1984.
28. Hughes, R.E., *Development, Qualification and Measurements in Two Curved Channels with 40 to 1 Aspect Ratio*, M.S. Thesis, Naval Postgraduate School, Monterey, California, September 1989.

29. Dage-MTI CCD-72 Series Video Camera, *Service Manual*, 1989.

INITIAL DISTRIBUTION LIST

		No. Copies
1.	Defense Technical Information Center Cameron Station Alexandria, VA 22304-6145	2
2.	Library, Code 52 Naval Postgraduate School Monterey, CA 93943-5002	2
3.	Dean of Science and Engineering, Code 06 Naval Postgraduate School Monterey, CA 93943-5000	1
4.	Research and Administration Office, Code 08 Naval Postgraduate School Monterey, CA 93943-5000	1
5.	Department Chairman, Code ME Department of Mechanical Engineering Naval Postgraduate School Monterey, CA 93943-5000	1
6.	Naval Engineering Curricular Office, Code 34 Department of Mechanical Engineering Naval Postgraduate School Monterey, CA 93943-5000	1
7.	Professor P.M. Ligrani, Code ME/Li Department of Mechanical Engineering Naval Postgraduate School Monterey, CA 93943-5000	3
8.	Professor C.S. Subramanian, Code ME/Su Department of Mechanical Engineering Naval Postgraduate School Monterey, CA 93943-5000	1
9.	Dr. K. Civinskas Propulsion Directorate U.S. Army Aviation Research and Technology Activity AVSCOM NASA-Lewis Research Center Cleveland, OH 45433	2
10.	LT W.A. Fields, USN 118 Brownell Circle Monterey, CA 93940-4824	1